

UNCLASSIFIED

AD 265 599

*Reproduced
by the*

ARMED SERVICES TECHNICAL INFORMATION AGENCY
ARLINGTON HALL STATION
ARLINGTON 12, VIRGINIA



UNCLASSIFIED

NOTICE: When government or other drawings, specifications or other data are used for any purpose other than in connection with a definitely related government procurement operation, the U. S. Government thereby incurs no responsibility, nor any obligation whatsoever; and the fact that the Government may have formulated, furnished, or in any way supplied the said drawings, specifications, or other data is not to be regarded by implication or otherwise as in any manner licensing the holder or any other person or corporation, or conveying any rights or permission to manufacture, use or sell any patented invention that may in any way be related thereto.

265599

ASTIA
25 NOV 60

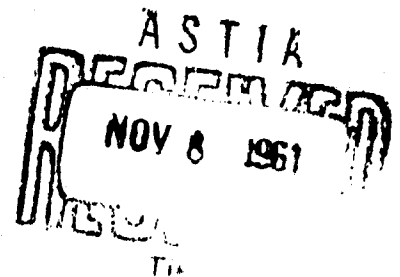
THERMOPILE GENERATOR FEASIBILITY STUDY

PART II — MATERIALS INVESTIGATIONS

J. H. BREDT, EDITOR
GENERAL ELECTRIC COMPANY
SCHENECTADY, N. Y.

AUGUST 1960

62 1-2
XEROX



WRIGHT AIR DEVELOPMENT DIVISION

**Best
Available
Copy**

NOTICES

When Government drawings, specifications, or other data are used for any purpose other than in connection with a definitely related Government procurement operation, the United States Government thereby incurs no responsibility nor any obligation whatsoever; and the fact that the Government may have formulated, furnished, or in any way supplied the said drawings, specifications, or other data, is not to be regarded by implication or otherwise as in any manner licensing the holder or any other person or corporation, or conveying any rights or permission to manufacture, use, or sell any patented invention that may in any way be related thereto.



Qualified requesters may obtain copies of this report from the Armed Services Technical Information Agency, (ASTIA), Arlington Hall Station, Arlington 12, Virginia.



This report has been released to the Office of Technical Services, U. S. Department of Commerce, Washington 25, D. C., for sale to the general public.



Copies of WADD Technical Reports and Technical Notes should not be returned to the Wright Air Development Division unless return is required by security considerations, contractual obligations, or notice on a specific document.

THERMOPILE GENERATOR FEASIBILITY STUDY
PART II — MATERIALS INVESTIGATIONS

J. H. BREDT, EDITOR

GENERAL ELECTRIC COMPANY
SCHENECTADY, N. Y.

AUGUST 1960

FLIGHT ACCESSORIES LABORATORY

FINAL REPORT
CONTRACT No. AF 33(616)-5281
PROJECT No. 3145
TASK No. 60199

FLIGHT ACCESSORIES LABORATORY
WRIGHT AIR DEVELOPMENT DIVISION
AIR RESEARCH AND DEVELOPMENT COMMAND
UNITED STATES AIR FORCE
WRIGHT-PATTERSON AIR FORCE BASE, OHIO

FOREWORD

This is the final report covering the work performed by the General Electric Company for the United States Air Force under Contract No. AF 33 (616)-5281 entitled "Thermopile Generator Feasibility Study." This program was carried out by several components within the Company under the overall cognizance of the Aircraft Accessory Turbine Department. The contract was administered under the direction of the Aeronautical Accessories Laboratory of the Wright Air Development Center, (presently called Flight Accessories Laboratory, Wright Air Development Division) Wright-Patterson Air Force Base, Ohio. Lt. R. G. Leiby was Task Engineer during the early part of the contract, and Mr. R. N. Cooper acted as Task Engineer during the remaining portion.

The report is written in four parts, of which this is Part II. It covers the entire period of the contract, from 1 July 1957 through 31 March 1960.

In addition to the editor of Part II and the authors of the various appendices, Dr. R. H. Vought contributed materially to the writing of this part of the report.

ABSTRACT

This report contains a detailed description and summary of a research and development study to determine means of employing thermopile generators as sources of electrical power in future air and space weapon systems. The following major areas of work were involved: 1) Materials development, 2) Junction fabrication and test, 3) Thermoelectric generator applications studies, and 4) Thermoelectric generator design.

The report consists of four parts as follows:

Part I - Summary - This presents an over-all summary of the entire program.

Part II - Materials Investigations - This contains the details of the work on materials development.

Part III - Performance Studies - This presents in detail the work on junction thermoelectric generator applications studies as well as the more general aspects of thermoelectric generator design.

Part IV - Generator Design - This contains the details of the work on fabrication and test and thermoelectric generator design for specific applications.

This is Part II of the report and contains detailed descriptions of the investigations carried out on various classes of materials and on instrumentation for measuring material properties. These descriptions are in the form of a series of appendices, each covering a separate aspect of the investigations.

TABLE OF CONTENTS

	<u>Page</u>
INTRODUCTION	1
APPENDIX A - METALLIC MATERIALS FOR THERMOPILE GENERATORS--John P. Denny	3
APPENDIX B - POWER PER UNIT VOLUME-- John P. Denny	21
APPENDIX C - THERMOELECTRIC POWER OF METALLIC ALLOYS AND TRANSITION METAL HYDRIDES--John P. Denny	25
APPENDIX D - THERMOELECTRIC POWER OF METALLIC ALLOYS AND TRANSITION METAL HYDRIDES--John P. Denny	35
APPENDIX E - THE FEASIBILITY OF USING REFRACTORY MATERIALS FOR THERMOELECTRIC GENERATOR (TEG) ELEMENTS--Hans J. Borchardt	51
APPENDIX F - SEEBECK VOLTAGE AND RESISTIVITY OF "REFRACTORY METALS"--John R. Gambino	83
APPENDIX G - THERMOELECTRIC POWER OF REFRACTORY BORIDES, CARBIDES, NITRIDES, AND SILICIDES--John R. Gambino	91
APPENDIX H - SOME PRELIMINARY RESULTS IN THE STUDY OF OXIDE THERMOELECTRIC GENERATOR MATERIALS--John R. Gambino	115
APPENDIX I - SEEBECK VOLTAGE AND RESISTIVITY OF COMPOSITIONS BASED ON CHROMIUM OXIDE--John R. Gambino	123
APPENDIX J - A STUDY OF OXIDES FOR THERMOELECTRIC GENERATOR APPLICATIONS--John R. Gambino	135
APPENDIX K - SUMMARY OF MEASUREMENTS OF RESISTIVITY AND SEEBECK COEFFICIENT OF FERRITES AND TITANATES AT TEMPERATURES UP TO 1000°K--Philipp H. Klein	161
APPENDIX L - SUMMARY OF THERMOELECTRIC INVESTIGATIONS OF ENCAPSULATED INTERMETALLIC AND LIQUID SEMICONDUCTORS--E. Fischer-Colbrie	189
APPENDIX M - GROWTH OF SINGLE CRYSTALS OF TRANSITION METAL OXIDES AND MEASUREMENT OF THEIR THERMAL CONDUCTIVITY--F.H. Horn, R. Newman, G.A. Slack	223
APPENDIX O - THERMAL CONDUCTIVITY STUDIES WITH THE POWELL METHOD--A.I. Dahl	249
APPENDIX P - THE POWELL METHOD OF MEASURING THE THERMAL CONDUCTIVITY OF SOLIDS--A.I. Dahl	271
APPENDIX Q - ANALYSIS OF RADIATION HEAT LOSSES IN MEASUREMENT APPARATUS--S.B. Dunham	281
APPENDIX R - MEASUREMENTS - Z METER--F.A. Ludewig, Jr.	287

LIST OF ILLUSTRATIONS

<u>Figure</u>		<u>Page</u>
C-1	Thermal EMF Versus Temperature of Alloys Referred to Platinum	26
C-2	Resistivity of Nickel and Nickel Alloys	28
C-3	Thermal EMF Maxima in Systems Ni-Cr, Ni-Mo and Ni-W . . .	29
C-4	Thermoelectric Power of Pd-H Alloys (Pt = Reference Junction)	31
C-5	Thermoelectric Power of Various Metals and Alloys (Pt = Reference Junction)	32
D-1	Thermal EMF of Annealed Cu-Co Alloys	37
D-2	Seebeck Coefficient (Thermoelectric Power) of Annealed 96.9 Cu 3.1 Co Alloy (Referred to Pt)	37
D-3	Thermal EMF of Copper versus Cold Worked, Solution Treated, and Annealed 96.9 Cu 3.1 Co Alloy	38
D-4	Seebeck Coefficient of 96.9 Cu 3.1 Co in Cold Worked, Solution Treated, and Annealed Conditions (Referred to Pt)	38
D-5	Plateau Vapor Pressure in Systems Zirconium-Hydrogen and Titanium-Hydrogen	41
D-6	Seebeck Coefficient of Zirconium-Hydrogen Alloys (Referred to Pt)	41
E-1	Resistivity and Thermal Conductivity Versus Temperature. .	78
E-2	Thermal Electric Power Versus Temperature	79
F-1	Temperature Dependence of Seebeck Voltage for Borides . . .	85
F-2	Temperature Dependence of Seebeck Voltage for Carbides . . .	86
F-3	Temperature Dependence of Seebeck Voltage for Nitrides . . .	87
F-4	Temperature Dependence of Seebeck Voltage for Silicides . .	89
G-1	Schematic Diagram of a Thermoelectric Generator Circuit . .	92

LIST OF ILLUSTRATIONS (CONT'D)

<u>Figure</u>		<u>Page</u>
G-2	Efficiency of Materials with Figures of Merit as a Function of Temperature	94
G-3	Specimen Holder for Seebeck Voltage Measurements	97
G-4	Temperature Dependence of Seebeck Voltage for Borides	98
G-5	Temperature Dependence of Seebeck Voltage for Carbides	99
G-6	Temperature Dependence of Seebeck Voltage for Nitrides	100
G-7	Temperature Dependence of Seebeck Voltage for Silicides	101
G-8	Seebeck Voltage of Disilicides as a Function of Temperature	103
G-9	Seebeck Voltage of Monosilicides	104
G-10	Seebeck Voltage of Solid Solutions of the Disilicides	105
G-11	Effect of Impurities on the Seebeck Voltage of Chromium Disilicide	106
G-12	Effect of Impurities on the Seebeck Voltage of Manganese Disilicide	107
G-13	Close-packed Layers in Some Disilicides	108
H-1	Seebeck Voltage as Function of Time During Reaction of ZnO and Fe_2O_3 ($T = 760^\circ\text{C}$)	117
I-1	Temperature Dependence of Resistivity Containing 1 Mole % Additives Having Valency > 3	124
I-2	Temperature Dependence of Resistivity Containing 1 Mole % Additives Having Valency < 3	125
I-3	Temperature Dependence of Resistivity Containing 1 Mole % Additives Having Valency of 3	126
I-4	Temperature Dependence of Chromium Oxide Containing Additives of Manganese Oxide	128

LIST OF ILLUSTRATIONS (CONT'D)

<u>Figure</u>		<u>Page</u>
I-5	Effect of Recrystallization and Oxygen Pressure on the Resistivity of Chromium Oxide	129
I-6	Temperature Dependence of Seebeck Voltage of Chromium Oxide Compositions Containing 1 Mole % Additives Having Valency of > 3	130
I-7	Temperature Dependence of Seebeck Voltage of Chromium Oxide Compositions Containing 1 Mole % Additives Having Valency of < 3	131
I-8	Temperature Dependence of Seebeck Voltage of Chromium Oxide Compositions Containing 1 Mole % Additives Having Valency of 3	132
J-1	Specimen Holder for Seebeck Voltage Measurements	137
J-2	The Effect of TiO_2 Additives on the Conductivity of Cr_2O_3	138
J-3	The Effect of NiO Additives on the Conductivity of Cr_2O_3	139
J-4	Temperature Dependence of Resistivity of Cr_2O_3 Without Additives	140
J-5	Resistivity of Cr_2O_3 Compositions with Additives Having Valency of > 3	142
J-6	Seebeck Voltage of Chromium Oxide Compositions Containing 1 Mole % Additives Having Valency > 3	143
J-7	Resistivity of Cr_2O_3 Compositions with Additives Having Valency < 3	144
J-8	Seebeck Voltage of Chromium Oxide Compositions Containing 1 Mole % Additives Having Valency < 3	145
J-9	Resistivity of Cr_2O_3 Compositions Containing MnO_2 Additives	147
J-10	Resistivity of Cr_2O_3 as a Function of Composition (MnO_2)	148

LIST OF ILLUSTRATIONS (CONT'D)

<u>Figure</u>		<u>Page</u>
J-11	Resistivity of Cr_2O_3 as a Function of Composition (NiO)	149
J-12	Resistivity of Cr_2O_3 as a Function of Composition (CuO)	150
J-13	Resistivity of Cobalt Oxides	153
J-14	Seebeck Voltage of Cobalt Oxides	154
J-15	Seebeck Voltage of CoO with 1 Mole % Additives	155
J-16	Seebeck Voltages of Co_3O_4 with Additives	156
J-17	Resistivity of Cobalt Oxides with Additives	157
K-1	Schematic Diagram of Two-probe S- ρ Meter	163
K-2	Sample Placement in Two-probe S- ρ Meter	164
K-3	Measuring Circuit for Two-probe Equipment	165
K-4	Sample Placement in Four-probe S- ρ Meter	167
K-5	Exploded View of Four-probe Apparatus	168
K-6	Resistivity Data for a Group of Titanates	170
K-7	Seebeck Coefficients of a Variety of Titanates	171
K-8	Variation of Resistivity of a Number of Ferrites as a Function of Temperature	173
K-9	Seebeck Coefficients of the Ferrites whose Resistivities are Shown in Figure K-8	174
K-10	Effect of Temperature on the Resistivities of a Number of Compounds of Mainly Academic Interest	175
K-11	Seebeck Coefficients of Materials whose Resistivities are Shown in Figure K-10	176

LIST OF ILLUSTRATIONS (CONT'D)

<u>Figure</u>		<u>Page</u>
K-12	Effect of Reduction in a Vacuum on Strontium Titanate of Two Initial Degrees of Purity	178
K-13	Seebeck Coefficients of Strontium Titanates Whose Resistivities are Shown in Figure K-12	179
K-14	Resistivities of Doped, Ultra-pure Strontium Titanate Compared with Undoped Samples	180
L-1	Encapsulation in Quartz Glass Vessel	192
L-2	Encapsulation by Sealing to Ceramics	192
L-3	TE Cell with Improved Conditions for Temperature Measurements	199
L-4	Resistivity vs Temperature, Lead Telluride	202
L-5	Seebeck Coefficient vs Temperature, Lead Telluride	203
L-6	Figure of Merit vs Temperature, Lead Telluride	204
L-7	Resistivity vs Reciprocal Temperature, Sb_2Se_3	206
L-8	Resistivity vs Reciprocal Temperature, As_2Se_3	207
L-9	Seebeck Coefficient vs Temperature, Bismuth - Antimony	208
L-10	Seebeck Coefficient vs Temperature, Indium - Antimonide	210
L-11	Resistivity vs Temperature, Indium - Antimonide	211
L-12	Seebeck Coefficient vs Temperature, Lead - Antimony Alloys	213
L-13	Resistivity vs Temperature, Zinc - Antimonide	214
L-14	Seebeck Coefficient vs Temperature, Zinc - Antimonide	215
L-15	Figure of Merit vs Temperature, Zinc - Antimonide	217
L-16	Best Performing TE Materials - April 1959	220
L-17	Temperature Dependence of Some Figures of Merit	222

LIST OF ILLUSTRATIONS (CONT'D)

<u>Figure</u>		<u>Page</u>
M-1	Flame Fusion Apparatus	224
M-2	Halide Decomposition Apparatus	226
M-3	Device for Measuring Thermocouple Conductivity	228
M-4	Thermal Conductivity vs Temperature for MgO	230
M-5	Thermal Conductivity vs Temperature for Various High-Purity Oxides	233
M-6	Average Phonon Mean Free Path, λ vs Reduced Temperature, (T/θ) for MgO	236
M-7	Average Phonon Mean Free Path, λ vs Reduced Temperature, (T/θ) for Various Oxides	237
M-8	Thermal Conductivity, (K) vs Temperature, (T) for NiO . .	240
M-9	Thermal Conductivity, (K) vs Temperature, (T) for MnO . .	241
M-10	Thermal Conductivity, (K) vs Temperature, (T) for MnO with Various Additions	242
M-11	Thermal Conductivity, (K) vs Temperature, (T) for NiO with Various Additions	244
O-1	Schematic of Mounted Metal Spheres Showing Imbedded Thermocouples	250
O-2	Schematic of Mounted Metal Spheres Showing Imbedded Thermocouples	252
O-3	Comparator No. 3	254
O-4	Comparator No. 3A, Loading vs Response	257
O-5	Comparator No. 3A, Response vs Conductivity	258
O-6	Comparator No. 3B, Loading vs Response	260
O-7	Comparator No. 3B, Response vs Conductivity	261
O-8	Photograph of Comparator No. 4	263

LIST OF ILLUSTRATIONS (CONT'D)

<u>Figure</u>		<u>Page</u>
O-9	Comparator No. 4, Loading vs Response	264
O-10	Comparator No. 4, Response vs Conductivity	264
O-11	Comparison of Conduction and Radiation Heat Transfer Rates, Contacting Sphere to Test Sample	267
P-1	Schematic of Mounted Metal Spheres	271
P-2	The Resistance Between Two Consecutive Equipotential Surfaces of the Figure is 1/6 of the Total Construction Resistance in One Contact Member	276
P-3	Equivalent Electric Contact Network	277
P-4	Equivalent Electrical Circuit, 1/4" Silver Sphere, Stainless Steel Slab	279
R-1	Z Meter Apparatus	290
R-2	Sample Holder	292
R-3	Measuring Circuitry	293
R-4	Room Temperature Sample Holder Design	295
R-5	Cross Section of Oven and Sample	299
R-6	Ratio Actual Thermal Conductivity to Indicated Thermal Conductivity for Various Conditions	311
R-7	Ratio Actual Thermal Conductivity to Indicated Thermal Conductivity for Various Thermal Conductivities	312
R-8	Electrical Resistivity Measuring Device Excluding Contact Resistance Measurement	315
R-9	Contact Resistance vs Pressure. Estimated Values from Available Data. Plane Surfaces, Ground Finish in Vacuum	316

LIST OF TABLES

<u>Table</u>		<u>Page</u>
A-1	Thermoelectric Power of Metallic Materials	7
A-2	Thermoelectric Materials Negative to Platinum	9
A-3	Elements Thermoelectrically Positive to Platinum	10
A-4	Thermoelectric Properties of Alloy Systems	11
A-5	Thermoelectric Data on Various Alloys (Pt = Reference Junction)	15
D-1	Thermoelectric Power of Copper Standard	43
D-2	Thermoelectric Power of Nickel Standard	44
D-3	82 Ni 18 Mo Alloy	45
D-4	60 Au 40 Pd Alloy	46
D-5	Constantan (45Ni 55Cu)	47
D-6	Chromel P (90Ni 10Cr)	49
E-1	Data on MoSi_2	80
E-2	Properties of Thermoelectric Materials	81
G-1	Properties of Some Refractory Carbides, Borides, Nitrides, and Silicides	110
G-2	Radius Ratios of a Number of Refractory Carbides, Borides, Nitrides, and Silicides	111
G-3	Seebeck Voltage of Two Grades of Silicon used in the Study	112
G-4	Room Temperature Resistivities of Compositions Based on Chromium Silicides	112
G-5	Room Temperature Resistivity of Compositions Based on Manganese Disilicide	113
G-6	Maximum Seebeck Voltage of Various Disilicides	113

LIST OF TABLES (CONT'D)

<u>Table</u>		<u>Page</u>
G-7	Maximum Seebeck Voltage of Various Monosilicides	114
G-8	Figure of Merit and Efficiency of Several Silicide Compositions	114
H-1	Seebeck Voltage Per Degree of Various Oxides as a Function of Temperature	119
H-2	Seebeck Voltage of Cr_2O_3 Compositions as a Function of Temperature	119
H-3	Seebeck Voltage of ZnO and Cr_2O_3 Powder Mixtures as a Function of Time	120
H-4	Seebeck Voltage of ZnO and Fe_2O_3 Powder Mixtures as a Function of Time	120
H-5	Change in Seebeck Voltage of ZnO During Heating with 2 Mole % Fe_2O_3 at 760°C	121
H-6	Seebeck Voltage of Reacted Oxide Mixtures	121
H-7	Effect of Stoichiometry on Seebeck Voltage of Selected Oxides	122
H-8	Resistivity of Cr_2O_3 as a Function of Temperature	122
J-1	Effect of Hot Pressing on the Resistivity of Cr_2O_3 Compositions	159
J-2	Effect of Heat Treatment on the Resistivity of Cr_2O_3	159
J-3	Effect of Atmosphere on the Resistivity of Cr_2O_3 Compositions	159
J-4	Effect of Mixtures of Additives on the Seebeck Voltage and Resistivity of Cr_2O_3	160
J-5	Seebeck Voltage of Various Oxides as a Function of Temperature	160
J-6	Figure of Merit of Oxidic Compositions	160
K-1	The Dependence of the Activation Energy for Conduction on Time of Reduction of Strontium Titanate	181

LIST OF TABLES (CONT'D)

<u>Table</u>		<u>Page</u>
K-2	Electrical Resistivities and Seebeck Coefficients of the Oxidic Semiconductors Studies at Three Selected Temperatures	184
K-3	Activation Energies for Conduction of Materials Studied .	186
L-1	List of High Temperature Contact Materials to Thermo-electric Materials	195
L-2	Materials and Work Done	196
L-3	Thermal Conductivity of ZnSb	216
M-1	Table of Crystals Studied	229
M-2	Relative Therman Conductivity vs Reduced Temperature for Phonon-Phonon Scattering	232
M-3	Physical Constants of Some Oxide Crystals	234
M-4	Fraction of Disordered Spins as a Function of Temperature for $J = 5/2$	239
O-1	Data Obtained with Thermal Comparator No. 3A	256
O-2	Calibration Response - Comparator No. 4	262
O-3	Calculation Data	266
O-4	Radiation Data	268
O-5	Compiled Values	268
P-1	Mechanical Properties	273
P-2	Contact Dimensions	273
P-3	Thermal Properties	275
P-4	Silver Sphere - SS Slab, 0.0006" Radius Contact	278
P-5	Charging Times Silver Sphere - SS Slab, 0.0006" Radius Contact	280

LIST OF TABLES (CONT'D)

<u>Table</u>		<u>Page</u>
Q-1	Summary of Results	285
R-1	Radiation Heat Transfer Coefficient (h_r)	318
R-2	Effective Pressure on Contact Resistance	321

INTRODUCTION

In this part of the report, we have collected the primary source material for the work done under the materials investigations section of the contract. This consists of the reports prepared by those who did the actual work on each task. All of the material presented here has appeared previously in the form of exhibits attached to the Technical Progress Reports which were submitted during the course of the contract, and the only alterations which have been made have been in the format, to obtain uniformity. Duplications and redundancies have been avoided as far as possible, but some do exist because we have included the whole text of each report which contained significant material that was not presented elsewhere, whether it also contained information included in other reports or not.

Items and materials used in the study, and called out in the four parts of this report by trade name or specifically identified with a manufacturer, were not originated for use in this specific study or for the applications necessary to this study. Therefore, the failure of any one of the items or materials to meet the requirements of the study is no reflection on the quality of a manufacturer's product. No criticism of any item or material is implied or intended. Nor is any indorsement of an item or material by the United States Air Force implied or intended.

Manuscript released August 1960 for publication as a Technical Report.

APPENDIX A - METALLIC MATERIALS FOR THERMOPILE GENERATORS

John P. Denny

September, 1957

Metallic materials have been surveyed for potential applicability in thermopile generators. Primary emphasis has been placed on those metals and alloys having a large thermoelectric power, since the efficiency of a generator is directly proportional to the thermoelectric power in accordance with the following three relationships previously discussed by D. L. Kerr (A-1).

$$Z = \frac{\alpha^2}{\rho k} \quad (A-1)$$

where Z is the "figure of merit"

α is the thermoelectric power in microvolts per degree Kelvin

ρ is the electrical resistivity in ohm-cm

k is the thermal conductivity in watts per centimeter per degree Kelvin

$$M = \sqrt{1 + 1/2 Z (T_1 + T_2)} \quad (A-2)$$

where M is the optimum resistance ratio

T_1 is the hot junction temperature in degrees Kelvin

T_2 is the cold junction temperature

$$\eta_{opt} = \frac{T_1 - T_2}{T_1} \frac{M-1}{M + \frac{T_2}{T_1}} \quad (A-3)$$

where η_{opt} is the optimum efficiency.

It is instructive to first consider those elements in the periodic table for which the quantities α , ρ , and k are known. These are presented in Table A-1 in ascending order of thermoelectric power, with all thermoelectric quantities referred to platinum at 0°C. The elements silicon and tellurium are respectively at opposite ends of the table, silicon having a thermoelectric power of -367 microvolts per °C and tellurium exhibiting +526 microvolts per °C.

The last column of the table presents values for the Wiedemann-Franz-Lorenz constant. The Wiedemann-Franz-Lorenz relationship is

$$\rho k = (2.45) (10^{-8}) T$$

where T is the absolute temperature and the constant $(2.45) (10^{-8})$ is the Wiedemann-Franz-Lorenz value. Most metals and alloys obey this relationship with small deviations. The theoretical basis for the relationship is the electronic nature of both electrical and thermal conductivity in metals.

The form of equation (A-1) shows that the Lorenz constant should be as low as possible. Examination of Table A-1 shows that indium $(0.73)(10^{-8})$, iridium $(1.06)(10^{-8})$, rhodium $(1.40)(10^{-8})$, and cobalt $(1.47)(10^{-8})$ show maximum deviation in the optimum direction.

Concurrently equation (A-1) contains the thermoelectric power squared, and the most significant changes in figure of merit can be effected by variations in the thermoelectric power. Table A-2 presents the figure of merit of those elements which are thermoelectrically negative with respect to platinum, and Table A-3 presents the thermoelectrically positive elements. Bismuth $(.47)(10^{-3})$ and antimony $(.29)(10^{-3})$ are the most attractive. From the standpoint of those elements which are strictly metallic in nature, cobalt $(.072)(10^{-3})$ and molybdenum $(.11)(10^{-3})$ are best.

Using the equation (A-1),

$$Z = \frac{(\alpha_p + \alpha_n)^2}{\left[\sqrt{\rho_p k_p} + \sqrt{\rho_n k_n} \right]^2} \quad (A-4)$$

figures of merit for junctions made from these elements are as follows:

<u>Junction</u>	<u>Figure of Merit ($^{\circ}\text{K}^{-1}$)</u>
Bi-Sb	$(0.38)(10^{-3})$
Bi-Pt	$(0.13)(10^{-3})$
Co-Mo	$(.094)(10^{-3})$

Improvements in the figure of merit are possible by alloying, as evidenced (A-1) by the reported figure of merit for Zn Sb-Bi Sb of $(1)(10^{-3})^{\circ}\text{K}^{-1}$.

The search reported herein has been directed primarily toward metallic systems. In general, semi-conductors are superior from the figure of merit standpoint, and metals and ceramics permit higher operating temperatures leading to potential gains in efficiency and power.

Table A-4 summarizes the thermoelectric power of metallic systems uncovered in the present search. Certain systems exhibit minima and others exhibit maxima over the composition range. The location of the minimum or maximum value in four metallic systems is defined approximately by an electron:atom ratio of 3:5.

<u>System</u>	<u>Inflection Point (Atomic%)</u>	<u>Electron:Atom Ratio</u>
Ni-Cu	45 Ni 55 Cu	2.75:5
Ni-Cr	90 Ni 10 Cr	3:5
Ni-Mo	85 Ni 15 Mo	4.5:5
Au-Pd	45 Au 55 Pd	2.25:5

The two metalloid-containing systems (Zn-Sb and Cd-Sb) exhibit inflection points at an electron to atom ratio of 19:5.

Theoretical or other means by which the inflection points may be predicted are not known. On the basis of the 3:5 ratio, the optimum atomic compositions in the Fe-Al and Au-Ni systems should be 80 Fe 20 Al and 60 Au 40 Ni.

Table A-5 presents thermoelectric data on various alloys. Maximum figures of merit in the table are 60 Au 40 Pd ($0.24-0.33 \times 10^{-3}$) and 79 Ni 20 Mo 1 Mn (0.27×10^{-3}).

In calculating these values and most other Z values, the ρk product has been assumed to be equal to the ρk product of the major constituent. This assumption introduces small errors but is reasonable as evidenced by the following data from the system iron-nickel.

Alloy	ρ ohm-cm	k watts/cm ² K	ρk
100 Ni	$6.84(10^{-6})$.921	$(2.34)(10^{-6})$
50 Ni 50 Fe	$48(10^{-6})$.134	$(2.19)(10^{-6})$
30 Ni 70 Fe	$82(10^{-6})$.0921	$(2.58)(10^{-6})$
25 Ni 75 Fe	$48(10^{-6})$.134	$(2.19)(10^{-6})$
100 Fe	$9.71(10^{-6})$.754	$(2.50)(10^{-6})$

Ingersoll (A-2) reports the following data for iron-nickel alloys referred to copper. The polarity of the thermoelectric power is not clear from his work. If the alloys are positive to copper, the couple 47.1 Ni-52.9 Fe produces a thermoelectric power of 50.1 microvolts/^oC, which is higher than any alloy reported in Table A-5. This should be confirmed experimentally.

Alloy	Thermoelectric Power Against Copper 0-96 ^o C Microvolts/ ^o C
21.0 Ni 79.0 Fe	23.5
22.1 Ni 77.9 Fe	21.0
26.4 Ni 73.6 Fe	16.7
35.1 Ni 64.9 Fe	9.8
40.0 Ni 60.0 Fe	22.4
45.0 Ni 55.0 Fe	29.0
47.1 Ni 52.9 Fe	31.9

Primary sources of data in the tables are given in references (A-3) through (A-8). The contributions of M. E. Ihnat of the Instrument Laboratory were very significant and are gratefully acknowledged.

Various methods have been considered for improving thermoelectric power over and above the values given in the table.

One method is to utilize thermoelectric error resultant from cladding of a surface. Using equations developed in reference (A-9), it is possible to increase the output of an alumel-chromel thermocouple at $400^{\circ}\text{F}/32^{\circ}\text{F}$ from 8.31 mv to 11.91 mv by cladding the alumel with bismuth and the chromel with antimony. The primary advantage of such an approach is the elimination of bismuth to antimony or similar junctions. If separate junctions can be made, they are preferable from the standpoint of total thermoelectric power.

Alloy development is a very fertile field. Most data reported in the literature pertains to thermocouples, and linearity is a requisite in such an application. In the thermoelectric generator on the other hand, one is primarily concerned with the emf which can be developed under a given set of operating conditions, and numerous metallic systems have not been studied.

TABLE A-1
THERMOELECTRIC POWER OF METALLIC MATERIALS

Element	Thermoelectric Power (α) Range of Thermoelectric Measurement	Electrical Resistivity (ρ) Microhm-cm at 20°C	Thermal Conductivity (k) Watts/cm ² K at 20°C	Wiedemann-Franz- Lorenz Constant $\frac{(\rho)(k)}{293}$
		$\mu\text{V}/^\circ\text{C}$		(All values times 10^{-8})
Si	0-300°C	-367	0.84	24200
Bi	0-200°C	-67.85	.084	3.31
Co	0-800°C	-17.5	.68	1.47
Pd	0-1500°C	-15.2	.71	2.63
Ni	0-1100°C	-12.4	.92	2.15
Li	0-100°C	-11.2	.71	2.29
Hg	0-200°C	-6.65	.084	2.76
Ca	0-300°C	-6.2	1.26	1.88
Pt	Reference Junction	10.6	.71	2.59
Th	0-1200°C	+3.3	-	-
Na	-100 - 0°C	+5.0	1.34	2.10
Sn	0-200°C	+5.35	.67	2.94
Mg	0-200°C	+5.5	1.59	2.05
Pb	0-300°C	+6.37	.35	2.46
In	0-100°C	+6.9	.24	.73
Tl	0-300°C	+7.2	.39	2.22
K	-200 - 0°C	+8.05	1.00	2.35
Al	0-600°C	+8.6	2.2	2.05
Ti	0-900°C	+12.8	.15	2.83
Zn	0-400°C	+13.2	.113	2.29

TABLE A-1 (Cont'd.)

Element	Thermoelectric Power (α) Range of Thermoelectric Measurement	Electrical Resistivity (ρ) Microhm-cm at 20 C	Thermal Conductivity (k) Watts/cm ² K at 20 C	Wiedemann-Franz- Lorenz Constant $\frac{(\rho)(k)}{293}$
Re	0-1200°C	+14.0	21.1	5.12
Cd	0-300°C	+14.1	7.4	2.32
Fe	0-1000°C	+14.64	9.71	2.49
Ir	0-1500°C	+15.0	5.3	1.06
Rh	0-1500°C	+16.9	4.7	1.40
Au	0-1000°C	+17.09	2.3	1.88
C	0-1100°C	+17.7	1375 (0°C)	113.
Ta	0-1200°C	+17.8	13.5	2.53
Ag	0-900°C	+18.0	1.59	2.29
Cu	0-1000°C	+18.2	1.673	2.25
Mo	0-1200°C	+30.8	5.7	2.85
W	0-1200°C	+31.5	5.5	3.75
Sb	0-600°C	+48.1	42.	2.70
Ge	0-300°C	+306	100000.	20000.
Te	20-40°C	+526	(5.2) (10 ⁶)	32000.
				(All values times 10 ⁻⁸)

TABLE A-2

THERMOELECTRIC MATERIALS NEGATIVE TO PLATINUM

<u>Elements</u>	<u>Range of Thermoelectric Measurement</u>	<u>Thermoelectric Power</u>		<u>Figure of Merit</u> $\frac{\alpha^2}{\rho k} (^{\circ}\text{K}^{-1})$
		α	$\mu\text{Volts}/^{\circ}\text{C}$	
1. Bi	0-200°C	-67.85		.47 (10 ⁻³)
2. Co	0-800°C	-17.5		.072 (10 ⁻³)
3. Pd	0-1500°C	-15.2		.030 (10 ⁻³)
4. Ni	0-1100°C	-12.4		.024 (10 ⁻³)
5. Li	0-100°C	-11.2		.019 (10 ⁻³)
6. Ca	0-300°C	-6.2		.0070 (10 ⁻³)
7. Hg	0-200°C	-6.65		.0055 (10 ⁻³)
8. Si	0-300°C	-367		.0019 (10 ⁻³)

TABLE A-3

ELEMENTS THERMOELECTRICALLY POSITIVE TO PLATINUM

Elements	Thermoelectric Power		Figure of Merit $\frac{\alpha^2}{\rho k} (^{\circ}\text{K}^{-1})$
	Range of Thermoelectric Measurement	α Microvolts/ $^{\circ}\text{C}$	
1. Sb	0-600 $^{\circ}\text{C}$	+48.1	.29 (10 ⁻³)
2. Mo	0-1200 $^{\circ}\text{C}$	+30.8	.11 (10 ⁻³)
3. W	0-1200 $^{\circ}\text{C}$	+31.5	.090 (10 ⁻³)
4. Ir	0-1500 $^{\circ}\text{C}$	+15.0	.072 (10 ⁻³)
5. Rh	0-1500 $^{\circ}\text{C}$	+16.9	.069 (10 ⁻³)
6. Au	0-1000 $^{\circ}\text{C}$	+17.09	.053 (10 ⁻³)
7. Cu	0-1000 $^{\circ}\text{C}$	+18.2	.050 (10 ⁻³)
8. Ag	0-900 $^{\circ}\text{C}$	+18.0	.049 (10 ⁻³)
9. Ta	0-1200 $^{\circ}\text{C}$	+17.8	.043 (10 ⁻³)
10. Fe	0-1000 $^{\circ}\text{C}$	+14.64	.029 (10 ⁻³)
11. Cd	0-300 $^{\circ}\text{C}$	+14.1	.029 (10 ⁻³)
12. Zn	0-400 $^{\circ}\text{C}$	+13.2	.026 (10 ⁻³)
13. In	0-100 $^{\circ}\text{C}$	+ 6.9	.022 (10 ⁻³)
14. Ti	0-900 $^{\circ}\text{C}$	+12.8	.020 (10 ⁻³)
15. Re	0-1200 $^{\circ}\text{C}$	+14.0	.013 (10 ⁻³)
16. Al	0-600 $^{\circ}\text{C}$	+ 8.6	.012 (10 ⁻³)
17. K	-200 - 0 $^{\circ}\text{C}$	+ 8.05	.0094 (10 ⁻³)
18. Tl	0-300 $^{\circ}\text{C}$	+ 7.2	.0080 (10 ⁻³)
19. Pb	0-300 $^{\circ}\text{C}$	+ 6.37	(.0057) (10 ⁻³)
20. Mg	0-200 $^{\circ}\text{C}$	+ 5.5	(.0050) (10 ⁻³)
21. Na	-200 - 0 $^{\circ}\text{C}$	+ 5.0	(.0041) (10 ⁻³)
22. Sn	0-200 $^{\circ}\text{C}$	+5.35	(.0033) (10 ⁻³)
23. Ge	0-300 $^{\circ}\text{C}$	+306	(.0016) (10 ⁻³)
24. C	0-1100 $^{\circ}\text{C}$	+17.7	(.0000946) (10 ⁻³)

TABLE A-4

THERMOELECTRIC PROPERTIES OF ALLOY SYSTEMS
(Pt = Reference Junction)

Sn-Pb				Sn-Cu			
(0 - 100°C exp. range)				(0 - 100°C exp. range)			
Wgt. %		Microvolts/°C		Wgt. %		Microvolts/°C	
0 Sn	100 Pb	+4.4		0 Sn	100 Cu	+7.6	
10 Sn	90 Pb	+4.4		10 Sn	90 Cu	+5.3	
20 Sn	80 Pb	+4.4		20 Sn	80 Cu	+5.6	
30 Sn	70 Pb	+4.4		30 Sn	70 Cu	+6.5	
40 Sn	60 Pb	+4.5		40 Sn	60 Cu	+6.5	
50 Sn	50 Pb	+4.5		50 Sn	50 Cu	+6.9	
60 Sn	40 Pb	+4.4		60 Sn	40 Cu	+7.2	
70 Sn	30 Pb	+4.4		70 Sn	30 Cu	+6.2	
80 Sn	20 Pb	+4.3		80 Sn	20 Cu	+5.4	
90 Sn	10 Pb	+4.2		90 Sn	10 Cu	+4.8	
100 Sn	0 Pb	+4.2		100 Sn	0 Cu	+4.2	

Au-Ag				Au-Pd			
(0 - 100°C exp. range)				(0 - 100°C exp. range)			
Wgt. %		Microvolts/°C		Wgt. %		Microvolts/°C	
100 Au	0 Ag	+7.4		0 Au	100 Pd	-5.7	
90 Au	10 Ag	+5.5		10 Au	90 Pd	-8.5	
80 Au	20 Ag	+4.8		20 Au	80 Pd	-12.5	
70 Au	30 Ag	+4.7		30 Au	70 Pd	-14.2	
60 Au	40 Ag	+4.7		40 Au	60 Pd	-16.9	
50 Au	50 Ag	+4.8		50 Au	50 Pd	-24.4	
40 Au	60 Ag	+4.9		60 Au	40 Pd	-29.7	
30 Au	70 Ag	+4.9		70 Au	30 Pd	-26.3	
20 Au	80 Ag	+5.0		80 Au	20 Pd	-4.6	
10 Au	90 Ag	+5.9		90 Au	10 Pd	-0.5	
0 Au	100 Ag	+7.8		100 Au	0 Pd	+7.8	

TABLE A-4 (Cont'd.)

Zn-Cu

(0 - 100°C exp. range)

<u>Wgt. %</u>	<u>Microvolts/°C</u>
0 Zn 100 Cu	+7.6
10 Zn 90 Cu	+5.4
20 Zn 80 Cu	+5.3
30 Zn 70 Cu	+5.4
40 Zn 60 Cu	+5.1
50 Zn 50 Cu	+5.4
60 Zn 40 Cu	+4.7
70 Zn 30 Cu	+8.7
80 Zn 20 Cu	+6.6
90 Zn 10 Cu	+9.8
100 Zn 0 Cu	+7.6

(0 - 100°C exp. range)

<u>Wgt. %</u>	<u>Microvolts/°C</u>
0 Ni 100 Cu	+7.6
10 Ni 90 Cu	-26.3
20 Ni 80 Cu	-30.8
30 Ni 70 Cu	-35.4
40 Ni 60 Cu	-40.3
50 Ni 50 Cu	-36.4
60 Ni 40 Cu	-30.6
70 Ni 30 Cu	-25.4
80 Ni 20 Cu	-24.9
90 Ni 10 Cu	-19.3
100 Ni 0 Cu	-14.8

Sn-Bi

(0 - 100°C exp. range)

<u>Wgt. %</u>	<u>Microvolts/°C</u>
0 Sn 100 Bi	-73.4
10 Sn 90 Bi	+40.0
20 Sn 80 Bi	+35.2
30 Sn 70 Bi	+25.6
40 Sn 60 Bi	+21.0
50 Sn 50 Bi	+17.7
60 Sn 40 Bi	+11.4
70 Sn 30 Bi	+9.5
80 Sn 20 Bi	+7.8
90 Sn 10 Bi	+6.0
100 Sn 0 Bi	+4.2

Sb-Cd

(0 - 100°C exp. range)

<u>Wgt. %</u>	<u>Microvolts/°C</u>
0 Sb 100 Cd	+9.0
10 Sb 90 Cd	+15.2
20 Sb 80 Cd	+28.8
30 Sb 70 Cd	+64
40 Sb 60 Cd	+122
50 Sb 50 Cd	+231
60 Sb 40 Cd	+444
70 Sb 30 Cd	+215
80 Sb 20 Cd	+128
90 Sb 10 Cd	+81
100 Sb 0 Cd	+48.9

TABLE A-4 (Cont'd.)

Sb-Bi

(0 - 100°C exp. range)

<u>Wgt. %</u>	<u>Microvolts/°C</u>
0 Sb 100 Bi	-73.4
10 Sb 90 Bi	-88.2
20 Sb 80 Bi	-73.1
30 Sb 70 Bi	-56.6
40 Sb 60 Bi	-40.5
50 Sb 50 Bi	-25.1
60 Sb 40 Bi	-10.6
70 Sb 30 Bi	+3.2
80 Sb 20 Bi	+17.9
90 Sb 10 Bi	+33.1
100 Sb 0 Bi	+48.9

Ni-Cr

(25-1000°C exp. range)

<u>Wgt. %</u>	<u>Microvolts/°C</u>
99.6 Ni, 0 Cr, 0.4 Mn	-12.9
97.6 Ni, 2 Cr, 0.4 Mn	+15.6
94.6 Ni, 5 Cr, 0.4 Mn	+28.6
89.6 Ni, 10 Cr, 0.4 Mn	+32.0
84.6 Ni, 15 Cr, 0.4 Mn	+27.8
79.6 Ni, 20 Cr, 0.4 Mn	+22.9
Chromel P (nominal 90 Ni 10 Cr)	+32.7
76.2 Ni, 19.1 Cr, 4.8 Al	+17.0
76.2 Ni, 19.1 Cr, 4.8 Si	+17.9

Ni-Mo-Cr

(25-1000°C exp. range)

<u>Wgt. %</u>	<u>Microvolts/°C</u>
Ni, 5 Mo, 9.4 Cr	+30.7
Ni, 10 Mo, 8.9 Cr	+30.2
Ni, 15 Mo, 8.4 Cr	+28.4
Ni, 18.8 Mo, 5 Cr	+30.0
Ni, 17.8 Mo, 10 Cr	+25.2
Ni, 13.8 Mo, 3.2 Cr	+35.0
Ni, 6.9 Mo, 6.6 Cr	+33.9

TABLE A-4 (Cont'd.)

Ni-Mo		Fe-Mo	
<u>(25-1000°C exp. range)</u>		<u>(25 - 1000°C exp. range)</u>	
<u>Wgt. %</u>	<u>Microvolts/°C</u>	<u>Wgt. %</u>	<u>Microvolts/°C</u>
Ni, 5 Mo, 1 Mn	+6.5	Fe, 1 Mo, 1 Mn	+14.6
Ni, 10 Mo, 1 Mn	+29.0	Fe, 7 Mo, 1 Mn	+20.8
Ni, 16 Mo, 1 Mn	+35.7		
Ni, 20 Mo, 1 Mn	+41.0		
Ni, 20 Mo, 3 Mn	+29.2		
Ni, 20 Mo, 5 Mn	+30.4		
Ni, 25 Mo, 1 Mn	+38.9		
Ni, 30 Mo, 1 Mn	+38.4		

Zn-Sb	
<u>(0-400°C exp. range)</u>	
<u>Wgt. %</u>	<u>Microvolts/°C</u>
30 Zn 70 Sb	225
36 Zn 64 Sb	265
38 Zn 62 Sb	246
40 Zn 60 Sb	230
43 Zn, 56.5 Sb, 0.5 Al	210
45 Zn, 54.5 Sb, 0.5 Al	144

TABLE A-5

THERMOELECTRIC DATA ON VARIOUS ALLOYS*
(Pt = Reference Junction)

Alloy	Approx. Melting Point °C	Est. Max. Opr. Temp. in Air °C	α	ρ	k	Z	Z Value Assumes
Constantan (45 Ni 55 Cu)	1290	875	-43.9 (0-900°C)	49	.228	.16 (10^{-3})	
40 Pd 60 Au	1460	1300	-42.8 (0-900°C)			.33 (10^{-3})	ρ k of Au
50 Pd 50 Au	1485	1300	-38.4 (0-900°C)	27.5		.24 (10^{-3})	ρ k of Pd
30 Pd 70 Au	1425	1275	-31.7 (0-900°C)			(.27) (10^{-3})	ρ k of Au
60 Pd 40 Au	1500	1300	-31.0 (0-900°C)			(.19) (10^{-3})	ρ k of Pd
70 Pd 30 Au	1515	1300	-25.6 (0-900°C)			(.13) (10^{-3})	ρ k of Pd
80 Pd 20 Au	1535	1300	-20.2 (0-900°C)			(.13) (10^{-3})	ρ k of Pd
90 Pd 10 Au	1550	1300	-15.7 (0-900°C)			(.086) (10^{-3})	ρ k of Pd
Driver Harris No. 99 Alloy (.02 C, .01 Mn, .01 Si, Bal Ni)	1450	1100	-10.4 (0-900°C)			(.053) (10^{-3})	ρ k of Pd
				6.84	.92	(.032) (10^{-3})	ρ k of Pd
						(.017) (10^{-3})	ρ k of Ni

* Symbols and units in this table are as follows:

α Thermoelectric Power Microvolts/°K
 ρ Electrical Resistivity Microhm-cm
 k Thermal Conductivity Watts/cm°K
 Z Figure of Merit 1/°K

TABLE A-5 (Cont'd.)

Alloy	Approx. Melting Point °C	Est. Max. Opr. Temp. in Air °C	α	ρ	k	Z	Z Value Assumes
Alumel (94 Ni, 2Al, 3 Mn, 1 Si)	1400	1100	-8.8 (0-900°C)	72		(.012) (10 ⁻³)	ρ k of Ni
20 Pd 80 Au	1375	1225	-8.3 (0-900°C)			(.012) (10 ⁻³)	ρ k of Au
98 Pt 2 Pd	> 1552	1300	-1.25 (0-1200°C)			(.00021) (10 ⁻³)	ρ k of Pt
10 Pd 90 Au	1265	1100	+2.3 (0-900°C)			(.00096) (10 ⁻³)	ρ k of Au
94 Pt 6 Pd	> 1552	1300	+3.25 (0-1200°C)			(.0014) (10 ⁻³)	ρ k of Pt
98 Pt 2 Rh	1790	1300	+3.58 (0-1200°C)			(.0017) (10 ⁻³)	ρ k of Pt
88 Pt 12 Pd	> 1552	1300	+5.1 (0-1200°C)			(.0035) (10 ⁻³)	ρ k of Pt
98 Pt 2 Ir	1780	600	+5.75 (0-1200°C)			(.0044) (10 ⁻³)	ρ k of Pt
94 Pt 6 Rh	1825	1300	+7.75 (0-1200°C)			(.0080) (10 ⁻³)	ρ k of Pt
98 Pt 2 Ru	> 1774	Not rec- ommended in air.	+9.2 (0-1200°C)			(.011) (10 ⁻³)	ρ k of Pt
90 Pt 10 Rh	1840	1300	+9.9 (0-1200°C)	18.3		(.013) (10 ⁻³)	ρ k of Pt

TABLE A-5 (Cont'd.)

Alloy	Approx. Melting Point °C	Est. Max. Opr. Temp. in Air °C	α	ρ	k	Z	Z Value Assumes
18-8 Stain. Steel	1420	900	+10.0 (0-900°C)	69	.159	(.0091) (10 ⁻³)	ρ of Pt
88 Pt 12 Rh	1865	1300	+10.4 (0-1200°C)			(.014) (10 ⁻³)	ρ of Pt
87 Pt 13 Rh	1870	1300	+11.0 (0-1200°C)			(.016) (10 ⁻³)	ρ of Pt
84 Pt 6 Ir	1790	600	+11.7 (0-1200°C)			(.018) (10 ⁻³)	ρ of Pt
80 Pt 20 Rh	1900	1300	+12.3 (0-1200°C)			(.020) (10 ⁻³)	ρ of Pt
98 Pt 2 Os	> 1774	600	+12.9 (0-1200°C)			(.022) (10 ⁻³)	ρ of Pt
70 Pt 30 Rh	1930	1300	+13.5 (0-1200°C)			(.024) (10 ⁻³)	ρ of Pt
60 Pt 40 Rh	1950	1300	+14.2 (0-1200°C)			(.027) (10 ⁻³)	ρ of Pt
Driver-Harris No. 525 Alloy (1.37 Mn, .14 Si, 16.02 Cr, 36.4 Ni, Bal Fe)	1525	900	+13.1 (0-900°C)			(.027) (10 ⁻³)	ρ of 50 Fe, 50 Ni
98 Pt 2 Fe	1745	600	+14.6 (0-1200°C)			(.028) (10 ⁻³)	ρ of Pt
99 Pt 1 Re	> 1774	1200	+15.0 (0-1200°C)			(.030) (10 ⁻³)	ρ of Pt
98 Pt 2 Re	> 1774	1200	+15.6 (0-1200°C)			(.032) (10 ⁻³)	ρ of Pt

TABLE A-5 (Cont'd.)

Alloy	Approx. Melting Point °C	Est. Max. Opr. Temp. in Air °C	α	ρ	k	Z	Z Value Assumes
10 Ir 90 Rh	>1966	600	+16.2 (0-1200°C)			(.064) (10^{-3})	ρ k of Rh
90 Ir 10 Rh	>1966	600	+16.5 (0-1200°C)			(.087) (10^{-3})	ρ k of Ir
90 Pt 10 Ir	1780	600	+15.4 (0-900°C)			(.032) (10^{-3})	ρ k of Pt
96 Pt 4 Fe	1740	600	+16.7 _o (0-1200°C)			(.037) (10^{-3})	ρ k of Pt
94 Pt 6 Ru	>1774	Not rec. in air.	+16.9 (0-1200°C)			(.038) (10^{-3})	ρ k of Pt
88 Pt 12 Ir	1800	600	+17.7 _o (0-1200°C)			(.042) (10^{-3})	ρ k of Pt
25 Ir 75 Rh	>1966	600	+17.9 (0-1200°C)			(.043) (10^{-3})	ρ k of Rh
85 Pt 15 Ir	1820	600	+16.2 (0-900°C)			(.035) (10^{-3})	ρ k of Pt
75 Ir 25 Rh	>1966	600	+18.5 (0-1200°C)			(.11) (10^{-3})	ρ k of Ir
40 Ir 60 Rh	>1966	600	+19.1 (0-1200°C)			(.088) (10^{-3})	ρ k of Rh
60 Ni, 24 Fe, 16 Cr	1350	1000	+17.2 (0-900°C)	98.1	.15	(.020) (10^{-3})	ρ k of 80 Ni, 14 Cr, 6 Fe
60 Ir 40 Rh	>1966	600	+19.2 (0-1200°C)			(.12) (10^{-3})	ρ k of Ir

TABLE A-5 (Cont'd.)

Alloy	Approx. Melting Point °C	Est. Max. Opr. Temp. in Air °C	α	ρ	k	Z	Z Value Assumes
Nichrome V (80 Ni 20 Cr)	1351	1100	+20.4 (0-900°C)	109.8 (100°C)	.134 (100°C)	(.028) (10^{-3})	
94 Pt 6 Os	> 1774	Not rec. in air.	+22.2 (0-1200°C)			(.066) (10^{-3})	ρ k of Pt
88 Pt 12 Os	> 1774	"	+30.0 (0-1200°C)			(.12) (10^{-3})	ρ k of Pt
Nirex (13 Cr, 6 Fe, Bal Ni)	1425	1000	+25.1 (0-900°C)	98.1	.15	(.043) (10^{-3})	
Driver-Harris No. 105 Alloy (2.11 Mn, .11 Si, 3.85 Cr, Bal Ni)	1440	1050	+25.4 (0-900°C)			(.044) (10^{-3})	ρ k of 80 Ni, 14 Cr, 6 Fe
Chromel P (90 Ni 10 Cr)	1430	1100	+32.1 (0-1200°C)	72		(.070) (10^{-3})	ρ k of 80 Ni 20 Cr
82 Ni 18 Mo	1400	700	+36.8 (0-900°C)			(.21) (10^{-3})	ρ k of Ni
79 Ni, 20 Mo, 1 Mn	1400	700	+41.0 (25-1000°C)			(.27) (10^{-3})	ρ k of Ni

REFERENCES

- A-1. "Thermopile Generator Feasibility Study", Prepared for Wright Air Development Center, WADC PR No. 19587, Submitted by Rectifier Department, General Electric Company, February 8, 1957.
- A-2. Ingersoll, Physical Review, 16, 126 (1920).
- A-3. American Institute of Physics, "Temperature - Its Measurement and Control in Science and Industry", Reinhold Publishing Company, 1941.
- A-4. American Society for Metals, "Metals Handbook", 1948.
- A-5. Smithells, C. J., "Metals Reference Book", Interscience Publishers, 1955.
- A-6. McCollum, P. A. and Betts, A. L., "Unconventional Electric Power Sources," WADC Technical Report 54-409, September, 1954 (Part I) September, 1955, and September, 1956 (Part II).
- A-7. Franklin Institute, "Development of Thermocouples for Use in Thermoelectric Generators", Signal Corps Project 162B, ASTIA No. U50025, 5/10/47 - 12/31/51.
- A-8. M. E. Ihnat, Private Communication.
- A-9. Ness, A. J., "Calculation of Thermocouple Error Voltage Caused by Metal Cladding", Aircraft Nuclear Propulsion Department, General Electric Company, January 11, 1955.

APPENDIX B - POWER PER UNIT VOLUME

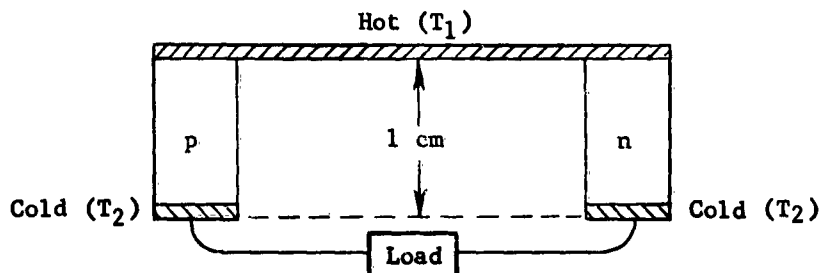
John P. Denny

August 1958

INTRODUCTION

A mathematical equation relating to power per unit volume is used in the text of this report, and will be referred to again in subsequent reports. For reference purposes, the equation is derived in the following.

DERIVATION OF POWER PER UNIT VOLUME RELATIONSHIP



Consider the above thermoelectric generator configuration, wherein thermoelectric elements "p" and "n" are one centimeter long with respective cross-sectional areas of A_p and A_n .

Let α_p = thermoelectric power of positive element

α_n = thermoelectric power of negative element

T_1 = hot junction temperature

T_2 = cold junction temperature

$$m = \frac{R_E}{R_I} = \frac{\text{external load resistance}}{\text{internal resistance}}$$

ρ_p = resistivity of positive element

ρ_n = resistivity of negative element

P = power output = $I^2 R_E$ loss in external circuit

$$= \frac{E^2 R_E}{(R_E + R_I)^2}$$

$$\begin{aligned}
 P &= \frac{(\alpha_n + \alpha_p)^2 (T_1 - T_2)^2 R_E}{(R_E + R_I)^2} \\
 &= \frac{(\alpha_n + \alpha_p)^2 (T_1 - T_2)^2 \frac{R_E}{R_I^2}}{\left(\frac{R_E + R_I}{R_I}\right)^2} \\
 &= \frac{(\alpha_n + \alpha_p)^2 (T_1 - T_2)^2 m}{(m + 1)^2 (R_I)}
 \end{aligned}$$

Considering that internal losses are in the thermoelectric elements only:

$$P = \frac{(\alpha_n + \alpha_p)^2 (T_1 - T_2)^2 m}{(m + 1)^2 \left(\frac{\rho_p l_p}{A_p} + \frac{\rho_n l_n}{A_n}\right)}$$

By taking the partial derivative of this equation with respect to m and equating the result to zero, maximum power output results at $m = 1$. Maximum power per unit

volume occurs when $\frac{A_n}{A_p} = \sqrt{\frac{\rho_n}{\rho_p}}$. Then since $l_n = l_p = l$,

$$\begin{aligned}
 \left(\frac{P}{V_t}\right)_{\max} &= \frac{1}{4} \frac{(\alpha_n + \alpha_p)^2 (T_1 - T_2)^2}{\left(\frac{\rho_p}{A_p} + \frac{\rho_n}{A_n}\right) (A_n + A_p)} \\
 &= \frac{1}{4} \frac{(\alpha_n + \alpha_p)^2 (T_1 - T_2)^2}{\rho_p \frac{A_n}{A_p} + \rho_n + \rho_n \frac{A_p}{A_n} + \rho_p} \\
 &= \frac{1}{4} \frac{(\alpha_n + \alpha_p)^2 (T_1 - T_2)^2}{\rho_p \sqrt{\frac{\rho_n}{\rho_p}} + \rho_n + \rho_n \sqrt{\frac{\rho_p}{\rho_n}} + \rho_p}
 \end{aligned}$$

$$\begin{aligned}
 \left(\frac{P}{V_t}\right)_{\max} &= \frac{1}{4} \frac{(\alpha_n + \alpha_p)^2 (T_1 - T_2)^2}{\sqrt{\rho_p \rho_n} + \rho_n + \sqrt{\rho_p \rho_n} + \rho_p} \\
 &= \frac{1}{4} \frac{(\alpha_n + \alpha_p)^2 (T_1 - T_2)^2}{(\sqrt{\rho_n} + \sqrt{\rho_p})^2}
 \end{aligned}$$

APPENDIX C - THERMOELECTRIC POWER OF METALLIC ALLOYS AND TRANSITION METAL HYDRIDES

John P. Denny

July 1958

INTRODUCTION

The purpose of this appendix is to present details of experimental work conducted on the systems nickel-tungsten and palladium-hydrogen, and to present a tabular summary of the thermoelectric properties of other metals and alloys as derived from the literature.

NICKEL TUNGSTEN ALLOYS

Based on periodic table relationships and electron: atom ratios, it was predicted^(C-1) that the system nickel-tungsten would exhibit a maximum in a plot of thermal e.m.f. versus composition. Experimental data obtained in the present study, coupled with data derived from the literature^(C-2) confirm this hypothesis. The system nickel-tungsten bears a striking thermoelectric similarity to nickel-chromium and nickel-molybdenum, as subsequently shown in Figure C-3.

It is pertinent that W, Cr, and Mo all lie in the same vertical row of the periodic table (Group VIa).

Three nickel-tungsten alloys, of nominal composition 87 Ni 13 W, 81 Ni 19 W, and 74 Ni 26 W, were processed into .025 inch wire. The alloy constituents were arc melted in an inert atmosphere and cast in the form of ingots, following which the materials were homogenized, swaged, drawn to the desired diameter, and annealed twenty minutes in hydrogen at 1000°C. Thermal e.m.f. measurements in hydrogen* were then made using nickel as the second element of each thermocouple. Nickel versus 82 Ni 18 Mo was used as the reference couple; this couple is used in a number of General Electric industrial heating furnaces for temperature control in hydrogen atmospheres. Standard tables covering the range 0-1300°C are available. The reference couple used was also checked against an iron-constantan couple and agreement was obtained within 0.7 millivolts (15°C) over the temperature range 0-1000°C.

Results of the e.m.f.-temperature measurements, converted to a platinum reference junction, are presented in Figure C-1. The thermoelectric powers of the nickel-tungsten alloys are inferior to that of Ni 18 Mo, with values over the range 0-1000°C as follows:

<u>Alloy</u>	<u>Thermoelectric Power (0-1000°C)</u>
	<u>Microvolts per°C</u>
82 Ni 18 Mo	+38.4
74 Ni 26 W	+34.9
81 Ni 19 W	+29.9
87 Ni 13 W	+21.2

*Hydrogen is here used to prevent oxidation. Molybdenum, Nickel, and Tungsten do not form hydrides, and H₂ solubilities are very low.

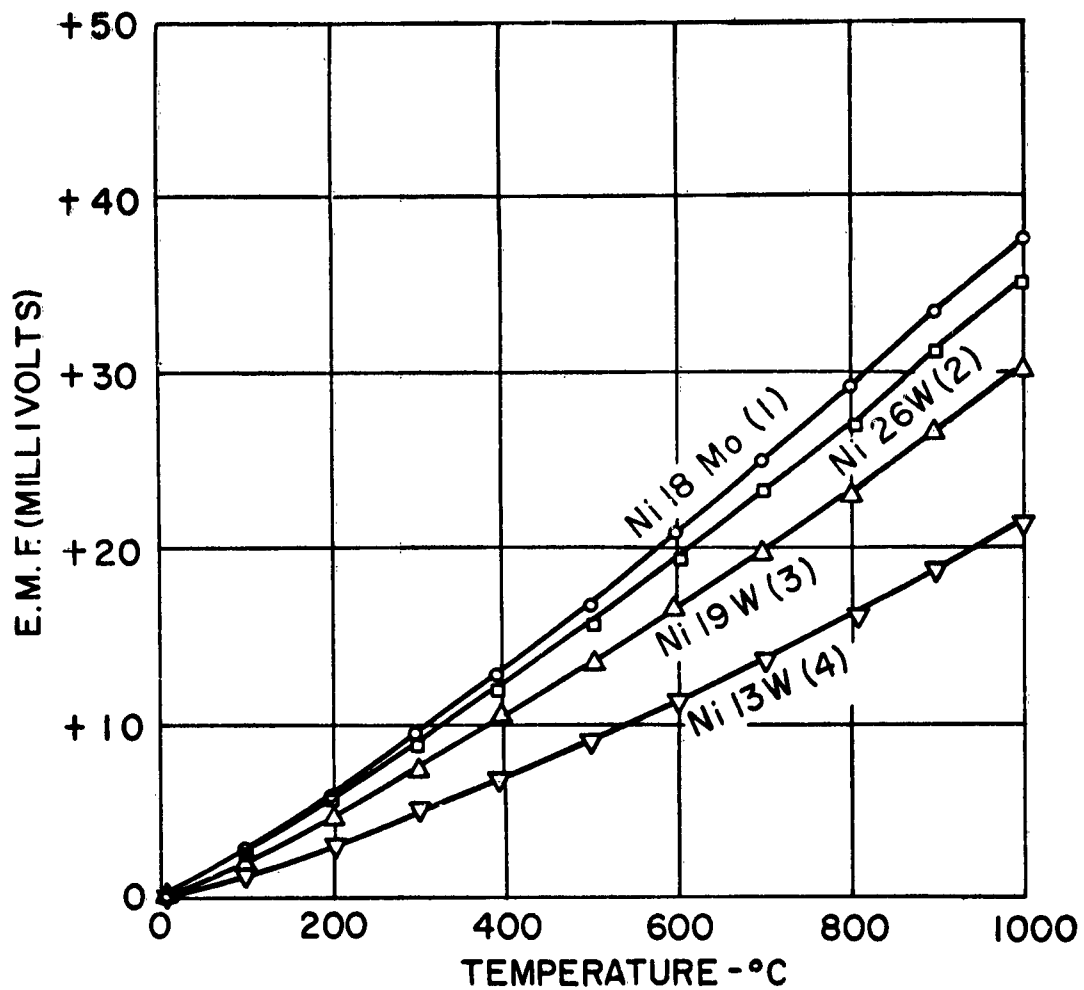


Figure C-1: Thermal EMF versus Temperature of Alloys Referred to Platinum.

(1) 82% Ni + 18% Mo
 (2) 74% Ni + 26% W

(3) 81% Ni + 19% W
 (4) 87% Ni + 13% W

Concurrently, the 74 Ni 26 W alloy can be used at slightly higher temperatures than 82 Ni 18 Mo (1400°C in hydrogen as opposed to 1300 C in hydrogen). Should it be possible to use 1400°C in the final generator, the merit of the two materials would be reversed.

Resistivity measurements were made on each of the alloys by passing 0.5 amperes through the alloy wire and measuring the voltage drop across a ten inch length. The specimens were contained in a furnace at consecutive constant temperatures, and purified nitrogen was passed through the furnace at a rate of four liters per minute to minimize oxidation. Results are presented in Figure C-2, and in the following tabulation.

Alloy	Resistivity of Alloys Microhm cm					
	Temperature (°C)					
	23	200	400	600	800	1000
82 Ni 18 Mo	84.9	88.5	93.6	97.9	102.1	109.6
74 Ni 26 W	74.4	78.6	86.1	91.1	98.6	105.3
81 Ni 19 W	49.9	56.0	64.0	71.1	80.3	90.1
87 Ni 13 W	38.9	47.4	52.4	62.4	69.9	80.6

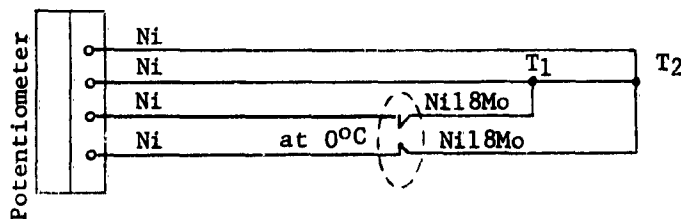
Using the parameter $\frac{\alpha^2}{\rho}$ which relates to power per unit volume, Ni 18 Mo has marginal advantages over Ni 26 W and is considerably better than Ni 19 W or Ni 13 W.

Figure C-3 illustrates the previously discussed maxima observed in the systems Ni-Cr, Ni-Mo, and Ni-W. Increasing atomic weight shifts the location of the maxima to more highly alloyed compositions: thus the Ni-W maximum is at approximately 26% W whereas the Ni-Cr maximum is at approximately 10% Cr.

PALLADIUM HYDROGEN

Holmes (C-4) has previously studied the system Pd-H over the temperature range 20-280°C. He reports a large deviation from linearity over this temperature range, $\frac{dE}{dT}$ dropping from -7 microvolts/°C at 20°C to -35 at 280°C. Experimental work has been conducted to determine the magnitude of this effect at elevated temperatures. Modest values of thermoelectric power have been found at the higher temperatures, and it is possible that the effect reported by Holmes represents a non-equilibrium condition.

Palladium wire, .025" in diameter and three inches long, was placed in a temperature gradient within a furnace. Separate nickel and Ni 18 Mo leads, joined to each end of the palladium, were brought out of the furnace. E.M.F. measurement across different lead combinations then gave the temperature at each end of the palladium, and the e.m.f. generated by the Pd. Introduction of hydrogen gave similar data for Pd (H).



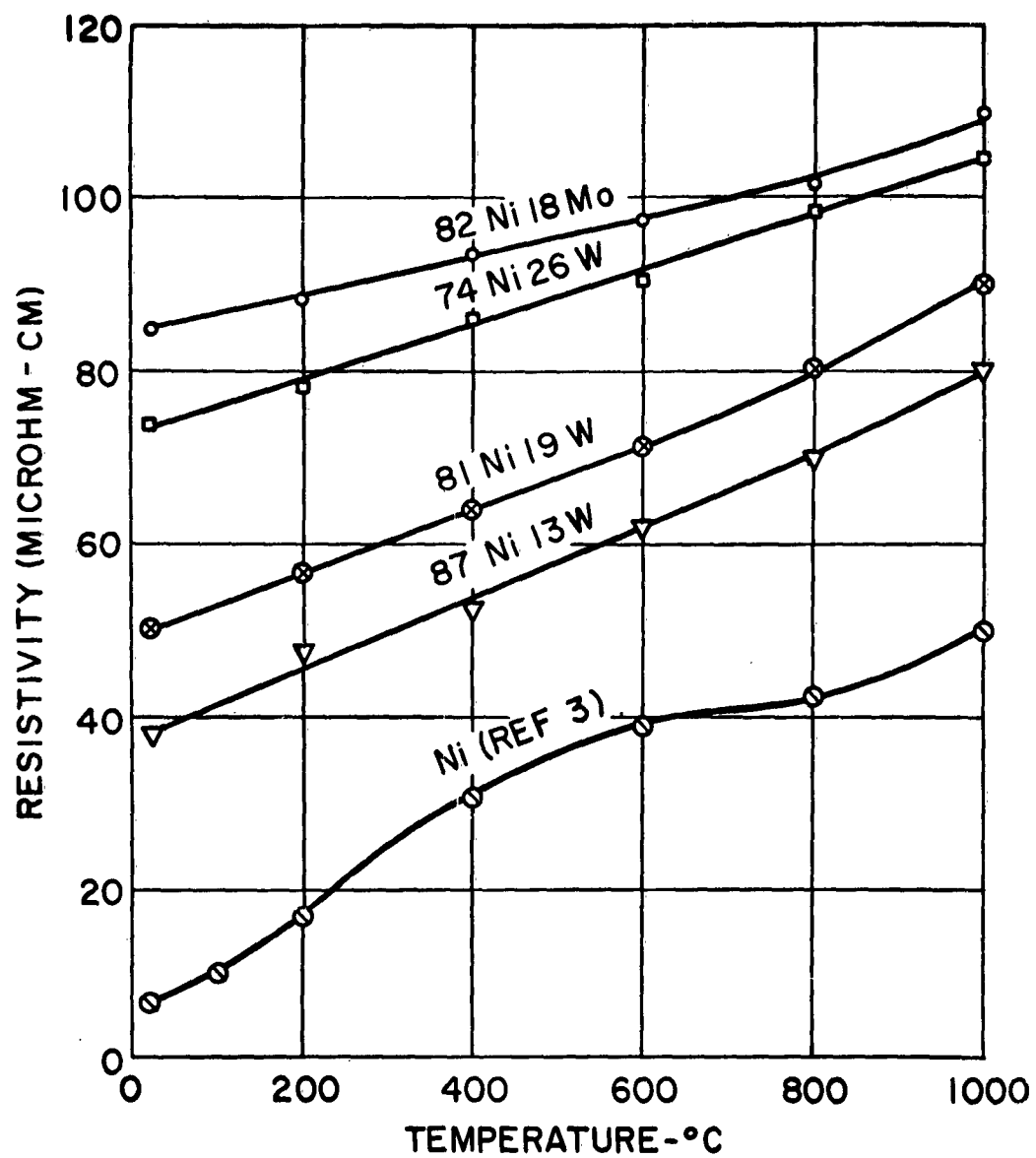


Figure C-2: Resistivity of Nickel and Nickel Alloys

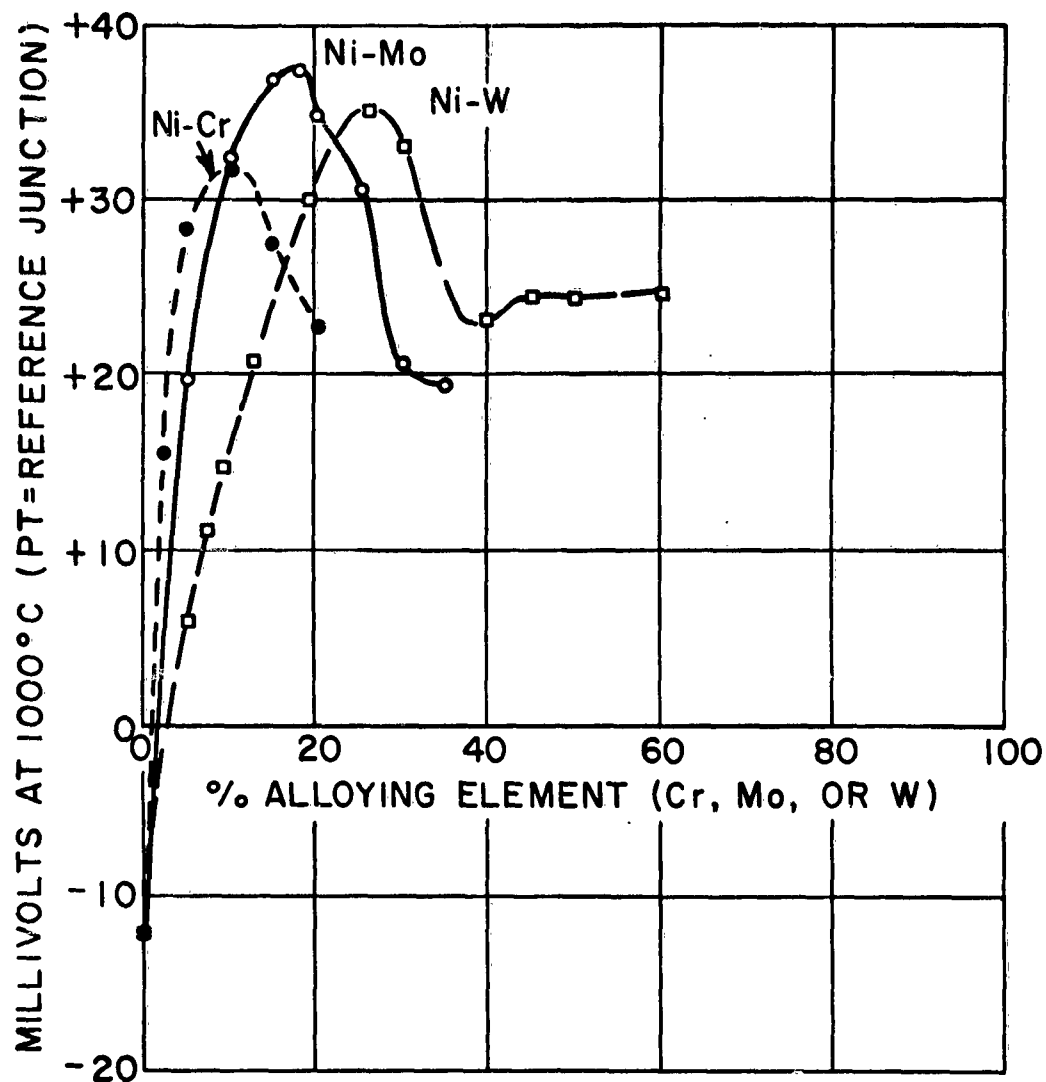


Figure C-3: Thermal EMF Maxima in Systems Ni-Cr, Ni-Mo and Ni-W.

The thermoelectric power was calculated by dividing the Pd or Pd (H) e.m.f. by the temperature difference, which was of the order of 50°C in these tests. It is necessary to correct for the e.m.f. of nickel over the temperature gradient in order to convert the data to a platinum reference junction. This has been done, and results are presented in Figure C-4.

The solid Pd (H) curve in Figure C-4 is felt to represent the most reliable data, with Pd (H) exhibiting a thermoelectric power of -19 to -24 microvolts per °C at elevated temperatures. These data represent tests in which the Pd (H) was heated in hydrogen over an eight hour period prior to measurement. For comparison purposes the thermoelectric power of palladium metal as derived from the literature is also presented in Figure C-4. The effect of hydrogen is to make the thermoelectric power of palladium more negative.

The dashed Pd (H) curve in Figure C-4 is felt to represent non-equilibrium conditions. The thermal history of these tests was as follows:

(a) Pd heated in argon atmosphere for six hours to 650°C, hydrogen passed through furnace for 45 minutes, and specimen cooled in hydrogen overnight.

(b) Pd (H) heated to 600°C over five hour period, during which time the plotted measurements were obtained.

A sharp minimum is to be observed in this curve, at -66 microvolts per °C.

Palladium will absorb large quantities of hydrogen. Smithells^(C-6) indicates that 100 grams of palladium will absorb 5800 c.c. of hydrogen at 120°C and 700 mm Hg pressure. Additional data given in this same reference show the following:

<u>Temperature</u>	<u>Hydrogen Solubility in Palladium cc (STP) per 100 grams at 760 mm pressure</u>
300	164
400	126
500	103
600	92.7
700	87.0
800	84.0

It is apparent that considerable amounts of hydrogen will be evolved on heating a palladium specimen which has been cooled in hydrogen overnight, and that non-equilibrium thermoelectric effects may accordingly be produced.

The hydride work is being extended to systems with higher temperature stability. Thermoelectric properties of the system Ti-H, including the compound TiH₂, will be studied during the coming month.

METALLIC SYSTEMS SURVEY

A survey of the thermoelectric properties of metals and alloys was initiated on the original WADC contract and completed using Company funds during the period preceding reactivation of the contract. Results of this survey are summarized graphically in Figure C-5, which is a partial thermoelectric spectrum of known metals and alloys, and are given in detail in Appendix A.

Figure C-5 is a partial thermoelectric spectrum of known metals and alloys.

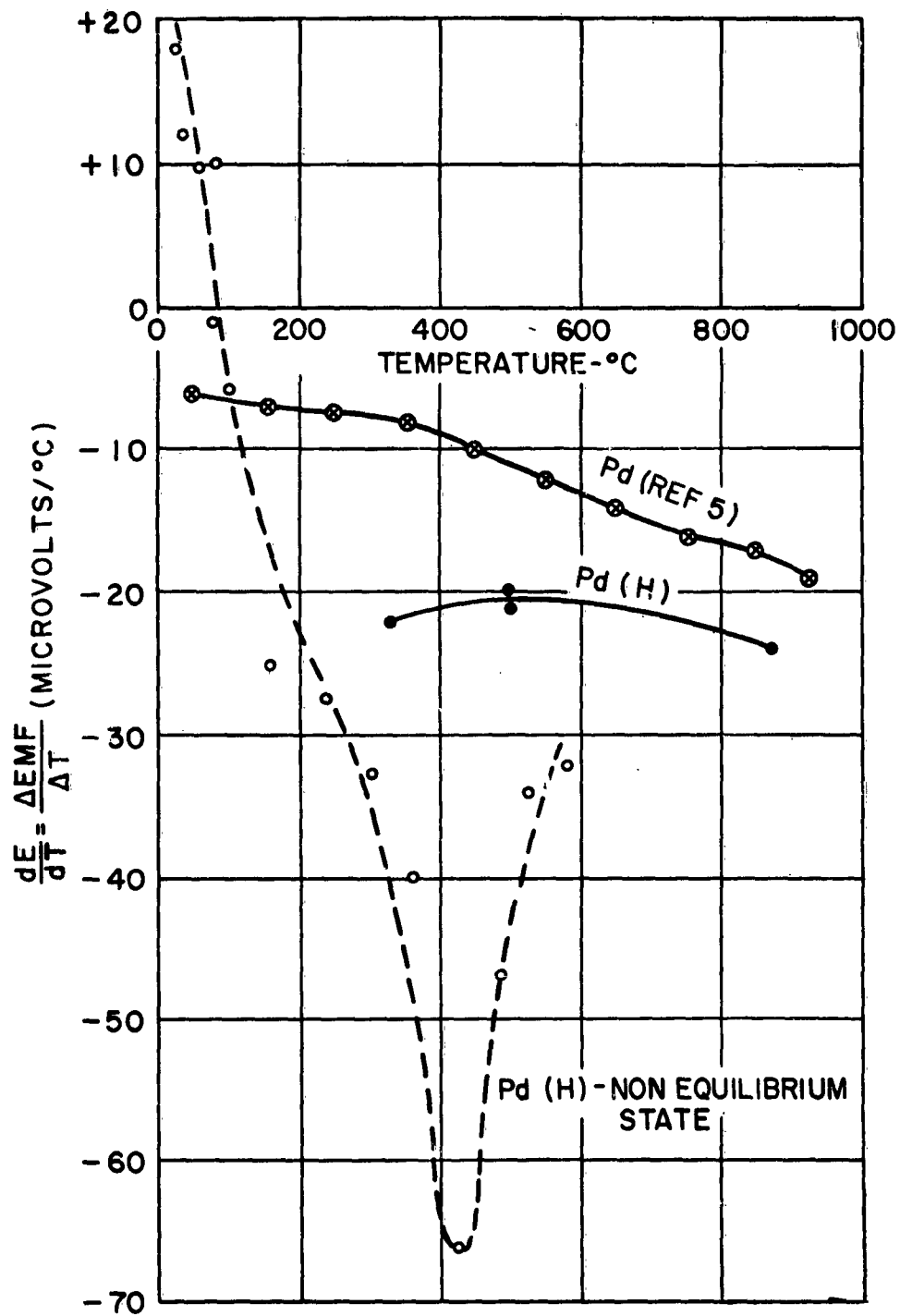


Figure C-4: Thermoelectric Power of Pd-H Alloys.
(Pt = Reference Junction)

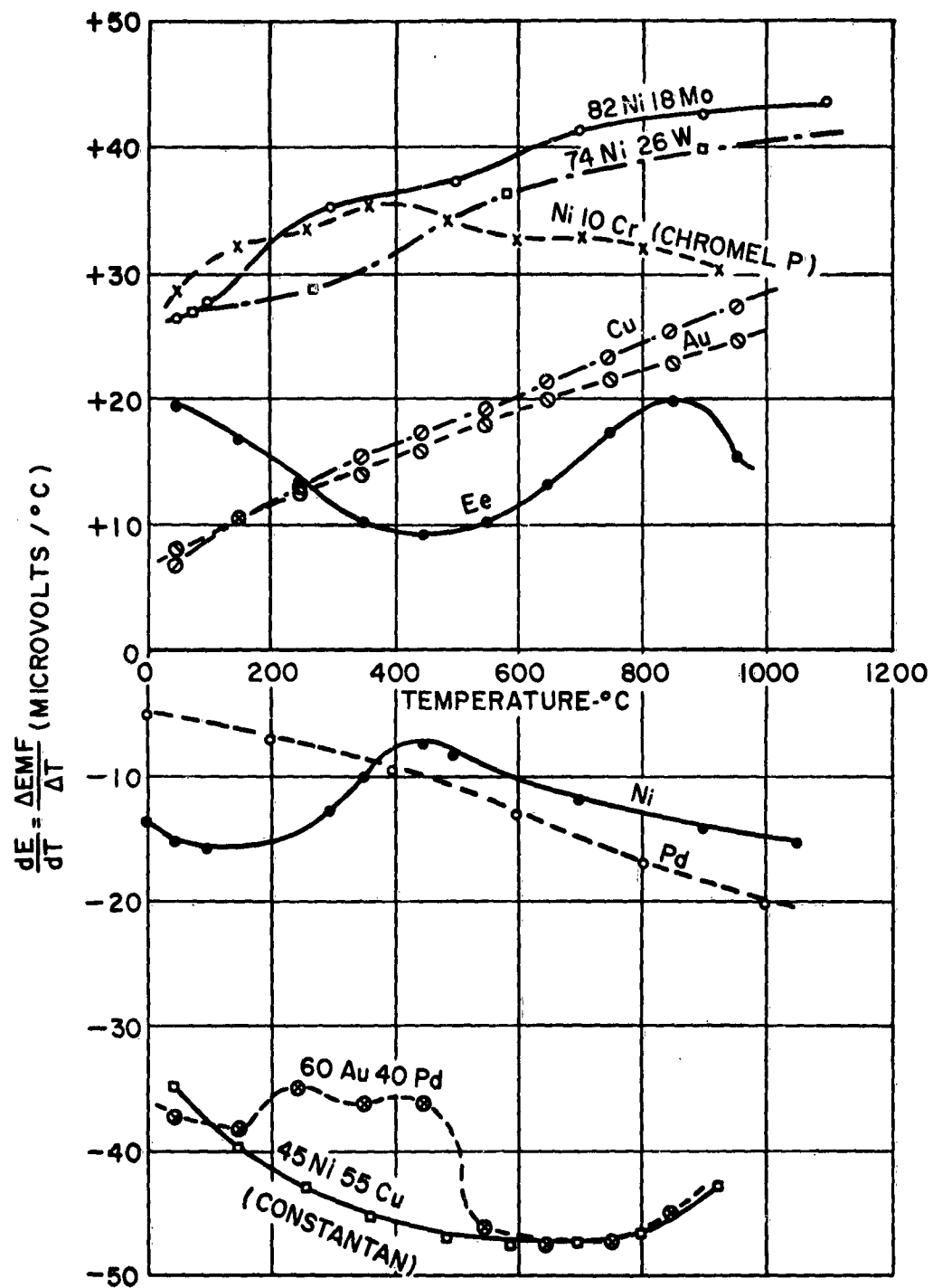


Figure C-5: Thermoelectric Power of Various Metals and Alloys
(Pt = Reference Junction)

The most outstanding materials are 82 Ni 18 Mo (positive), 60 Au 40 Pd (negative), and 45 Ni 55 Cu (negative). The differential plot in Figure C-5 permits precise estimates of thermoelectric power over any desired temperature range. To illustrate an 82 Ni 18 Mo element operating with hot junction at 800°C and cold junction at 700°C would have a thermoelectric power of 42 microvolts per °C.

REFERENCES

1. Thermopile Generator Feasibility Study, Prepared for Wright Air Development Center, WADC PR 08580, Submitted by Rectifier Department, General Electric Company, 4 April 1958.
2. F.C. Kelley, Electrical Engineering, (1942), pp 468-475.
3. Metals Handbook, American Society for Metals, (1948).
4. R.M. Holmes, Physical Review, 22, (1923), pp 137-147.
5. R.F. Vines, The Platinum Metals and Their Alloys (book), International Nickel Company, 1941.
6. C.J. Smithells, Metals Reference Book, Vol. II, Interscience Publishers, Inc., New York, 1955.
7. American Institute of Physics, Temperature - Its Measurement and Control in Science and Industry, Reinhold Publishing Company, 1941.
8. P.A. McCollum and A.L. Betts, Unconventional Electric Power Sources, WADC Technical Report 54-409, September, 1954 (Part I), September, 1955 and September, 1956 (Part II).
9. Franklin Institute, Development of Thermocouples for Use in Thermoelectric Generators, Signal Corps Project 162B, ASTIA No. U50025, 5/10/47-12/31/51.
10. M.E. Ihnat, Private Communication.

APPENDIX D - THERMOELECTRIC POWER OF METALLIC ALLOYS AND TRANSITION METAL HYDRIDES

John P. Denny

April 1959

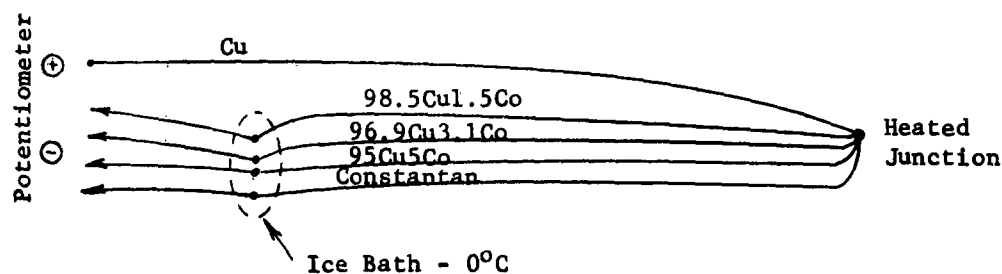
INTRODUCTION

The purpose of this appendix is to provide experimental details covering work on the systems copper-cobalt and zirconium-hydrogen, and to present the thermoelectric properties of selected metals and alloys as derived from the literature and the present investigation.

COPPER-COBALT ALLOYS

A tabular value from a security classified source (D-1) indicates that the thermoelectric power of the alloy Cu + 3.1% Co has an exceptionally outstanding value for a metallic system. The present study finds that the thermoelectric power of annealed Cu + 3.1% Co varies from -12 to +3 microvolts/°C over the range room temperature to 800°C, and is in marked disagreement.

The starting materials in the present investigation were electrolytic cobalt and high purity (99.999% pure) copper. Three alloys, 98.5 Cu 1.5 Co, 96.9 Cu 3.1 Co, and 95 Cu 5 Co were prepared in wire form by inert arc melting, casting, swaging and drawing. After drawing, the wires were given a fifteen minute anneal at 760C in nitrogen and furnace cooled. The ends of the three alloy wires and standard copper and constantan wires were then joined into a single junction by inert arc welding, and heated in a furnace under argon atmosphere using ice bath cold junctions. Periodic emf measurements were taken at different temperatures using a Leeds and Northrup type 8662 potentiometer. The experimental arrangement is shown in the following sketch.



(D-1) Henry E. Robison, "The Design, Development, and Construction of a Heat Production and Distribution Device," Armour Research Foundation of Illinois Institute of Technology, Technology Center, Chicago, Illinois; Project No. L029-1, Contract No. DA-44-109-qm-1154, DA Project No. 7-82-04-001; Final Report, September 30, 1953; for Office of the Quartermaster General Research and Development Division, Washington 25, D.C., ASTIA No. 54834, Table A-1, Page A-2.

The output of the copper-constantan couple was approximately 2-1/2 times greater than any of the copper versus copper-cobalt couples, as shown in Figure D-1.

Thermoelectric powers were calculated from the data of Figure D-1, and from copper versus platinum data taken from the literature and reproduced in Table D-1. The approximation: Seebeck Coefficient $\left(\frac{dE}{dT}\right) = \text{Thermoelectric Power } \left(\frac{\Delta \text{emf}}{\Delta T}\right)$ was used in all cases. ΔT never exceeded 100°C, and the approximation is quite reasonable for the systems under consideration. Algebraic addition of the alloy versus copper coefficient $\left(\frac{\Delta \text{emf}}{\Delta T}\right)$ and the copper versus platinum coefficient (at the average temperature) yields the thermoelectric power.

The thermoelectric power of the alloy 96.9 Cu 3.1 Co is plotted in Figure D-2. The values are intermediate between those of copper and Constantan. The coefficients of 98.5 Cu 1.5 Co and 95 Cu 5 Co are essentially identical to 96.9 Cu 3.1 Co and have been omitted from Figure D-2 for purposes of clarity.

In two further attempts to duplicate the previously reported value, specimens were tested in the cold worked and solution treated conditions. The solid solubility of cobalt in copper decreases from 5% at 1110C to almost nil at 500C, and the specimens were solution treated by heating in an inert atmosphere for one hour at 1050C followed by a water quench. The cold worked specimens studied were produced by wire drawing, 99% reduction in area being employed. Junctions to the solution treated and cold worked wires were made mechanically to avoid metallurgical changes.

The results of tests on the solution treated and cold worked wires are presented in Figures D-3 and D-4. The effect of each is to lower the thermoelectric power approximately 12 microvolts/°C at room temperature. Metallurgical changes (precipitation, stress relief) occur on heating, particularly at temperatures about 200°C, and the cold worked and solution treated materials are not stable at elevated temperatures. In any event, order of magnitude changes were not produced by either processing technique.

It is possible that the originally reported value for this particular alloy is a typographical error. Results of the present work are being sent to the original author for comments.

ZIRCONIUM-HYDROGEN

Commercially pure zirconium wire was resistance welded between a pair of Ni-82Ni 18Mo thermocouples, progressively hydrided, and periodically placed in a temperature gradient for thermal emf measurement in accordance with the following experimental arrangement.

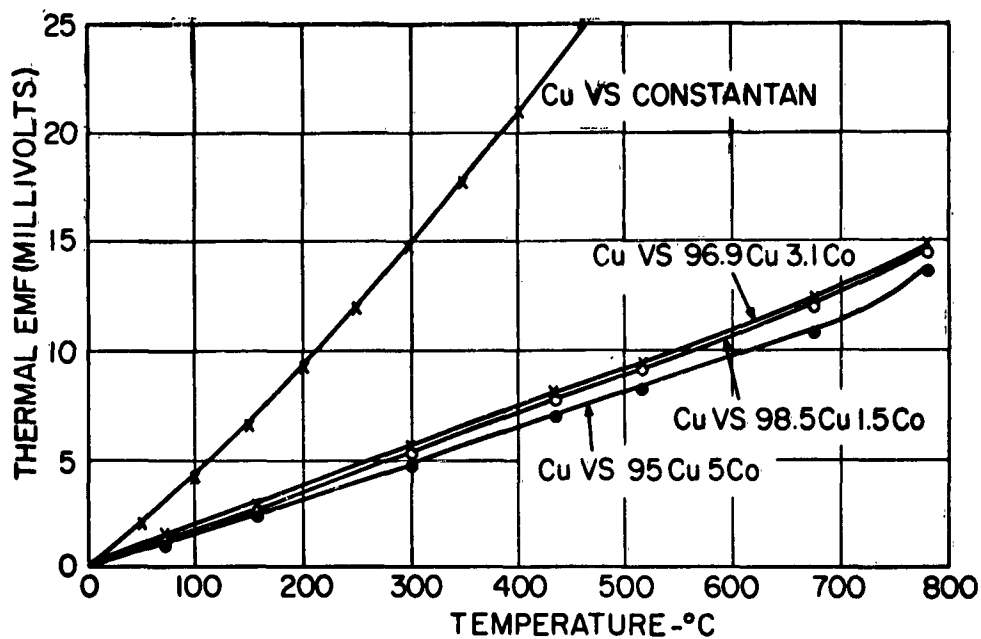


Figure D-1: Thermal EMF of Annealed Cu-Co Alloys

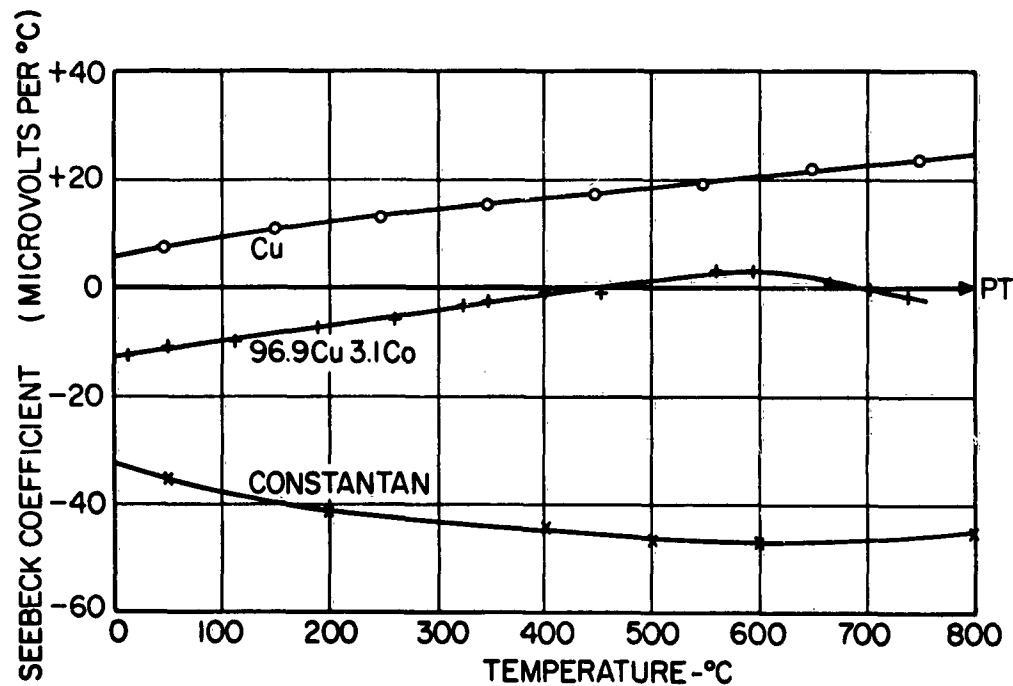


Figure D-2: Seebeck Coefficient (Thermoelectric Power) of Annealed 96.9 Cu 3.1 Co Alloy. (Referred to Pt)

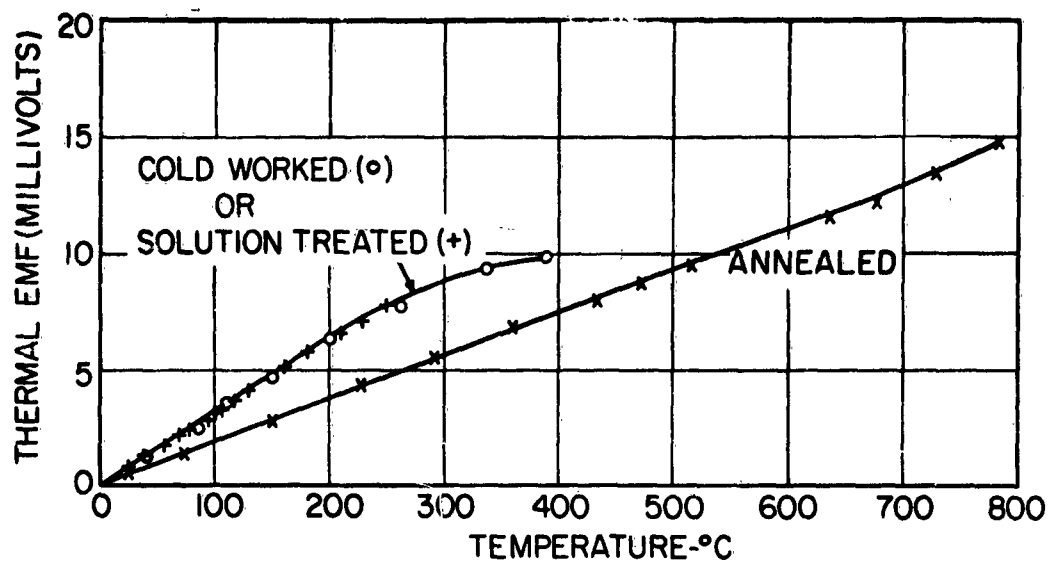


Figure D-3: Thermal EMF of Copper versus Cold Worked, Solution Treated, and Annealed 96.9 Cu 3.1 Co Alloy.

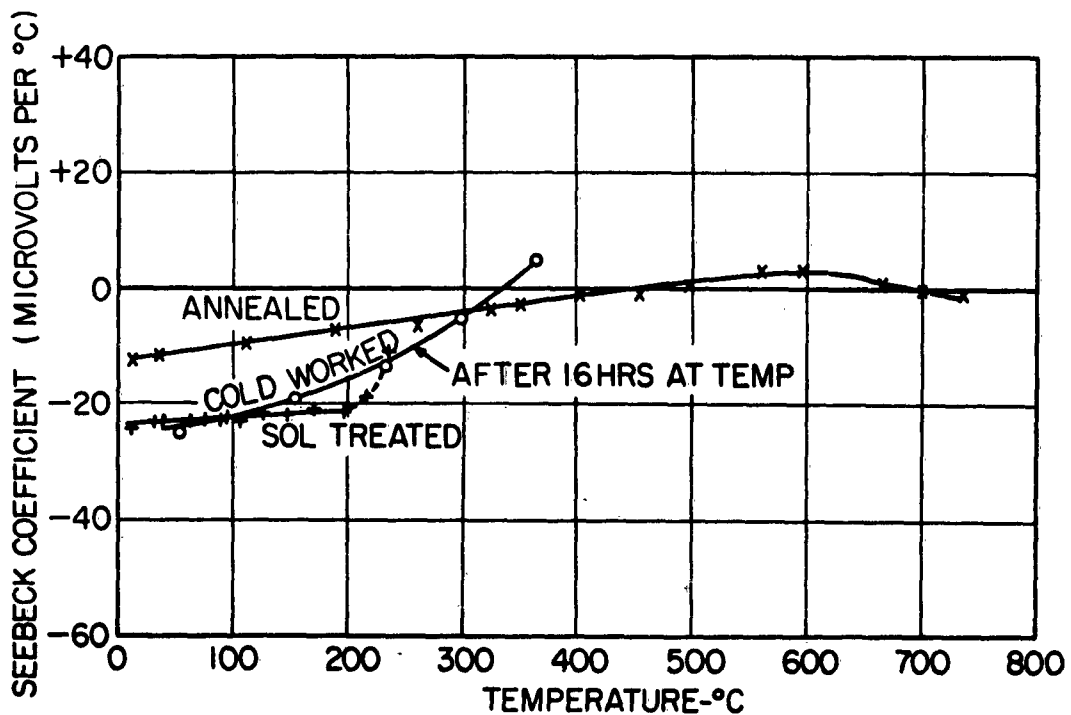
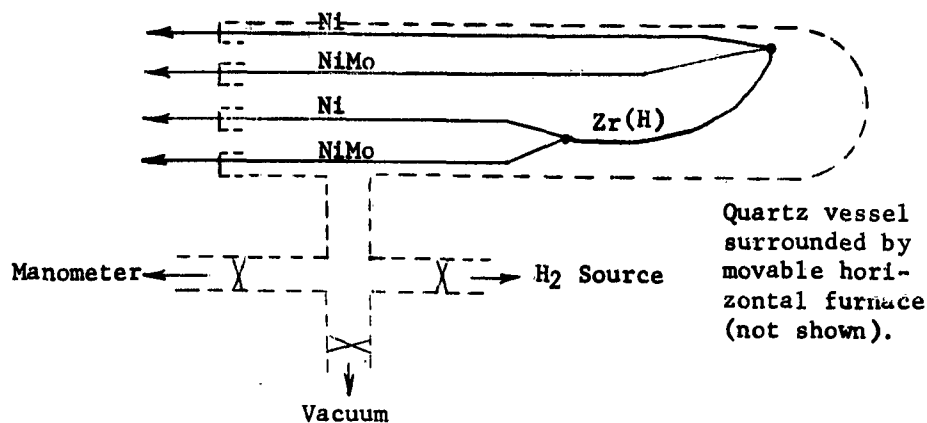


Figure D-4: Seebeck Coefficient of 96.9 Cu 3.1 Co in Cold Worked, Solution Treated, and Annealed Conditions. (Referred to Pt)



In the above sketch, the two Ni-NiMo thermocouples measure the temperature of each end of the Zr(H).

The thermal emf of Zr(H) over any particular temperature range is obtained by measuring the potential in the circuit Ni-Zr(H)-Ni. The thermoelectric power of Zr(H)-Ni over the temperature range is then simply the quotient, thermal emf generated in the Ni-Zr(H)-Ni circuit divided by the temperature difference along the length of the Zr(H) wire. Algebraic addition of the Zr(H)-Ni thermoelectric power, and the Ni-Pt thermoelectric power at the average temperature (Table D-2) gives the thermoelectric power of Zr(H) with respect to platinum.

All measurements were checked by similar measurements using the circuit NiMo-Zr(H)-NiMo, along with data on the thermoelectric power of NiMo-Pt (Table D-3). Results of the two sets of measurements agreed within two microvolts per °C in all cases.

Prior to thermal studies, the system was outgassed under vacuum at 700°C. The hydrogen source was a heated flask of TiH_2 , and adjustment of flask temperature permitted controlled hydrogen additions. The solubility of hydrogen in nickel and molybdenum (the thermocouple constituents) is essentially nil, permitting the Zr wire to absorb the hydrogen progressively. The zirconium was outgassed at 700°C prior to hydriding to increase the absorption kinetics by cleaning the surface, and hydriding was carried out at 600°C. The thermoelectric determinations were conducted at temperatures below 400°C to minimize extraneous effects which could be caused by Zr(H) dissociation or hydrogen absorption during test. The plateau vapor pressure of Zr(H) is 10^{-4} mm at 400°C and this increases progressively at elevated temperatures as shown in Figure D-5.

The following tabulation summarizes hydrogen additions and resultant products.

Summary of Successive Hydrogen Additions to Zr Wire

Pressure mm	Volume cc (STP)	Moles Hydrogen	Total moles Hydrogen	Product (Moles Zr = .00264)
2.01	3.61	.000322	.000322	ZrH _{1.12}
3.26	5.86	.000523	.000845	ZrH _{1.32}
7.83	14.06	.001253	.002098	ZrH _{1.80}
8.92	16.01	.001429	.003527	ZrH _{1.34}
7.28	13.08	.001168	.004695	ZrH _{1.78}
2.07	3.72	.000332	.005027	ZrH _{1.91}

Results of the determinations are summarized in Figure D-6. Hydrogen is found to increase the thermoelectric power of zirconium to a moderate degree, as may also be seen from the following tabulation.

Temperature	Composition	Thermoelectric Power
250°C	Zr	$\mu\text{V}/^\circ\text{C} + 12.9$
"	ZrH _{1.12}	+ 13.6
"	ZrH _{1.32}	+ 14.0
"	ZrH _{1.80}	+ 17.8
"	ZrH _{1.34}	+ 18.8
"	ZrH _{1.78}	+ 14.6
"	ZrH _{1.91}	+ 22.2

MISCELLANEOUS METALS AND ALLOYS

Tables D-3 through D-6 summarize the thermoelectric characteristics of 82Ni 18Mo, 60Au40Pd, Constantan, and Chromel P, which are representative of the better alloys from the thermoelectric standpoint. Resistivity and thermal conductivity data are included when such information is known. For figure of merit and related calculations on metallic systems, the Weidemann-Franz-Lorenz relationship $\rho k = (2.45) (10^{-8} T)$ may be used with reasonable accuracy, where ρ is the electrical resistivity in ohm-cm, k is the thermal conductivity in watts per cm per $^\circ\text{K}$, and T is the absolute temperature in $^\circ\text{K}$.

A. Schultz in Metallwirtschaft, vol. 18, 1939, pp 249 and 315 reports that Pallaplat, a Pt-Pd-Au alloy, has an unusually high emf in comparison to other metallic systems. The exact composition of this alloy is not reported. Analysis of the data yields the following.

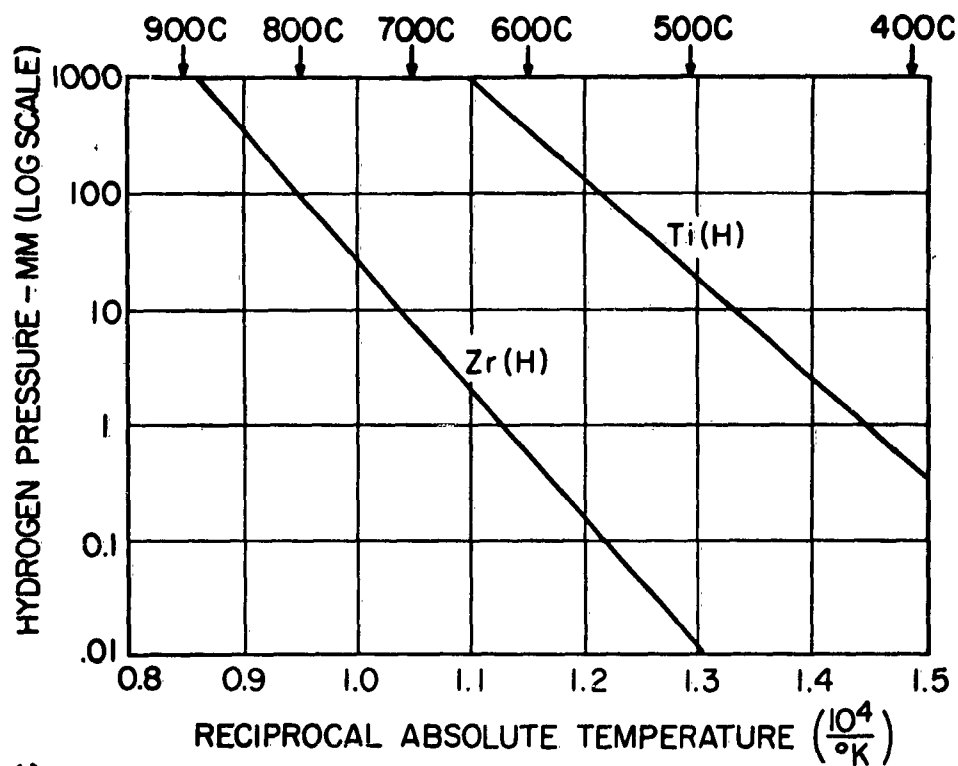


Figure D-5: Plateau Vapor Pressure in Systems Zirconium-Hydrogen and Titanium-Hydrogen.

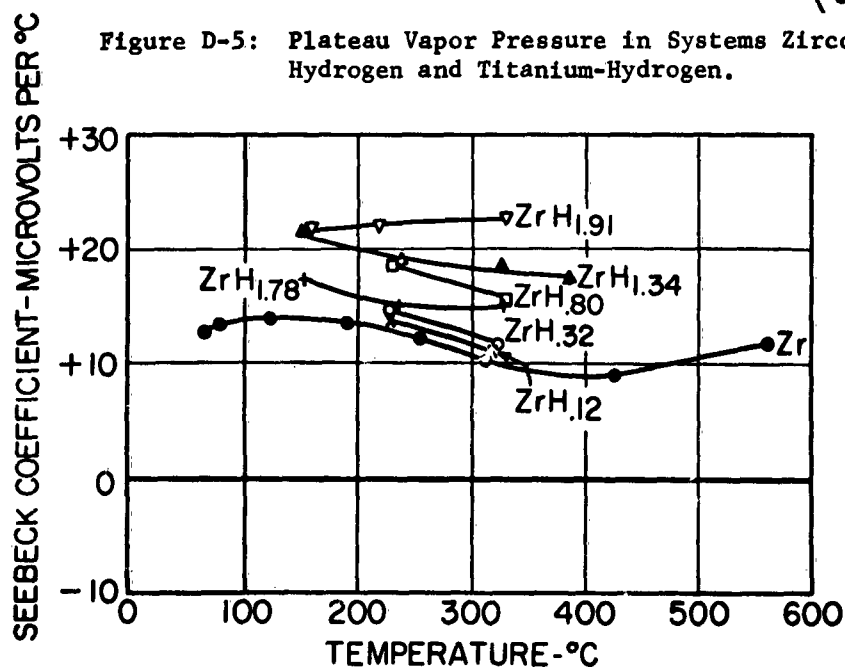


Figure D-6: Seebeck Coefficient of Zirconium - Hydrogen Alloys.
(Referred to Pt)

Pallaplat - Pt Pd Au Alloy

Avg Temp. °C	Thermoelectric Power $\frac{(\Delta \text{emf})}{\Delta T} \mu\text{V}/^\circ\text{C}$
150	40
450	51.5
850	56.0
1150	52.0

These values if correct are superior to other known metallic systems, but are not sufficiently better to warrant detailed work directed toward the intended power generation applications.

TABLE D-1

THERMOELECTRIC POWER OF COPPER STANDARD

Temp.	Thermal EMF (D-2) Cu vs. Pt. mv.	Avg. Temp. °C	Thermoelectric Power $\left(\frac{\Delta \text{emf}}{\Delta T}\right)$ V/°C
0	0	50	+ 7.6
100	+ 0.76	150	+10.7
200	+ 1.83	250	+13.2
300	+ 3.15	350	+15.3
400	+ 4.68	450	+17.3
500	+ 6.41	550	+19.3
600	+ 8.34	650	+21.5
700	+10.49	750	+23.5
800	+12.84	850	+25.7
900	+15.41	950	+27.9
1000	+18.20		

(D-2) R. F. Vines, "The Platinum Metals and Their Alloys," International Nickel Company, 1941

TABLE D-2

THERMOELECTRIC POWER OF NICKEL STANDARD

Temp. °C	Thermal EMF ^(D-2) Ni vs. Pt. mv.	Avg. Temp. °C	Thermoelectric Power $\left(\frac{\Delta \text{emf}}{\Delta T}\right)$ V/°C
0	0		
100	- 1.48	50	-14.8
200	- 3.10	150	-16.2
300	- 4.59	250	-14.9
400	- 5.45	350	- 8.6
500	- 6.16	450	- 7.1
600	- 7.04	550	- 8.8
700	- 8.10	650	-10.6
800	- 9.35	750	-12.5
900	-10.69	850	-13.4
1000	-12.13	950	-14.4
1100	-13.62	1050	-14.9

(D-2) R. F. Vines, "The Platinum Metals and Their Alloys", International Nickel Company, 1941.

TABLE D-3

82 Ni 18 Mo Alloy

(a) Thermoelectric Power

Temp. °C	Thermal EMF (D-3) 82 Ni 18 Mo vs. Pt. mv.	Avg. Temp. °C	Thermoelectric Power $(\frac{\Delta \text{emf}}{\Delta T})$ V/°C
0	0		
100	+ 2.64	50	+26.4
200	+ 5.96	150	+33.2
300	+ 9.50	250	+35.4
400	+13.04	350	+35.4
500	+16.65	450	+36.1
600	+20.57	550	+39.2
700	+24.67	650	+41.0
800	+28.84	750	+41.7
900	+33.11	850	+42.7
1000	+37.42	950	+43.1
1100	+41.78	1050	+43.6

(b) Resistivity

Temp. °C	Resistivity (microhm-cm)
23	84.9
200	88.5
400	93.6
600	97.9
800	102.1
1000	109.6

(D-3) G.E. Publication GET-1415A

TABLE D-4

60 Au 40 Pd Alloy

(a) Thermoelectric Power

Temp. °C	Thermal EMF ^(D-2) 60 Au 40 Pd vs. Pt. mv	Avg. Temp. °C	Thermoelectric Power $\left(\frac{\Delta \text{emf}}{\Delta T}\right)$ V/°C
0	0		
100	- 3.7	50	-37
200	- 7.5	150	-38
300	-11.0	250	-35
400	-15.4	350	-44
500	-20	450	-46
600	-24.6	550	-46
700	-29.3	650	-47
800	-34.0	750	-47
900	-38.5	850	-45
1000	-43.0	950	-45

(b) Resistivity

Temp. °C	Resistivity (microhm-cm)
20	26.5

(D-2) R. F. Vines, "The Platinum Metals and Their Alloys", International Nickel Company, 1941.

TABLE D-5
Constantan (45 Ni 55 Cu)

(a) Thermoelectric Power

Temp. °F	Thermal EMF ^(D-4) Constantan vs. Pt.	Avg. Temp. °C	Thermoelectric Power $\left(\frac{\Delta \text{emf}}{\Delta T}\right)$ V/°C
32	0		
100	- 1.27	18.9	-33.6
200	- 3.26	65.6	-35.4
300	- 5.39	121.1	-38.4
400	- 7.64	176.7	-40.5
500	- 9.98	232.2	-42.1
600	-12.40	287.8	-43.6
700	-14.88	343.3	-44.6
800	-17.41	398.9	-45.5
900	-19.97	454.4	-46.1
1000	-22.55	510.0	-46.4
1100	-25.15	565.6	-46.8
1200	-27.77	621.1	-47.1
1300	-30.39	676.7	-47.1
1400	-32.99	732.2	-46.8
1500	-35.58	787.8	-46.6
1600	-38.14	843.3	-46.1
1700	-40.66	898.9	-45.4
1800	-43.13	954.4	-44.5

(D-4) Metals Handbook, American Society for Metals, 1948, p. 1062.

TABLE D-5 (continued)

(b) Resistivity

Temp. °C	Resistivity (Microhm-cm)
20	49
500	49

(c) Thermal Conductivity

Temp. °C	Thermal Conductivity (Watts/cm ² K)
20	0.228

TABLE D-6^(D-5)

Chromel P (90Ni 10Cr)

(a) Thermoelectric Power

Temp. °F	Thermal EMF Chromel P vs Pt	Avg. Temp. °C	Thermoelectric Power $\left(\frac{\Delta \text{emf}}{\Delta T}\right)$ V/°C
32	0	18.9	+26.5
100	1.00	65.6	+29.0
200	2.61	121.1	+30.8
300	4.32	176.7	+31.8
400	6.11	232.2	+33.5
500	7.97	287.8	+33.8
600	9.85	343.3	+34.6
700	11.77	398.9	+34.4
800	13.68	454.4	+34.6
900	15.60	510.0	+34.4
1000	17.51	565.6	+34.2
1100	19.41	621.1	+33.5
1200	21.27	676.7	+33.2
1300	23.11	732.2	+32.8
1400	24.93	787.8	+32.2
1500	26.72	843.3	+31.7
1600	28.48	898.9	+31.7
1700	30.24	954.4	+31.5
1800	31.99		

(D-5) Chromel vs. constantan data obtained from internal G. E. publication entitled "GEL Tables of Thermocouple Characteristics". This then converted to values with respect to platinum by use of Table D-5.

TABLE D-6 (continued)

(b) Resistivity

Temp. °C

Resistivity (Microhm-cm)

0

70 - 110

APPENDIX E - THE FEASIBILITY OF USING REFRACTORY MATERIALS FOR THERMOELECTRIC GENERATOR (TEG) ELEMENTS

Hans J. Borchardt

November, 1957

OBJECT

To ascertain from a literature survey whether the use of refractory materials for TEG elements appears feasible.

BACKGROUND

Materials which have been examined for TEG application are, for the most part, conventional metals and some semiconductors. Certain semiconductors such as bismuth telluride (Bi_2Te_3) with large thermoelectric powers and favorable thermal conductivity and electrical resistivity characteristics appear promising at the present time and are being actively investigated. Applications can readily be visualized, particularly for aircraft, where operation at elevated temperatures (1000 - 1500°C) is required. In cases where waste heat reservoirs would be utilized (such as hot exhaust gases) efficiency of conversion, as such, is of secondary interest; maximum power output per unit weight and/or volume of generator being the primary goal. Intermetallic compounds such as Bi_2Te_3 are less suitable for this particular type of application since they are characterized by low melting points, relatively high efficiencies (~2%) but limited power generation. The present survey is, therefore, aimed at finding materials capable of operating at high temperatures and of delivering appreciable power with less emphasis on the efficiency of conversion.

SCOPE

The present effort was limited to two-man weeks, hence, is definitely not to be taken as exhaustive. The material included herein was taken primarily from Chemical Abstracts, Government Publications, and selected reference books.

Oxides, sulfides, and thermocouples using graphite are discussed in Section E-1. Systems are included irrespective of their apparent suitability for the present application. The more promising systems are discussed at the conclusion of the report. Included are values for figure of merit, efficiency, and power output per unit area and length. Caution should be observed in viewing these figures if the values for thermoelectric power, resistivity, and thermal conductivity come from different sources, i.e., measurements performed on different samples. References are indicated on the right margin; the numbers refer to the references which immediately follow and the letters to the books listed in Section E-IV.

Two types of calculated parameters will be encountered; parameters with respect to a couple and parameters with respect to a single material. These are respectively defined as follows:

Figure of merit with
respect to a couple:

$$Z = \frac{(\alpha_p + \alpha_n)^2}{\left[\sqrt{\rho_p K_p} + \sqrt{\rho_n K_n} \right]^2}$$

Figure of merit with respect to a single material:

$$Z = \frac{\alpha^2}{\rho K}$$

where α is the thermoelectric power relative to a standard, usually platinum. Symbols, subscripts and dimensions are consistent with those in the proposal. Optimum efficiencies are defined in a similar manner. Power generated per junction per unit area and length is calculated from

$$P = \frac{(\alpha_n + \alpha_p)^2 \Delta T^2}{4 (\sqrt{\rho_n} + \sqrt{\rho_p})^2}$$

for a couple and for a single material from

$$P = \frac{\alpha^2 \Delta T^2}{4 \rho}$$

where α is again the thermoelectric power relative to platinum and ΔT the temperature difference between hot and cold junctions. ΔT is based on a reasonable estimate of operating temperature range.

In Section E-II is a tabulation of data on refractory hard "metals", i.e., carbides, borides, nitrides, and silicides. This class of materials is characterized by high temperature stability in an inert atmosphere (melting points $\sim 3000^\circ\text{K}$, negligible volatility to above 2000°K) and metallic resistivities ($\sim 10^{-5}$ ohm-cm, increasing slowly with temperature). Unfortunately, information on the thermoelectric power of these materials was not found in most cases. On the other hand, most metallic elements have thermoelectric powers relative to platinum of the order of 10 microvolts/ $^\circ\text{C}$. Assuming a value for thermoelectric power of 10 microvolts/ $^\circ\text{C}$ and, taking a reasonable operating temperature range and the given values of resistivity, one finds that the power output per junction per unit area and length is quite comparable to that of Bi_2Te_3 . Since, in addition, these materials have superior thermal properties, it was felt that their inclusion was justified.

Section E-III contains references which were encountered during this survey which may be pertinent to the other aspects of this program.

A critical summary is included at the end of the report.

SECTION E-1: GRAPHITES, OXIDES, AND SULFIDES

A. COUPLES USING GRAPHITE AS ONE ELEMENT

1. GRAPHITE - SILICON CARBIDE (SiC)

a. Thermoelectric power

$$= \text{approximately } 200 \times 10^{-6} \text{ V/}^{\circ}\text{C} \quad (1)$$

$$= 286 \times 10^{-6} \text{ V/}^{\circ}\text{C at } 1840^{\circ} \quad (1)$$

$$\text{Thermal emf} = 0.5 \text{ V at } 1650^{\circ}\text{C} \quad (\text{A})$$

b. Resistivity

$$\text{Graphite} - 1.5 \times 10^{-3} \text{ ohm cm} \quad (1)$$

Varies from 1×10^{-3} at

25°C to 9×10^{-4} at 500°C

(min) to 1.2×10^{-3} at 1800°C (A)

$$\text{SiC} - 0.21 - 1.88 \text{ ohm cm} \quad (1)$$

$$0.309 - 500^{\circ}\text{C} \quad (2)$$

$$0.215 - 1000^{\circ}\text{C}$$

$$0.29 - 1500^{\circ}\text{C}$$

$$0.36 - 1800^{\circ}\text{C}$$

c. Thermal conductivity

$$\text{Graphite} - \sim .4 \text{ watts/cm}^{\circ}\text{C} \quad (\text{A})$$

decreases slightly with temperature

$$\text{SiC} - \sim .4 \text{ watts/cm}^{\circ}\text{C} \quad (\text{A})$$

$$20 - 425^{\circ}\text{C}$$

d. Figure of merit

$$Z = 2.3 \times 10^{-7}$$

$$\text{For } \alpha = 2.86 \times 10^{-4}$$

$$\rho_G = 1.5 \times 10^{-3}$$

$$\rho_{\text{SiC}} = 0.32$$

$$K_G = 0.4$$

$$K_{SiC} = 0.4$$

e. Optimum efficiency

$$7.2 \times 10^{-3} \%$$

$$T_1 - T_2 = \Delta T$$

$$= 1800 - 500 = 1300^\circ\text{C}$$

$$M = 1.00032$$

f. Power generated

$$0.11 \text{ watt}$$

$$\Delta T = 1300^\circ$$

(REFERENCES)

- (1.) Funagashi, V. and Hisamota, A. - "The Graphite SiC Thermocouple" - Tokai Technol. J., 12, 34-9 (1948). C.A. 48:9763b

Thermoelectric power and resistivity given to 2000°C.
 α is approximately $200 \times 10^{-6} \text{ V/}^\circ\text{C}$. At 1840°C, $\alpha = 286 \times 10^{-6} \text{ V/}^\circ\text{C}$. ρ of carbon 0.0015 ohm-cm and of SiC 0.21 - 1.88 ohm-cm. Upper useful temperature limit is 1800°C.

- (2.) Norton Company - "Heating Elements" (Indust. lit.) p 6.

- (3.) Varsonovich, V. K. - "Carbon - SiC Thermoelements for Measuring High Temperatures (to 1800°C)" - Ukrain. Nauch. - Issledovatel. Inst. Ognevpoporov. Kisloto-uporov, 44, 114-5 (1938). C.A. 33:2770³

"A brief description is given."

- (4.) Dodero, M. - "The Thermoelectric Power of the Couple Graphite - SiC" - Compt. rend., 206, 660-1 (1938). C.A. 32:3225⁶

The thermoelectric power-temperature curve of Cu-SiC and graphite Si-C shows a change in direction at about 900° on heating and 700° on cooling -- attributed to the transformation in SiC. Also a change at 1300°.

- (5.) Bonnot, M. - "The Graphite-SiC Thermocouple: Its Use in Metallurgy" - Rev. met., 37, 16-19 (1940); Chem. Zentr. 1940 I, 2986. C.A. 36:2822⁹

Discusses "Fitterer" (C-SiC) couple.

- (6.) Uya Funabashi - "Contacting Point for C-SiC T.C." - Patent, Japan 4298 (1950) December 16. C.A. 46:9901^b

An adhesive prepared from powdered artificial graphite

50%, pitch 40%, tar 10%, is heated at 150° and coated on SiC rod.

- (7.) Losana, Luigi - "Thermoelements for High Temperatures" - Met. ital. 32, 239-41 (1940); Chem. Zentr. 1941 I, 247. C.A. 36:6844¹

Combinations of graphite with SiC or W are recommended for thermoelements for use at high temperatures, (e.g., above 1500°). An electrically insulated SiC rod is introduced into a graphite tube so that the lower end of the rod presses against the graphite screw closing the tube. The upper end is surrounded by a Cu jacket cooled by running water. In the graphite-W element, a W wire 0.8 mm in diameter passes through the graphite screw closing the tube. The free end is fused to a ball and allowed to fall free in the tube. Calibration curves for these thermoelements are reported for temperatures up to 2000°.

- (8.) Tyler, W. W. and Wilson, Jr., A. C. - "Thermal Conductivity, Electrical Resistivity and Thermoelectric Power of Graphite" - (Knolls Atomic Power Laboratory), Phys. Rev. 89, 870-5 (1953). C.A. 47:4884^a

Data 20 - 300°K.

- (9.) Eatherly, W. P. and Rasor, N. S. - "The Thermoelectric Power of Graphite, Dependence on Temperature, Type and Neutron Irradiation" - Unclassified Report, North American Aviation Inc., Downey, California (Contract AT11-1-Gen-8), 21 November 1952 (NAA-SR-196).
- (10.) Kmetko, E. A. - "Electronic Properties of Carbons and Their Industrial Bisulfate Compounds" - J. Chem. Phys., 21, 2152-8 (1953). C.A. 48:4277
- (11.) Hirabayashi, H. and Toyoda, H. - "Electrical Properties of Amorphous Carbon" - J. Phys. Soc. Japan, 7, 337-8 (1952). C.A. 47:11839^d

Conductivity and Thermoelectric power between 20 - 300°C.

- (12.) Ref: 7.2 Reference Index.

2. GRAPHITE-TUNGSTEN

a. Thermoelectric Power

$\alpha = 6.9 \times 10^{-6}$ V/°C at 1650°C (A)
 Thermal emf = 0.038 V at 1650°C (A)
 (mean = 23×10^{-6} V/°C)

b. Resistivity

Tungsten	5.5×10^{-6} ohm-cm	25°C	(B)
	25.3	727°C	

41.4	1227°C
59.4	1727°C
98.9	2727°C

c. Thermal conductivity

Tungsten	1.7 watts/cm°C	25°C	(C)
----------	----------------	------	-----

d. Figure of merit

$$Z = 8.1 \times 10^{-9}$$

$$\alpha = 23 \times 10^{-6} \text{ V/}^\circ\text{C}$$

$$\rho_w = 6 \times 10^{-5}$$

graphite data as above

e. Power generated

0.28 watts	$\Delta T = 1800^\circ\text{C}$
------------	---------------------------------

(REFERENCES)

- (1.) "New Construction of a W-Graphite Thermocouple" - Zavodskaya Lab. 14, 632-3 (1948). C.A. 43:6474^a

T.C. suitable for many hours at 12 - 1700°, with better protection to 2000°.

- (2.) "Measurement of Temperature of Molten Steel by Means of a W-C Thermoelement" - Ceram. Abstracts, 18, #10, 275. C.A. 34:7246⁴

3. GRAPHITE - B₄C

a. Thermoelectric power

Thermal emf = 0.7 volts at 2500°C	(A)
(assume average $\alpha = 280 \times 10^{-6} \text{ V/}^\circ\text{C}$)	

b. Resistivity

B ₄ C - 0.3 - 0.8 ohm-cm	(A)
-------------------------------------	-----

c. Thermal conductivity

B ₄ C - 0.29 - 0.84 watts/cm°C	(A)
---	-----

d. Figure of merit

$$2.6 \times 10^{-7}$$

$$\rho_{B_4C} = 0.3$$

$$K_{B_4C} = 0.3$$

e. Power generated

0.35 watts	$\Delta T = 1500^\circ\text{C}$
------------	---------------------------------

(REFERENCES)

- (1.) Ridgway, Raymond R. (to Norton Co.) - "Patent Thermocouple" - Can. 386, 183, (Jan. 9, 1940). C.A. 34:1520⁷

Structural details are described of a thermocouple having contact elements of B₄C and graphite.

B. OXIDES

1. Cr₂O₃

a. Thermoelectric power

~ - 700×10^{-6} v/°C
Relative to lead

(D)

b. Resistivity

ohm-cm

1.3×10^3	350°C	(A)
2.3×10^1	1200°C	
5×10^3	740°C (70 cm O ₂)	(1)
6.8×10^{-3}	600°C	(A)
4.5×10^{-3}	1100°C	

c. Thermal conductivity

Not found, assume 0.5 watt/cm°C

d. Figure of merit

$$*Z = 1.6 \times 10^{-4}$$

e. Optimum efficiency

*15.5%

$$\rho = 6 \times 10^{-3}$$
$$T_1 - T_2 = \Delta T$$

$$1300^\circ\text{K} - 200^\circ\text{K} = 1000^\circ\text{K}$$
$$M = 1.06$$

f. Power generated

*20.4 watts
 1.2×10^{-4} watts

$$\rho = 6 \times 10^{-3}$$
$$\rho = 10^3$$

(REFERENCES)

- (1.) Bevan, D. J. M., Shelton, Anderson, J. S. - "Properties of Some Simple Oxides

*Probably mismatched data

and Spinel at High Temperatures" - J. Chem. Soc. 1948, 1729-41. C.A. 43:4533¹

Electrical conductivity of ZnO, Fe₂O₃, Cr₂O₃, ZnFe₂O₄, ZnCr₂O₄, MgFe₂O₄, and MgCr₂O₄ to 1000°.

2. Co₃O₄ (PLUS ADDITIVES)

a. Thermoelectric power

$$\alpha = 234 \times 10^{-6} \text{ V/}^\circ\text{C (mean } 51^\circ\text{C} - 751^\circ\text{C)}$$

b. Resistivity

$$0.285 \text{ ohm cm}$$

c. Thermal conductivity

$$\text{Assume } K = 0.1 \text{ watt/cm}^\circ\text{C}$$

d. Figure of merit

$$Z = 1.9 \times 10^{-6}$$

e. Power generated

$$P = 0.049 \text{ watts}$$

(REFERENCES)

- (1.) Fischer, F., Dehn, K., Sustmann, H. - "Increase of Thermal emf of Oxides by Use of Oxide Mixtures" - Ann. Physik 15, 109-26 (1932). C.A. 27:26124

Single oxides and mixture up to 5 components in the form of compressed tablets were systematically investigated. Sometimes the contact surface of the tablets were silvered by pressing on a layer of Ag₂O and heating. The best results for positive emf (current at hot junction flows from Cu to oxide) were obtained with ((Co₃O₄ + 10% CuO) + 5% Bi₂O₃) + 2% Ta₂O₅) + 2% MgO; this mixture developed 0.418 watt for a temperature difference of 700°C.

For negative emf Co₃O₄ with silvered surfaces was best with 0.175 V and 0.042 watt for a temperature difference of 704°.

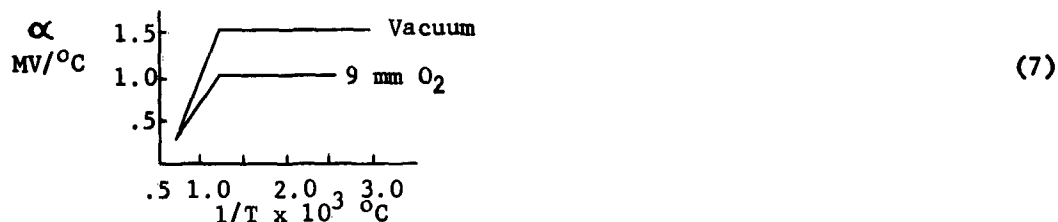
(Note: The above applies to disks
12 mm diameter and 2 mm thick)

- (2.) Fischer, F., Dehn, K. and Sustmann, H. - "Increase in Thermoelectric Force of Oxides by Admixtures of Other Oxides II" - Ges. Abhandl. Kenntnis Kohle, 12, 516-26 (1937); Chem. Zentr. 1937 II, 3863. C.A. 33:6172³

Oxide mixtures showing a negative thermo emf against the special steel serving as reference material were investigated. The best two component mixture so far studied consists of CdO with 3 - 5% MgO. This was therefore used as the basis material for further studies of three component mixtures. The best of these mixtures as regarding thermo emf and energy production was (CdO + 3% MgO) + 1% NiO. Four component mixtures using this mixture as a basis material gave poorer results in every case. When this best negative mixture (against reference materials) was combined with the best positive mixture of ((Co₃O₄ + 10% CuO) + 5% Bi₂O₃) + 2% Ta₂O₅) + 2% MgO, an energy production of 0.67 watts was obtained for a temperature difference of 700°C. The method of production, temperature, duration of heating had considerable influence on the thermo emf and also on the ease with which the material could be pressed into tablet form. Because of the thermal conductivity of the mixture, thin tablets gave lower thermo emfs than infinitely thick ones, e.g., the variation amounted to 7% for a thickness of 2 mm. From a discussion of the construction of a thermo battery from oxide tablets, it is shown that with suitable construction quite efficient conversion of thermal energy into electric energy can be obtained, the efficiency approaching that of modern heat engines (to 22%).

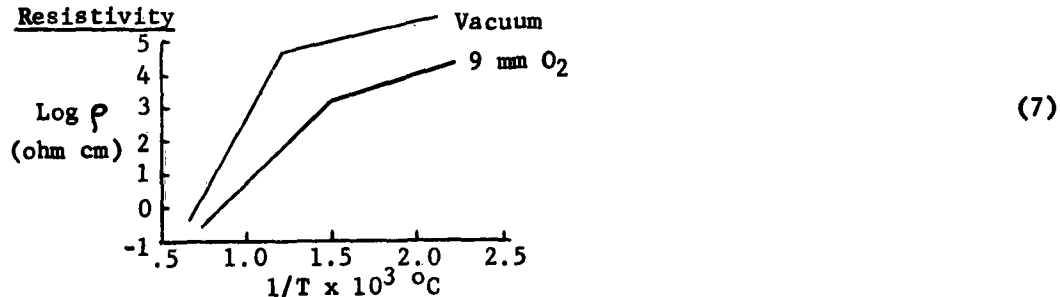
3. Cu₂O

a. Thermoelectric Power



$$\alpha \simeq 500 \times 10^{-6} \text{ V/°C at } P(\text{O}_2) = 100 \text{ mm.} \quad (4)$$

b. Resistivity



$$\rho = .25 \text{ ohm-cm at } P(\text{O}_2) = 100 \text{ mm} \quad (4)$$

c. Thermal conductivity

Not found, assume 0.1 watt/cm°C

d. Figure of merit

$$Z = 10^{-5} \quad (100 \text{ mm O}_2)$$

e. Efficiency

$$\begin{aligned} 0.2\% \quad \Delta T &= 1030^\circ - 30^\circ = 1000^\circ\text{C} \\ m &= 1.004 \end{aligned}$$

f. Power generated

.25 watts

(REFERENCES)

- (1.) Vogt, W. - "Electrical and Optical Properties of Semiconductors III." "Electrical Determinations with Cu₂O" - Ann. Physik, 7, 183-204 (1931). C.A. 25:3215⁵

A study of Cu₂O, which is a semiconductor, was made to determine its electric conductivity and thermoelectric force, Hall constant and heat conductivity between -70° and +70°. A tabulation of the values of conductivity, Hall constant, dissociation work ϵ , and electron number, n_0 . The effect of temperature and length of mean free path of the electrons on the thermoelectric force is shown.

- (2.) Monch, G. - "Thermoelectric and Volta Potential of Cu₂O" - Naturwissen-Schaffen, 21 367 (1933). C.A. 27:4743²

A metal-Cu₂O-metal thermoelement has a potential of 1 MV/°. (Vogt - C.A. 25:3215⁵). This potential is largely due to differences in electron concentration in the semiconducting Cu₂O. A similar potential appears between two ends of an insulated piece of Cu₂O if they are kept at different temperatures. (0.4 to 0.5 V/100° for polycrystalline Cu₂O). The change in volta potential of the free Cu₂O surfaces is 0.15 V/100°.

- (3.) Hakhberg, B. M. and Kvasha, O. G. - "Thermoelectric Processes in Cu₂O" - J. Exptl. Theoret. Phys. (U.S.S.R.) 5, 46-53 (1935). C.A. 29:7765²

Cu-Cu₂O T.C.'s with varying oxygen content were prepared. Electrical conductivity varied by 10⁴. Thermo emf remained approximately constant at 0.49 to 0.95 MV/°C in range -150° to +500°. Conductivity 1/T but emf/degree constant and fell only above 750°. These

results are contrary to present theories.

- (4.) Hogarth, C. A. - "Some Conducting Properties of the Oxides of Zinc and Copper" - Z. Physik. Chem. 198, 30-40 (1951). C.A. 46:4873^e

Electrical conductivity and thermopower of ZnO and Cu₂O measured f (T) to 100° and O₂ pressure 100 - 0.04 mm.

- (5.) Okada, T. - "Electric Conduction of Cu₂O Semiconductor" - Busseiron Kenkyu, 19 15-29 (1949). C.A. 47:3069^c

Electrical conductivity and α between R.T. and 450° under P(O₂) 5-20 mm.

- (6.) Greenwood, N. N. and Anderson, J. S. - "Conductivity and Thermoelectric Effect in Cu₂O" - Nature, 164 346-7 (1949). C.A. 44:2815¹

Reproducible results by equilibrating Cu₂O with Cu⁰ at 1050°. Conductivity - temperature and thermopower - temperature given.

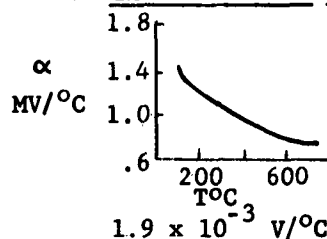
- (7.) Anderson, J. S. and Greenwood, N. N. - "The Semiconducting Properties of Cu₂O" - Proc. Roy. Soc. (London) 215A 353-70 (1952). C.A. 47:4158^e

Electrical conductivity and thermopower 20 - 1030°. α remains constant in region where number of current carrier depend strongly on temperature. All details given. Fifty references.

- (8.) "Measurements of Thermoelectric Forces of Cu₂O at High Temperatures" - Z. Naturforsch., 7a 211-12 (1952). C.A. 46:8914^e

4. Bi₂O₃

a. Thermoelectric power

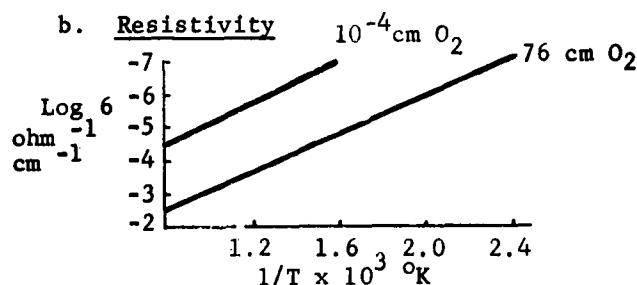


(1)

1.9 x 10⁻³ V/°C

(D)

b. Resistivity



(1)

c. Thermal conductivity

Assume 0.05 watts/cm°C

d. Figure of Merit

At 500°C

$$7 \times 10^{-10}$$

$$= 3 \times 10^4 \text{ ohm cm}$$

$$= 10^{-3} \text{ V/°C}$$

(REFERENCES)

- (1.) Mansfield, R. - "The Electrical Properties of Bi_2O_3 " - Proc. Phys. Soc. (London) 62B 476-83 (1949). C.A. 44:1299^f

Conductivity and thermoelectric power of Bi_2O_3 measure from 150 - 680° and at O_2 pressure 76×10^{-4} cm. Variation with pressure less than 10% except below 10^{-3} cm where sign changes > 550°. Conductivity due to excess O or Bi^{+3} deficiency. Conductivity by holes.

5. CdO

a. Thermoelectric power

$$\alpha = 60 \times 10^{-6} \text{ V/°C at } 300^\circ\text{K}$$

(1)

$$\alpha = 135 \times 10^{-6} \text{ V/°C at } 800^\circ\text{K}$$

(1)

b. Resistivity

$$\rho = 4 \times 10^{-3} \text{ at } 300^\circ\text{K}$$

(1)

$$\rho = 2 \times 10^{-2} \text{ at } 800^\circ\text{K}$$

(1)

c. Thermal conductivity

Assume K - 0.1 watts/cm°C

d. Figure of merit

$$9 \times 10^{-6} \text{ at } 300^\circ\text{K}$$

$$9 \times 10^{-6} \text{ at } 800^\circ\text{K}$$

e. Power generated

$$P = 0.06 \text{ watts}$$

$$\Delta T = 500^\circ\text{K}$$

$$\alpha = 1 \times 10^{-4} \text{ V/°C}$$

$$\rho = 10^{-2}$$

(REFERENCES)

- (1.) Wright, R. W. - "Variation with Temperature of the Electrical Properties of a WADD TR60-22, Pt. II

Degenerate Electronic Semiconductor as Exemplified by CdO" - Proc. Phys. Soc. (London) 64A 350-62 (1951). C.A. 45:8346

Strong strip specimens are prepared from CdO powder such that they possess an electrical conductivity $\sim 300 \text{ ohm}^{-1} \text{ cm}^{-1}$ at room temperature. Simultaneous measurements of the Hall constant and the electrical conductivity are made through the temperature range 0 - 500° and the thermopower is measured immediately afterwards on the same specimen. The properties are found to resemble those of a metal. Theory developed. Satisfactory agreement. Theory predicts that α and ρ be directly proportional to T^0K . Experimental results confirm this.

- (2.) Hogarth, C. A. and Andrews, J. P. - "Variation with Oxygen Pressure of the Thermoelectric power of CdO" - Phil. Mag., 40 273-82 (1949). C.A. 44:5174^d

Thermopower $\sim (\log P_{O_2})$. Between 240 and 570°C thermopower given by $dE/dT = -a + bT$ at constant P_{O_2} .

- (3.) Andrews, J. P. - "Thermoelectric Power of CdO" - Proc. Phys. Soc. 59 990-8 (1947). C.A. 42:1776^c

The thermopower of CdO vs. Pt over -110° to 800°.

6. NiO

a. Thermoelectric power

$\alpha \approx 300 \times 10^{-6} \text{ V/}^\circ\text{C}$ pure NiO (1)
 $\alpha = 5 - 600 \times 10^{-6} \text{ V/}^\circ\text{C}$ impure (1)
 $\alpha = 100 \times 10^{-6} \text{ V/}^\circ\text{C}$ with Li_2O impurity (1)

b. Resistivity

Minimum for sample containing Li_2O as impurity
10 ohm cm 25°C
Decreases slowly with temperature (1)

c. Thermal conductivity

Assume 0.1 watt/cm°C

d. Figure of merit

10^{-8}

e. Power generated

2.5×10^{-4} watts

$\Delta T = 1000^\circ\text{C}$

(REFERENCES)

- (1.) Paravano, G. - "Thermoelectric Behavior of NiO" - (Franklin Inst.) J. Chem. Phys. 23, 5-10 (1955). C.A. 49:5049^a

NiO containing Li₂O, CeO₂, Ag₂O, NiCl₂, Cr₂O₃ and W₂O₃. Measured α .

- (2.) Hogarth, C. A. - "Conduction Properties of Oxides of Cd and Ni" - Proc. Phys. Soc. (London) 64B, 691-700 (1951). C.A. 48:11864^b

$$\rho = \frac{1}{3 \times 10^{-5}} \quad \text{Black NiO}$$

$$\rho = \frac{1}{1.6 \times 10^{-2}} \quad \text{Green NiO}$$

- (3.) Wright, R. W. and Andrews, J. P. - "Temperature Variation of the Electrical Properties of NiO" - Proc. Phys. Soc. (London) 62A, 446-55 (1949). C.A. 44:4248

NiO prepared in coherent strips. Conductivity, Hall coefficient to 700°. Thermopower thereafter, deficit semiconductor, hole conduction.

7.1 (BaSr)O

a. Thermoelectric power

$$\alpha = 2.17 \times 10^{-3} \text{ V/}^\circ\text{C at } 1000^\circ\text{K} \quad (1)$$

b. Resistivity

$$\rho = 5 \times 10^2 \text{ ohm cm at } 1000^\circ\text{K} \quad (1)$$

c. Thermal conductivity

Assume K = 0.01 watt/°C cm

d. Figure of merit

$$Z = 9 \times 10^{-7} \text{ at } 1000^\circ\text{K}$$

7.2 BaO

a. Thermoelectric power

$$\alpha = 2.12 \times 10^{-3} \text{ V/}^\circ\text{C at } 1000^\circ\text{K} \quad (1)$$

b. Resistivity

$$\rho = 10^3 \text{ ohm cm} \quad (2)$$

c. Thermal conductivity

Assume $K = 0.01 \text{ watt/}^\circ\text{C cm}$

d. Figure of merit

$$Z = 4 \times 10^{-7} \text{ at } 1000^\circ\text{K}$$

(REFERENCES)

- (1.) Young, J. R. - "Electrical Conductivity and Thermoelectric Power of (BaSr)O and BaO" - J. Applied Phys., 23, 1129-38 (1952). C.A. 47:373¹

Electrical conductivity and thermopower and thermo-emission between 300 - 1100°K on different base metals.

$$\begin{aligned}\alpha &= 2.0 \text{ MV/}^\circ \text{ 1100}^\circ\text{K} \\ &2.5 \text{ MV/}^\circ \text{ 800}^\circ\text{K} \\ &1 - 0.5 \text{ MV/}^\circ \text{ 500}^\circ\text{K}\end{aligned}$$

- (2.) Noga, Kinichi - "Thermoelectromotive Force of BaO and (Ba, Sr)O" - J. Phys. Soc. Japan 6 124-5 (1951) (in English). C.A. 45:5998^e

Thermo-emf values of 1.8 - 2.8 MV/°C were obtained from 750 - 1200°K. Over the same temperature range chemical potentials of 1.8 - 2.6 e.v. were found. The activation values were 0.4 - 0.6 e.v. The sign of thermo-emf showed the N-type of semiconductor for (BaSr)O, the P-type appearing for the very poorly activated state.

8. MgO

a. Thermoelectric power

$$\alpha = 1.1 \times 10^{-3} \text{ V/}^\circ\text{C} \quad (1)$$

950° - 1400°C

b. Resistivity

$$\rho = 10^7 \text{ ohm cm at } 1000^\circ\text{C} \quad (1)$$

(REFERENCES)

- (1.) Mansfield, R. - "The Electrical Conductivity and Thermoelectric Power of MgO" - Proc. Phys. Soc. (London) 66B 612-14 (1953). C.A. 47:9577^e

Data on sintered MgO 600 - 1500°.

9. TiO₂

a. Thermoelectric power

248×10^{-6} V/°C relative to Ni (1)

b. Resistivity

1.51 ohm cm 20°C decreases ~1%/°C at 20° (1)

c. Thermal conductivity

Not found, assume 0.5 watt/cm°C

d. Figure of merit

$Z = 8.1 \times 10^{-8}$

(REFERENCES)

- (1.) Henisch, H. K. - "Thermoelectric Power and Conductivity Properties of Blue TiO₂" - Elec. Comm. 25 163-77 (1948). C.A. 42:61298

C. SULFIDES

1. CrS

a. Thermoelectric power

$\alpha = 20 \times 10^{-6}$ V/°C (1)

b. Resistivity

$\rho = 4 \times 10^{-4}$ ohm cm (1)

c. Thermal conductivity

Assume K = 0.1 watt/cm°C

d. Figure of merit

$Z = 10^{-5*}$

e. Efficiency

Assume $\Delta T = 1000^\circ\text{C}$ 1300°K - 300°K
0.25%*

f. Power generated

25 watts*

*Mismatched data? See Reference (1)

(REFERENCES)

- (1.) Fakidov, I. G. and Grazhdankina, N. P. - "Electrical Properties of Chromium Sulfides" - Trudy. Inst. Fiz. Metal., Akad. Nauk S.S.S.R., Ural Filial, 15, 65-9 (1954). C.A. 49:13721e

Electrical conductivity of CrS with 50 - 59 atomic %S has maximum at 54 atomic %S with sp. resistivity of 4×10^{-4} ohm cm. Temperature coefficient is plus between 0 - 233°K for comp. between 50 - 53 %S but becomes - above 233°K. With 54 %S, CrS shows curie points at -110° and 30°. α is 0.02 MV/°C for the ferromagnetic form.

- (2.) Watanabe, H. and Tsuya, N. - "The Properties of Chromium Sulfides and Iron Sulfide I" - Science Reports Research Insts., Tohoku Univ., Ser. A2 503-6 (1950). C.A. 46:4304c

Sulfides heated 900° $\rho_{\text{CrS}_{1.17}} = 3 \times 10^{-4}$ ohm cm.
 $\rho_{\text{CrS}_{1.33}} = 5.2 \times 10^{-4}$ ohm cm.

2. NiS

a. Thermoelectric power

$$\alpha = 6.5 \times 10^{-6} \text{ V/}^\circ\text{C} \quad (1)$$

b. Resistivity

$$\rho = 2 \times 10^{-4} \text{ ohm cm} \quad (1)$$

c. Thermal conductivity

Assume $K = 0.5$ watts/cm°C

d. Figure of merit

$$4.2 \times 10^{-7}$$

(REFERENCES)

- (1.) Hauffe, K. and Flindt, H. G. - "The Electrical Conductivity and the Thermoelectric Force of NiS" - Z. Physik. Chem. 200, 199-209 (1952). C.A. 47:3071

Conductivity independent of S pressure below 150 mm.
Conductivity $4800 \text{ ohm}^{-1} \text{ cm}^{-1}$ at 700°.

3. BaS

a. Thermoelectric power

$$\alpha = 2.5 \times 10^{-3} \text{ V/}^\circ\text{C} \quad (1)$$

970 - 1270°K

b. Resistivity

$$\rho = 10^5 \text{ ohm cm} \quad (1)$$

(REFERENCES)

- (1.) Grattidge, W. and Hohn, H. - "The Electronic Properties of BaS" - J. App. Phys., 23 1145-51 (1952). C.A. 47:961e

$$\alpha = 2.5 \text{ MV/}^\circ \text{ between } 970 - 1270^\circ\text{K}$$
$$\rho = 10^{+5} \text{ ohm cm}$$

4. PbS

See Franklin Institute Report F1992-13

5. SnS

a. Thermoelectric power

$$\alpha = 630 \times 10^{-6} \text{ V/}^\circ\text{C} \quad (1)$$

b. Resistivity

$$\rho = 28 \text{ ohm cm} \quad (1)$$

(REFERENCES)

- (1.) Anderson, J. S. and Morton, Mrs. M. C. - "Semiconducting Properties of Stannous Sulfide II. Thermoelectric Effect" - Trans. Farad. Soc. 43 185-94 (1947).

Au-SnS-Au -80° to 420°C, thermopower and conductivity.

SECTION E-II: REFRACTORY HARD METALS

(REFERENCES A AND E)

(Unless otherwise indicated, data is for room temperature)

A. SILICIDES

1. MoSi₂

M.P. 1870°C with decomposition (E) (2030 ± 50°C Moly Chem. Bull. Cdb. 6.)

a. Thermoelectric power

$$\begin{aligned}\alpha &= 5.13 \times 10^{-6} \text{ V/}^\circ\text{C } 60^\circ\text{C} \\ \alpha &= 15.3 \times 10^{-6} \text{ V/}^\circ\text{C } 600^\circ\text{C}\end{aligned}\quad (1)$$

b. Resistivity

$$\rho = 21.5 \times 10^{-6} \text{ ohm cm} \quad (E)$$

c. Thermal conductivity

$$K = 0.314 \text{ watts/cm}^\circ\text{C} \quad (E)$$

d. Figure of merit

$$\begin{aligned}3.9 \times 10^{-6} & \text{ } 60^\circ\text{C} \\ 3.5 \times 10^{-5} & \text{ } 600^\circ\text{C (room temperature values for p and K)}\end{aligned}$$

e. Power generated

$$2.72 \text{ watts} \quad \Delta T = 1000^\circ \quad \alpha = 15.3 \times 10^{-6}$$

(REFERENCES)

- (1.) "Thermoelectric Effects in MoSi₂" - J. Appl. Phys. 24 498 (1953). (Note) C.A. 47:10935

Thermal emf of MoSi₂ vs. Pt, in range 60 - 600° is given by

$$E = 5.13t + 1/2 (3.76) 10^{-2} t^2 - 1/3 (15.65) 10^{-6} t^3. \text{ Microvolts.}$$

2. OTHER SILICIDES

<u>Compound</u>	<u>Resistivity</u> <u>micro ohm-cm</u>	<u>Thermal cond.</u> <u>watts/cm°C</u>	<u>M. P.</u> <u>°C</u>
TaSi ₂	8.5		2400
WSi ₂	33.4		2150
NbSi ₂	6.3		1950
MoSi ₂	21.5	.314	1870
VSi ₂	9.5		1750
CrSi ₂			1570
TiSi ₂	123		1540
ZrSi ₂	161		1520

3. CARBIDES

HfC	109		3890
NbC	74	.14	3500
TaC	20	.22	3880
TiC	105	.17	3250
W ₂ C (β)	81		2700
WC	12		2630
VC	156		2830
ZrC	63.4	.20	3175
Mo ₂ C	97		2690

4. BORIDES

<u>Compound</u>	<u>Resistivity micro ohm-cm</u>	<u>Thermal cond. watts/cm°C</u>	<u>M. P. °C</u>
TiB ₂	15 - 28	0.261	2980
ZrB ₂	9.2 - 28.8 87.6 at 1600°C 118.2 at 2305°C 139.1 at 2635°C	0.23	3040
VB ₂	16		2100
NbB ₂	28 - 65	0.17	> 2900
TaB ₂	68 - 86	0.11	3000
CrB	64		1550
CrB ₂	21		1850
HfB ₂	10		3250
Mo ₂ B	40		2000
MoB α	45		2180
MoB β	25		
MoB ₂	45		2100
WB			2860
W ₂ B			2770

5. NITRIDES

TaN	135 - 25°C 116.3 - 2840°C	3090
ZrN	11.5 - 160 - 25°C 320 M. P.	2980
TiN	21.7 - 130 - 25°C 340 M. P.	2930
NbN	200 - 25°C 450 - 2050°C	2050
VN	85.9 - 200 - 25°C 850 M. P.	2050

SECTION E-III: MISCELLANEOUS REFERENCES

1. Schulze, A. - "Metallic Materials for Thermoelements" - Metallwirtschaft, 18 249-54, 271-6, 315-20 (1939). C.A. 33:5792³

A systematic consideration of all metals shows that but a few base metals are suitable for practical thermoelectric measurements above 1000°. Of these, only Ni and its alloys (up to 10%) with Cr, Mo, W are really useful. Several types of thermopiles for the measurement of radiation are described.

2. Schulze, A. - "Metallic Materials for Thermoelements" - Warne, 62 127-9 (1939). C.A. 33:6092⁶

A record is given of the progress made in the use of various noble metals, noble metal combinations, and common metal alloys as elements of thermocouples. The sensitivity of some of these in temperature measurements is compared.

3. Schulze, A. - "Metallic Materials for Thermocouples" - J. Inst. Fuel 12 41-85 (1939). C.A. 34:2213³

T.C.'s for temperatures > 1500°. Data on thermoelectric force and useful temperature range of a large number of noble and base metal couples included.

4. Laure, Yvon - "The Electrical Measurement of High Temperatures" - Electricite 23 183-90 (1939). C.A. 33:6092⁷

Resistance thermometers for precision and industrial use are described, also their construction, measuring methods, and calibration. In use for precision T.C.'s are:

SiC vs graphite
50% Ni + 50% Cu vs. 84% Ni + 16% Mo

For industrial purposes:

Pt vs. 92% Pt + 8% Re
Pt vs. 90.5% Pt + 4.5% Re + 5% Rh
Rh vs. 99.92% Rh + 0.08% Re
Au vs. 68% Au + 32% Pd
Pd vs. 60% Pt + 40% Pd
Te vs. Pt
Pt vs. 99% Te + 1% Sb
95% Pt Rh + 5% Re vs. Pd + Au
60% Fe + 40% Cr vs. Pd
Ni vs. graphite
NiCr vs. NiAl
W vs. 75% W + 25% Mo

The millivolts are given for all the elements and calibration curves are shown for most of them.

5. Morgan, F. H. - "Refractory Thermocouples and Emissivity Determinations" - (Bartol Research Foundation, Swarthmore, Pa.), Phys. Rev. 78, 353 (1949) C.A. 45:6053^f

Thermoelectric power

W - Ta
W - Mo
Ta - Mo
W - W/Mo (50 - 50)

6. Morgan, F. H. and Danforth, W. E. - "Thermocouples of the Refractory Metals" - J. App. Phys., 21, 112-13 (1950). C.A. 44:7595^d

W - Ta
W - Mo
Ta - Mo
W - W/Mo (50 - 50)

7. Domenicali, C. A. and Otter, F. A. - "Thermoelectric Power and Electrical Resistivity of Dilute Alloys of Si in Cu, Ni, and Fe" - (Franklin Inst.), J. Appl. Phys., 26 377-80 (1955). C.A. 49:8643^d

Data are given for the thermoelectric power and resistivity of dilute alloys Cu-Si, Ni-Si, Fe-Si from -195° to +500°.

8. Troy, W. C. and Stevens, G. - "Thermocouple" - Patent US 2,588,988 March 11, 1952 W-Ir. C.A. 46:4864^f

W-Ir

9. Boltaks, B. I. and Zhuze, V. P. - "Semiconductive Properties of Some Metallic Compounds" - Invest. Akad. Nauk S.S.S.R. Ser. Fiz., 16 155-68 (1952). C.A. 46:10753^a

Mg_3Sb_2 , Mg_2Sn , Mg_2Pb , Cs_3Sb , $SbZn$

10. Mesnard, G. and Uzan, R. - "Conductivity and other Electrical Properties of Thoria" - Le Vide, 6 1052-62, 1091-7 (1951). C.A. 46:800¹
11. Kitaro, Fujii - "Studies and Applications of the Thermoelectric Properties of Inorganic Compounds" - Proc. World Eng., Congr., Tokyo, 1929 22 331-2 (1931). C.A. 25:5604ⁿ

A thermoelectric series of crystals, microcrystals and amorphous masses of metals or inorganic compounds that conduct electricity is set up. Inorganic thermocouples are superior to metallic. The sensitivity of a thermopile of 20 elements of CuS and PbS was 3 - 5 times higher

than that of elements of Bi-Sb, Bi-Ag, or constantan-mangnus.

12. Perrot, M. and Peri, G. - "Particulate Thermoelectric Elements" - Compt. rend. 239 537-9 (1954). C.A. 49:3587^a

When a powdered oxide of Al, Be, or Th is compressed between two metallic plates, a difference in temperature between the two plates results in an emf. When the oxide is moist, the positive pole is always the colder one, but the oxide is dry, the positive pole is always the warmer one. However, with dry oxide, the intensity of polarization is very weak, whereas with wet Al_2O_3 of 20 sq cm surface, 1 mm thickness and 50 ohms resistance, $\Delta T = 22^\circ\text{C}$ a potential of 0.5 volts was generated and a current of 1 ma delivered for 3 hours through a resistance of 400 ohms. Considerable variation was found in the voltage and current produced with different samples of Al_2O_3 . Moreover, the curves of E or I vs. ΔT are not linear and appear to approach a limiting value. The decrease in E as ΔT is reduced back to zero is not instantaneous.

13. Hirahara, Eiji - "Physical Properties of Cu_2S Semiconductors: I. Electric Conductivity and Anomalous Heat Capacity, II. Thermal Properties" - Proc. Phys. Soc. Japan, 4, (I) 10-12, (II) 12-14, (1949). C.A. 44:10422^a

From ionic conductivity and electric conductivity and heat capacity, two transition points are found. Anomalous thermal emf explained by Cu diffusion in Cu_2S phase.

SECTION E-IV: GENERAL REFERENCES

- A. Campbell, I. E. (Ed) - "High Temperature Technology" - John Wiley, New York (1956).
- B. "Handbook of Chemistry and Physics" - 38th Ed., Chem. Rubber Publishing Co. (1957)
- C. "American Institute of Physics Handbook" - McGraw-Hill (1957).
- D. Zwikker, C. - "Physical Properties of Solid Materials" - Interscience, New York (1954).
- E. Schwarzkopt, P. and Kieffer, R. - "Refractory Hard Metals" - Macmillan, New York (1953).

SECTION E-V: SUMMARY

In order to evaluate the materials described, they are compared to Bi_2Te_3 with respect to figure of merit, optimum efficiency, and power generation per unit area and length. These parameters for Bi_2Te_3 are tabulated below. They are based on the Battelle data in the proposal for this contract.

Bi_2Te_3

Operating Temperature Range: 300 - 500°K

<u>Cold Junction</u> <u>300°K</u>	<u>Hot Junction</u> <u>T°K</u>	<u>Figure of Merit</u> <u>°C⁻¹</u>	<u>Optimum</u> <u>Efficiency</u>	<u>Power</u> <u>Generated*</u> <u>Watts</u>
	350	5.4×10^{-4}	.65 percent	.0096
	400	3.2×10^{-4}	.79 percent	.0305
	450	1.8×10^{-4}	.68 percent	.0594
	500	1.0×10^{-4}	.50 percent	.0704

*Resistivity at mean sample temperature used, assuming linear temperature gradient.

On the basis of data in Table 5.4.1-2 given in the proposal, the figure of merit of Bi_2Te_3 is 2×10^{-3} . Assuming an operating temperature span of 200°K and using room temperature data for thermoelectric power and resistivity (Table 5.4.1-2), the power generated is 0.5 watts.

The materials found which generate comparable power are as follows:

MoSi_2 - 2.7 watts
CrS - 0.25 watts
 Cu_2O - 0.25 watts
W-C - 0.28 watts
C-SiC - 0.11 watts

Of these, MoSi_2 is by far the outstanding from a number of viewpoints and is discussed in detail below:

MoSi_2

1. MELTING POINT

2030 \pm 50°C (Moly. Chem. Bull. cdb-6)
(E)

Decomposes at M.P.

2. TEMPERATURE STABILITY

MoSi_2 one of the most stable refractories known today. It is stable in an oxidizing atmosphere to 1700°C. Because of this property, it is often used as a coating material over less stable high temperature materials.

3. PREPARATION

A considerable technology has developed in the preparation and forming of this material. This information is available in manufacturers' brochures.

4. MECHANICAL PROPERTIES

The principal disadvantage of MoSi_2 is its relatively poor thermal shock resistance. Information on this and other mechanical properties is also available from manufacturers.

5. RESISTIVITY AND THERMAL CONDUCTIVITY

These data are available over limited temperature ranges. Some data are shown in Figure E-1. The Lorenz number has been measured between 200 - 800°C. It deviates from constancy by 7%, having a scattering range of 3.83 - 4.09.

6. THERMOELECTRIC POWER

The thermoelectric power has been measured to 600°C. For the purpose of the calculations below, the data has been extrapolated to 1600°C by use of the equation in Reference 1, Section E-II of this report. A plot of thermoelectric power versus temperature is shown in Figure E-2.

Needless to say, considerable uncertainty must be attached to the extrapolated values. In particular, the decrease in thermoelectric power above 1400°C is hardly acceptable on the basis of the data available.

In view of the reported properties of MoSi_2 , further investigation of this material as a thermoelement seems desirable. It would also appear worthwhile to examine other materials in the class of refractory hard "metals" for which data on thermoelectric power is not now available.

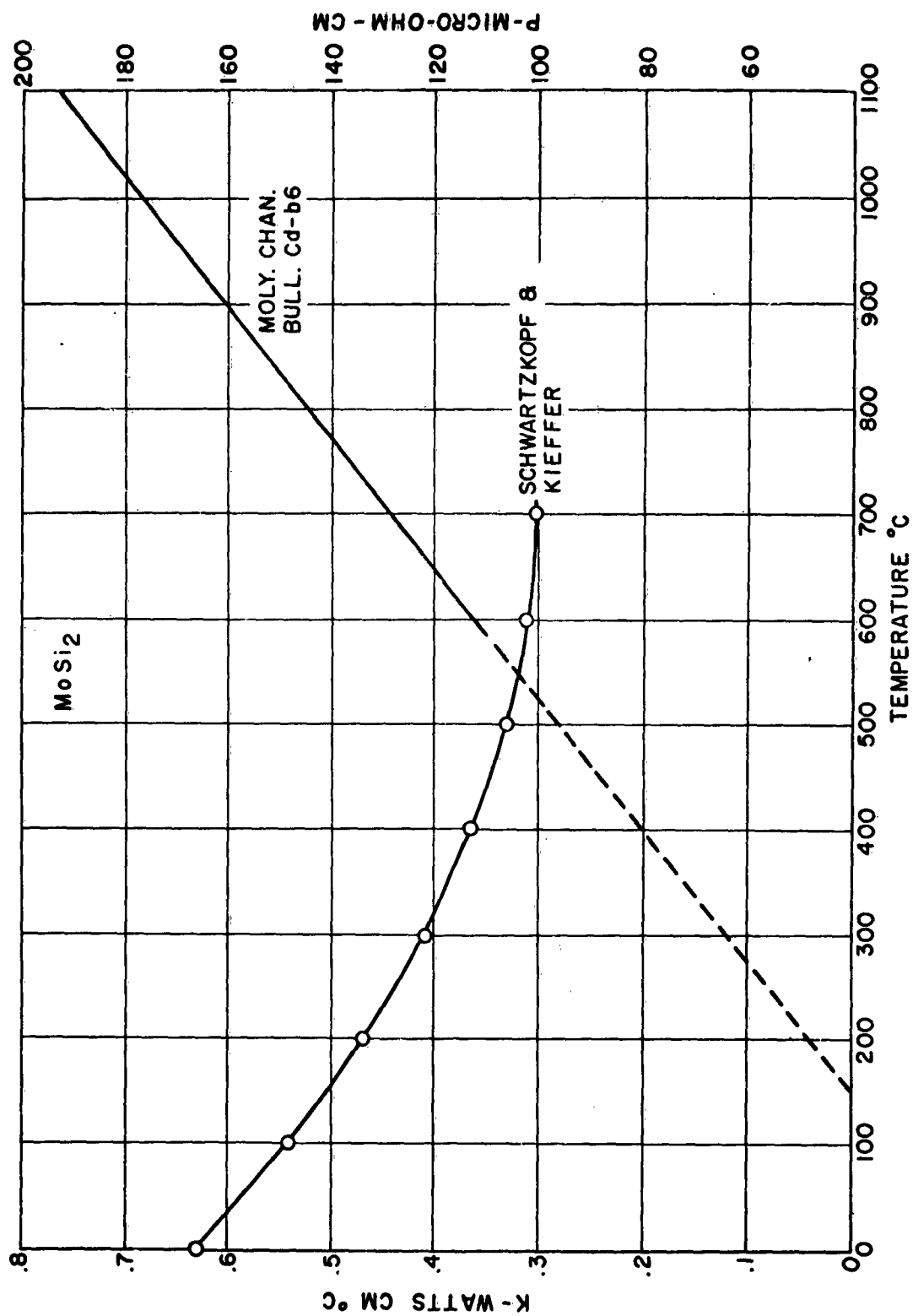


Figure E-1: Resistivity and Thermal Conductivity Versus Temperature.

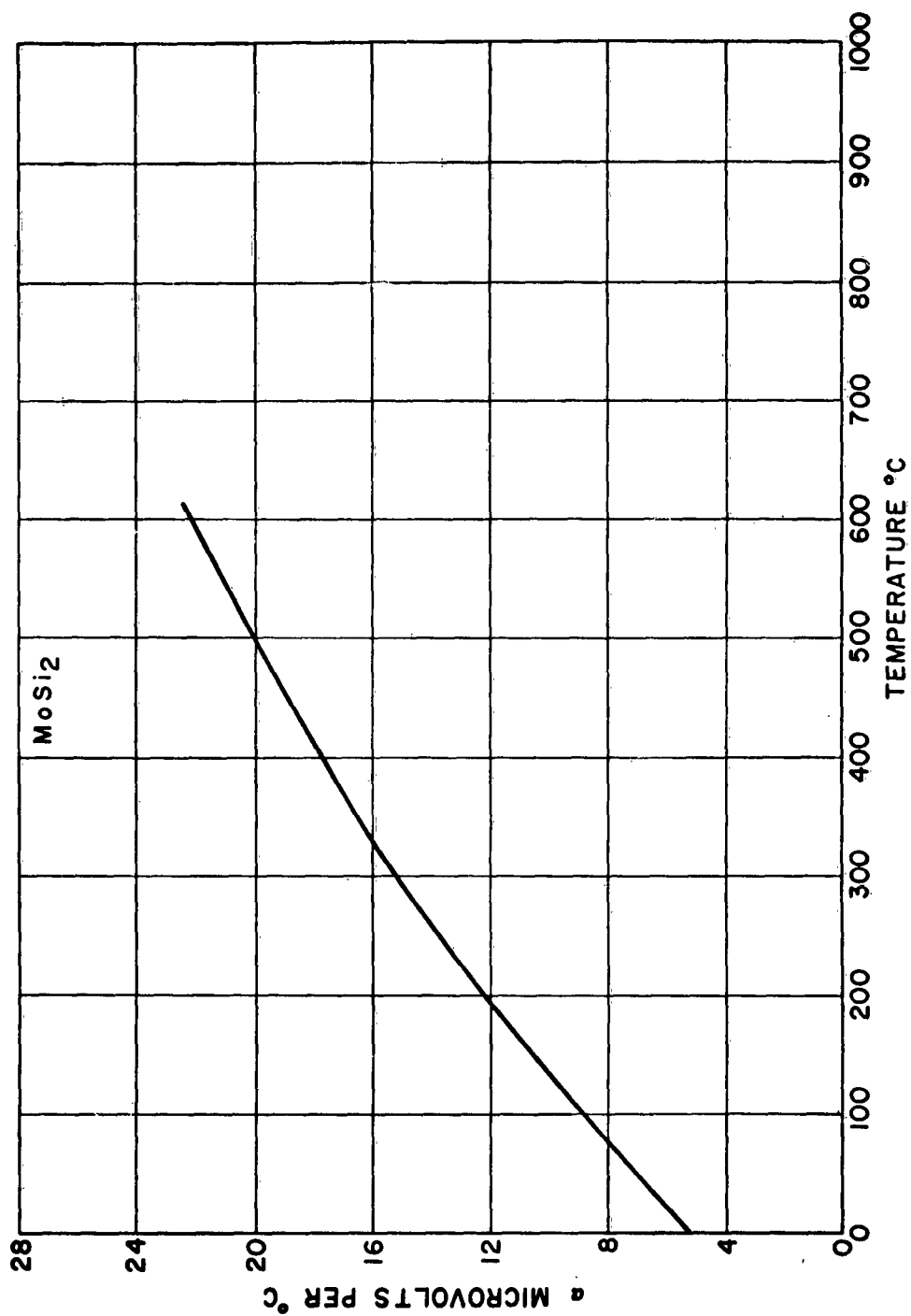


Figure E-2: Thermoelectric Power Versus Temperature.

TABLE E-1 - DATA ON MoSi₂

Temperature °C	Thermal Conductivity watts/cm°C (1)	$\rho \times 10^5$ ohm watts/°C (2)	Thermo Power $\times 10^6$ volts/°C	Figure of Merit $\frac{1}{\text{°K}}$	Power Generated watts/cm ³ (4)	Optimum (4) Efficiency %
200	0.469	1.87	12.02	7.7×10^{-6}	0.009	0.02
400	0.367	2.67	17.67	1.2×10^{-5}	0.12	0.09
600	0.310	3.46	22.06	1.4×10^{-5}	0.42	0.17
800		4.25	25.19	1.5×10^{-5}	0.87	0.26
1000		5.04	27.08	1.5×10^{-5}	1.41	0.33
1200		5.83	27.27	1.3×10^{-5}	1.86	0.36
1400		6.63	27.15	1.1×10^{-5}	2.27	0.35
1600		7.42	24.65	8.2×10^{-6}	2.23	0.31
1700		7.81	27.27 (5)	9.5×10^{-6}	2.96	0.39

(1) Data calculated from equation on P2 Moly. Chem. Bull. cdb-6 (Jan. 1956).

(2) From average Lorenz number of 3.96×10^{-8} ohm watt/°K².

(3) Extrapolated data below dotted lines.

(4) Cold junction at 100°C. Value of resistivity at mean sample temperature.

(5) Taking leveling-off value.

TABLE E-2 - PROPERTIES OF THERMOELECTRIC MATERIALS

Material	Graphite - SiC	Graphite - Tungsten	Graphite - B ₄ C	MoSi ₂ - Platinum
Thermopower micro-volts/°K	28.6	23	280	+27.3
Resistivity micro-ohm - cm	1.5×10^{-3}	3.2×10^{-5}	$.3-.8 \times 10^6$	161 at 900°C
Thermal conductivity watt/cm ² °K	0.4	0.4	.29 - .84	.47
Figure of merit $\times 10^3$ °K ⁻¹	2.3×10^{-4}	8.1×10^{-6}	2.6×10^{-4}	1.5×10^{-5} at 900°C
Tl max. °K	2100	2000	2500°	2000°(2)
η max. %	7.2×10^{-3} (1)			.39
(P/V _c) max. watts/cm ³	.11	.28	.035	2.96

Notes: (1) T₂ = 800°K

(2) without protection.

APPENDIX F - SEEBECK VOLTAGE AND RESISTIVITY OF "REFRACTORY METALS"

John R. Gambino

November, 1958

INTRODUCTION

This appendix summarizes the results obtained so far on the class of compounds called refractory hard "metals". This class of compounds is characterized by their melting points, hardness, and "metallic" electrical and thermal conductivity. Although the conductivity is essentially metallic in character, the definite chemical composition, hardness, and crystal structure indicates some amount of covalent bonding.

The refractory nature of these materials would allow their use over a large temperature range. If their thermoelectric power were about the same order as metals, $10\mu\text{volts}/^\circ\text{C}$ versus platinum, the power output per unit volume would be comparable to semiconductors, such as Bi_2Te_3 with their limited temperature range.

The Wiedemann-Franz ratio for these materials generally is of the order observed in metals. For this reason, the study has been concerned primarily with measurement of thermoelectric power. Since this property is and electrical conductivity is not independent of state of aggregation, specimen fabrication was greatly simplified. No attempt was made to densify the specimens. Thermoelectric power data was almost completely lacking for this class of materials.

An empirical approach was used consistent with a survey type study of this sort. Materials were selected based on several criteria: (1) availability in reasonable purities, (2) representative compositions in each of the classes; borides, carbides, nitrides, and silicides, and (3) materials with representative resistivities either greater or less than that of the parent metal. For instance, the resistivity of TaSi_2 is about half that of tantalum while ZrSi_2 is four times greater than that of zirconium. Such high resistances could be indications of semi-metallic behavior. Generally, the non-metal atoms having a much smaller size than the metal atoms occupy interstitial sites in the lattice. The non-metal forms Si-Si or B-B linkages in some compounds and these should contribute to the covalent nature of bonding and non-metallic behavior. Some compounds were included because of the possibility of this type of bonding.

MATERIALS

Compounds studied included the following:

1. Borides: ZrB_2 , TiB_2 , LaB_6
2. Carbides: TiC , MoC , Cr_3C_2
3. Nitrides: TiN , ZrN , MoN
4. Silicides: MoSi_2 , TiSi_2 , ZrSi_2 , CrSi_2 , Mo_3Si_2

The Cr_3C_2 , TiN , ZrN , MoN , TiSi_2 , ZrSi_2 , CrSi_2 , and Mo_3Si_2 were prepared by synthesis from the elements. The other compositions were obtained from commercial sources. Synthesis generally involved cold pressing and sintering or hot pressing powder mixtures so that frequently the reacted specimen was in a suitable form for measurement.

Sintering was accomplished in an argon or hydrogen atmosphere; hot pressing was done in air so that the atmosphere around the specimen was mainly N_2 and CO . Interaction with the graphite molds was minor. The oxide layers which might exist on the powder surfaces or could develop during synthesis or fabrication was considered the most important source of contamination.

EXPERIMENTAL METHODS

Sintered compacts were placed between two platinum sheets which had platinum-platinum 10% rhodium thermocouples attached to their outer surfaces. The temperature of each surface was measured and the ΔT obtained by difference. The end temperatures and the Seebeck emf, obtained by utilizing the platinum leg of the thermocouple, were measured with a G.E. precision potentiometer. The ΔT ranged from 30 to 50°C depending on the specimen size and the measurement temperature. The natural gradient of a tube furnace was used to provide the temperature difference.

RESULTS AND DISCUSSION

The temperature dependence of Seebeck voltage for typical borides, carbides, nitrides and silicides were studied in the temperature range 100 to 1000°C. The Seebeck voltages of the borides, shown in Fig. F-1, were uniformly low and on the basis of reported resistivity and conductivity for these compounds, these materials do not appear promising for thermoelectric power use. It is interesting to note that LaB_6 contains boron atoms linked in an infinite 3-dimensional network instead of the interstitial positions occupied in the closed-packed TiB_2 and ZrB_2 . B_4C which has a similar 3-dimensional network for boron atoms is a semiconductor in contrast to the "metallic" conduction and Seebeck voltage of LaB_6 . From these results, it can be concluded that similarities in bonding cannot be used as the sole basis for choosing materials for study. Further work on the borides should be concentrated on AlB_2 , FeB , and CoB . Boron atoms are linked into layers in AlB_2 and into chains in FeB and CoB .

Seebeck voltages of the carbides, shown in Fig. F-2, are low also. It should be mentioned that chromium carbide, Cr_3C_2 , has a structure not related to the parent metal as in interstitial carbides. (In this way, it might be considered representative of the group Fe, Mn, Co, and Ni carbides.) The carbon atoms form chain linkages throughout the structure somewhat analogous to B-B in FeB . Another type of carbide, those containing discrete C atoms, should be considered to complete the study of carbide structure types. These include Al_4C_3 and carbides with the CaC_2 structure such as LaC_2 , UC_2 , and VC_2 . Their metallic luster and conductivity are probably indicative of low Seebeck voltages also.

Interstitial nitrides had typically low Seebeck voltages, shown in Fig. F-3. Ionic and covalent nitrides are known; examples of the former are Ge_3N_4 and the latter BN or Si_3N_4 . The stability of the ionic nitrides and the high resistivity of the covalent nitrides makes it doubtful that such compounds should be investigated.

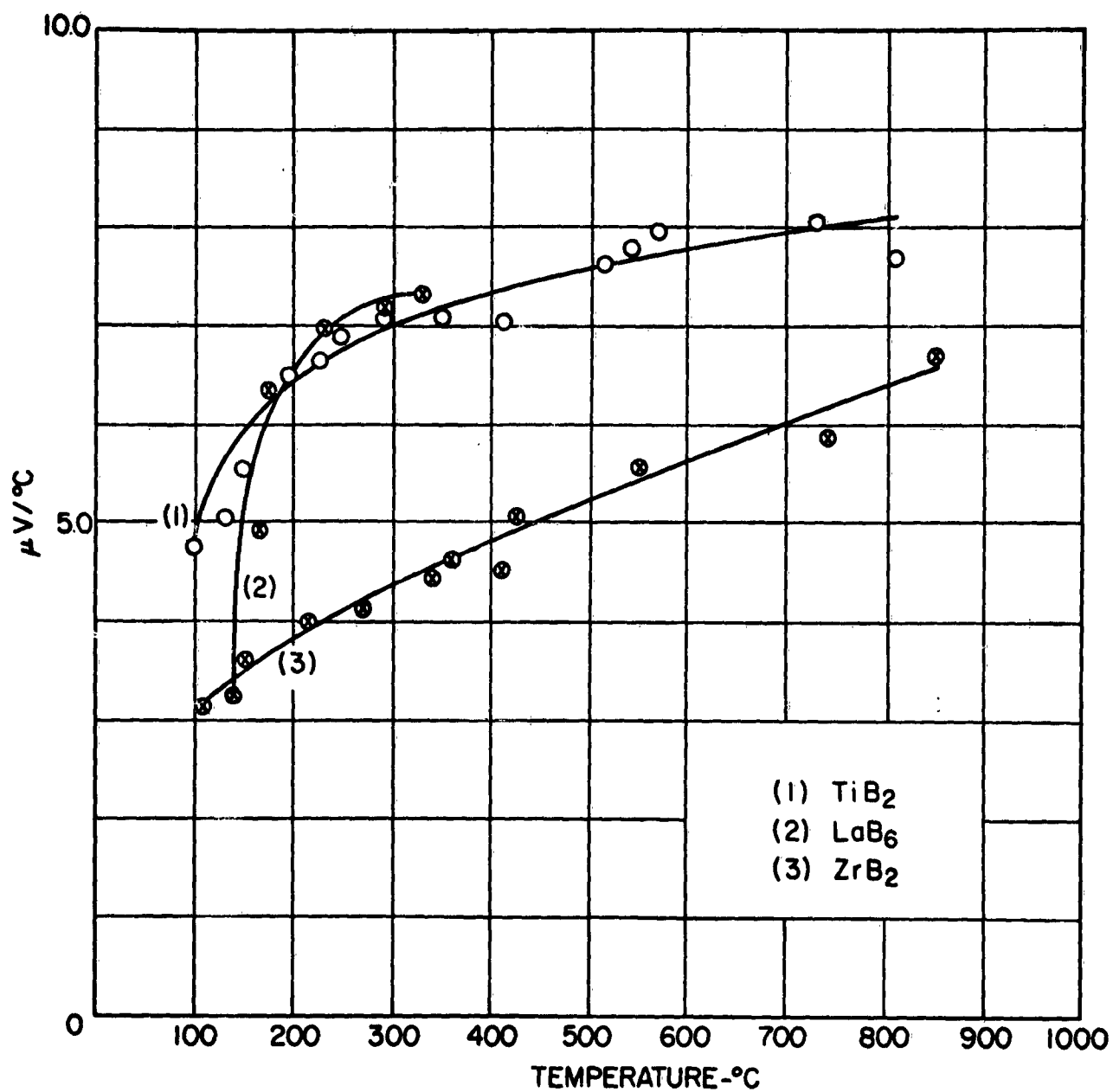


Figure F-1: Temperature Dependence of Seebeck Voltage for Borides.

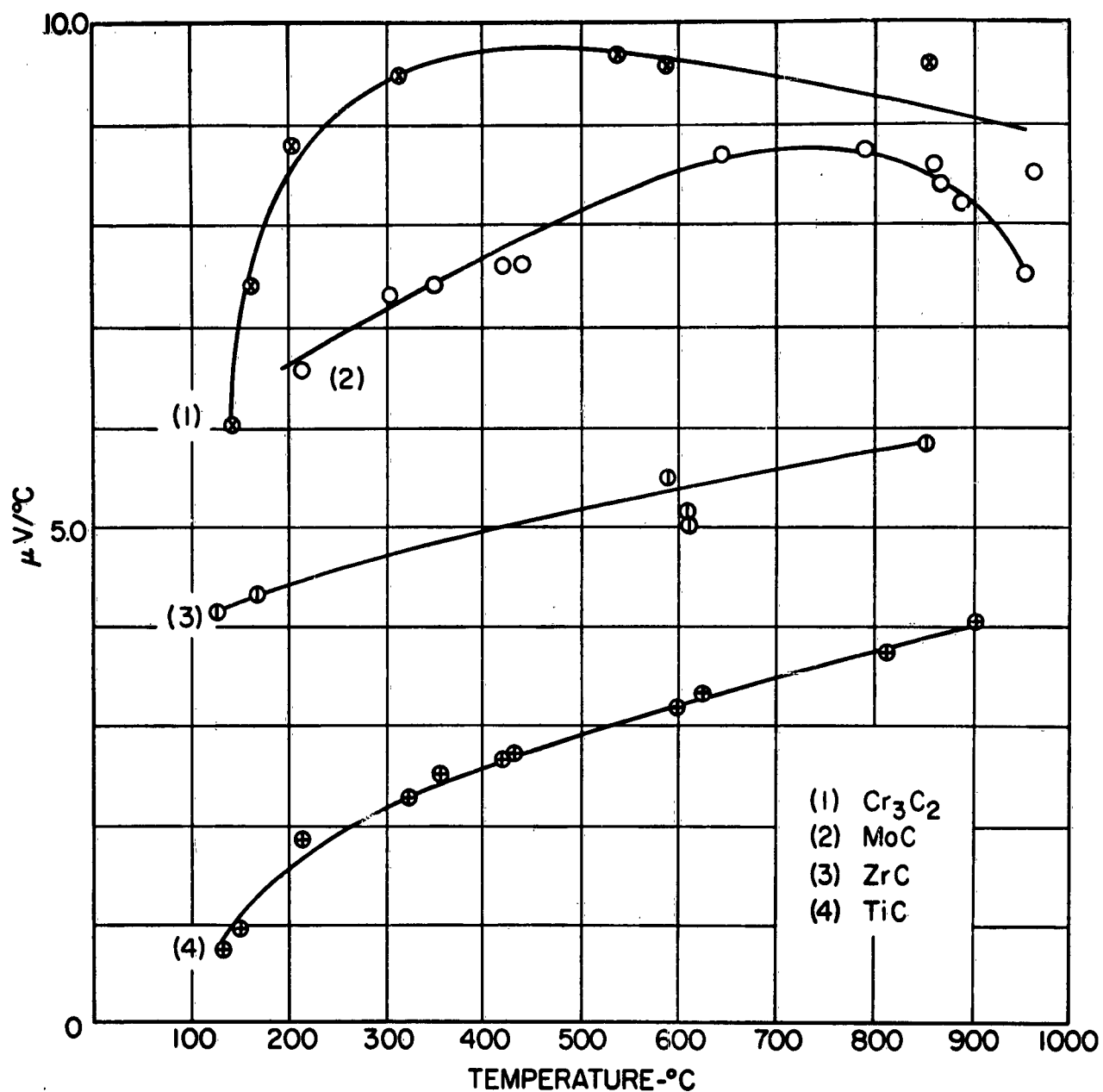


Figure F-2: Temperature Dependence of Seebeck Voltage for Carbides.

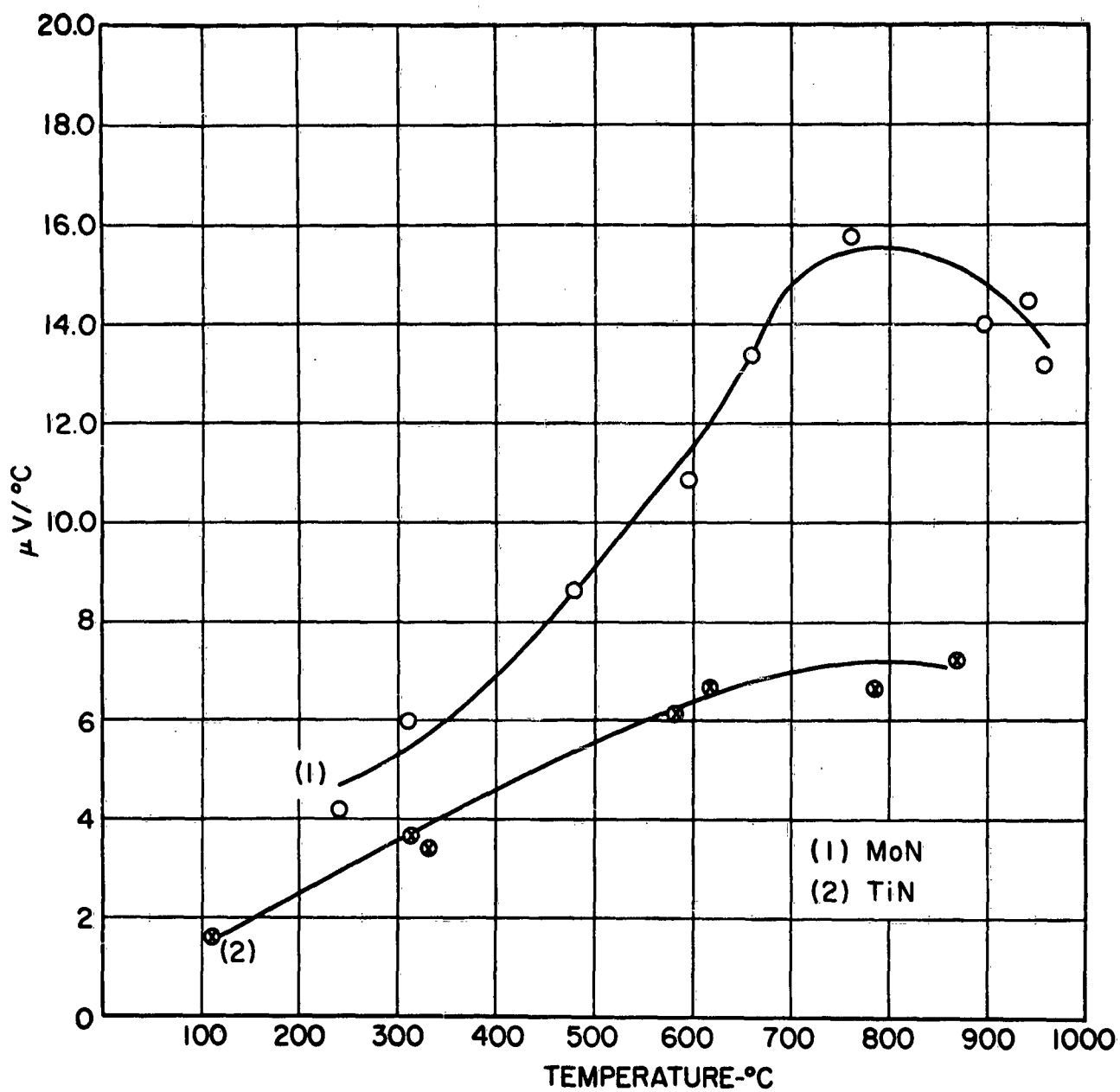


Figure F-3: Temperature Dependence of Seebeck Voltage for Nitrides.

The Seebeck voltages of silicide compositions are shown in Fig. F-4. The method of preparation had some influence on the Seebeck voltage; this was also observed in other classes of refractory metals studied. The differences observed for CrSi_2 can be attributed to loss of one or more constituent by volatilization. The effects of oxide impurities will be discussed later.

The silicides are the most promising class of materials studied. The Seebeck voltages are equal or somewhat better than the best high temperature metals. In addition, the refractory nature and oxidation resistance of this class of compounds makes them attractive from several standpoints. Molybdenum disilicide, for instance, is used for commercial heating elements which operate at 1600°C . Cladding, necessary for metals at these temperatures, can be omitted with a considerable saving in weight.

The disilicides of titanium, chromium, and molybdenum are related structurally in a very interesting way although the classes of structure are dissimilar, orthorhombic, hexagonal, and cubic, respectively. All are composed of close packed layers superposed in such a way to give 10 instead of 12-coordination. The differences is essentially the number of layers in the repeat unit, 4 in the TiSi_2 group, 3 in the CrSi_2 group, and 2 in the MoSi_2 group. The ten-fold increase in Seebeck voltage could be the result in the subtle difference in structure. The apparent relationship between structure and Seebeck voltage should be verified by making measurements on isomorphous silicides in the CrSi_2 group, such as VSi_2 and TaSi_2 , and in the MoSi_2 group such as CoSi_2 . Data on a isomorphous group of mono-silicides, CrSi , MnSi , FeSi , CoSi , and NiSi , reported by Russian investigators (F-1), indicated a wide variation, -1 to +102, in Seebeck voltages. In this group of silicides at least, isomorphous relationships are no guide to behavior. The decrease in Seebeck voltage of Mo_3Si_2 , as well as the data reported by the Russians, indicate that increasing the silicon content causes loss of metallic behavior. When the non-metal to metal atomic radius ratio is below 0.59, the non-metal occupies interstitial positions. In systems with values greater than 0.59, a metallic character can still be maintained but an entirely different structure results.

The addition of impurities to silicides with semiconductor properties should result in changes in the conductivity and Seebeck voltage. Optimization of these properties can best be accomplished by selecting one or two materials for study.

Auxiliary experiments were performed to determine whether oxide layer on the particles could be masking the true value of Seebeck voltage. The Seebeck voltage of oxides of molybdenum, MoO_2 and MoO_3 was found to be less than $10 \mu\text{V}/^\circ\text{C}$ for the former and $700 \mu\text{V}/^\circ\text{C}$ at 700°C for the latter. Lower oxides, undoubtedly present to some extent, should not affect the Seebeck voltage measurement appreciably. In one experiment with MoSi_2 , in which the atmosphere was inadvertently air instead of inert gas, a very large increase in Seebeck voltage was observed above the melting point of MoO_3 .

FIGURE OF MERIT AND EFFICIENCY

Although electrical and thermal conductivity measurements were not made for CrSi_2 , room temperature values have been reported (F-1). By assuming ρ_K does not

(F-1) E. N. Nikitin, Zhur. Tekh. Fiz., 28 23, (1958)

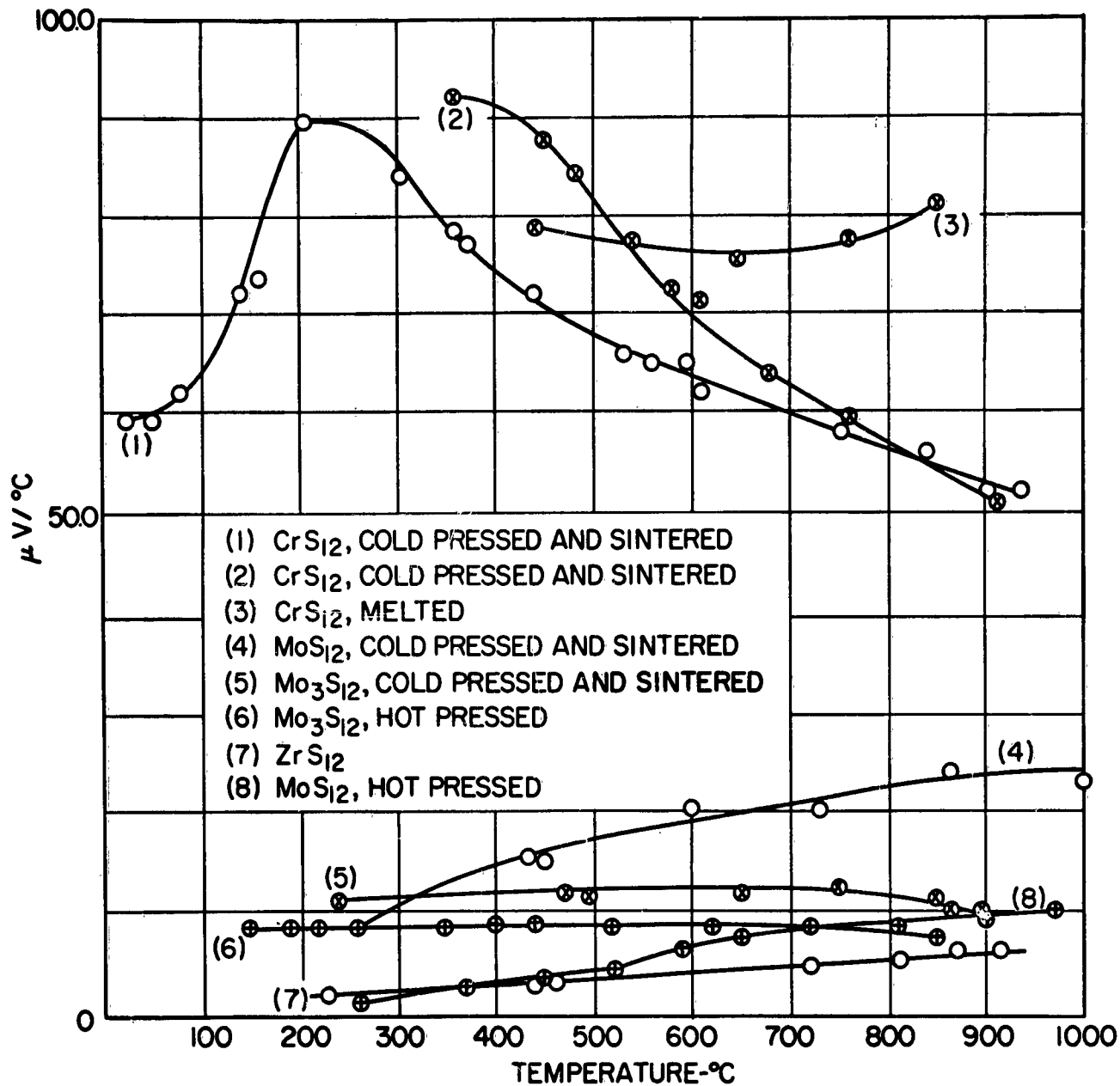


Figure F-4: Temperature Dependence of Seebeck Voltage for Silicides

change appreciably with temperature, a tentative figure of merit and efficiency can be calculated. These values are as follows:

Hot junction temperature	$T_1 = 1300^{\circ}\text{K}$
Cold junction temperature	$T_2 = 300^{\circ}\text{K}$
α avg ($\mu\text{V}/^{\circ}\text{K}$)	70.0
ρ , ohm-cm	1.47×10^{-3}
K , watt/cm $^{\circ}\text{C}$	0.060
($^{\circ}\text{K}^{-1}$)	5.54×10^{-5}
η , %	1.35
$\left[\frac{P}{Vt} \right]_{\text{max.}}$, watts/cm 3	1.88

Somewhat higher efficiencies were predicted^(F-1) for the same class of materials.

APPENDIX G - THERMOELECTRIC POWER OF REFRACTORY BORIDES, CARBIDES, NITRIDES, AND SILICIDES

John R. Gambino

April, 1959

INTRODUCTION

This appendix summarizes the results of an investigation of refractory carbides, borides, nitrides, and silicides for thermoelectric generator applications. The primary objective of this study was to develop materials having desirable properties for thermoelectric applications. A secondary consideration was to survey a broad group of materials and establish empirical relationships, whenever possible, between characteristics of materials and their properties of interest for thermoelectric applications. Such relationships are necessary in order to limit the number of compounds which need to be studied.

BACKGROUND

The practical application of energy conversion by means of thermoelectricity depends primarily on development of an element material which operates with a reasonable efficiency. The magnitude of the power delivered by an element, shown in Fig. G-1, is determined by the Seebeck voltage and the temperature difference. The resistance of the element produces losses due to IR drop and joule heating, therefore, the resistivity of the element should be as low as possible. The thermal conductivity should also be low so that a large temperature difference can be maintained across the element. These properties of the material, Seebeck voltage, resistivity, and thermal conductivity are related to efficiency by the following expressions:

$$\text{Figure of merit } Z = \frac{\alpha^2}{\rho K} \text{ } (^{\circ}\text{K}) \quad (\text{G-1})$$

where α is the Seebeck voltage, $\frac{V}{^{\circ}\text{K}}$, ρ is the resistivity (ohm-cm), and K is the thermal conductivity, watts/ $^{\circ}\text{C}/\text{cm}$.

$$\text{Optimum efficiency } N_{\text{opt}} (\%) = \frac{T_1 - T_2}{T_1} \cdot \frac{\frac{m - 1}{m + T_2}}{\frac{T_2}{T_1}} \quad (\text{G-2})$$

$$\text{where } m = \left[1 + \frac{1}{2} Z (T_1 + T_2) \right]^{1/2}$$

In this study, the evaluation of materials was based almost exclusively on measurement of the Seebeck voltage. The reason for this was that a number of these materials are known to have a Wiedemann-Franz ratio of the order observed in metals. For these cases, the measurement of the Seebeck voltage is sufficient to evaluate the material. Of course, if a large Seebeck voltage is observed, measurement of electrical and thermal conductivity is necessary.

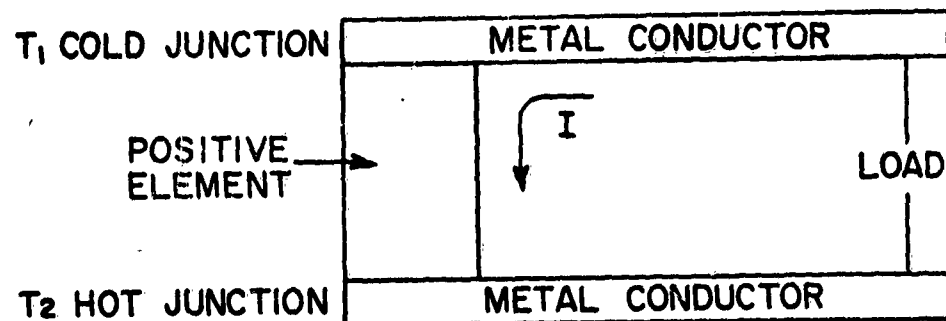


Figure G-1: Schematic Diagram of a Thermoelectric Generator Circuit.

The search for materials with favorable thermoelectric properties has been in progress for many years. Despite concerted efforts in recent years to develop better materials, not many major advances have been made. Few materials are available which have efficiencies greater than 1%. A philosophy was evolved in this study in order that an effort of this magnitude would lead to a significant contribution. The salient features were:

1. Materials or groups of materials should be studied which have not been extensively investigated in the past.
2. Materials should be studied which are capable of operating at much higher temperatures than those being currently investigated.
3. Empirical relationships should be developed whenever possible in order to limit the number of materials for study.

Improvement of existing materials by appropriate doping or changes in stoichiometry is, of course, important in developing a theory and in getting practical devices since some promising materials are available. The amount of improvement is necessarily limited and the return per unit effort much less than that possible in studying a new group of materials.

Materials which are capable of operating over a large temperature range, i.e., at high temperatures, have an advantage from an efficiency standpoint. The efficiencies of some hypothetical materials with various figures of merit as a function temperature range are shown in Fig. G-2. Efficiencies result from high temperature operation comparable to those obtained for materials such as Bi_2Te_3 having a high figure of merit but a limited temperature range. It is interesting to note that many materials have been studied at low temperatures for low temperature applications, i.e., Peltier cooling. Materials which are found to be unsatisfactory at low temperatures become more suitable at high temperatures since the electrical and thermal conductivity decrease with temperature while the Seebeck voltage is relatively insensitive to temperature. These materials examined at high temperatures are in a sense "new" materials.

The theory of thermoelectricity has not been developed to the point to provide much directivity in the selection and improvement of specific materials. Therefore, an empirical approach was used consistent with the survey nature of this study. The need for empirical relationships between characteristics of materials and their properties becomes evident when, as in this study, materials must be selected for study from a large number of possible compounds.

MATERIALS SELECTION

The class of materials of interest, the carbides, borides, etc., are frequently called, as a group, the refractory hard "metals". These materials are characterized by their high melting points, hardness, brittleness, and "metallic" electrical and thermal conductivity. The properties of some of these materials are listed in Table G-1. Although the luster and conductivity suggest a metallic character, the definite chemical composition, hardness, and crystal structure indicate some amount of covalent bonding.

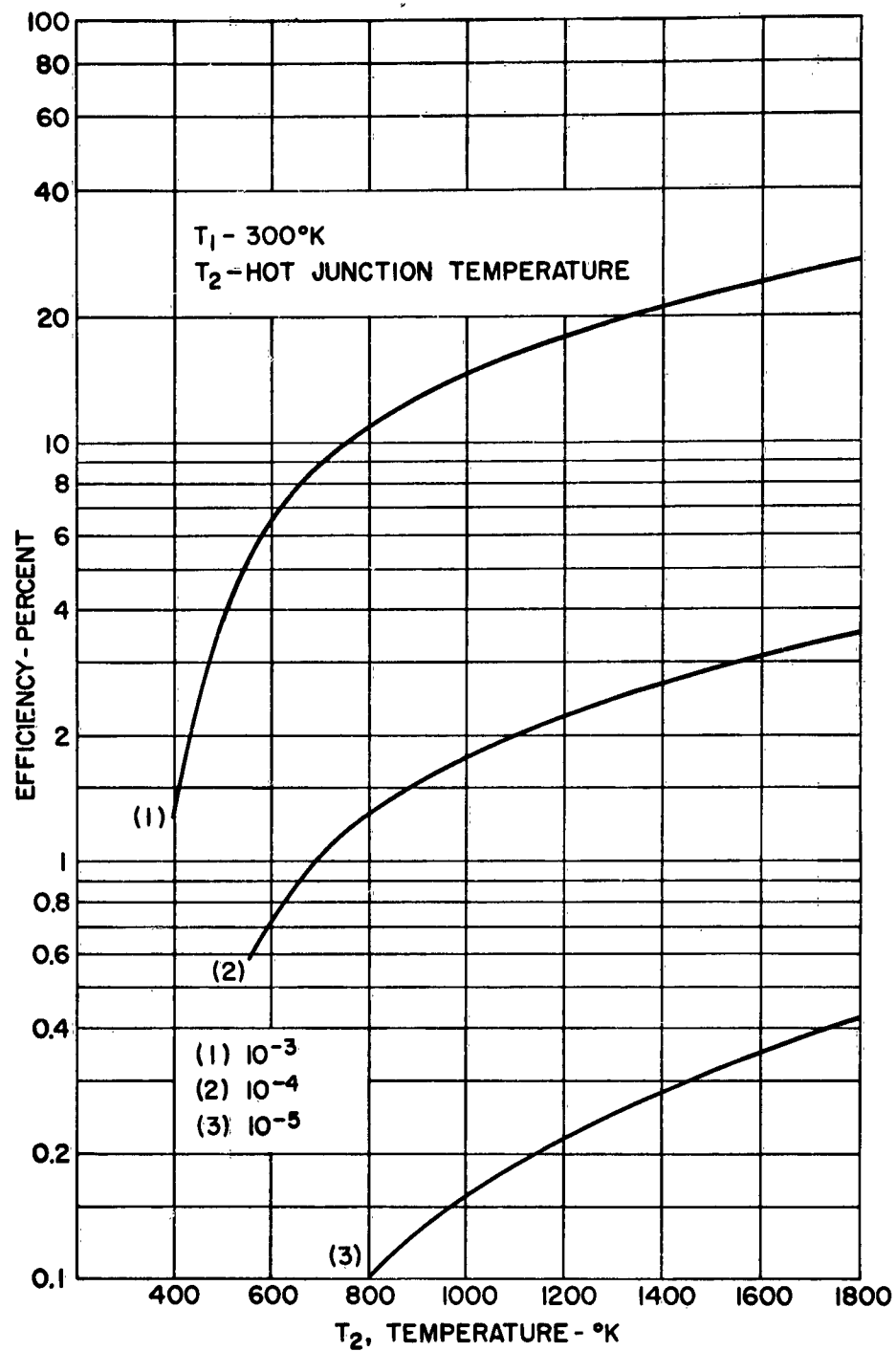


Figure G-2: Efficiency of Materials with Figures of Merit as a Function of Temperature.

Thermoelectric power data was almost completely lacking at the inception of the project. A number of investigators (G-2, G-3) recently reported data on these materials. This class of materials had not been extensively investigated previously and are capable of operating at high temperatures, hence, met requirements (1) and (2) above.

Specific materials were selected based on several criteria: (1) availability in reasonable purities, (2) representative compositions in each of the classes, borides, carbides, nitrides, and silicides, and (3) materials with representative resistivities. Impurities could consist of other metals beside the parent metal, non-metals other than the desired non-metals, or deviations from stoichiometry. Metal impurities would effect the resistivity more than the Seebeck voltage if these materials have essentially metallic behavior. The presence of other non-metals on deviations from stoichiometry could result in significant changes in Seebeck voltage. Such effects could best be determined by varying the composition of a material of interest.

The resistivities of these compounds were sometimes less than that of the parent metal; others were significantly higher. High resistances could be an indication of semi-metallic behavior. Some materials were selected because of the existence of a particular type of bonding which could influence the electrical properties.

MATERIALS AND EXPERIMENTAL METHODS

Representative compounds from each of the classes included the following:

1. Borides: ZrB_2 , TiB_2 , LaB_6
2. Carbides: TiC , MoC , Cr_3C_2
3. Nitrides: TiN , ZrN , MoN
4. Silicides: $MoSi_2$, $TiSi_2$, $ZrSi_2$, $CrSi_2$, Mo_3Si_2

The Cr_3C_2 , TiN , ZrN , MoN , $TiSi_2$, $ZrSi_2$, $CrSi_2$, and Mo_3Si_2 were prepared by synthesis from the elements. The other compositions were obtained from commercial sources.* Synthesis generally involved cold pressing and sintering or hot pressing powder mixtures so that frequently the reacted specimen was in a suitable form for measurement. Otherwise the material was crushed, re-pressed, and sintered. Sintering was accomplished in an argon or hydrogen atmosphere. For the very refractory materials, such as TiC , ZrB_2 , and TiB_2 , a special induction furnace capable of operating to $2000^\circ C$ was constructed. Even at these temperatures, densification and bonding was very slight. Hot pressing of these compositions at temperatures of $1800^\circ C$ and pressures of 2000 psi did not result in densification. Hot pressing was done in air so that the atmosphere in the graphite mold was mainly N_2 with some CO impurity. Temperature and time conditions were regulated to minimize interaction with the graphite molds. The oxide layer which might exist on the powder surface or could develop during synthesis or fabrication was considered the most important source of contamination.

As mentioned previously, the property of most interest was the Seebeck voltage. Since this property is and electrical conductivity is not independent of the state

*American Electro Metals Division of Firth Sterling, Inc., 220 Yonkers Ave., Yonkers, N. Y.

of aggregation, specimen fabrication was greatly simplified. No serious attempt was made to densify the specimens, and most specimens were less than theoretical density.

Seebeck voltage measurements were made by placing the sintered compacts between two platinum sheets which had platinum-platinum 10% rhodium thermocouples attached to their outer surfaces. The spring loaded holder is described in Fig. G-3. The temperature at each surface was measured and the ΔT obtained by the difference. The end temperatures and Seebeck emf obtained by utilizing the platinum leg of the thermocouple were measured with a G.E. precision potentiometer. The ΔT ranged from 30 to 50°C, depending on the specimen size and measurement temperature. The natural gradient of the tube furnace was used to provide the temperature difference. A number of different specimen shapes were utilized which varied with the mode of preparation; the length varied from 1.5 to 3.0 cm.

A few room temperature conductivities were measured using a four probe method (see Fig. G-3). Since this property is sensitive to state of aggregation and the macro and microstructure varied from sample to sample, the result of these measurements is subject to ambiguous interpretation.

SEEBECK VOLTAGE OF REPRESENTATIVE CARBIDES, BORIDES, NITRIDES, AND SILICIDES

The temperature dependence of Seebeck voltage of typical borides, carbides, nitrides, and silicides were studied in the temperature range 100 - 1000°C. The Seebeck voltages of ZrB_2 , TiB_2 , LaB_6 , shown in Fig. G-4, were uniformly low, below 10 $\mu V/^\circ C$. On the basis of reported electrical and thermal conductivity and the low Seebeck voltages observed, these materials do not appear promising for thermoelectric power use. The values of Seebeck voltage of carbides and nitrides shown in Figs. G-5 and G-6 were low also. The Seebeck voltage of some silicides, shown in Fig. G-7, were higher than the other classes of materials. An interesting relationship is apparent from these data. The significance of the higher Seebeck voltages of the silicides can be understood if the structure of the refractory hard "metals" is considered. It has been recognized (G-4, G-5) that the properties and structure of these compounds can be related to the ratio of the non-metal atom to the metal atom radius.

When the radius ratio is less than the critical value of 0.59, the resultant structure is the normal interstitial type. (This rule has its exceptions, notably in cases in which the radius ratio is close to 0.59 and the non-metal concentration is high.) When the radius ratio is exceeded, more complicated structures result. The new phases can still have "metallic" properties, however. The critical radius ratios for compounds of transition elements are shown in Table G-2. Compounds studied which had a radius ratio less than 0.59 all had Seebeck voltages of the order observed in metals. The silicides, all of which have radius ratios greater than 0.59, had high Seebeck voltages in some cases and low in others.

Some carbides, nitrides, and borides not studied have critical radius ratios somewhat greater than 0.59. The borides of vanadium and borides and carbides of chromium, manganese, iron, cobalt, and nickel are among these. Some of these have B-B and C-C bonding in the lattice which could be further reason for non-metallic behavior. LaB_6 contains boron atoms linked in an infinite three-dimensional network and yet has "metallic" conduction and Seebeck voltage.

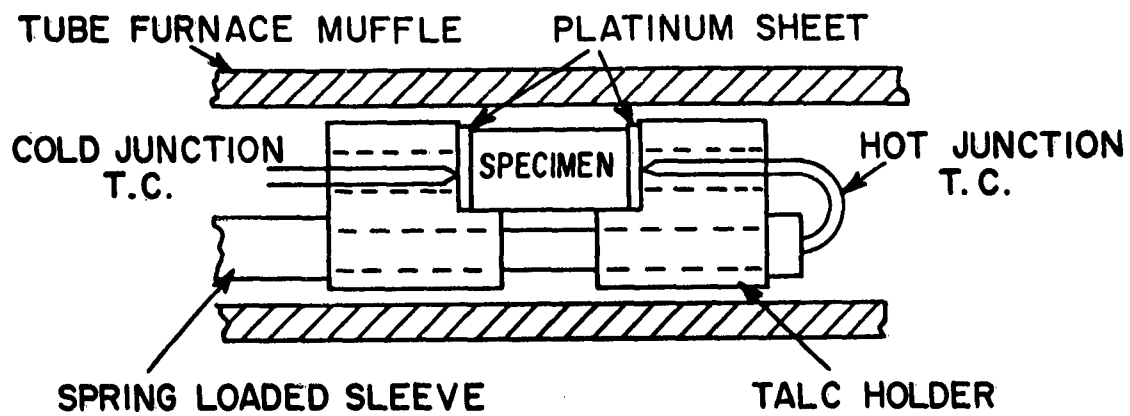


Figure G-3: Specimen Holder for Seebeck Voltage Measurements.

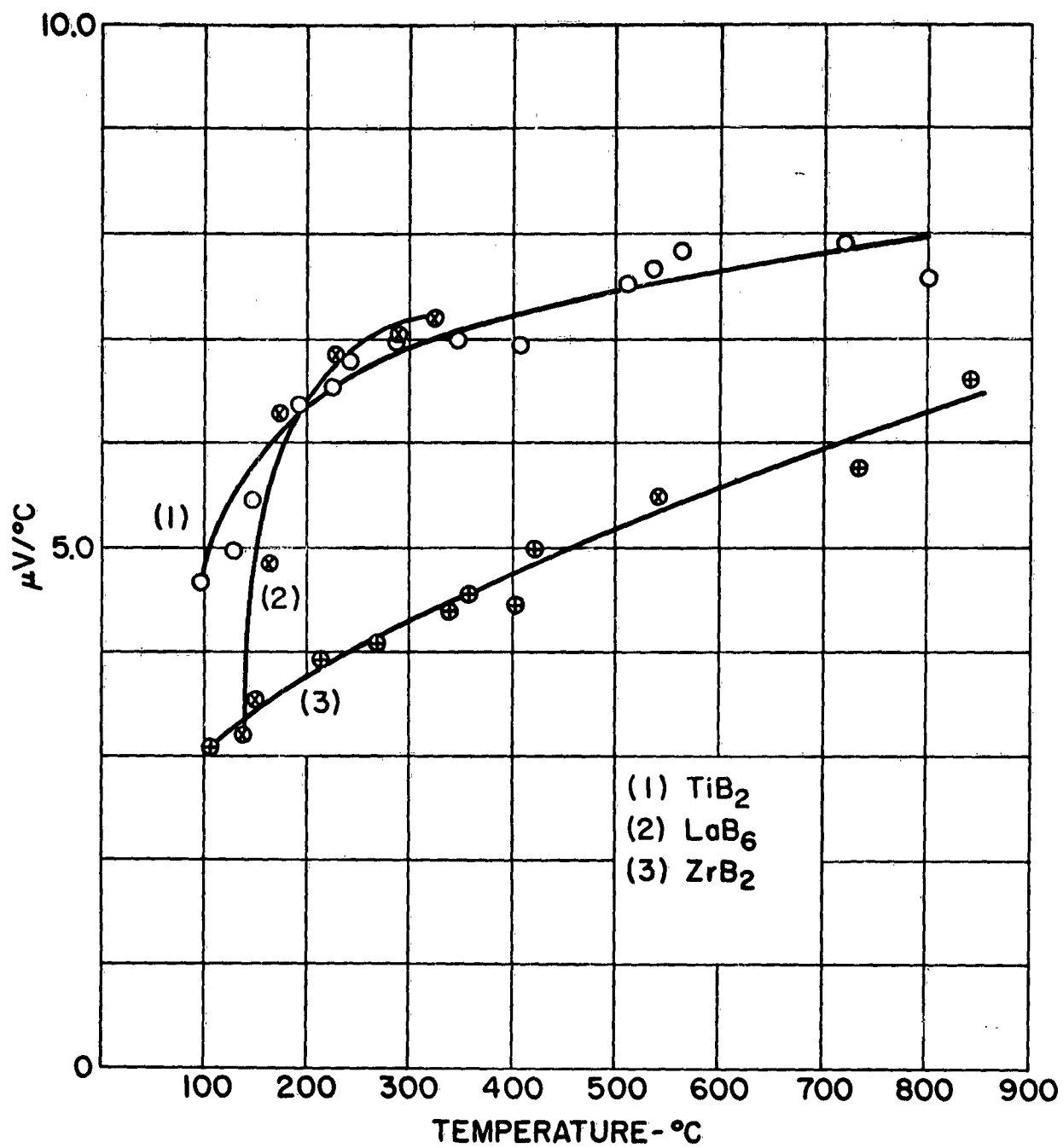


Figure G-4: Temperature Dependence of Seebeck Voltage for Borides.

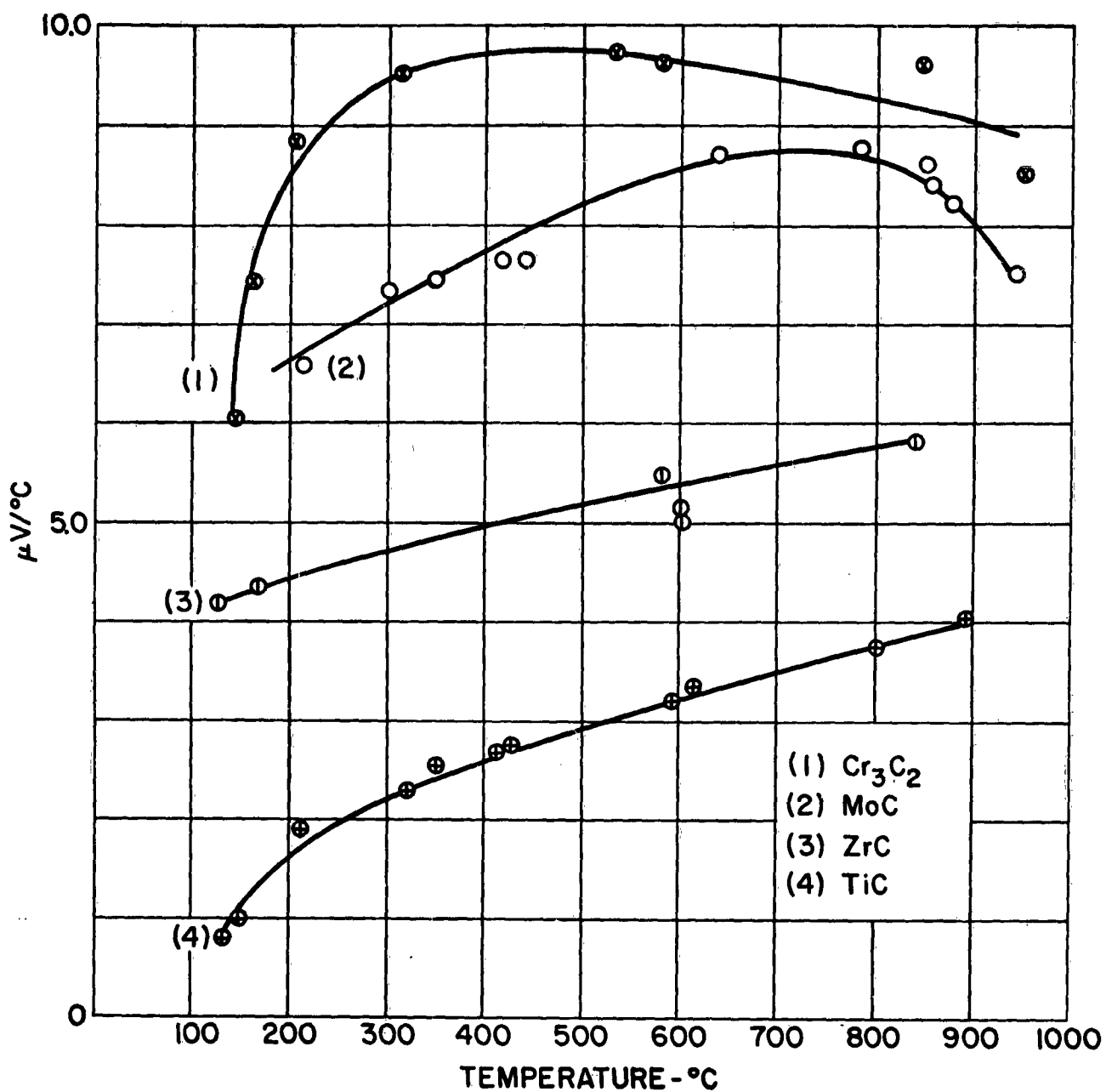


Figure G-5: Temperature Dependence of Seebeck Voltage for Carbides.

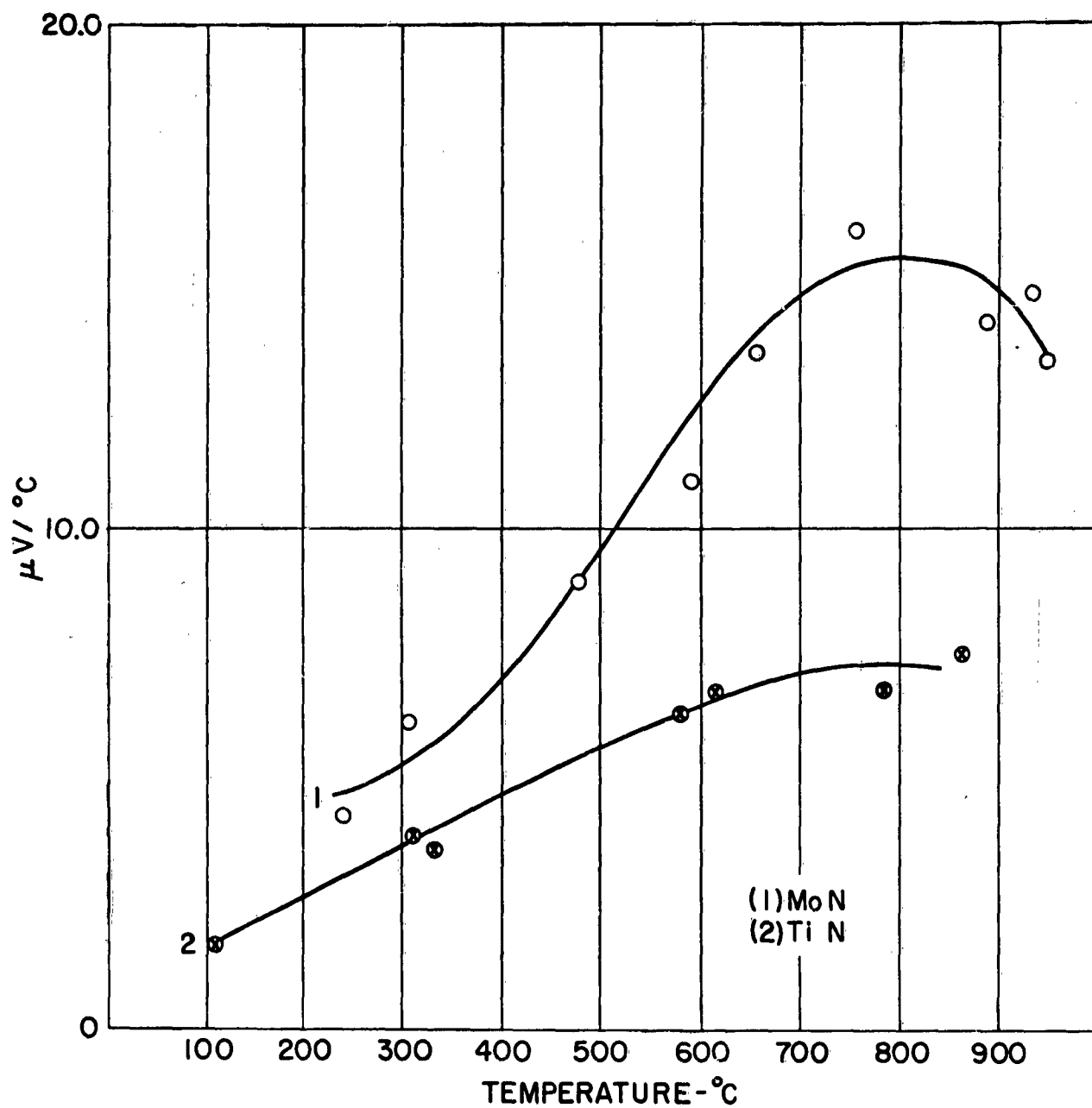


Figure G-6: Temperature Dependence of Seebeck Voltage for Nitrides.

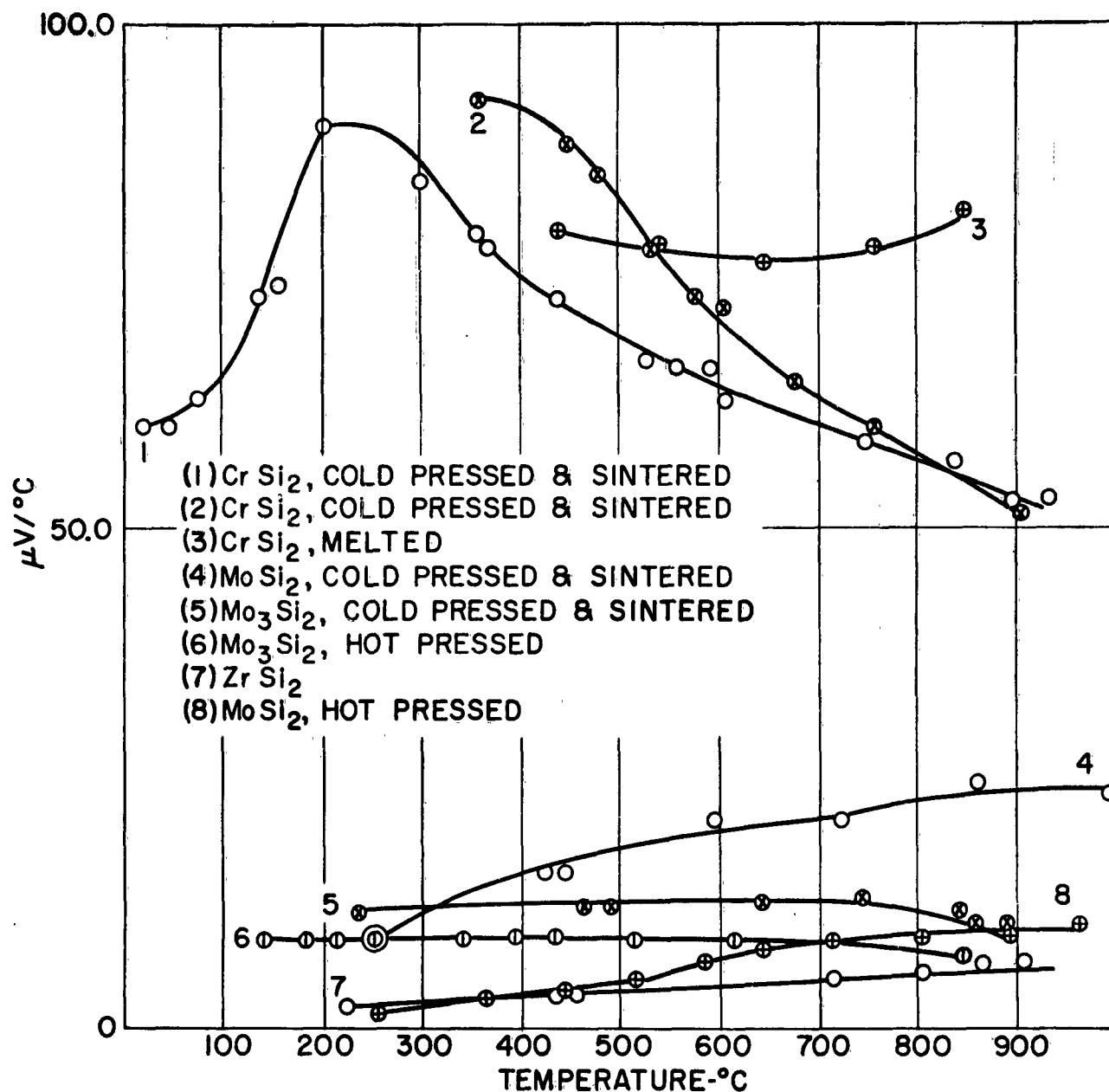


Figure G-7: Temperature Dependence of Seebeck Voltage for Silicides.

This behavior also was observed in Cr_3C_2 which contains C-C linkages. The directional variation in properties would be evidence of the importance of non-metal to non-metal bonding. Further effort was directed towards the investigation of silicides which already had shown some promise.

The silicides for this part of the investigation were prepared by mixing silicon and metal powders, cold pressing and sintering in an argon atmosphere. The silicon used, either an impure or a pure (99.95%) silicon, was designated in each case. The temperature dependence of Seebeck voltage of several disilicides are shown in Fig. G-8. A MnSi_2 composition had the highest Seebeck voltage. The Seebeck voltage of several monosilicides, shown in Fig. G-9 along with the room temperature values reported by others^(G-3), were lower than the disilicides. Solid solutions of the disilicides, shown in Fig. G-10, were intermediate between the values for the disilicides along. The addition of impurities to the CrSi_2 , shown in Fig. G-11 and to the MnSi_2 , shown in Fig. G-12, did not result in significant increases in the Seebeck voltage. The Seebeck voltage of two types of silicon are shown in Table G-3.

The room temperature resistivities of CrSi_2 compositions and MnSi_2 compositions are shown in Table G-4 and G-5, respectively.

The maximum Seebeck voltage of the various disilicides along with some other properties are shown in Table G-6. There appears to be some correlation between radius of the metal atom and Seebeck voltage. No correlation exists between crystal structure and Seebeck voltage, however. The crystal structures of CrSi_2 , MoSi_2 , and TiSi_2 are related in an interesting way^(G-6). The layers themselves are close-packed, but superimposed in such a way that the whole structure is not close-packed as shown in Fig. G-13. Each atom has ten nearest neighbors instead of 12 in cubic close-packed structure. The difference is in the number of layers making up the repeat unit.

The maximum Seebeck voltage of monosilicides, along with values reported by others^(G-3) are shown in Table G-7. These data indicate a wide variation in Seebeck voltage despite the fact they are isomorphous. If similarities in structure are important, at least impurity effects mask them.

FIGURE OF MERIT AND EFFICIENCY

Using room temperature values of electrical and thermal conductivity^(G-3), a tentative figure of merit and efficiency can be calculated if it is assumed that the ρ K does not change appreciably at higher temperatures. The temperature dependence of electrical and thermal conductivity which has been reported^(G-7) indicates this is a reasonable assumption. The figure of merit and efficiency of several silicide compositions are given in Table G-8. These values are high enough to warrant further investigation of the silicides.

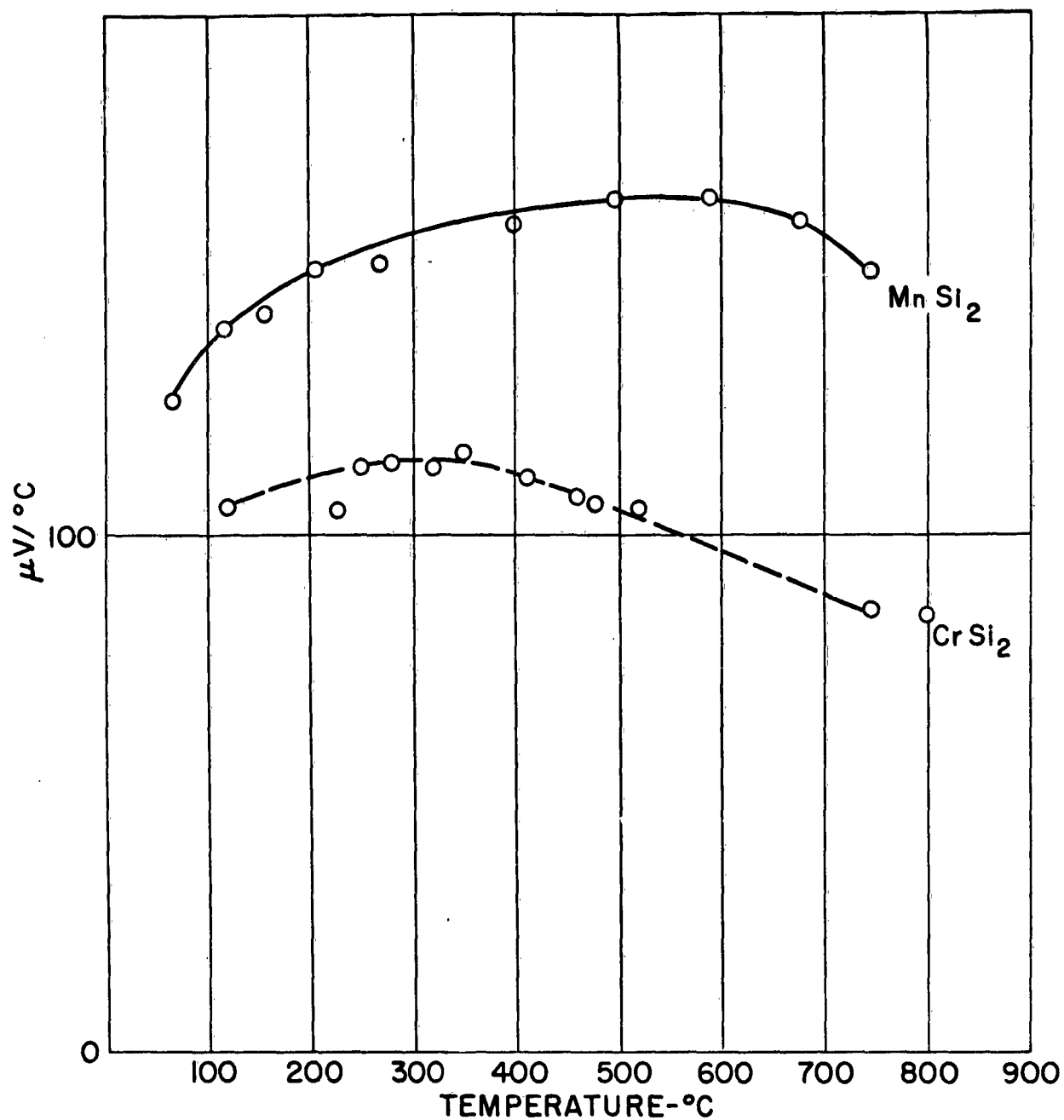


Figure G-8: Seebeck Voltage of Disilicides as a Function of Temperature.

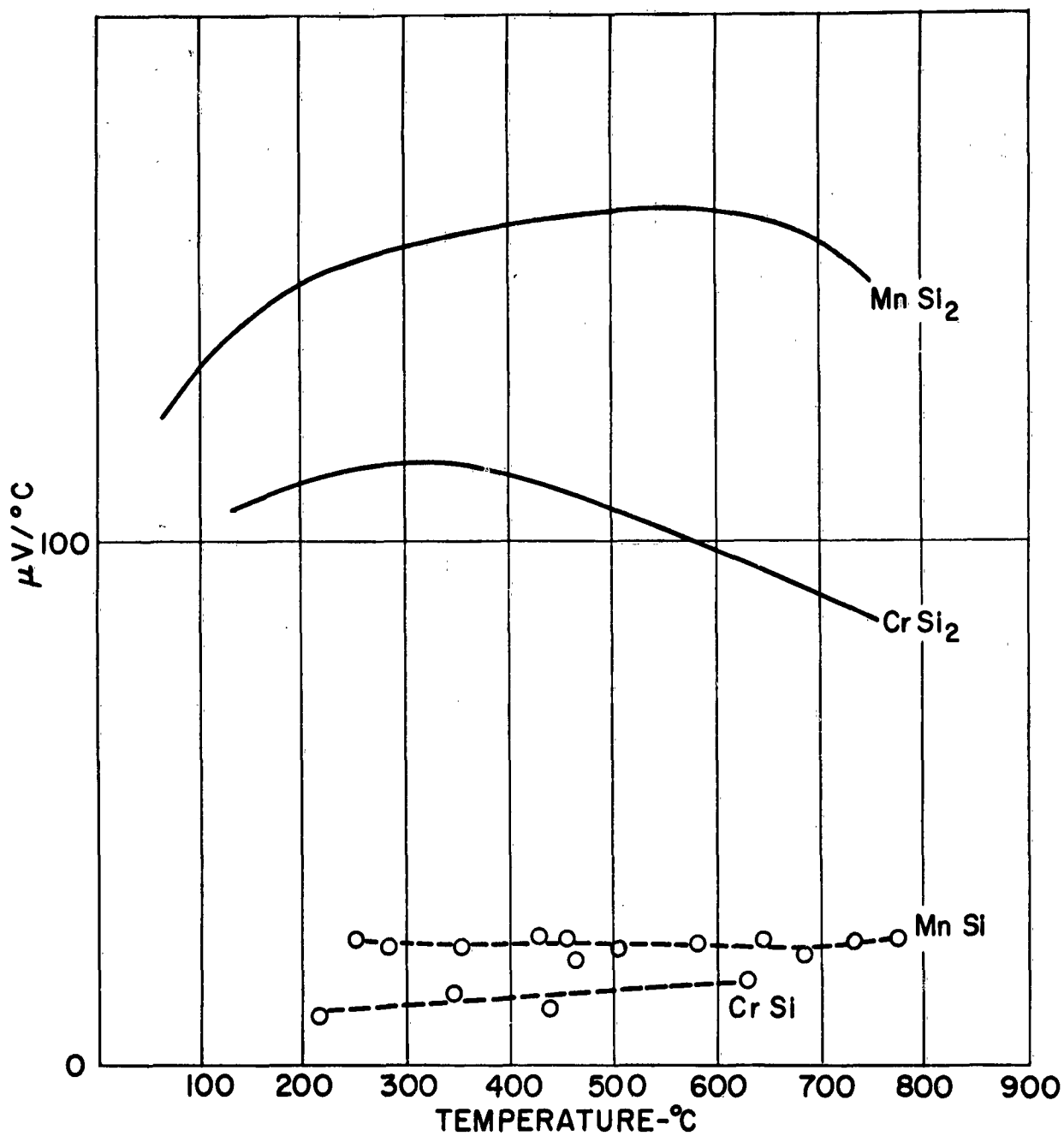


Figure G-9: Seebeck Voltage of Monosilicides.

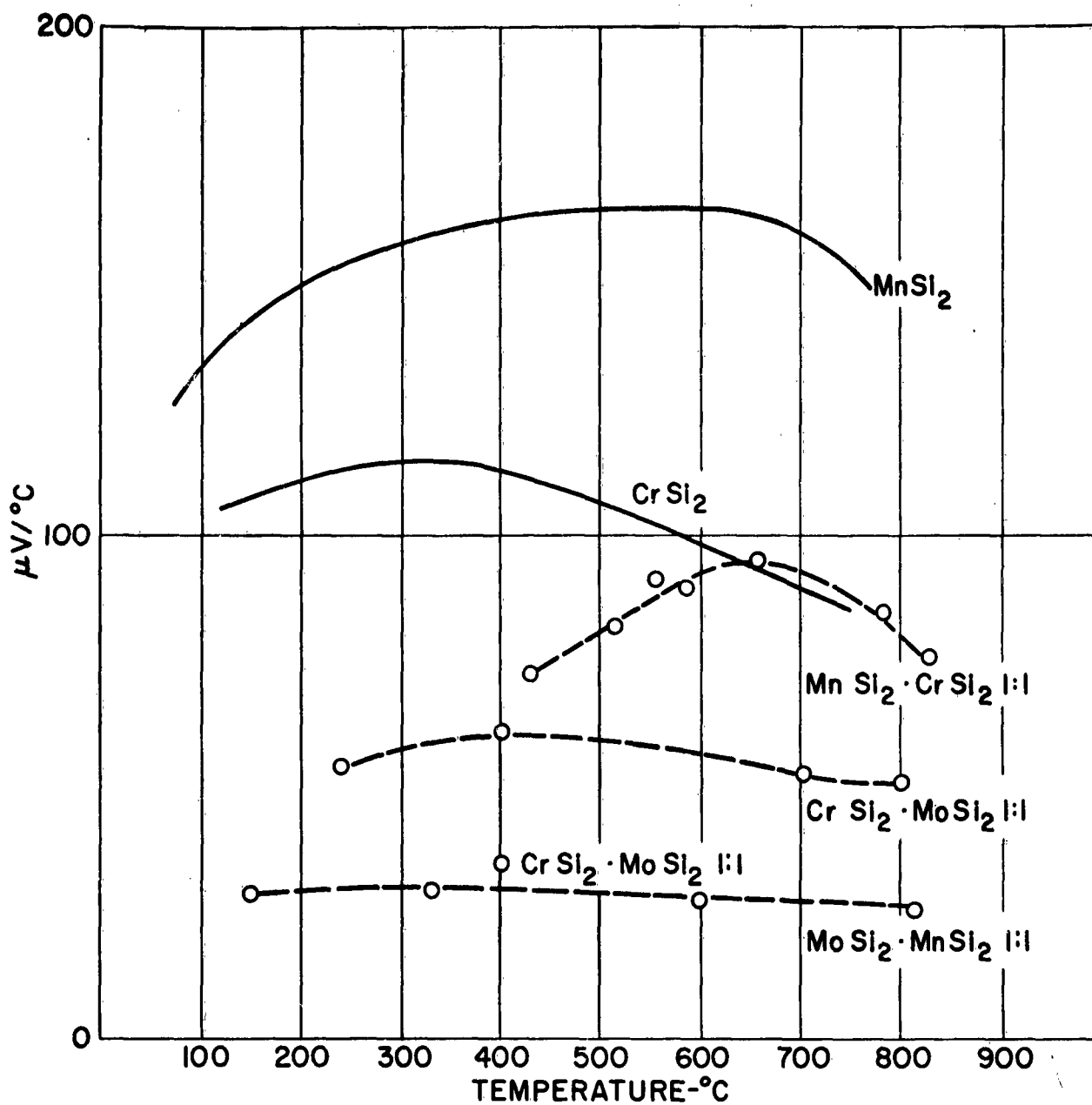


Figure G-10: Seebeck Voltage of Solid Solutions of the Disilicides.

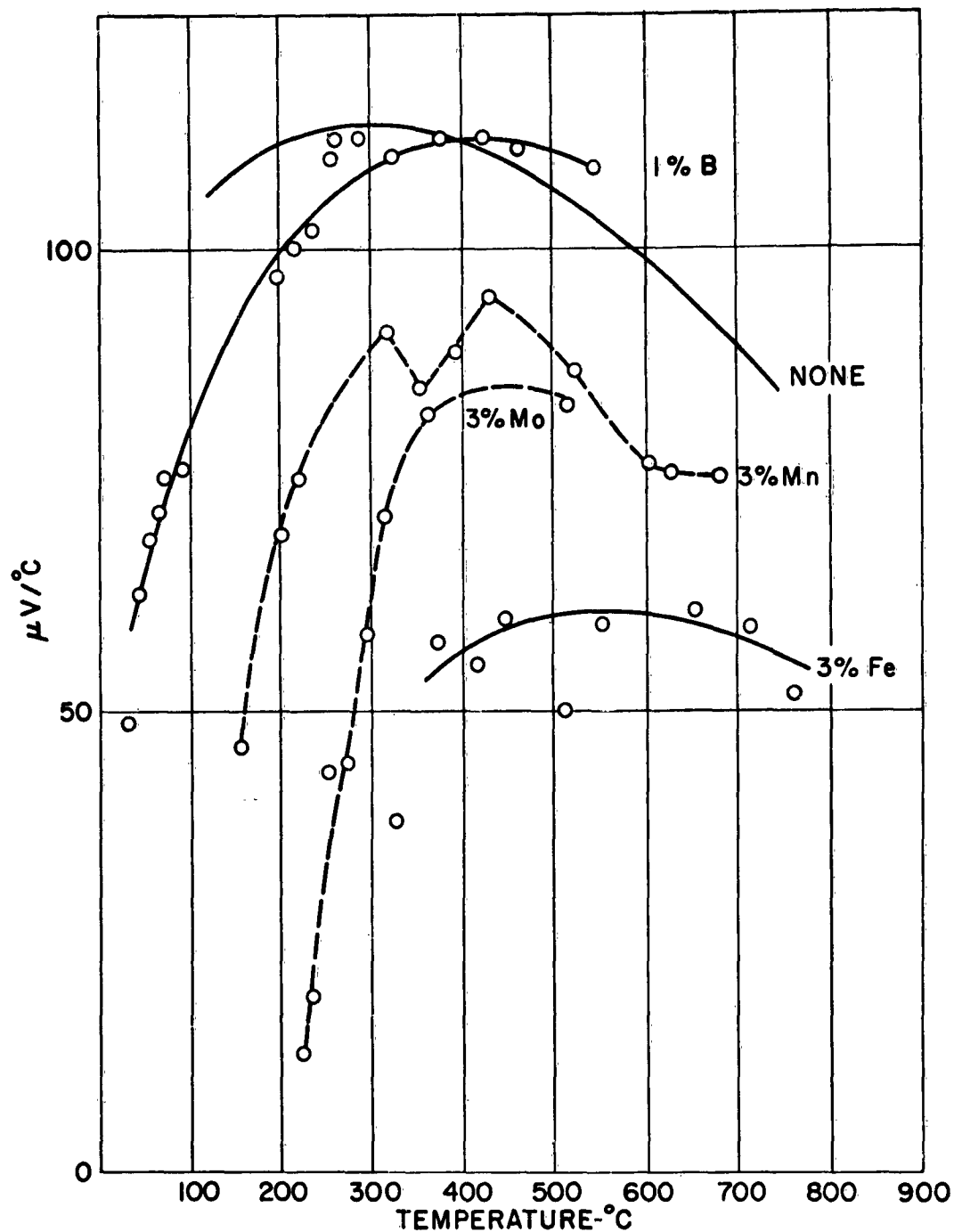


Figure G-11: Effect of Impurities on the Seebeck Voltage of Chromium Disilicide.

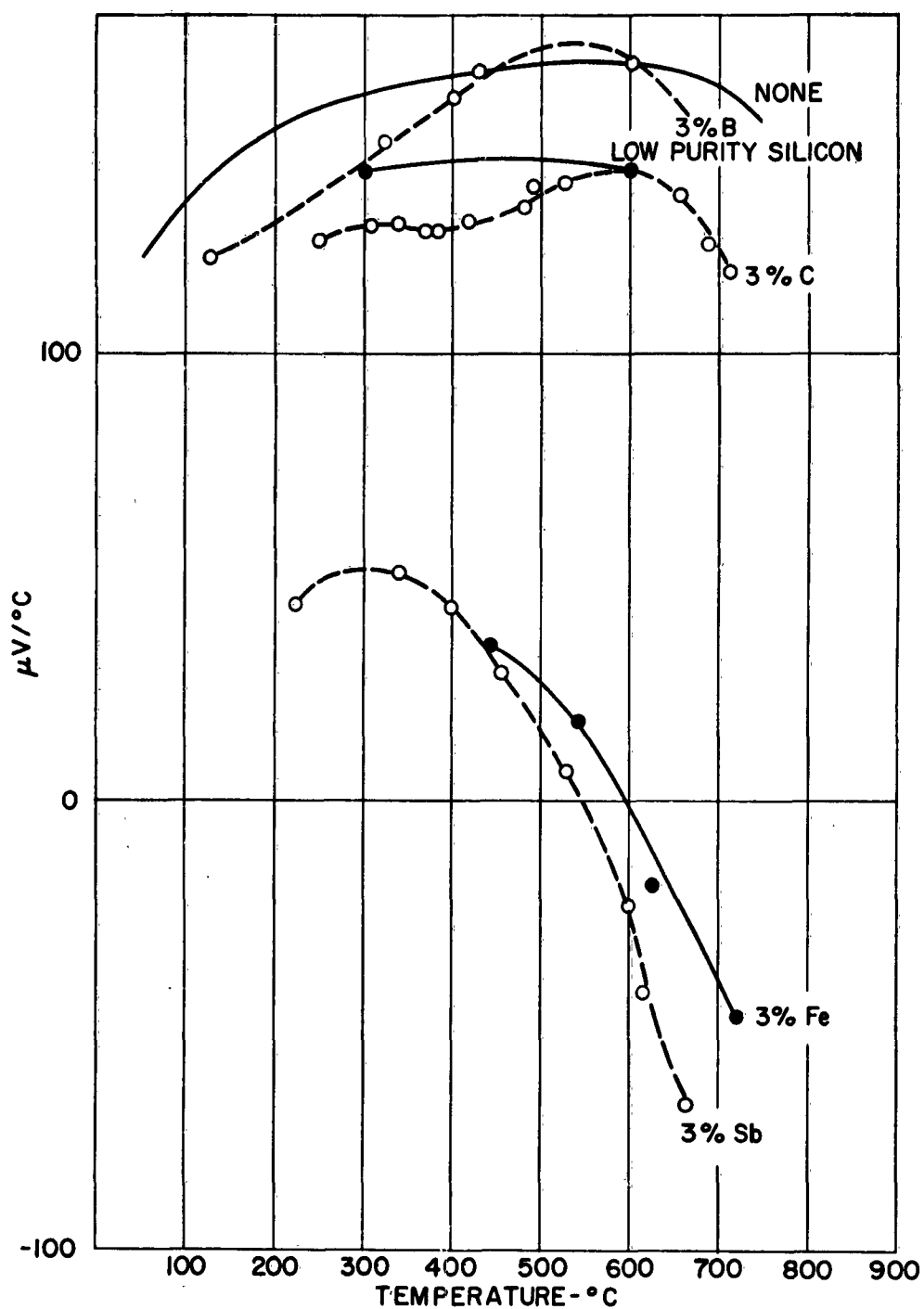


Figure G-12: Effect of Impurities on the Seebeck Voltage of Manganese Disilicide.

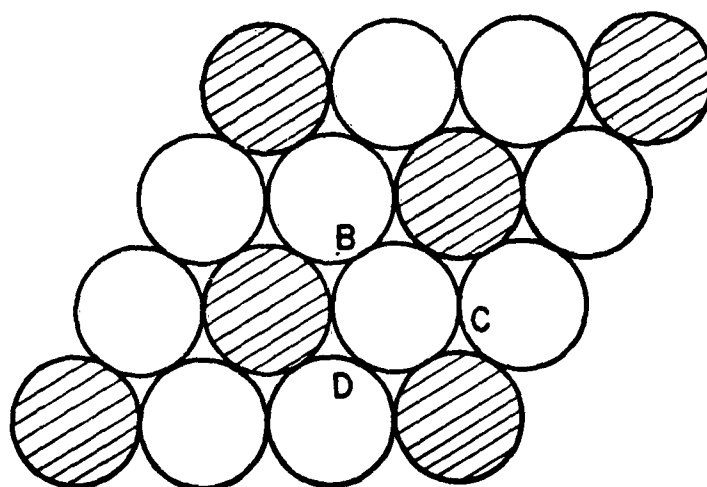


Figure G-13: Close-packed Layers in Some Disilicides.

REFERENCES

- G-1 P. Schwarzkopf and R. Kieffer, "Refractory Hard Metals", New York MacMillan Company, (1953)
- G-2 N. V. Kolomvets, et al., Zhur Tekh. Fiz., 28 (1) 2382 (1958)
- G-3 E. N. Nikitin, Zhur. Tekh. Fiz., 28 (1) 26 (1958)
- G-4 G. Hagg, Z. Phys. Chem. (B) 6 221 (1930)
- G-5 G. Hagg, Z. Phys. Chem. (B) 12 33 (1931)
- G-6 A. F. Wells, "Structural Inorganic Chemistry", Oxford University Press, Loudon (1952)
- G-7 E. N. Nikitin, Zhur, Tekh. Fiz. 28 (1) 23 (1958)

Table G-1

PROPERTIES OF SOME REFRACTORY CARBIDES, BORIDES, NITRIDES, AND SILICIDES

	<u>Compound</u>	<u>Resistivity*</u> <u>microhm - cm</u>	<u>Thermal Conductivity</u> <u>watts/cm</u>	<u>Melting Point</u> <u>°C</u>
<u>Carbides:</u>	NbC	74	0.14	3500
	TaC	20	0.22	3880
	TiC	105	0.17	3250
	ZrC	63.4	0.20	3175
	Mo ₂ C	97	---	2690
<u>Borides:</u>	TiB ₂	15 - 28	0.261	2980
	ZrB ₂	9.2 - 38.8 87.6 (1600°C) 118.2 (2305°C) 139.1 (2635°C)	0.23	3040
	NbB ₂	28 - 65	0.17	2900
	TaB ₂	68 - 86	0.11	3000
	Mo ₂ B	40	---	2180
	MoB	25	---	2100
	MoB	45	---	
	TaN	135 117.3 (2840°C)	---	3090
	ZrN	11.5 - 160 320 (2980°C)	---	2980
<u>Nitrides:</u>	NbN	200 450 (2050°C)	---	2050
	TiN	21.7 - 130 340 (2930°C)	---	2930

*Room temperature unless otherwise specified

Table G-1 (Continued)

PROPERTIES OF SOME REFRACTORY CARBIDES, BORIDES, NITRIDES, AND SILICIDES

	Compound	Resistivity* microhm - cm	Thermal Conductivity watts/cm	Melting Point °C
Silicides:	TaSi ₂	8.5	---	2400
	WSi ₂	33.4	---	2150
	NbSi ₂	6.3	---	1950
	MoSi ₂	21.5	---	1870
	CrSi ₂	---	---	1570
	TiSi ₂	123	---	1540
	ZrSi ₂	161	---	1520

*Room temperature unless otherwise specified

Table G-2

RADIUS RATIOS OF A NUMBER OF REFRACTORY CARBIDES,
BORIDES, NITRIDES, AND SILICIDES

Metal	Radius Ratios			
	Si (1.17 Å)	B (0.87 Å)	N (0.71 Å)	C (0.76 Å)
Ni (1.24 Å)	0.94	0.70	0.57	0.62
Co (1.25 Å)	0.94	0.70	0.57	0.61
Fe (1.26 Å)	0.93	0.69	0.56	0.60
Mn (1.26 Å)	0.93	0.69	0.56	0.60
Cr (1.27 Å)	0.92	0.69	0.56	0.60
V (1.34 Å)	0.88	0.65	0.53	0.57
Mo (1.39 Å)	0.84	0.63	0.51	0.55
W (1.39 Å)	0.84	0.63	0.51	0.55
Ti (1.47 Å)	0.80	0.59	0.48	0.52
Nb (1.46 Å)	0.80	0.60	0.49	0.53
Ta (1.46 Å)	0.80	0.60	0.49	0.53
Zr (1.60 Å)	0.73	0.58	0.44	0.48

Table G-3

SEEBECK VOLTAGE OF TWO GRADES OF SILICON USED IN THE STUDY

<u>Technical Grade Silicon</u>		<u>High Purity Silicon</u>	
<u>Temperature °C</u>	<u>Seebeck Voltage μV/°C</u>	<u>Temperature °C</u>	<u>Seebeck Voltage μV/°C</u>
350	- 360*	450	+ 300
415	- 325	500	+ 370
490	- 300	600	+ 310
515	- 260	645	+ 290

*Represent the average of at least two values

Table G-4

ROOM TEMPERATURE RESISTIVITIES OF COMPOSITIONS
BASED ON CHROMIUM SILICIDES

<u>Material*</u>	<u>Room Temperature Resistivity** ohm-cm</u>
CrSi ₂	2 x 10 ⁻³
CrSi ₂ + 1% B	3 x 10 ⁻³
CrSi ₂ + 3% Fe	3 x 10 ⁻³
CrSi ₂ + 3% Mn	5 x 10 ⁻³
CrSi ₂ + 3% Mo	4 x 10 ⁻³
CrSi	6 x 10 ⁻⁴

*Prepared from high purity silicon
by synthesis from the elements

**Resistivity measurements varied considerably
with treatment. The macro and microstructure
differed from specimen to specimen.

Table G-5

ROOM TEMPERATURE RESISTIVITY OF COMPOSITIONS
BASED ON MANGANESE DISILICIDE

<u>Material</u>	<u>Room Temperature Resistivity (ohm-cm)</u>
MnSi ₂	5×10^{-4}
MnSi ₂ (prepared from low purity silicon)	2×10^{-3}
MnSi ₂ + 3% B	3×10^{-3}
MnSi ₂ + 3% C	8×10^{-3}
MnSi ₂ + 3% Fe	5×10^{-3}
MnSi ₂ + 3% Sb	2×10^{-3}

Table G-6

MAXIMUM SEEBECK VOLTAGE OF VARIOUS DISILICIDES

<u>Material</u>	<u>Maximum Seebeck Voltage</u>	<u>Crystal Structure</u>	<u>Radius of Metal Atom</u>	<u>Layer Repeat Unit</u>
MnSi ₂	180	tetragonal	1.26	
CrSi ₂	120	hexagonal	1.27	3
MoSi ₂	30	tetragonal	1.39	2
TiSi ₂	10	orthorhombic	1.47	4
CoSi ₂	30	CaF ₂	1.25	

Table G-7

MAXIMUM SEEBECK VOLTAGE OF VARIOUS MONOSILICIDES

<u>Material</u>	<u>Seebeck Voltage Reported in this Study</u>	<u>Seebeck Voltage Reported by Russian Investigators</u>	
MnSi	+ 25	+ 102	(+ 51)*
CoSi		- 46	(- 33)
FeSi		+ 9	(- 1)
CrSi	+ 17	+ 5	(+ 10)
MiSi		+ 8	(+ 13)

*Values in parenthesis for silicides prepared from technical grade silicon

Table G-8

FIGURE OF MERIT AND EFFICIENCY OF SEVERAL SILICIDE COMPOSITIONS

	<u>MnSi₂</u>	<u>CrSi₂</u>	<u>MoSi₂</u>
T ₁ , hot junction temperature, °K	1000	1300	1500
T ₂ , cold junction temperature, °K	300	300	300
α avg., μV/°K	150	70	20
ρ ohm-cm, room temperature	5.4 x 10 ⁻⁴	1.47 x 10 ⁻³	2.15 x 10 ⁻⁵
K, watts/cm °K, room temperature	0.06*	0.060	0.47
Z, (°K ⁻¹) **	7 x 10 ⁻⁴	5.6 x 10 ⁻⁵	4 x 10 ⁻⁵
n _{opt} , %	9.7	1.4	1.2
$\frac{P}{V_t \text{ max.}}$ *** watts/cm ³ **	5.1	0.83	6.7

*Assumed value

**Based on room temperature values of ρ and K

***V_t is volume of thermoelectric materials assuming elements 1 cm. in length

APPENDIX H - SOME PRELIMINARY RESULTS IN THE STUDY OF OXIDE THERMOELECTRIC GENERATOR MATERIALS

John R. Gambino

July 1958

INTRODUCTION

The purpose of this appendix is (1) to summarize preliminary results in the study of oxide thermoelectric generator materials and (2) to demonstrate the usefulness of an experimental technique which has been used to determine the qualitative effects of various parameters in simple but rapid screening tests.

In work on oxide materials reported in the literature, the effect of numerous additives on the thermoelectric power of several oxides has been investigated. In addition, the influence of non-stoichiometry has been recognized. The state of aggregation, such as crystallinity, etc., should not in itself affect thermoelectric power but should influence electrical and thermal conductivity considerably. In many instances, thermoelectric power measurements have been used in conjunction with other types of measurements to elucidate the electronic structure of metal oxides. The present knowledge of oxidic semiconductors is such that existing theories are not generally applicable as a guide in developing a thermoelectric material.

The general approach taken in this work is that oxides with high thermoelectric powers in the pure state can be made more useful for generator applications if the means could be found to lower the resistivity without lowering the thermoelectric power. Chromium oxide was chosen for intensive study because its properties obtained in a preliminary literature survey (based on mismatched data) indicated that it was most attractive of the oxides for this application. In addition, this oxide was reported to be a "transition" semiconductor, one containing equivalent amounts of electrons and electron defects, a class of semiconductors which includes Co_3O_4 and CuO , two other oxides of interest for thermoelectric power applications. The conductivity of these materials reportedly increases with additions of high and lower valency cations. Additives were chosen having ionic radii comparable to Cr^{3+} to enhance solid solution and included higher and lower valency ions.

MATERIALS AND METHODS

Materials were prepared from C.P. chemicals. Additives were introduced as oxides or as salts which decomposed on heating into oxides. In experiments designed to study the time dependence of emf changes with interaction, a slurry of the constituents were agitated in a "Waring Blendor" to attain homogeneity in the product. Otherwise, the constituents were simply milled, reacted at the appropriate temperature, and milled again before recycling or pressing.

Pressed compacts coated on opposite faces with platinum paste were placed between platinum-platinum-10% rhodium foil. Powder samples, used when compacts could not be easily formed, were placed in vycor tubing between ceramic rods capped with the foil. The emf was measured with a G.E. potentiometric recorder. The temperature and differential temperature was measured using platinum-platinum-10% rhodium couples. The ends of the differential couples were inserted in magnesium silicate plates. It was recognized that the differential temperature was subject to considerable error. Because of the thermal resistance, the values obtained in

this study were generally lower than those reported in the literature for similar materials and consistent with the thermocouple placement. Reproducibility was good, however, and valid comparisons of the behavior of different compositions are possible since the errors are systematic.

RESULTS

The Seebeck voltage of the pure oxides studied in the temperature range 595 to 925°C are given in Table H-1. The data is for samples heated above 900°C and equilibrated thermally as well as with respect to oxygen pressure. Although thermal equilibrium was attained in five minutes, changes in emf due to defect structure changes required up to one hour. In the extreme case, Cu₂O heated at 700°C, increased from 400 to 850 $\mu\text{V}, ^\circ\text{C}^{-1}$ in three hours without equilibrating.

The Seebeck voltage per degree of Cr₂O₃ compacts made with various additives are shown in Table H-2. There is the possibility that some of these additives such as MgO and CoO did not react completely with the Cr₂O₃ in the times and temperature studied, since a small change in emf was observed. In other systems, there was a distinct possibility of formation of a second phase such as a ZnO-Cr₂O₃ when ZnO was added.

Several reactions of this latter type were studied in order to ascertain the effect of the second phase on the observed voltage and the time for the reaction to come to completion. In these studies, the change of Seebeck voltage of compacts was measured as a function of time. The individual oxides were previously calcined separately. The results found in the system ZnO-Cr₂O₃ and ZnO-Fe₂O₃ are shown in Table H-3 and H-4. A reaction profile is shown in Figure H-1 for ZnO and Fe₂O₃ at the temperature 760°C. The change of emf with time appears to follow some simple relationship, apparently connected with extent of reaction. Some preliminary attempts to derive kinetic data from these results will be described later. X-ray examination of the products at various stages have been made as an independent check.

The changes in Seebeck voltage with time of compositions containing 2 mole % ZnO are shown in Table H-5. The equilibrium values of these reactions and the previous ones in a 1:1 molar ratio are summarized in Table H-6. It is evident from these results that in the temperature range studied, reactions which form a second phase or diffusion processes are essentially complete in a few hours. The influence of stoichiometry (and crystallinity) on Seebeck voltage is evident by the change observed on heating uncalcined powders and equilibration (of defects) of calcined powders. A few selected examples are shown in Table H-7.

Some resistivity measurements were made on pressed compacts of oxides by applying a known voltage across the sample (using a regulated DC power supply) and measuring the voltage across a known shunt in series. The resistivity of some compositions, such as the Cr₂O₃ shown in Table H-8, decreased to values for which contact resistance could constitute a large part of the total measured resistance. This technique must, therefore, be supplemented in the low conductivity ranges by other methods in which contact resistance can be neglected.

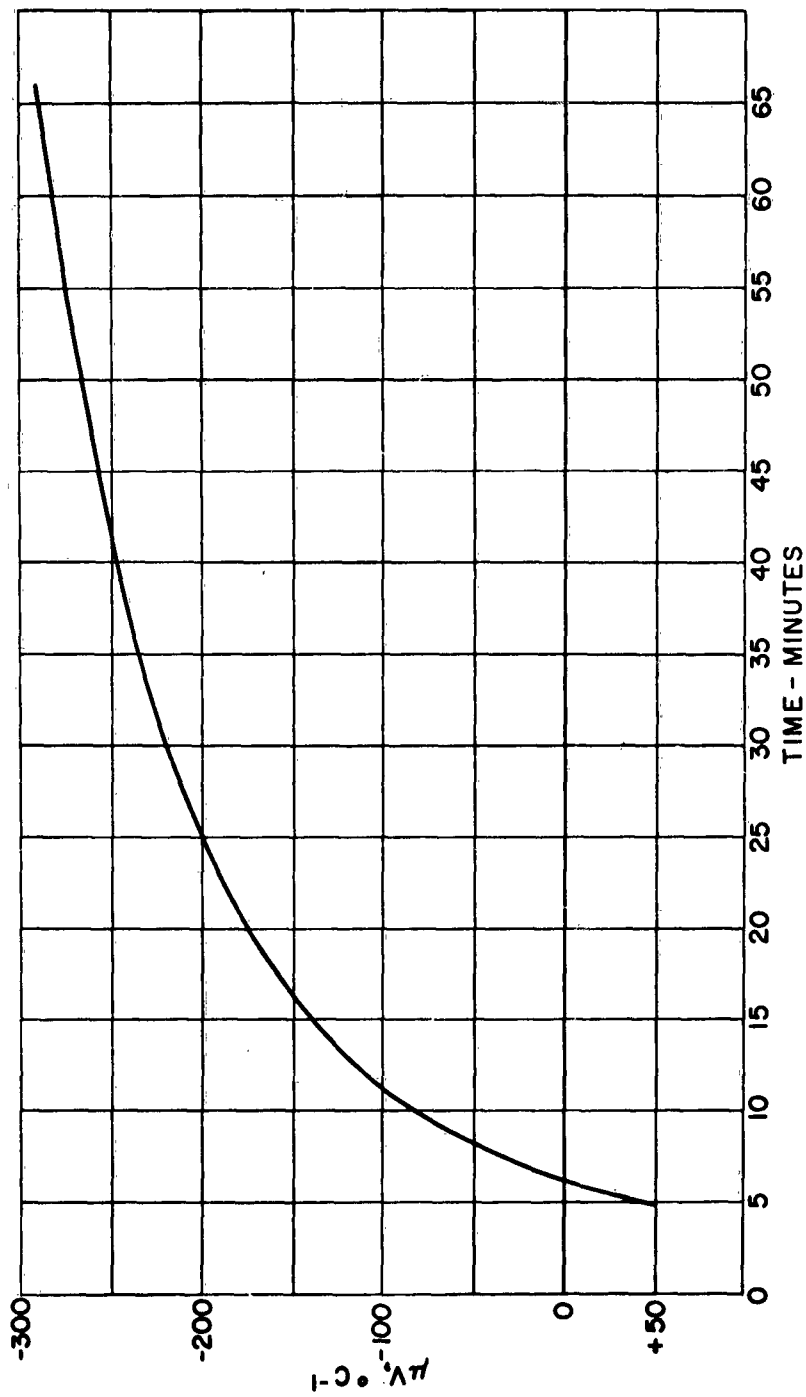


Figure H-1: Seebeck Voltage as Function of Time During Reaction of ZnO and Fe₂O₃.
T = 760°C

DISCUSSION OF RESULTS

The measurements of the time dependence of the Seebeck voltage were made originally to detect the presence of a second phase which could effectively mask the real value of a solid solution. Such a second phase could result from inhomogeneity caused by poor mixing or slow reactions. The utility of the method for obtaining the qualitative effects of various parameters and as a screening method become apparent. For instance, impurities should be studied over a wide range of composition which would necessitate large numbers of sample preparations if a representative number of oxides and impurities are studied. In systems involving only solid solutions, monotonically increasing or decreasing emf would indicate that no intermediate concentration of additives having a maximum effect on emf exists. The same qualitative results are possible in studying the effect of non-stoichiometry using an appropriate atmosphere instead of impurities.

If a large excess of impurities A are added to an oxide B, solid-solution would be expected until the solubility limit was reached at which time a second phase A_xB_y would appear.

It will be convenient to illustrate the manner in which quantitative interpretation of emf changes is possible based on chemical interaction by using systems in which a second phase, C, is formed. The measured voltage V as a function of time can be translated to the dependence of l_C , the thickness of the product layer by the expression:

$$V^0 - V = \frac{\Delta T}{2L^0} \left[\alpha_A n_A + \alpha_B n_B - 2\alpha_C n_C \right] l_C$$

where V^0 is the initial voltage

$\frac{\Delta T}{2L^0}$ is the temperature gradient assumed to be linear

α_K are the Seebeck coefficients for the reactants and products

n_K are the number of particles in a line normal to the electrodes

It is assumed that the molar volumes are approximately equal and the contribution of solid solution is negligible or at least constant. The rate of change might be reasonably expected to follow a parabolic law, i.e., depend on the thickness of the product layer. The variation of $(V^0 - V)^2 \simeq (l_C)^2$ in the reaction $ZnO-Cr_2O_3$ was observed to be approximately proportional to time at temperatures about 705°C. Reactions in the system $ZnO-Fe_2O_3$ appeared to obey a third power rather than a second power relationship.

Similar treatments can be used in analyzing emf changes which occur during changes in stoichiometry and reactions involving only solid solution formation.

TABLE H-1

SEEBECK VOLTAGE PER DEGREE OF VARIOUS OXIDES
AS A FUNCTION OF TEMPERATURESeebeck Voltage ($\mu\text{V}, ^\circ\text{C}^{-1}$) At Temperature $^\circ\text{C}$

<u>Material</u>	<u>595</u>	<u>650</u>	<u>705</u>	<u>760</u>	<u>815</u>	<u>870</u>	<u>925</u>
Cr_2O_3	570	540	530	530	500	490	480
Co_3O_4	330	370	440	460	450	480	-
NiO	290	300	320	330	340	370	-
ZnO	-	-	30	130	190	-	-
Cu_2O	700	-	850	-	690	-	750
Fe_2O_3	-	-	210	200	170	140	110

TABLE H-2

SEEBECK VOLTAGE OF Cr_2O_3 COMPOSITIONS AS A FUNCTION OF TEMPERATURESeebeck Voltage ($\mu\text{V}, ^\circ\text{C}^{-1}$) At Temperature $^\circ\text{C}$

<u>Additive 1 Cation %</u>	<u>595</u>	<u>650</u>	<u>705</u>	<u>760</u>	<u>815</u>	<u>870</u>	<u>925</u>
None	570	540	530	530	500	490	480
MgO	310	310	310	320	320	330	340
CoO	380	-	340	-	330	-	330
ZrO_2	190	200	190	-	250	-	-
Li_2O	-	-	230	-	240	-	240
ZnO	-	-	320	230	-	-	-
SnO_2	-	-	-	-	280	-	-
TiO_2	-	-	-	-	-	-	230

TABLE H-3

SEEBECK VOLTAGE OF ZnO AND Cr₂O₃ POWDER MIXTURES AS A FUNCTION OF TIMESeebeck Voltage ($\mu\text{V}, ^\circ\text{C}^{-1}$)

<u>Time</u> <u>Min.</u>	<u>716°C</u>	<u>750°C</u>	<u>816°C</u>
1	440	550	390
2	420	490	335
3	405	455	315
4	395	430	290
5	385	420	-
6	380	420	-
7	375	410	280
8	370	400	-
9	365	390	-
10	360	390	-
15	360	385	-
20	350	375	-

TABLE H-4

SEEBECK VOLTAGE OF ZnO AND Fe₂O₃ POWDER MIXTURES AS A FUNCTION OF TIMESeebeck Voltage ($\mu\text{V}, ^\circ\text{C}^{-1}$)

<u>Time</u> <u>Min.</u>	<u>650°C</u>	<u>705°C</u>	<u>760°C</u>
5	-	585	- 85
10	-	460	-140
15	-	340	-180
20	-	280	-200
25	230	180	-220
30	220	120	-230
35	-	90	-250
40	200	60	-250
50	180	-	-
80	130	-	-
100	100	-	-

TABLE H-5

CHANGE IN SEEBECK VOLTAGE OF ZnO DURING HEATING
WITH 2 MOLE % Fe_2O_3 AT 760°C

Seebeck Voltage ($\mu\text{V}, ^\circ\text{C}^{-1}$)

Time (Min.)

5	210
10	275
15	290
20	295
25	300

TABLE H-6

SEEBECK VOLTAGE OF REACTED OXIDE MIXTURES

Seebeck Voltage ($\mu\text{V}, ^\circ\text{C}^{-1}$)

<u>Material</u>	<u>590</u>	<u>650</u>	<u>705</u>	<u>760</u>	<u>815</u>	<u>870</u>	<u>925</u>
ZnO + 2 mole % Cr_2O_3	-	-	-	360	395	400	-
Cr_2O_3 + 2 mole % ZnO	-	-	-	360	-	-	-
ZnO · Cr_2O_3	420	-	390	-	360	-	470
ZnO · Fe_2O_3	-	-	100	-	255	-	280

TABLE H-7

EFFECT OF STOICHIOMETRY ON SEEBECK VOLTAGE OF SELECTED OXIDES

Seebeck Voltage ($\mu\text{V}, ^\circ\text{C}^{-1}$)

<u>Material</u>	<u>ZnO</u>	<u>Fe₂O₃</u>
<u>Temperature $^\circ\text{C}$</u>	<u>815</u>	<u>815</u>
<u>Time (Min.)</u>		
5	220	-
10	185	-
15	160	-
20	150	10
25	140	30
30	140	45
35	130	60
40	120	70

TABLE H-8

RESISTIVITY OF Cr_2O_3 AS A FUNCTION OF TEMPERATURE

<u>Temperature $^\circ\text{C}$</u>	<u>ρ, ohm-cm</u>
310	34.0
400	18.0
520	11.0
560	9.7
600	9.0
660	8.0
710	7.5
770	7.0
820	6.5
880	6.0

APPENDIX I - SEEBECK VOLTAGE AND RESISTIVITY OF COMPOSITIONS BASED ON CHROMIUM OXIDE

John R. Gambino

September, 1958

INTRODUCTION

This appendix summarizes data on the temperature dependence of Seebeck voltage and resistivity for compositions based on chromium oxide. Experimental results obtained primarily to perfect the method of following the time-dependence of Seebeck voltage will not be presented here but will be reported on at a later date. The results will be presented in a manner to show the usefulness of these compositions as thermoelectric generator materials; the significance of the results in enlarging on the present knowledge of the electronic structure of Cr_2O_3 and the development of compositions based on this knowledge will be reported later when more results are available.

MATERIALS

Compositions were prepared from C.P. chemicals. Additives were made as oxides or as salts which decomposed on heating to oxides. Oxide additives were mixed as an alcohol slurry in a "Waring Blendor", filtered, and dried, before pressing and heating to obtain reaction.

EXPERIMENTAL METHODS

The pressed compacts were painted with platinum paste for both resistivity and Seebeck voltage measurements. For Seebeck voltage measurements the samples were placed between two platinum sheets which had platinum-platinum 10% rhodium thermocouples attached to their outer surfaces. The temperature of each surface was measured and the ΔT obtained by difference. The end temperatures and the Seebeck emf, using the platinum leg of the thermocouple, were measured with a G.E. precision potentiometer. The ΔT ranged from 10 to 50°C depending on the specimen size and temperature.

A G.E. double bridge was used for measuring resistivity. Four platinum lead wires were attached to two platinum sheets for this method. This arrangement eliminated lead wire resistance but not contact resistance which can be neglected in most instances.

The errors inherent in these methods will be discussed in a later section.

RESULTS

Resistivity measurements were made in air between 550 and 1500°C. The temperature dependence of resistivity is shown for convenience in three parts, Figure I-1 to I-3, according to the valency of the additive cation. Thus, the resistivity of compositions made with cation additives in a valency state greater than 3 are shown in Figure I-1 and those with cations less than 3 are shown in Figure I-2. (The fact that the normal valency in the additive oxide has a certain

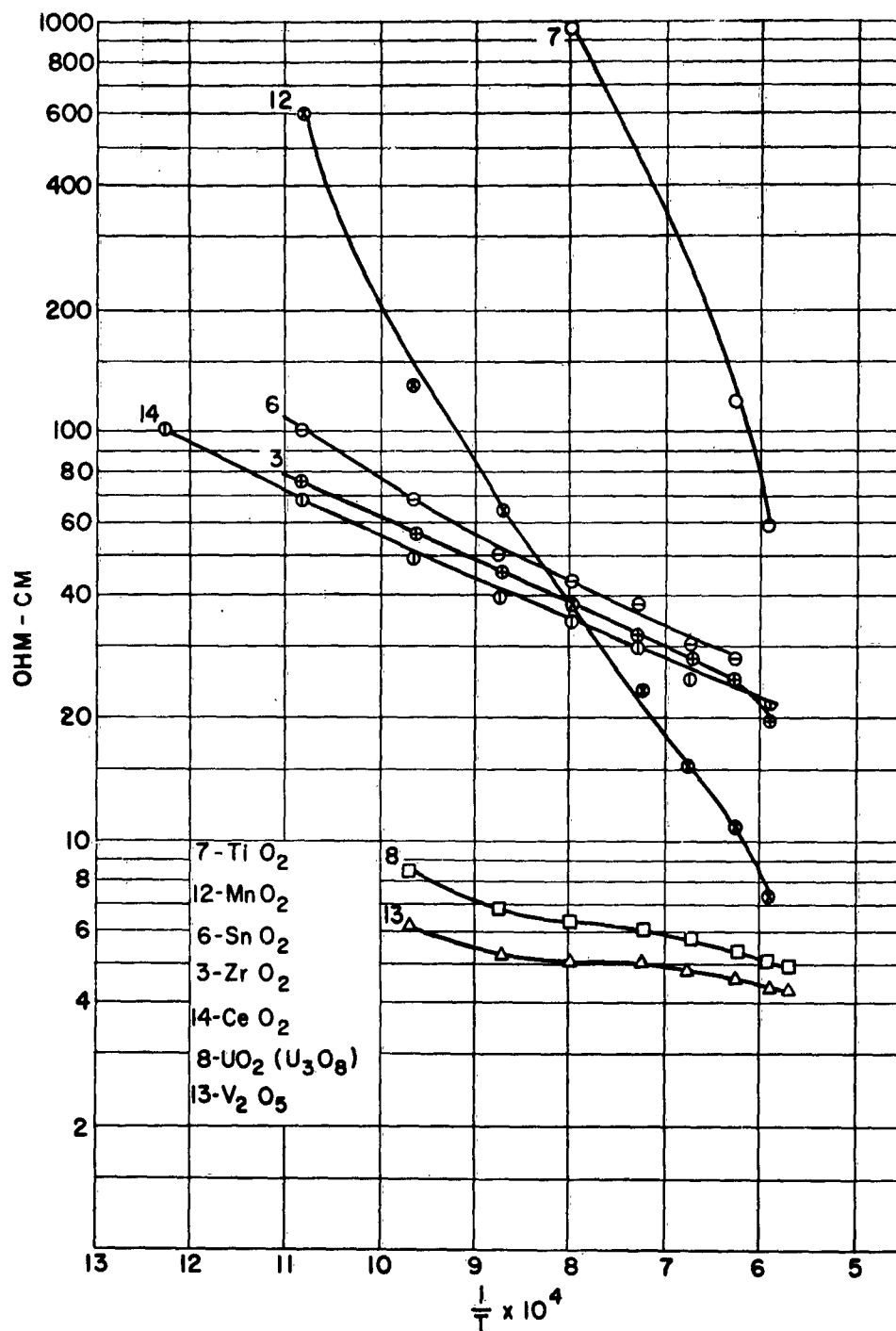


Figure I-1: Temperature Dependence of Resistivity
Containing 1 Mole % Additives Having
Valency > 3.

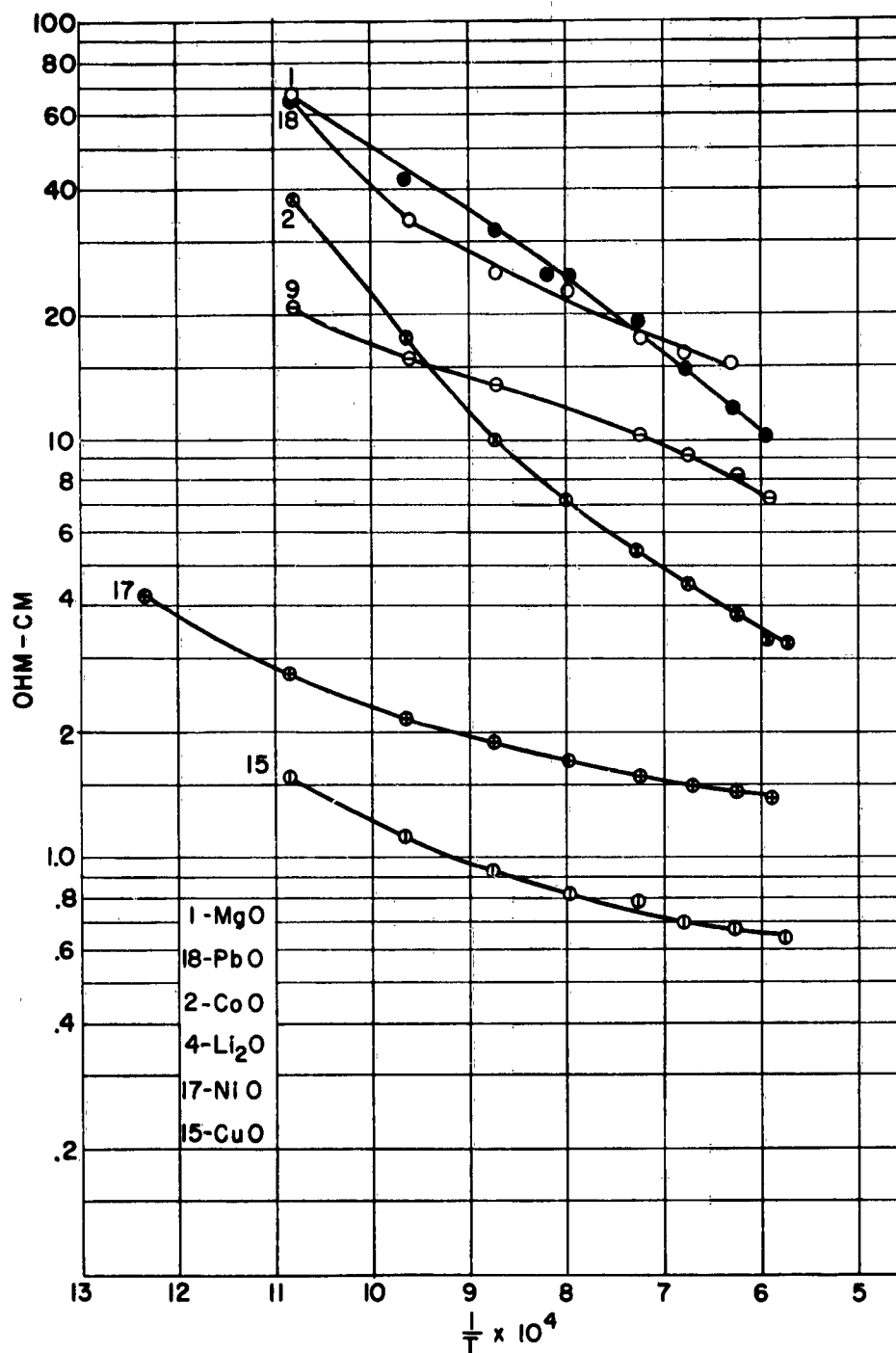


Figure I-2: Temperature Dependence of Resistivity
Containing 1 Mole % Additives Having
Valency <3.

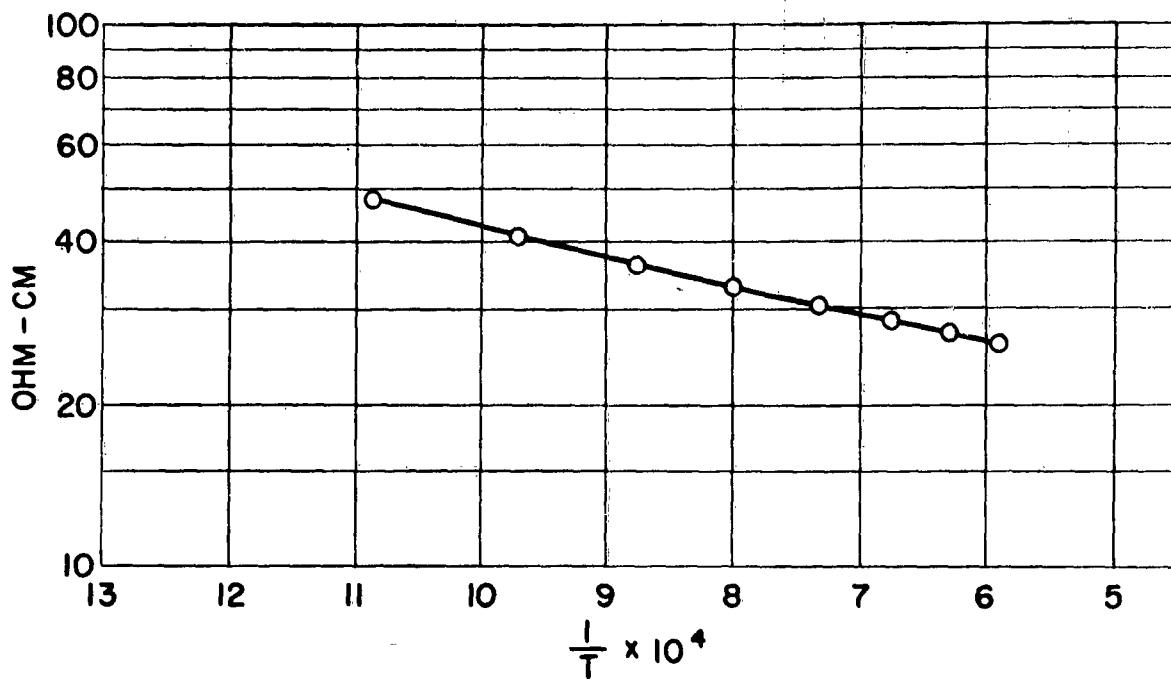


Figure I-3: Temperature Dependence of Resistivity Containing 1 Mole %
Additives Having Valency of 3.
(Y_2O_3)

value does not insure that the cation will exist in the chromium oxide structure with this same valency.)

In general, cations having a normal valency of greater than 3 tend to increase the resistivity of the chromium oxide. The primary exception is the uranium added as uranyl nitrate and decomposed to tetravalent and hexavalent uranium oxide during heating. The resistivities of compositions made with cations having a normal valency less than 3, shown in Figure I-2, were generally less than that of chromium oxide without additives. Lead oxide had a higher resistivity although it was added in the divalent state as $PbCrO_4$.

The resistivity of compositions with trivalent cations are shown in Figure I-3.

The effect of various amounts of MnO_2 on resistivity are shown in Figure I-4. The resistivity increases with increasing additions of manganese cations.

The effect of oxygen pressure and degree of sintering on the resistivity are shown in Figure I-5.

Seebeck voltage results are shown in Figure I-6 to I-8. The compositions having cation additions with valency greater than 3, shown in Figure I-6, had Seebeck voltages both greater and less than that of pure chromium oxide. The addition of cations less than 3 in valency, shown in Figure I-7, generally caused a decrease in Seebeck voltage. Trivalent cations, shown in Figure I-8, had little effect on Seebeck voltage. In general, the addition of cations to the chromium oxide compositions had much less effect on Seebeck voltage than on resistivity.

DISCUSSION OF RESULTS

The resistances were of the order of one-half ohm for compositions having resistivities about 2 ohm-cm. Since the contact resistance cannot be greater than one-half ohm, correction for contact resistance to the resistivity values greater than 10 ohm-cm could not be more than 10%. Of course, the low resistivity values could actually be much lower if the contact resistance was an appreciable part of the measured resistance.

Efforts were made to increase the density of chromium oxide compositions by recrystallization (prolonged heating) and hot pressing. Except for compositions containing appreciable amounts of vanadium oxide, no appreciable shrinkage was observed after sintering of chromium oxide compositions. Sintering proceeds by an evaporation-condensation mechanism, i.e., the samples retain their initial pressed density, about 60% of theoretical density. Prolonged heating results in recrystallization and a decrease in particle-to-particle contact resistance. But specimens of this porosity cannot have a conductivity much greater than one-half that of a dense recrystallized chromium oxide specimen.

Recrystallization was not very evident in hot pressed specimens after 20 hours of heating at $1500^{\circ}C$, indicating that solid-state transformation is not as effective as evaporation-condensation for recrystallization. The high resistivities of such specimens could be caused by localized high resistance regions at the grain boundaries.

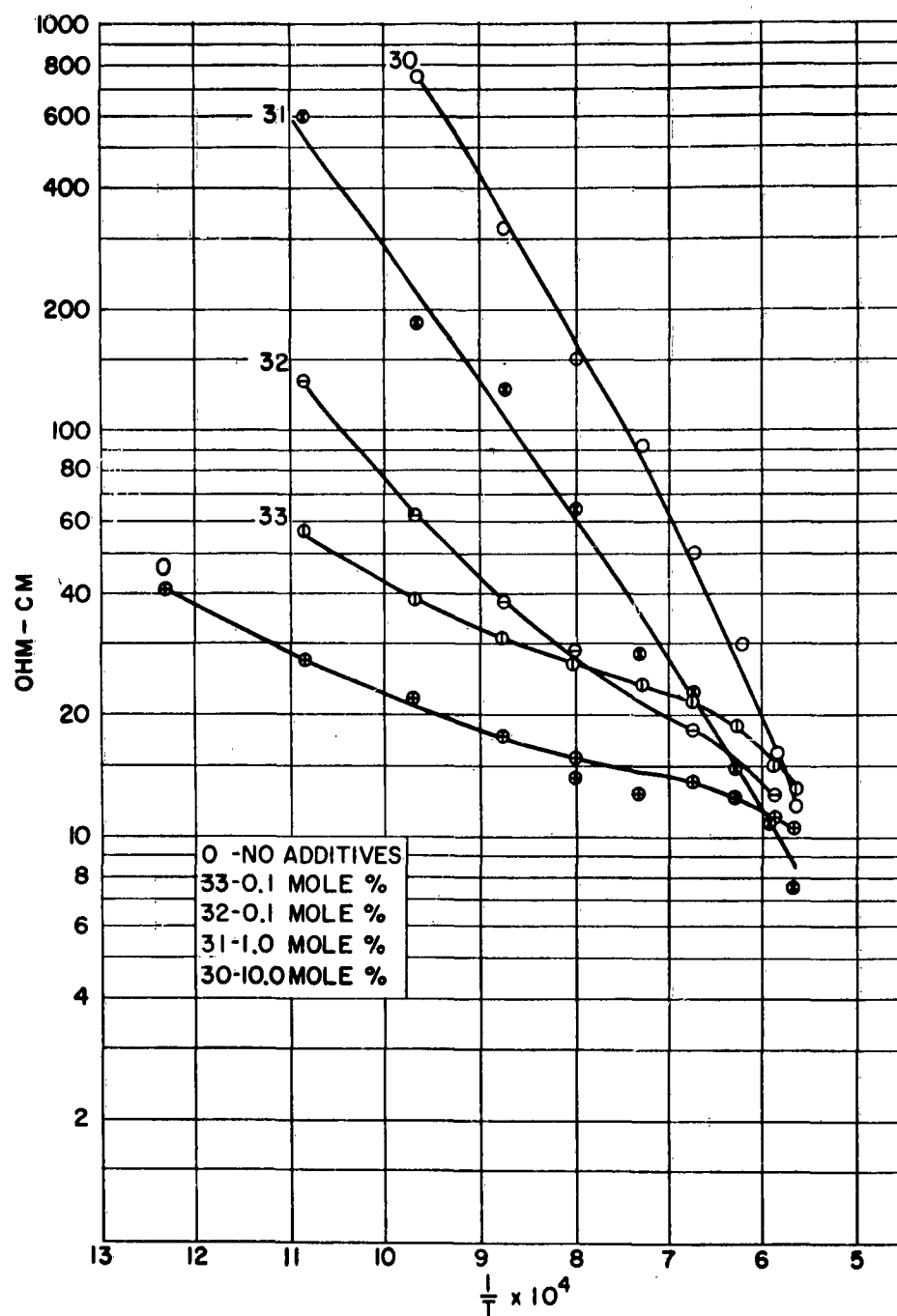


Figure I-4: Temperature Dependence of Chromium Oxide Containing Additives of Manganese Oxide.

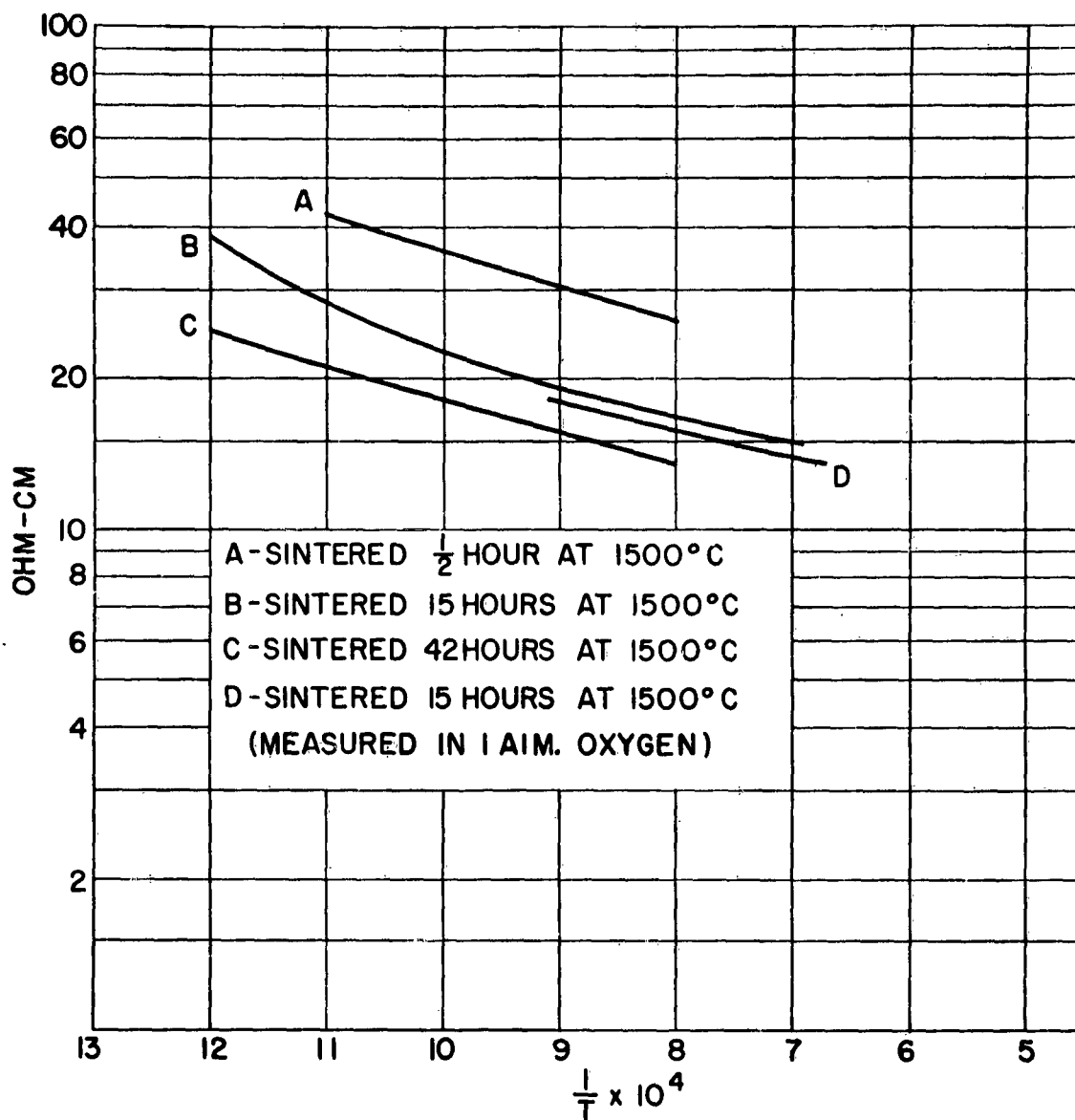


Figure I-5: Effect of Recrystallization and Oxygen Pressure on the Resistivity of Chromium Oxide.

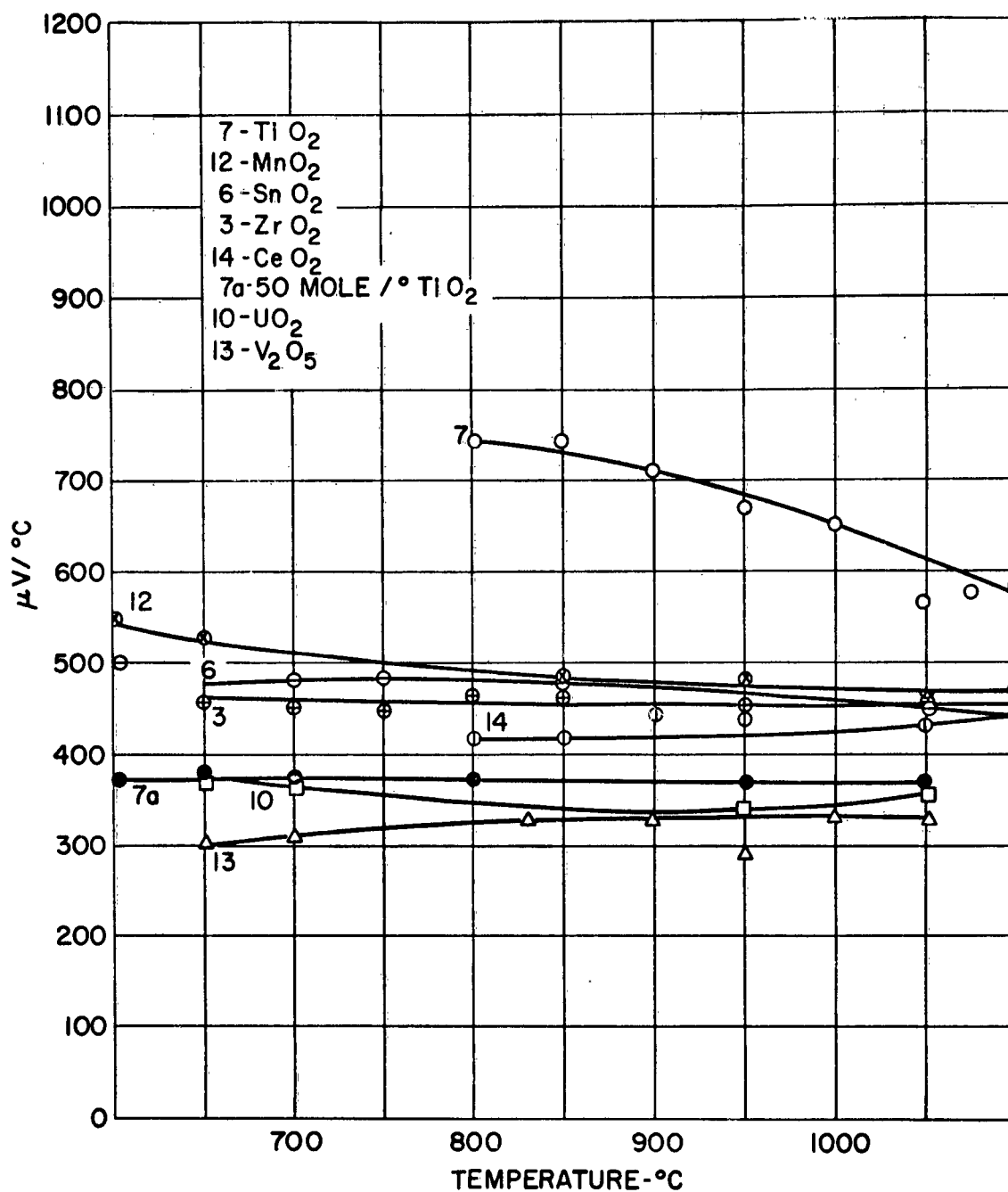


Figure I-6: Temperature Dependence of Seebeck Voltage of Chromium Oxide Compositions Containing 1 Mole % Additives Having Valency of >3 .

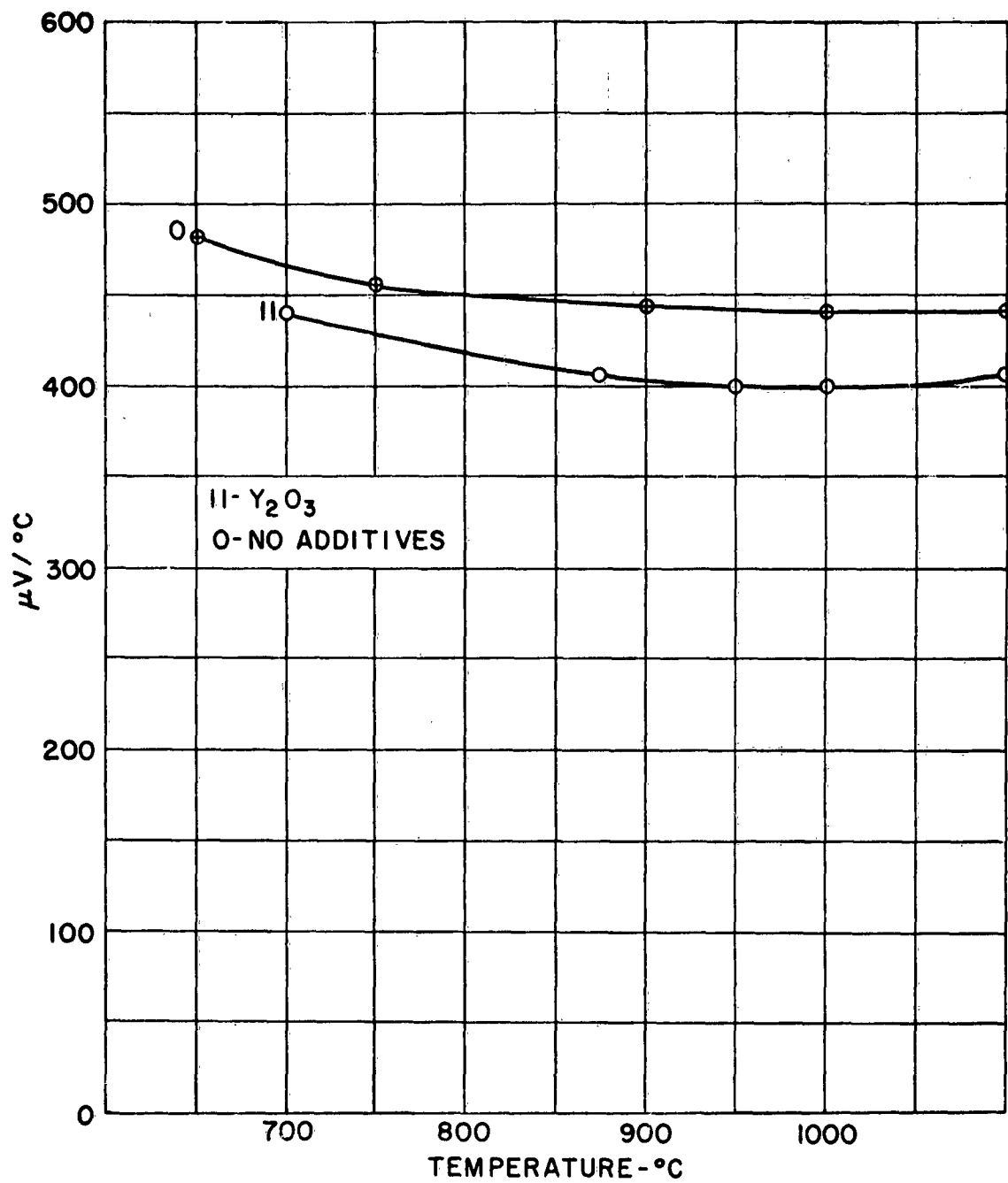


Figure I-7: Temperature Dependence of Seebeck Voltage of Chromium Oxide Compositions Containing 1 Mole % Additives Having Valency of < 3 .

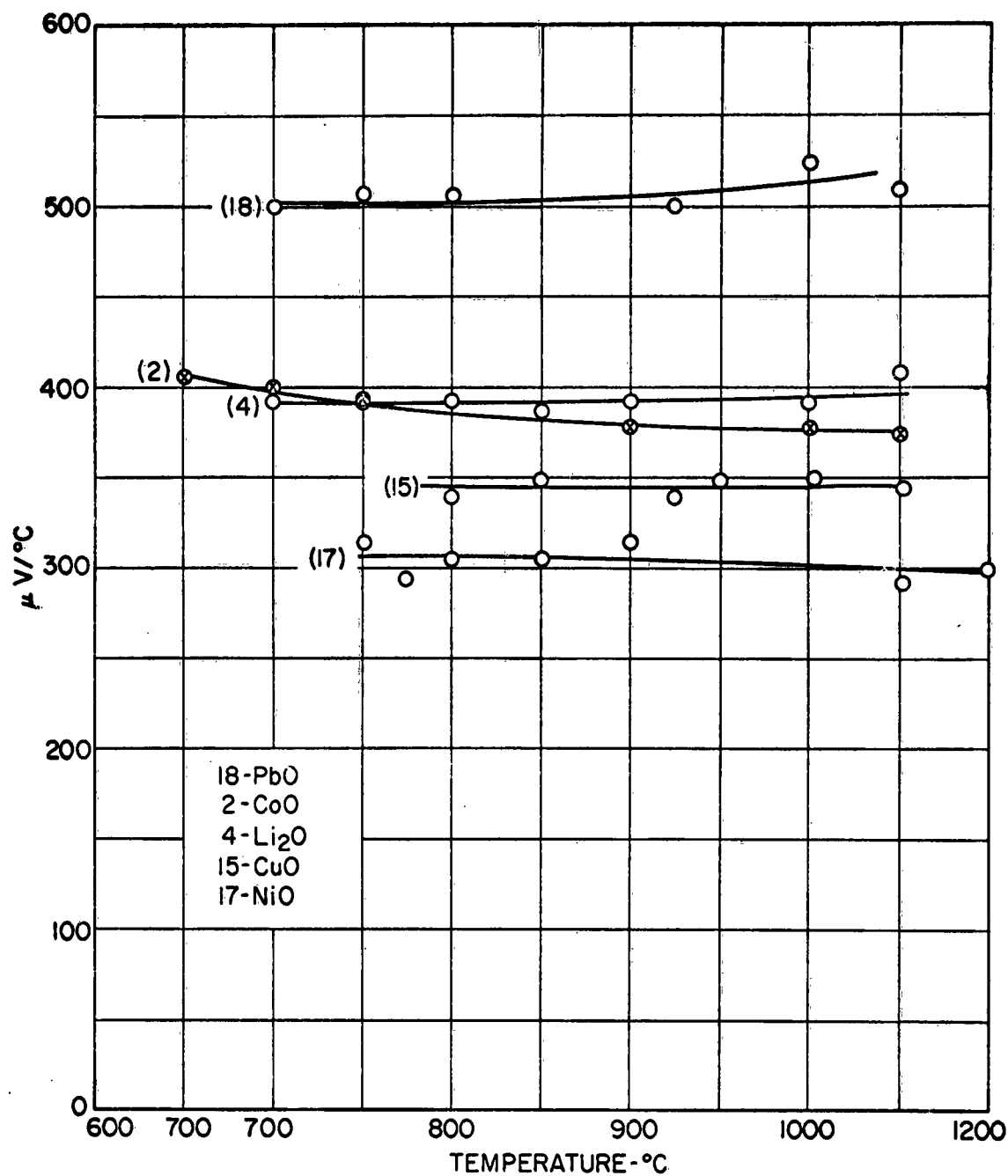


Figure I-8: Temperature Dependence of Seebeck Voltage of Chromium Oxide Compositions Containing 1 Mole % Additives Having Valency of 3.

The Seebeck voltages reported in this study are somewhat lower than those reported in the literature (for Cr_2O_3). This is consistent with the placement of the thermocouples at the outer surface of the end plates. A reasonable estimate would be that these reported values are at least 10% less than the real values.

FIGURE OF MERIT AND OPTIMUM EFFICIENCY

Based on presently available data, compositions with copper oxide additions have the highest figure of merit. Using an average Seebeck voltage of $400 \mu\text{V}/^\circ\text{C}$, an average resistivity of about 0.5 ohm-cm and assuming a thermal conductivity $0.1 \text{ watt/cm}^\circ\text{C}$ over the temperature range 500 to 1500°C , the figure of merit would be 3.0×10^{-6} . In this temperature range, the optimum efficiency, 0.2% , is one order of magnitude less than that calculated from data reported in the literature.

It is probable that optimization by varying the concentration and different placement of the probes to eliminate contact resistance would increase the figure of merit and optimum efficiency one order of magnitude.

APPENDIX J - A STUDY OF OXIDES FOR THERMOELECTRIC GENERATOR APPLICATIONS

John R. Gambino

April 1959

INTRODUCTION

This appendix summarizes the results of an investigation of oxides for thermoelectric applications. Prior to this investigation, a literature search was conducted^(J-1) in which it was found that a number of oxides had reported properties which made them promising as thermoelectric generator materials. In most cases, however, the data used for calculations of figure of merit or efficiencies were fragmentary and reported values varied widely. In the extreme case, values for electrical resistivity of chromium oxide varied from 10^3 to 10^{-3} ohm-cm at approximately the same temperature.

The choice of materials for study was based on such data. These materials, the oxides of chromium, cobalt, and copper, have very high resistivities at room temperatures. Because of this, the study was made in the temperature range of about 500°C to temperature of instability. In the case of Co_3O_4 , loss of oxygen at 900°C was considered limiting the temperature range. In Cr_2O_3 , the rapid volatilization of the material at 1500°C limited the temperature of the measurements. It is conceivable that these materials could be used at higher temperatures if appropriate encapsulation was provided. Major emphasis was placed on the Cr_2O_3 based compositions since on the basis of mismatched data in the literature, this material appeared most amenable to the improvement.

BACKGROUND

Since the theory of thermoelectricity has not been developed to the extent to provide directivity, an empirical approach was used in this study. The materials were chosen on the basis of their reported properties. The objectives were primarily to examine materials at higher temperature than previously studied and to obtain both resistivity and Seebeck voltage data on the same samples. In addition, optimization of properties critical to increasing the figure of merit was sought by control of the imperfections arising from nonstoichiometry and impurities.

EXPERIMENTAL

Compositions were prepared from CP materials. In oxides (especially the oxides considered in this study) the electrical conductivity and presumably Seebeck voltage are more insensitive to impurities than elemental semiconductors such as germanium and silicon. Because of this, additional purification of these oxides was not considered necessary.

Additives were oxides or salts which readily decomposed on heating to oxides. Oxide additives added as oxides were milled, pressed, reacted by heating, and, if needed, crushed, milled, repressed, and reheated. The oxide additives were sometimes mixed as an alcohol suspension in a "Waring Blendor", filtered and dried before pressing and heating to obtain reaction. This procedure was followed when simple milling did not result in satisfactory mixing. Additives of water soluble salts were made as aqueous solutions, mixed with the base oxide powder, dried slowly

at 100°C, and then at a temperature which would decompose the salt to the oxide. These compositions were then pressed and heated to achieve reaction and sintering. The compact size for cold pressed and sintered specimens was about 6 x 13 x 19 mm. Samples were pressed at 10,000 psi.

The ends of the pressed compacts were painted with platinum paste* for both resistivity and Seebeck voltage measurements. Measurements were made in an apparatus schematically described in Figure J-1. For Seebeck voltage measurements, the samples were placed between two platinum sheets and held in place by spring tension. Platinum-platinum 10% rhodium thermocouples attached to the outer surfaces of the platinum sheets were used to measure the end temperatures from which ΔT was obtained by difference. The emf generated by the sample was measured using the platinum legs of the thermocouples. A G.E. precision potentiometer was used for measuring the voltages. A switching device was incorporated in the system so that rapid change from one measurement to another could be accomplished. The specimen and holder were placed in a tube furnace; the natural temperature gradient was used to maintain a temperature difference. No attempt was made to keep the temperature difference constant since the natural gradient through the furnace varied with temperature. The temperature difference was usually $50 \pm 15^\circ\text{C}$ and within this range no significant variation in Seebeck voltage was observed. The temperature difference varied with specimen size, position in the furnace, and furnace temperature. Measurements were made in a tube furnace heated with a MoSi₂ resistance element which is capable of reaching temperatures of 1550°C. A nichrome wound tube furnace which operated up to 1100°C was used for some of the low temperature measurements.

The use of such large temperature differences could result in overlooking a major change in the Seebeck voltage if it occurred over a short temperature span. Since the measurements are made at close temperature intervals, the resulting α curve is an accurate average for the purposes of calculating the figure of merit and efficiency.

The specimen was brought up to the desired temperature, held at that temperature until it equilibrated before the measurement was made.

The same general procedure was used in measuring resistivity. Two platinum leads were attached to each platinum plate for these measurements. A double bridge was used for measuring resistivity but because of the placement of the leads, the lead wire resistance but not the contact resistance was eliminated.

COMPOSITIONS BASED ON CHROMIUM OXIDE

The Effect of Impurities on Electrical Properties

The importance of impurities on the electrical conductivity of semiconductor oxides is well known. Hauffe and Block^(J-2) reported that the addition of TiO₂ caused an increase in the resistivity of Cr₂O₃ as shown in Figure J 2. The reverse behavior was observed for additions of NiO, Figure J-3.

The resistivity of Cr₂O₃ reported by Hauffe and others ^(J-3,J-4) is shown in Figure J-4, together with the resistivities observed in this study. The variation

* Hanovia Chemical Manufacturing Company, No. 012

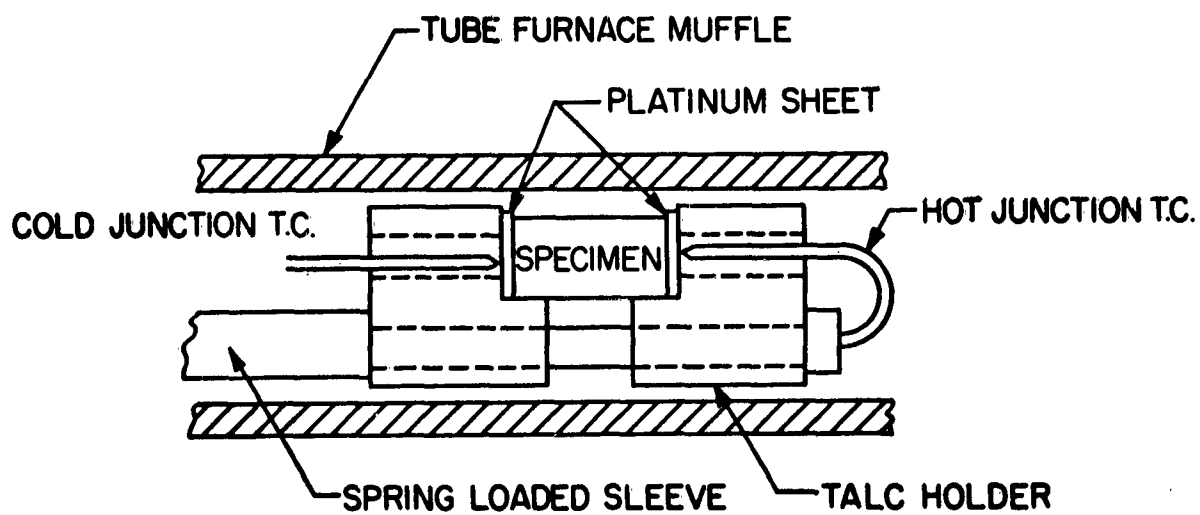


Figure J-1: Specimen Holder for Seebeck Voltage Measurements

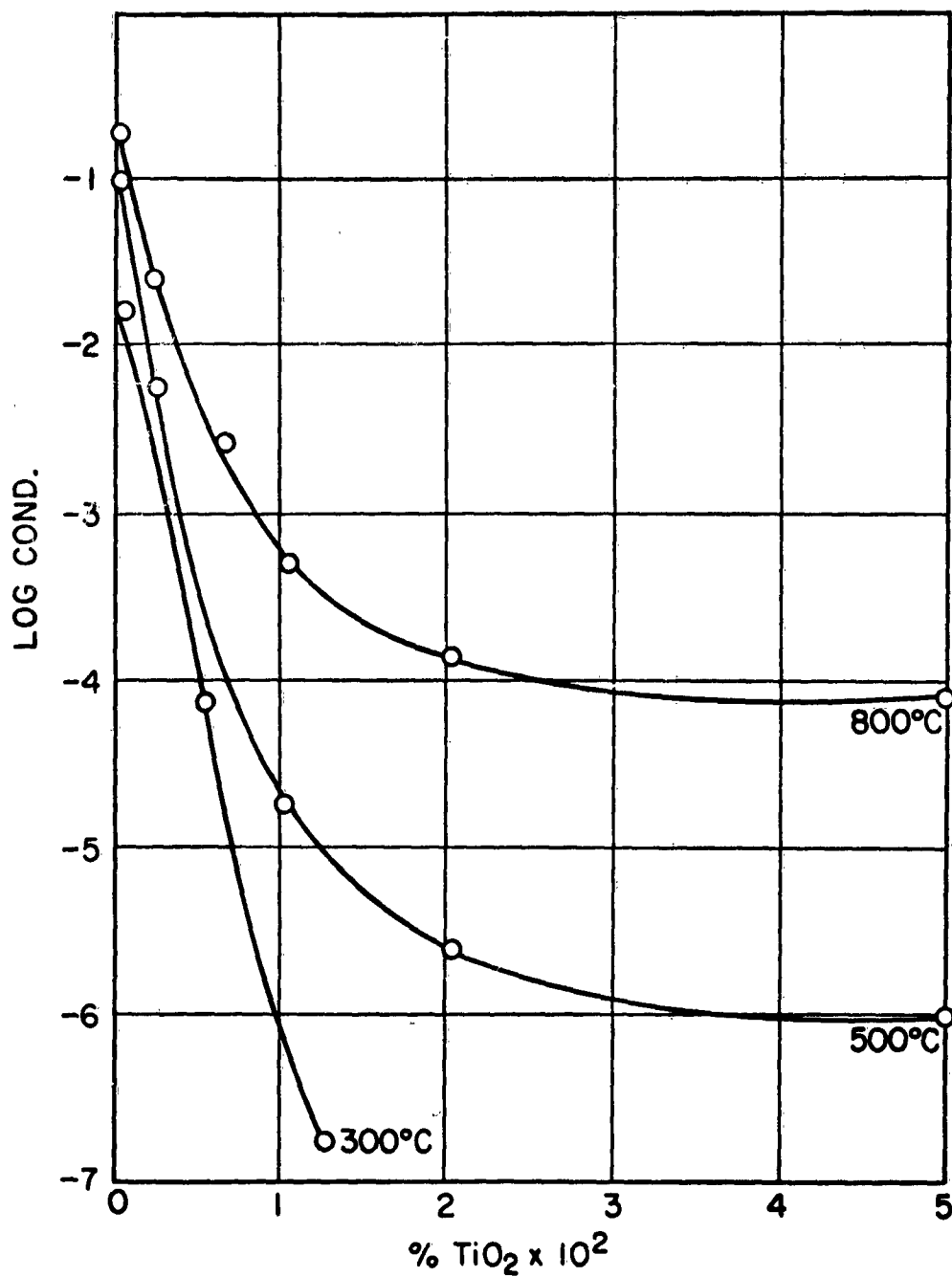


Figure J-2: The Effect of TiO₂ Additives on the Conductivity of Cr₂O₃.
(After Hauffe)

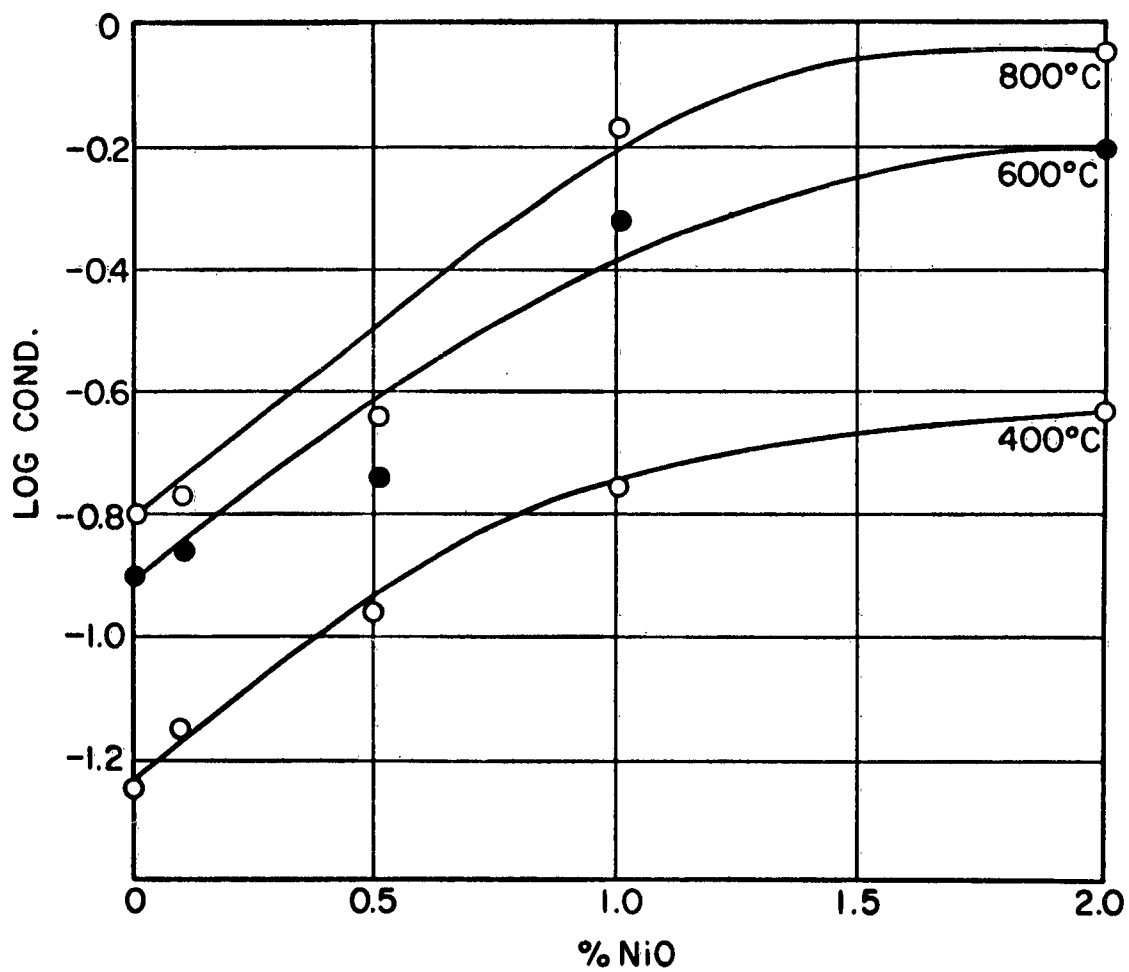


Figure J-3: The Effect of NiO Additives on the Conductivity of Cr₂O₃.
(After Hauffe)

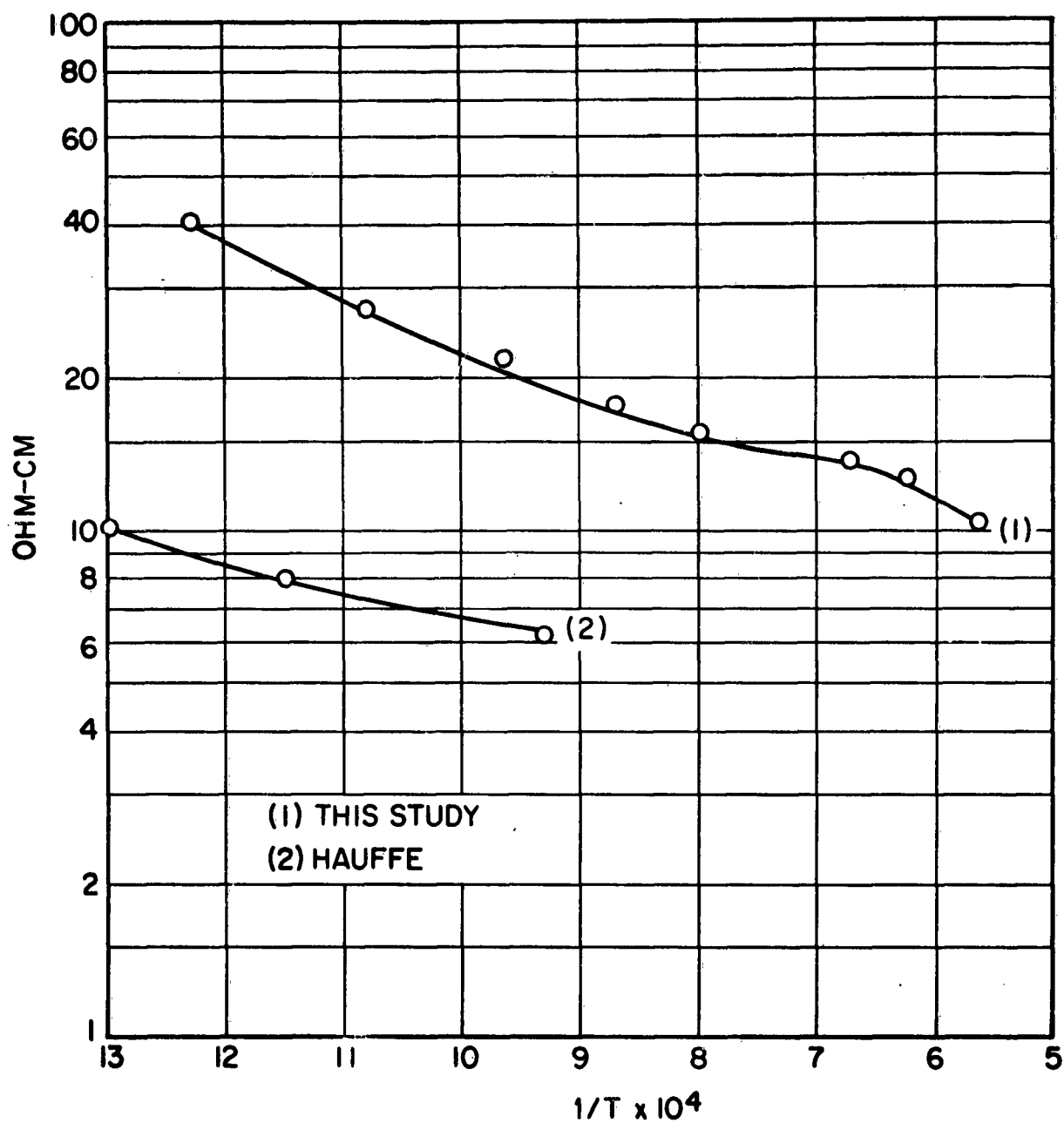


Figure J-4: Temperature Dependence of Resistivity of Cr_2O_3 Without Additives.

in resistivities is undoubtedly caused by the different treatments used in preparing the samples and impurities. In this study, no attempt was made to densify the majority of the specimens. Although the sintering conditions were severe, heating 15 hours at 1500°C, no appreciable shrinkage and, therefore, densification of the compact resulted. Attempts to densify Cr₂O₃ will be discussed later. If it is assumed that the impurities added had little influence on sintering behavior, i.e., the microstructure is determined by evaporation and condensation, the relative changes brought about by the various additives can be attributed to changes in electronic structure only.

The influence of impurities on the Seebeck voltage of Cr₂O₃ had not been extensively investigated. Some pentavalent ions were reported^(3,3) to decrease the Seebeck voltage and cause a change in sign. The objective of this study was to determine the relationships which exist between the change in resistivity and Seebeck voltage caused by additions of various additives. For convenience in presenting the data, the additives were classified into those existing in valency states greater than three, less than three, and those with a valency of three. The valency of the cation was established from its valency state in the parent oxide. The valency state in the Cr₂O₃ lattice need not be the same as shown by Parravano (Ref. J-6).

The resistivities of additives having valencies greater than three are shown in Figure J-5.

The impurities were added as oxides in amounts of 1 mole % of TiO₂, MnO₂, SnO₂, ZrO₂, CeO₂, UO₂, and V₂O₅. The valency of these metal ions except uranium and vanadium is four in the parent oxide at least. Most of these additives resulted in increases in resistivity. Compositions containing MnO₂, SnO₂, ZrO₂, and CeO₂ had resistivities about three times that of undoped Cr₂O₃. The TiO₂-Cr₂O₃ composition was two orders of magnitude greater at 1000°C. The two oxides which had lower resistivities than the undoped Cr₂O₃ were those which existed in pentavalent and hexavalent states in the parent oxides. The effect of the vanadium oxide could have been due partially to liquid phase sintering as evidenced by the shrinkage observed in this composition. The cations which had the least effect on the resistivity, Ce⁺⁴, Sn⁺⁴, Zr⁺⁴ had somewhat larger ionic radii than Cr³⁺ so that the concentration used could have exceeded the solubility limit for these cations. The effects of these additives on the Seebeck voltage shown in Figure J-6 were similar to those on resistivity, i.e., in the cases in which an increase in Seebeck voltage was observed, an increase in resistivity was also observed. The Seebeck voltage or resistivity was not measured at temperature about 1500°C in which intrinsic conductivity appeared to occur. At these temperatures, vaporization is so rapid that the utility of the material is doubtful.

The resistivities of additives having valencies less than three added in concentrations of 1 mole % are shown in Figure J-7. The resistivities of compositions containing Mg²⁺ and Pb²⁺ were slightly higher than that of undoped Cr₂O₃; those containing Li⁺¹, Co²⁺, and Cu²⁺ were lower than that observed for undoped Cr₂O₃. The magnesium and lead were added as the chromate, and the lithium, nickel, and copper were added as nitrates. The temperature dependence of Seebeck voltages for these compositions is given in Figure J-8. A decrease in Seebeck voltage was observed which corresponded qualitatively with the decrease in resistivity. The addition of a trivalent additive had little effect on the resistivity or Seebeck voltage.

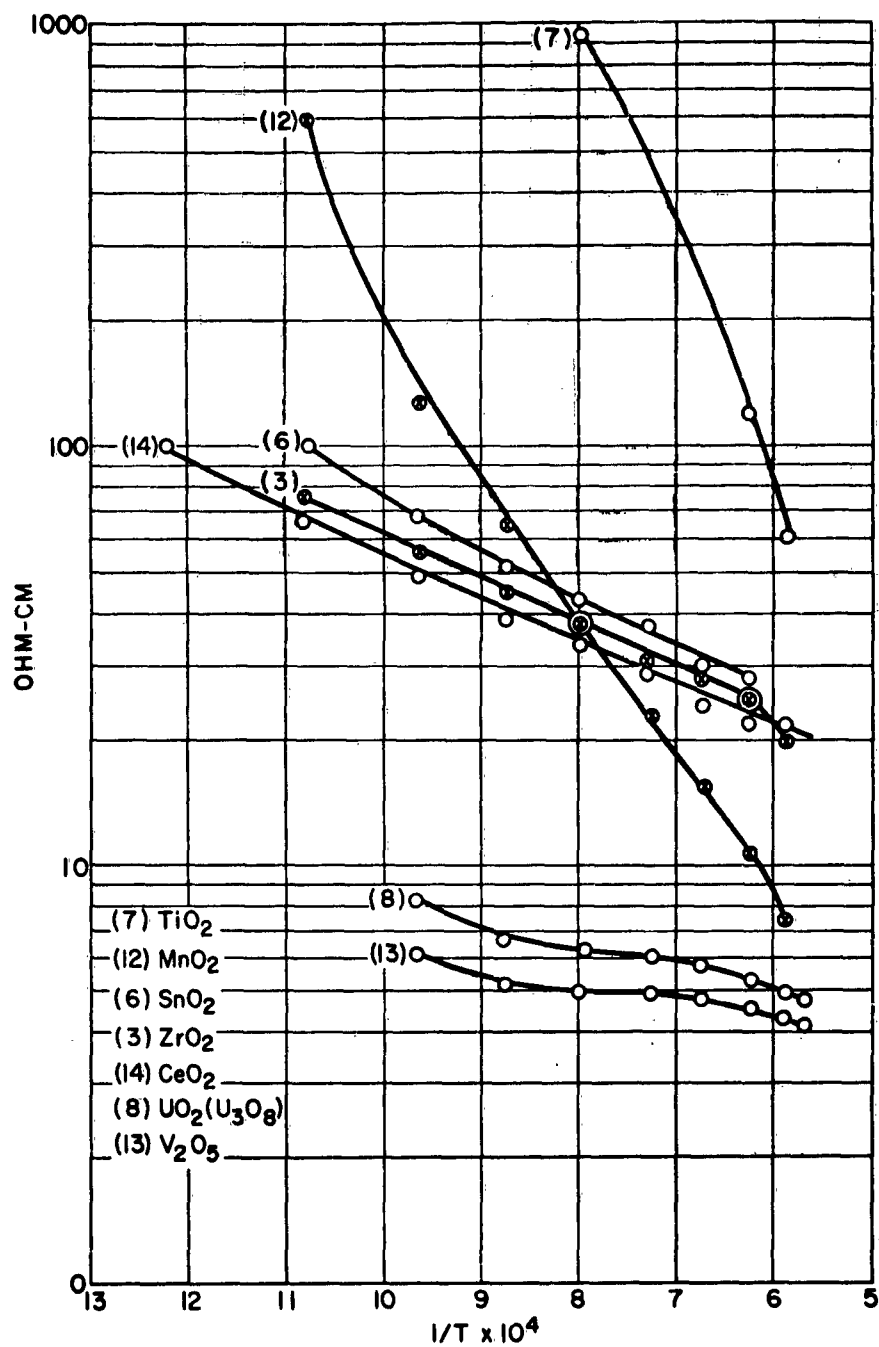


Figure J-5: Resistivity of Cr_2O_3 Compositions with Additives Having Valency of >3 .

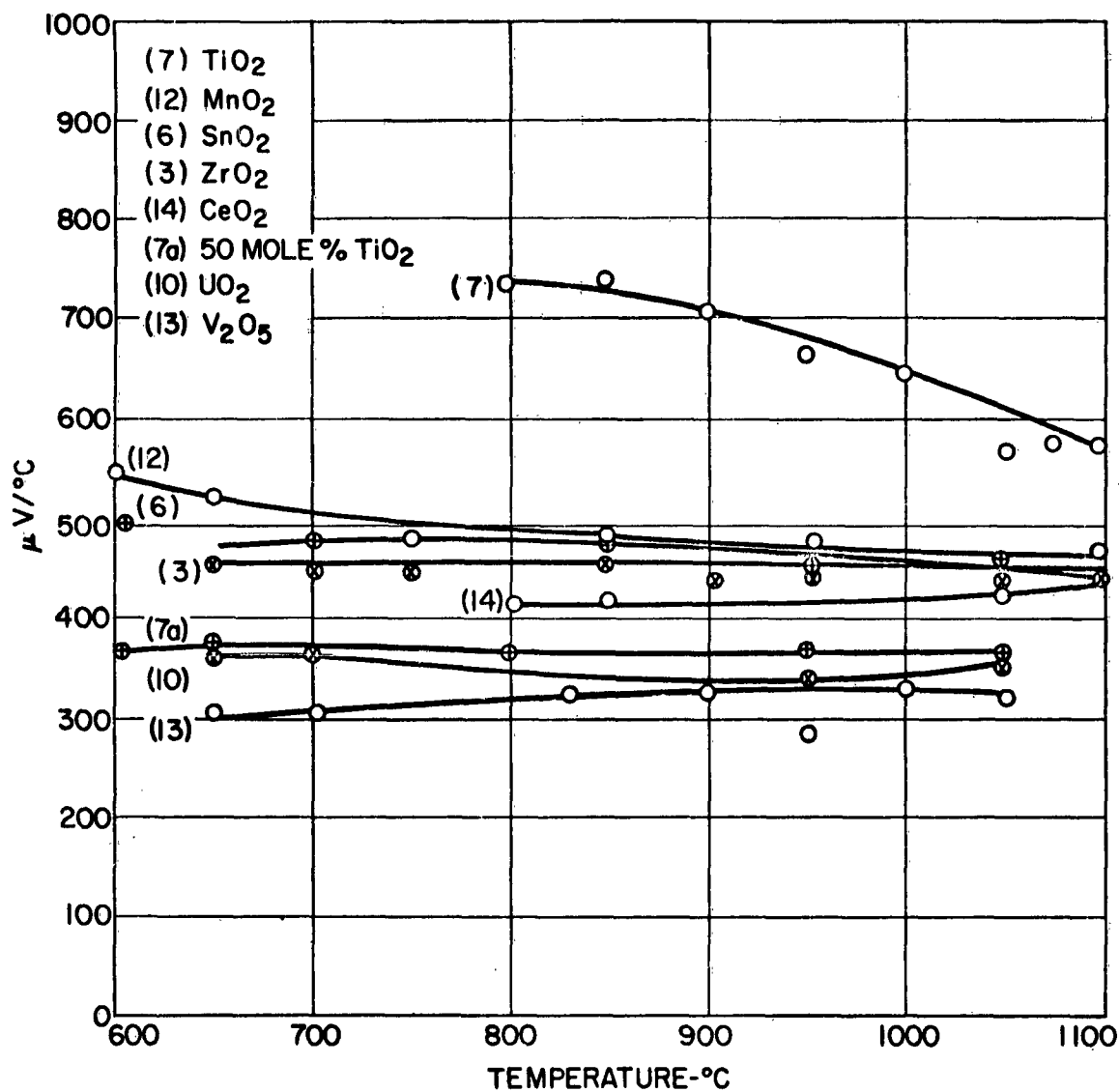


Figure J-6: Seebeck Voltage of Chromium Oxide Compositions Containing 1 Mole % Additives Having Valency > 3.

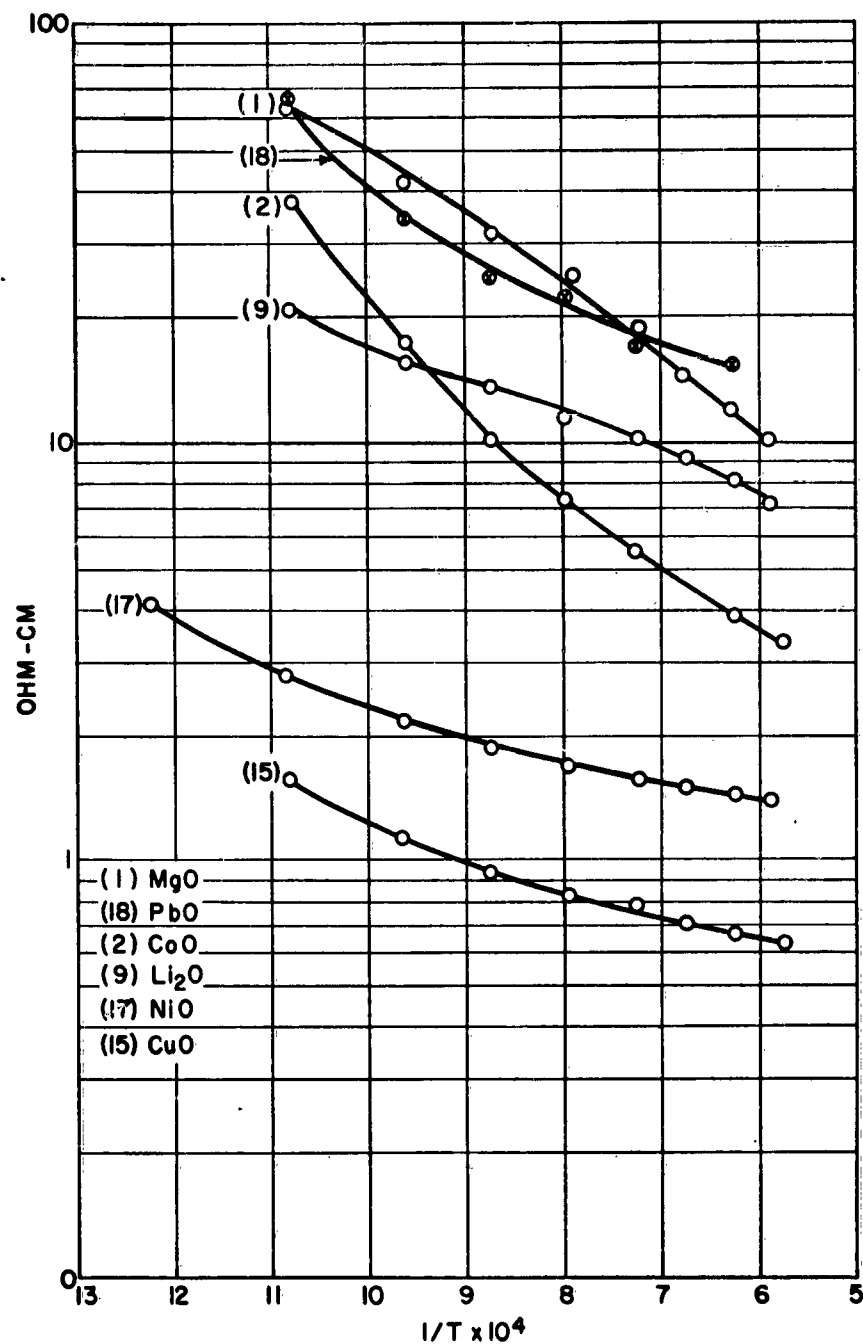


Figure J-7: Resistivity of Cr_2O_3 Compositions with Additives Having Valency < 3 .

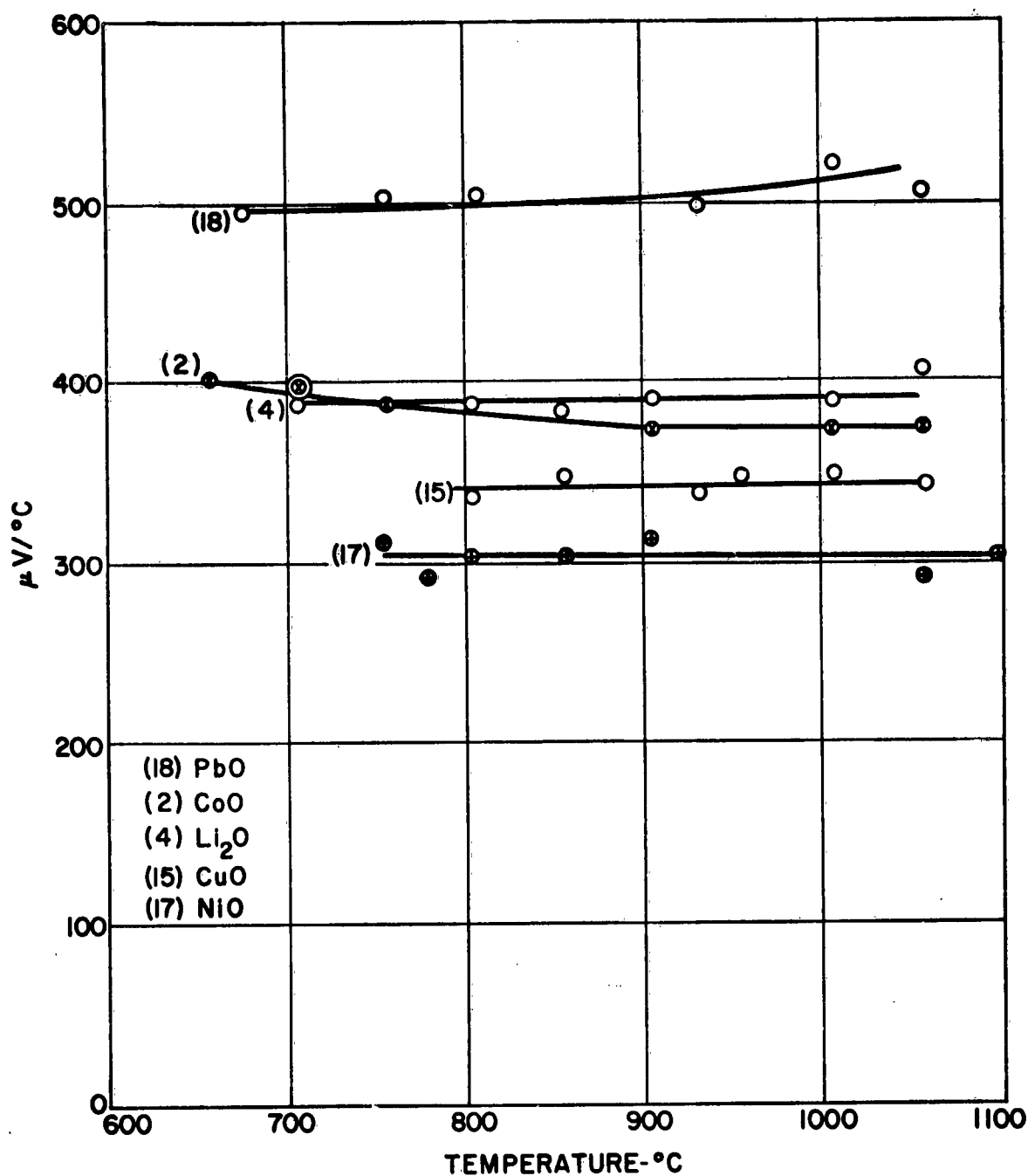


Figure J-8: Seebeck Voltage of Chromium Oxide Compositions Containing 1 Mole % Additives Having Valency < 3.

Assuming that the thermal conductivity is unaffected by the use of additives, it is apparent that the only significant improvement in $\frac{\alpha^2}{\rho}$ occurs with the lower valency additives. Further optimization of the properties, i.e., increase in $\frac{\alpha^2}{\rho}$, could be achieved by varying the amount of impurity used for doping. The resistivity-temperature values for different amounts of MnO_2 additives are shown in Figure J-9. The same data plotted as resistivity versus percent of MnO_2 for various temperatures is shown in Figure J-10. The resistivity versus percent of NiO and CuO are given for various temperatures in Figures J-11 and J-12. The resistivity, as well as the Seebeck voltage, generally decreased with impurity content. None of these compositions had resistivities low enough to indicate that Cr_2O_3 might be useful as a generator material.

Effect of Densification in the Resistivity of Cr_2O_3

Since the reported values of resistivity were very much lower than those observed in this study, an attempt was made to densify Cr_2O_3 compositions. Because of its high vapor pressure, it is likely that the Cr_2O_3 powder sinters by an evaporation-condensation mechanism which does not result in shrinkage. Very little shrinkage was observed during the sintering of all of these compositions with the exception of those containing V_2O_5 additives. In order to achieve theoretical densities, a number of possible approaches were used:

- (a) Sintering with concurrent application of stress.
- (b) The use of a "reactive" powder which would allow diffusional sintering to occur before the vapor pressure becomes appreciable.
- (c) The growth of single crystals from the vapor phase.

A standard hot pressing procedure was used. This involved filling a graphite die with the powder, pressing to 2000 psi at room temperature, heating the die by induction to the temperature desired with application of pressure to maintain 2000 psi, and holding at the desired temperature until no further reduction in pressure was noted. Hot pressing was done in air in the temperature range 1350 to 1750°C. The atmosphere in the die cavity was, therefore, primarily nitrogen with some CO likely.

The optimum temperature was found to be 1650°C. Below this temperature, theoretical densities could not be obtained in reasonable times, and at higher temperatures chromium carbide formation was extensive. The carbide formation was removed by oxidation and grinding. In general, the increase in density did not result in any significant permanent decrease in resistivity. On the contrary, some of the compositions with additives had higher resistivities when hot pressed into compacts having close to theoretical density. The resistivity of various compositions prepared by hot pressing are shown in Table J-1 with those prepared by cold pressing and sintering. The low values observed for some hot pressed specimens were markedly changed by prolonged exposure to oxidation at high temperatures (shown in parentheses). When the resistivity was not reduced by such treatment, the Seebeck voltage was found to be very low. The explanation for this increase in resistivity resulting from the hot pressing treatment is not immediately obvious. The relatively short heating time used in hot pressing could prevent grain growth and, hence, grain boundary resistance would be higher. For the same reason, diffusion of the impurities might have been inhibited so that the impurities remained at grain boundaries. The reducing atmosphere could be responsible also.

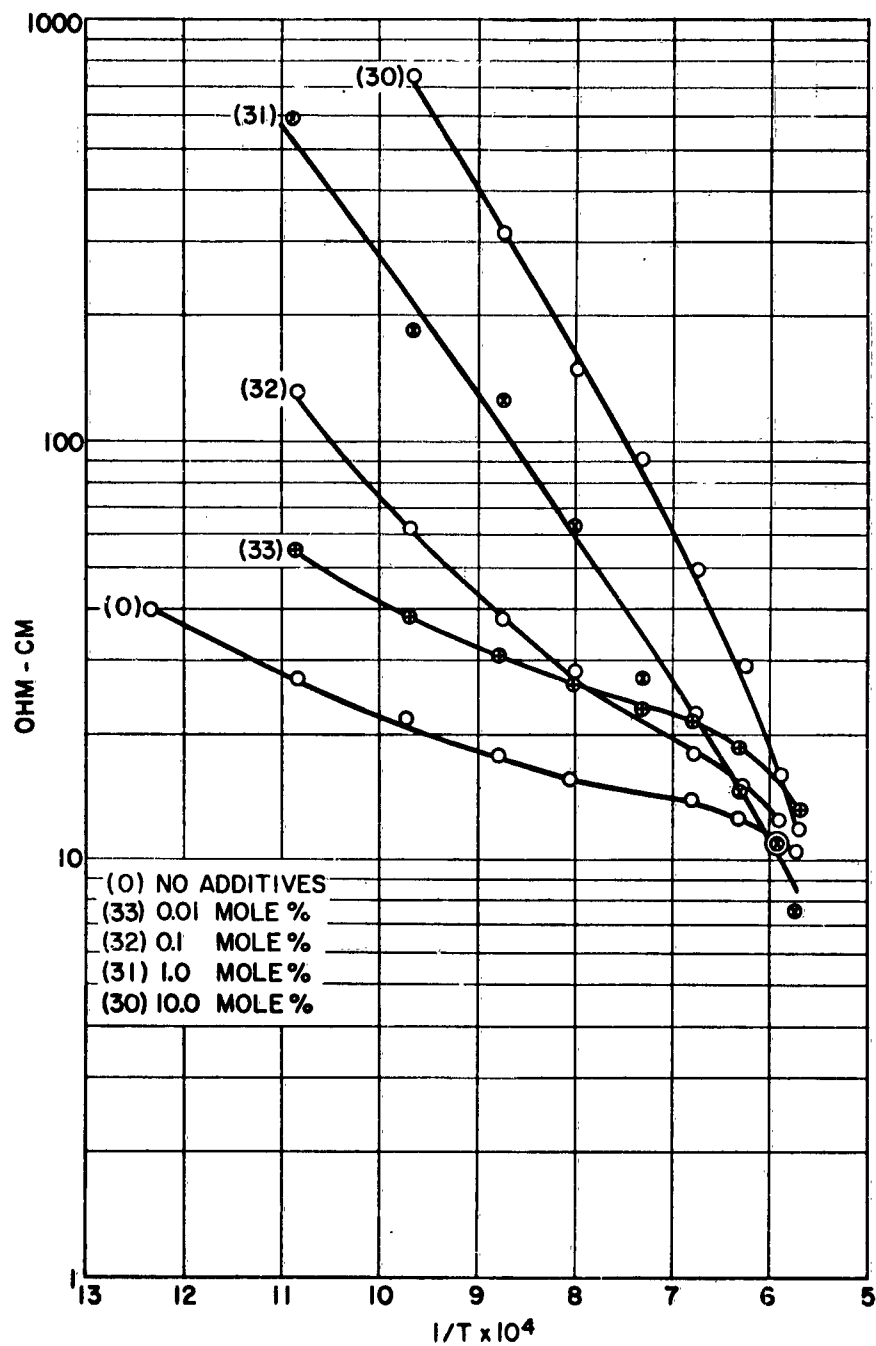


Figure J-9: Resistivity of Cr_2O_3 Compositions Containing MnO_2 Additives.

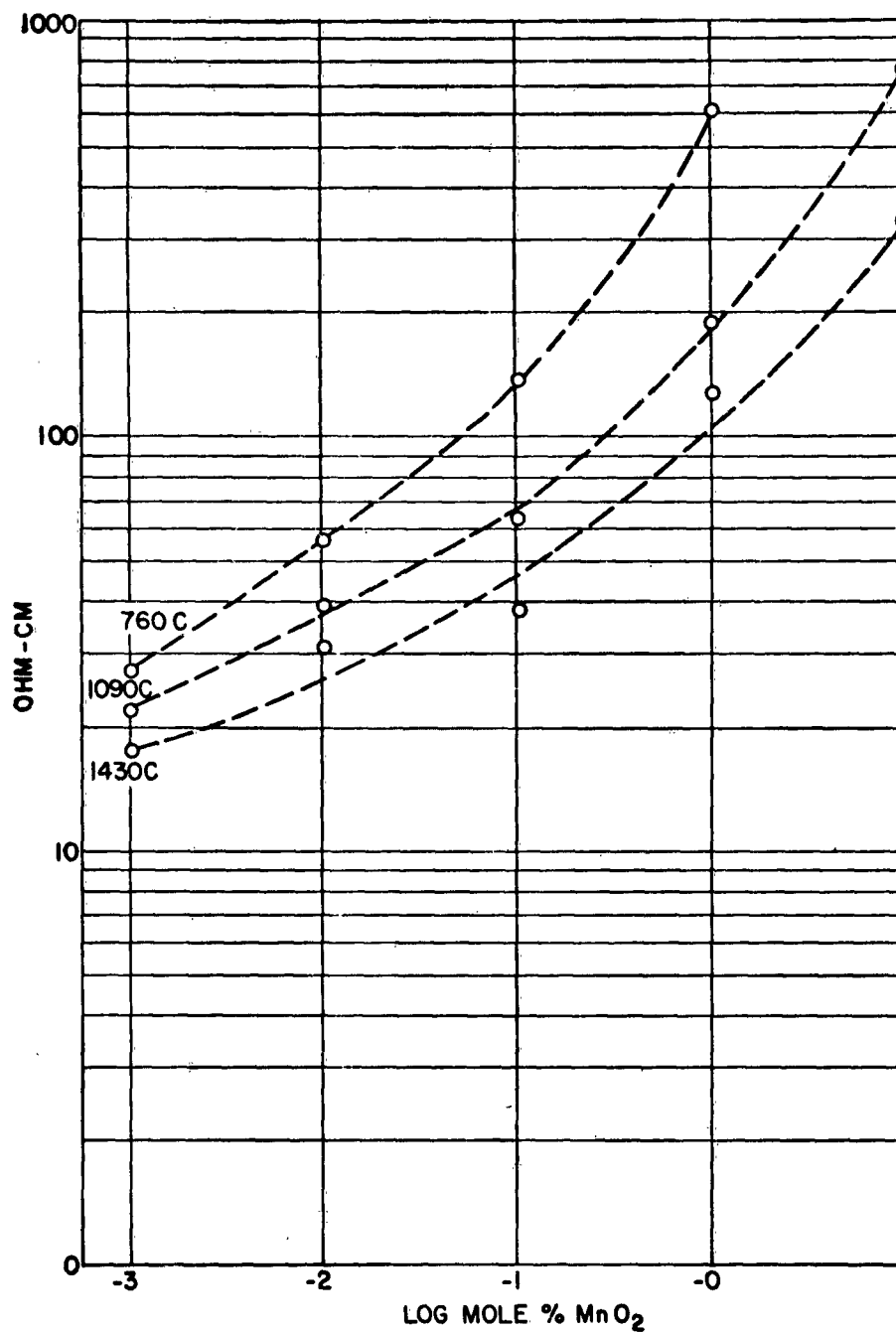


Figure J-10: Resistivity of Cr_2O_3 as a Function of Composition (MnO_2).

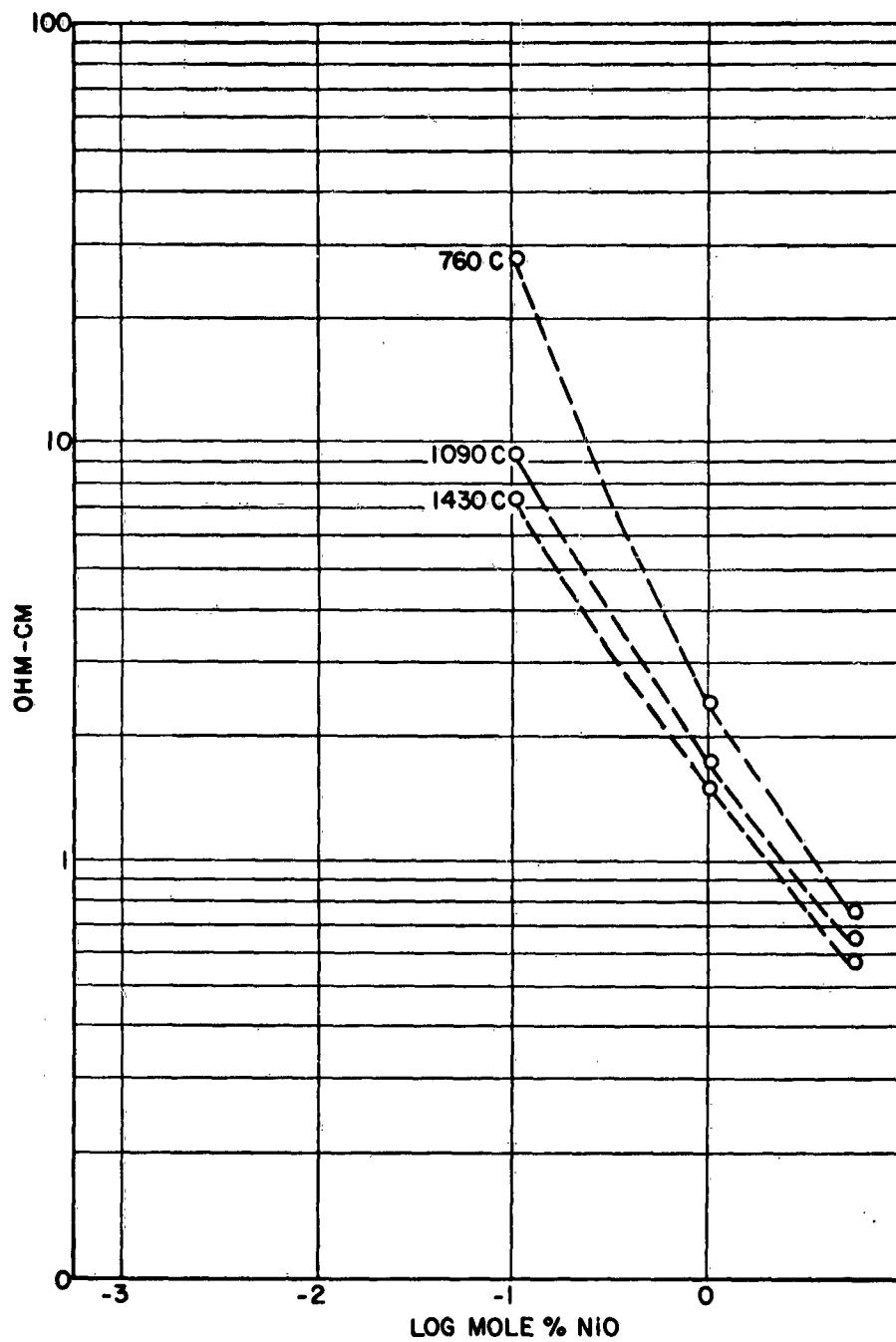


Figure J-11: Resistivity of Cr_2O_3 as a Function of Composition (NiO).

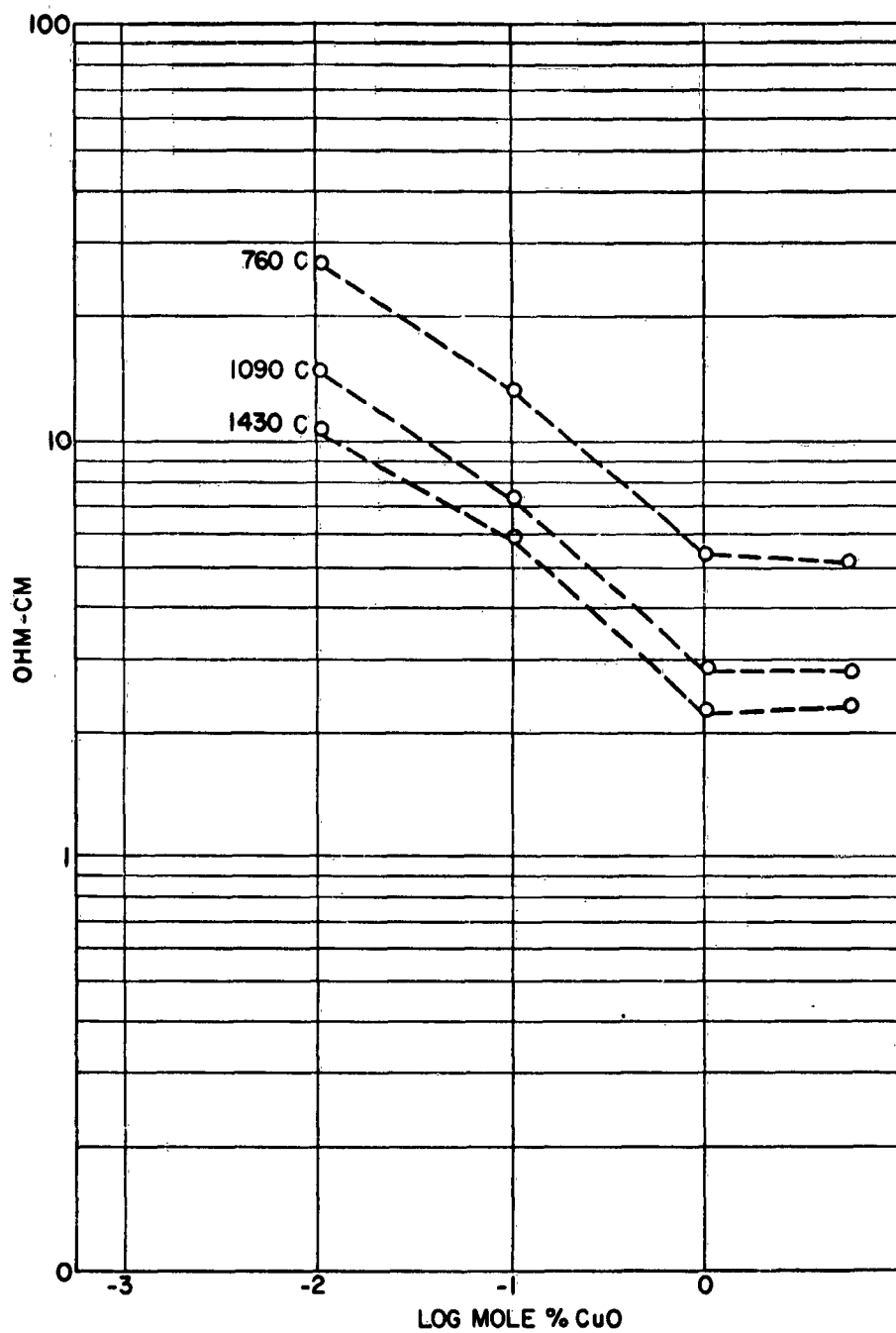


Figure J-12: Resistivity of Cr_2O_3 as a Function of Composition (CuO).

Attempts to densify the Cr_2O_3 compositions were not successful. "Reactive" powders prepared by low temperature decomposition of salts did not densify during sintering. Attempts to prepare single crystals by condensation of Cr_2O_3 vapors did not result in crystals large enough to measure.

The role of microstructure in determining the resistivity is complex unless the grain boundary effects are discounted. The oxide, when heated for long times at high temperatures, is changed from particles in contact into large crystals with much fewer grain boundaries. The geometry can be approximated as a continuous phase containing isolated voids. From geometrical considerations, a body of this type having 60% of theoretical density would have about twice the resistivity of a dense body. The exact increase would depend on the distribution and shape of pores.

The next case which can be considered if the role of the grain boundary is neglected is where evaporation and condensation have been proceeding to the extent that the radius of the contact area between grains is a small fraction, 1 to 10%, of the original grain size. Such a body would have about five times the resistance of a dense body.

The relative values of resistivities of samples, heated under different conditions, are shown in Table J-2. The agreement between the observed resistivities and those calculated from geometric considerations are evidence that grain boundary resistance is negligible in these samples. These data also indicate that the values for sintered but porous bodies are not so different from that of a dense body. Much lower resistivities are necessary to make Cr_2O_3 attractive for thermoelectric applications.

The change in resistivity as a function of atmosphere is shown in Table J-3. Changes in oxygen pressure did not have much effect on the resistivity. The treatment in a hydrogen atmosphere did cause a significant increase in resistivity. The reason for this increase is not understood. The samples treated in hydrogen were measured in an inert atmosphere because of the side effects hydrogen has on the platinum alloy thermocouples. The use of more than one additive did not result in any marked changes in Seebeck voltage or resistivity. Some of these results are shown in Table J-4. The values generally were intermediate between those obtained for the additives added singly. It would seem the effect of one was counteracted by the presence of the other.

COMPOSITIONS BASED ON COBALT OXIDES

Cobaltic oxide was another oxide which had reported properties which indicated some promise for development of this oxide into a usable generator material. An extensive investigation of compositions based on cobalt oxides was conducted (4-8, J-9) in the past. A combination of several additives was found to show the most improvement in properties. This study was limited to 700°C , and the effect of stoichiometry was not investigated. Also the amounts of additives used were made in such large amounts that it is likely that more than one phase existed.

The study of these compositions undertaken here had as its objective the investigation of stoichiometry and selected additives in influencing the properties of interest. Cobaltic oxide, Co_2O_3 , used in the preparation of the compositions loses oxygen on heating; at 900°C the composition becomes CoO . The properties as well as the crystal structure of these two compositions are different. The cobaltic oxide was heated and sintered at either 870 or 1100°C to give nominal compositions

corresponding to Co_3O_4 or CoO . The cobalt oxide, CoO prepared at 1100°C , did not appear to absorb significant amounts of oxygen during heating in air below 1000°C .

The resistivity of these oxides measured in an air and argon atmosphere is shown in Figure J-13. The resistivity of the cobalt oxide, CoO , measured in air drops off rapidly at temperatures below 900°C and then increases at temperatures above 900°C . The resistivity measured during cooling was lower than that observed during heating. These hysteresis effects were not evident for the Co_3O_4 compositions or CoO heated in argon.

The Seebeck voltage of CoO was about twice that of Co_3O_4 as shown in Figure J-14. A sharp decrease in Seebeck voltage was observed for CoO heated in air at temperatures above 800°C . This behavior and the anomalous increase in resistivity at around 900°C suggests that compositional changes were occurring due to absorption of oxygen.

A more careful study of the weight changes Co_3O_4 and CoO undergo during heating in air was made by heating powders in an automatic recording balance. CoO powder gained weight during heating in air in the temperature range 800 to 900°C , but lost the weight gained during the heating up at 900°C and above. The Co_3O_4 gained a small amount of weight during heat-up starting at 770°C , (indicating it was not quite stoichiometric Co_3O_4) but started to lose weight rapidly at 880°C . A constant weight was attained during holding the sample a short time at 960 . The weight gain of CoO can be attributed to oxygen absorption which resulted in the decrease in Seebeck voltage and resistivity which occurred in this temperature range. By analogy with the $\text{FeO} \cdot \text{Fe}_3\text{O}_4$ system, there is probably an extensive solid solubility in the $\text{CoO} \cdot \text{Co}_3\text{O}_4$ system.

The Seebeck voltages of CoO compositions containing various impurities are shown in Figure J-15. Additives of 1 mole % NiO , Cr_2O_3 , TiO_2 , and V_2O_5 caused an increase in the Seebeck voltage. Since these measurements were made in air, the decreases observed at the higher temperatures can be attributed to oxygen absorption also. The Seebeck voltage of CoO was not changed appreciably by the addition of magnesia, but an addition of 1 mole % lithium oxide resulted in much lower Seebeck voltage, $100 \mu\text{V}/^\circ\text{C}$ in the temperature range 300 to 900°C . The addition of lithium also caused a decrease in Seebeck voltage of Co_3O_4 , shown in Figure J-16. The Seebeck voltage of Co_3O_4 containing 1 mole % V_2O_5 decreased from $440 \mu\text{V}/^\circ\text{C}$ at 400°C to $190 \mu\text{V}/^\circ\text{C}$ at 915°C . No hysteresis effects were noted on cycling the Co_3O_4 compositions.

The resistivity of a number of CoO and Co_3O_4 compositions containing various additives is shown in Figure J-17. The addition of lithium resulted in the lowest resistivity.

OTHER OXIDE COMPOSITIONS STUDIED

Cuprous oxide had been studied by a number of investigators (J-10, J-11). The Seebeck voltage and resistivity were measured over a wide temperature range and under different pressures of oxygen. Although the properties of this material reported by these investigators indicated it had some potential usefulness as a generator material, the properties were very sensitive to deviations from stoichiometry brought about by exposure to different atmosphere conditions. Because of this, it was felt that the effect of impurities would be too difficult to study in this investigation. Work was limited to some preliminary measurements of Seebeck voltage shown in Table J-5, along with those obtained for some other oxides.

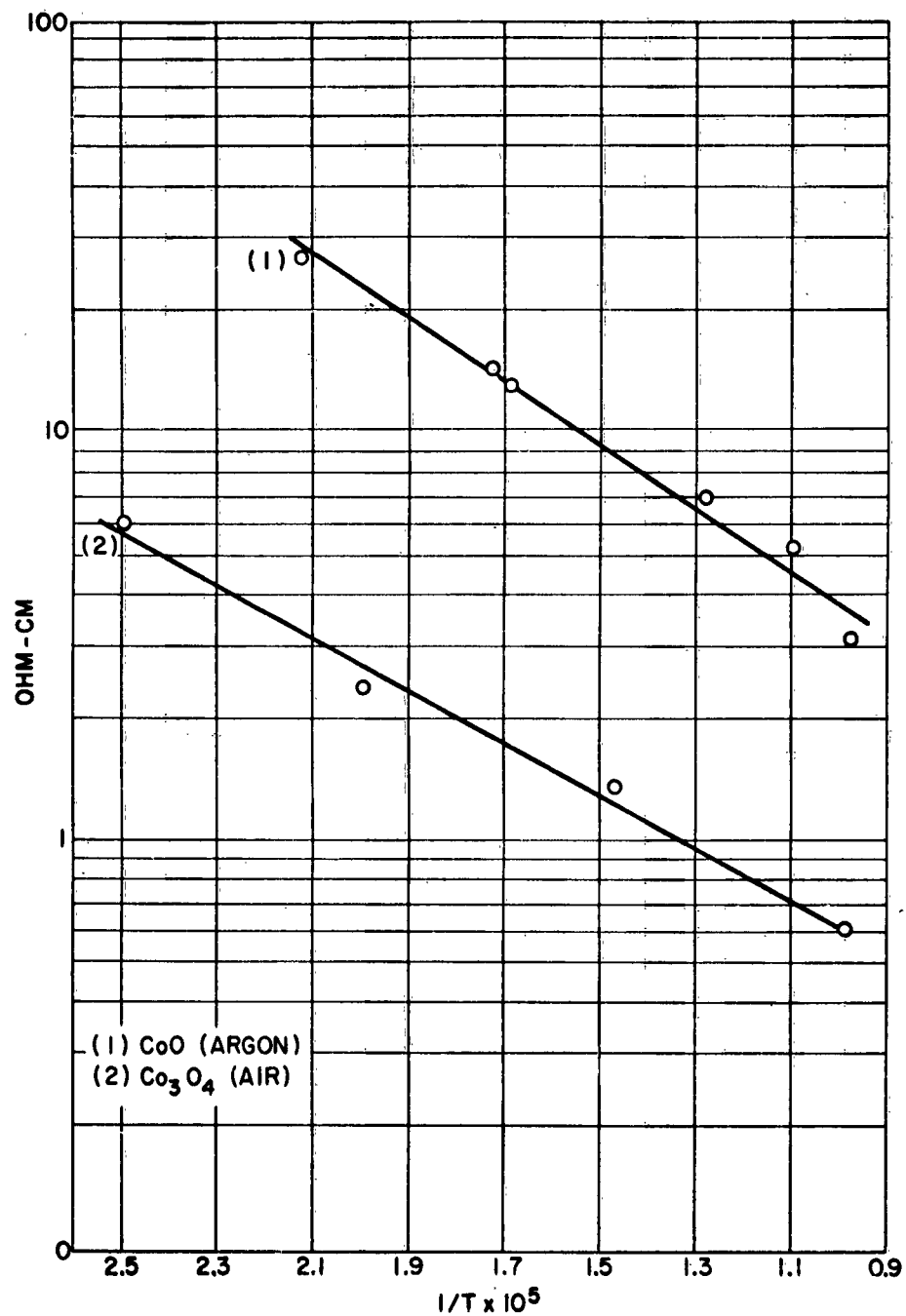


Figure J-13: Resistivity of Cobalt Oxides.

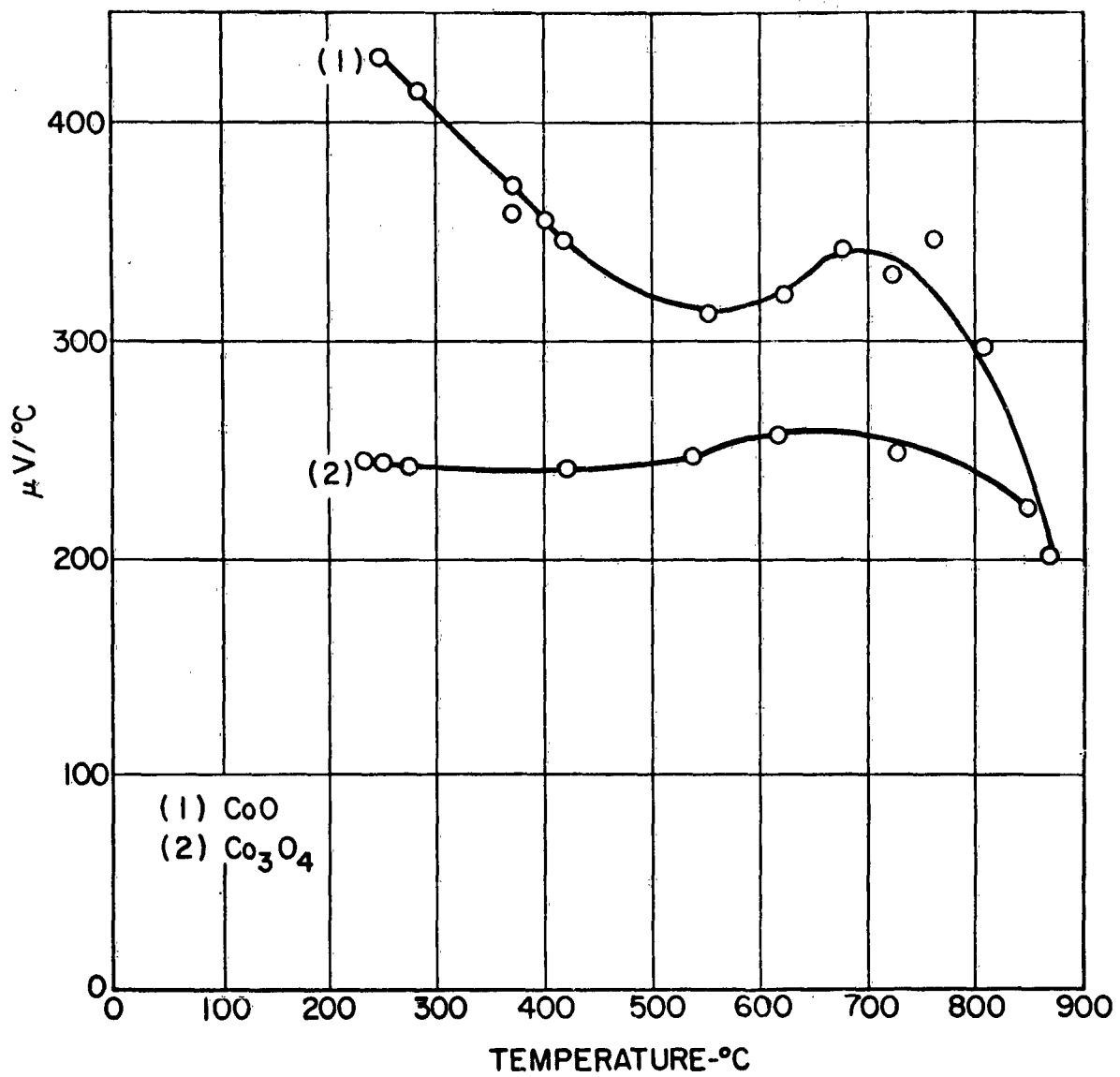


Figure J-14: Seebeck Voltage of Cobalt Oxides.

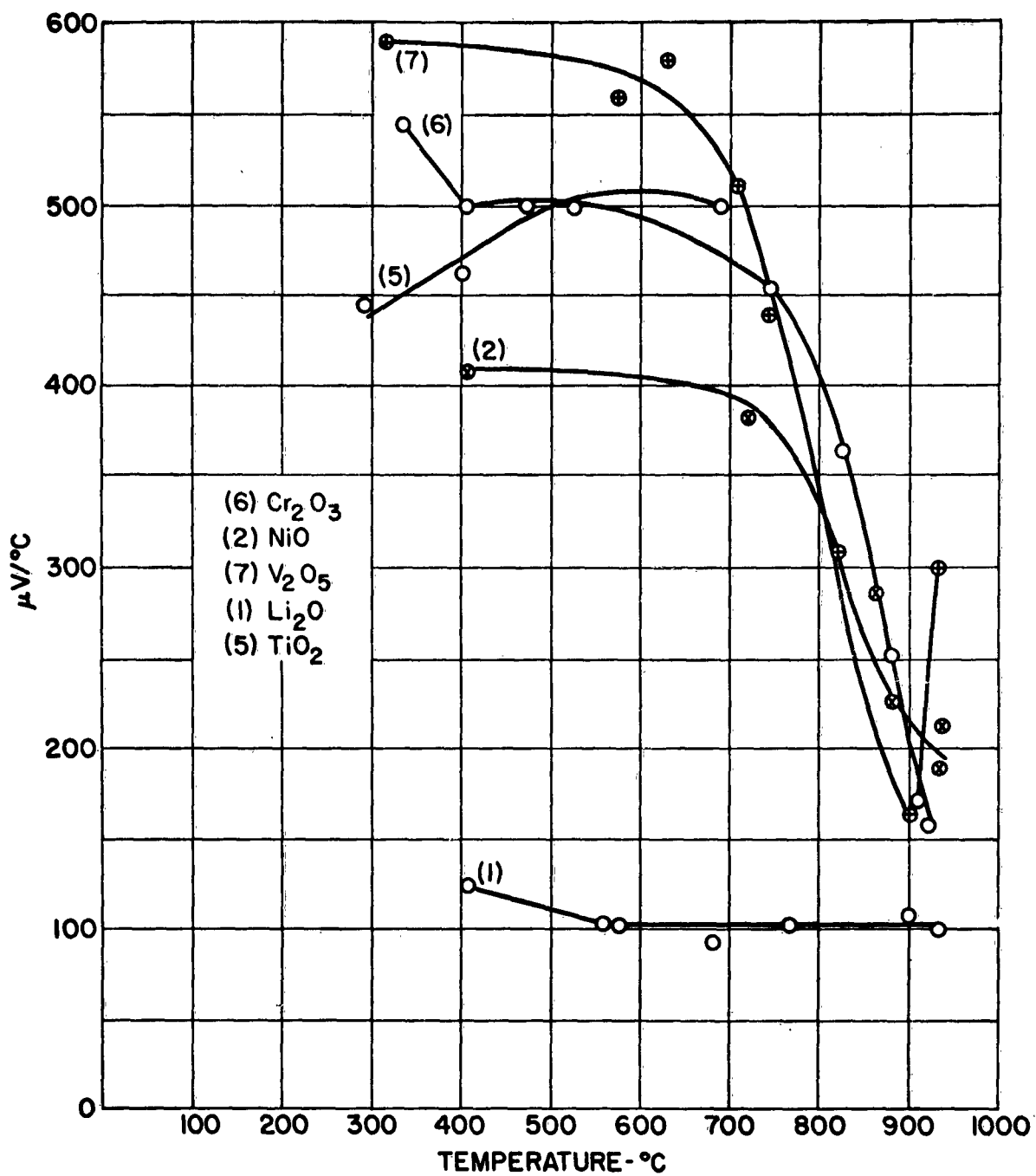


Figure J-15: Seebeck Voltage of CoO with 1 Mole % Additives.

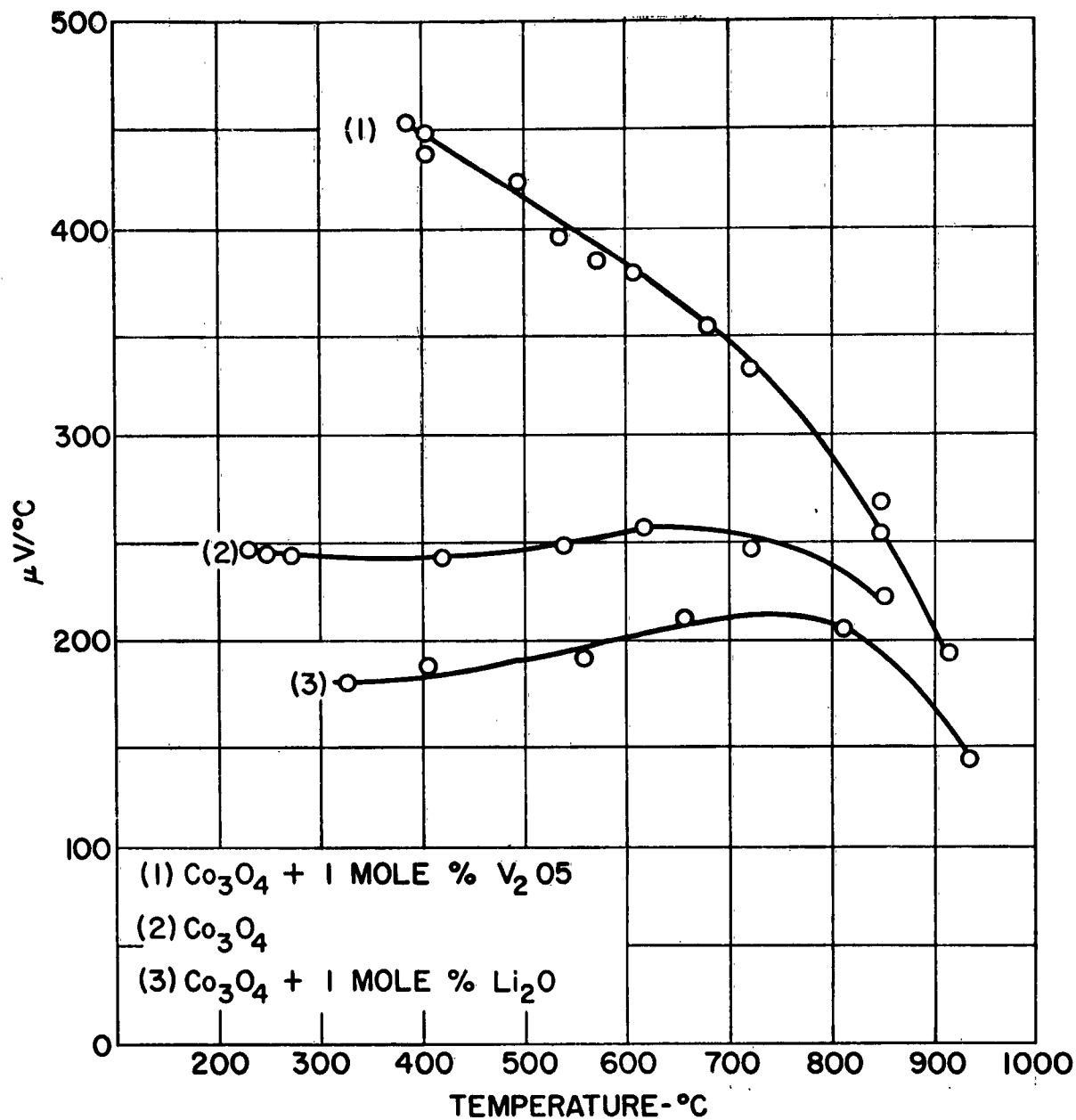


Figure J-16: Seebeck Voltages of Co_3O_4 with Additives.

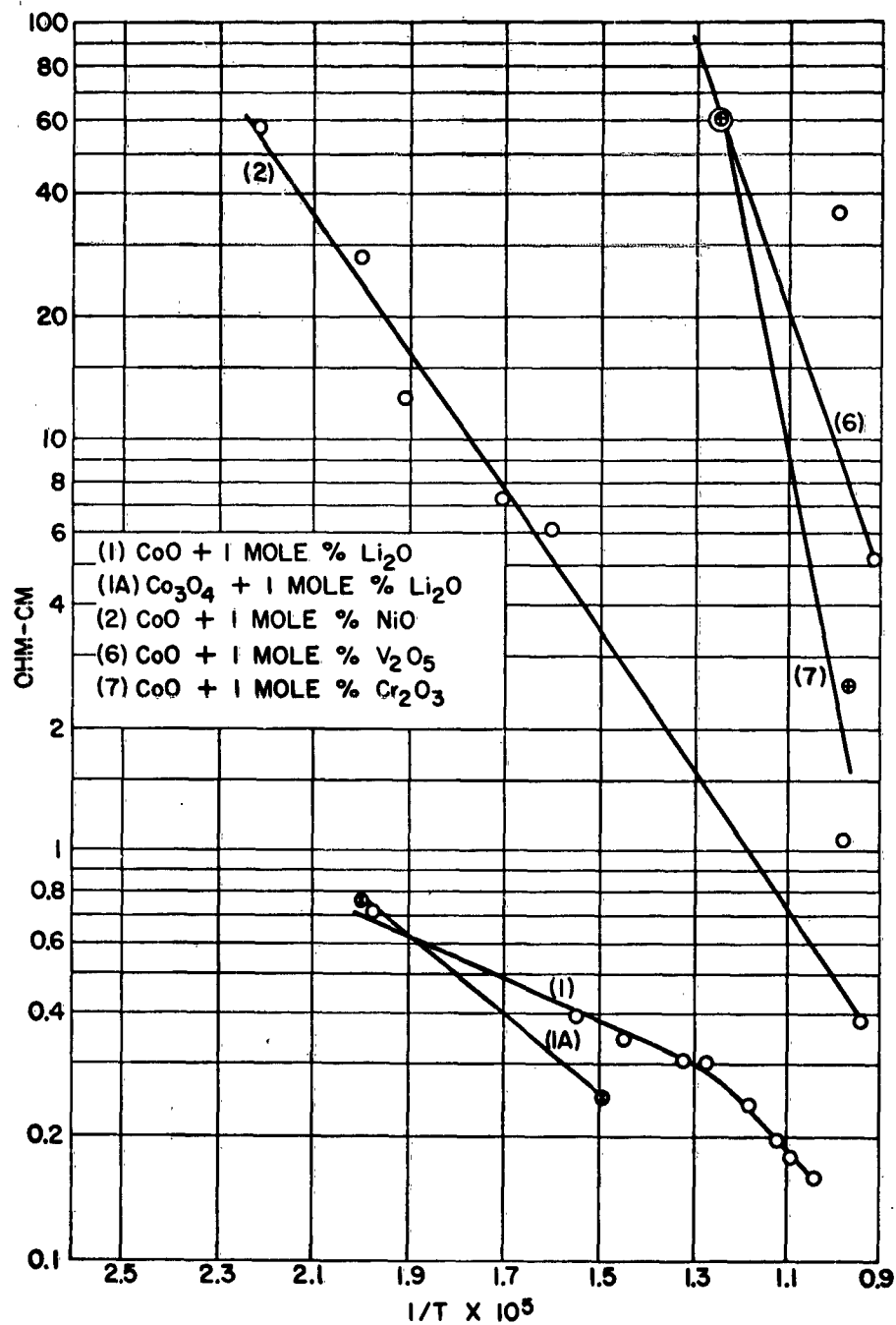


Figure J-17: Resistivity of Cobalt Oxides with Additives.

The measurement of Seebeck voltage of molybdenum trioxide was made at temperatures above its melting point also. Although a large amount of uncertainty in the values obtained was caused by the difficulties associated with measurement of this volatile, corrosive liquid, the Seebeck voltage did not appear to decrease above the melting point. The resistivity of the liquid was about one ohm-cm at 850°C.

FIGURE OF MERIT AND OPTIMUM EFFICIENCY OF OXIDIC COMPOSITIONS

The figure of merit and efficiency of oxide compositions are shown in Table J-6. Thermal conductivity measurements were not made or reported in the literature. Because of the low value of $\frac{\alpha^2}{\rho}$ obtained, a much lower value of thermal conductivity than that assumed would not increase the figure of merit sufficiently to make these compositions of interest for generator applications.

REFERENCES

- (J-1) Borchardt, H. J. "Refractory Materials for Thermoelectric Generator Elements," GEL Memorandum Report, Nov. 13, 1957.
- (J-2) Hauffe, K. and Block, J., Z. Physik Chem 198 232 (1951).
- (J-3) Bevan, D. J. M., Shelton, Anderson, J. S., J. Chem. Soc. 1948 1729.
- (J-4) National Research Council, International Critical Tables, McGraw-Hill Book Company, New York (1926).
- (J-5) Fisher, W. A., Lorenz, G., Arch Eswhuttew 28, 497 (1957).
- (J-6) Parravano, G., J. Chem. Physic, 23 5 (1955).
- (J-7) Gambino, J. R., unpublished results.
- (J-8) Fisher, F., Dehn, K., Sustman, H., Ann. Physik. 15 109-26 (1932).
- (J-9) Fisher, F., Dehn, K., Sustman, H., Ges Abhandl. Kenntners Kohle 12 516 (1937).
- (J-10) Greenwood, N. N., Anderson, J. S., Nature 164 346 (1949).
- (J-11) Anderson, J. S. and Greenwood, N. N., Proc. Roy. Soc. (London) 215A 353 (1952).

TABLE J-1
EFFECT OF HOT PRESSING ON THE RESISTIVITY OF Cr₂O₃ COMPOSITIONS

Temperature (°C)	Resistivity, ohm-cm mole % NiO							
	0.01		0.1		1.0		5.0	
	cold pressed	hot pressed	cold pressed	hot pressed	cold pressed	hot pressed	cold pressed	hot pressed
690	--	--	--	--	3.1	43.2	0.89	4.1
760	--	17.3*	26.8	78.0	2.4	24.8 (60.0)	0.78	2.0
870	--	12.7	18.8	59.0	2.0	14.8 (25.2)	0.71	1.2
980	--	9.8	16.5	35.6	1.9	9.6 (23.1)	0.67	0.8
1090	--	7.8	9.3	22.6	1.8	7.0 (16.0)	0.64	0.7
1200	--	5.7	7.9	16.0	1.6	5.0 (10.4)	0.62	0.5
1320	--	3.5	7.5	10.1	1.6	2.8 (6.0)	0.60	0.3
1430	--	2.7	7.2	4.3	1.5	1.9	0.60	0.2

*All hot pressed specimens heated in air for 1 hour at 1300°C. Values in parenthesis are for samples heated in air an additional 24 hours.

TABLE J-2
EFFECT OF HEAT TREATMENT ON THE RESISTIVITY OF Cr₂O₃

Heat Treatment	Resistivity at 980°C (ohm-cm)
1/2 hr. at 1500°C	29
15 hrs. at 1500°C	19
42 hrs. at 1500°C	15
Fused in oxy-gas flame	12
Hot pressed	0.3*

*Not affected by heating in air although low Seebeck voltage indicated some interaction to form carbides.

TABLE J-3
EFFECT OF ATMOSPHERE ON THE RESISTIVITY OF Cr₂O₃ COMPOSITIONS

Composition	Temperature (°C)	Resistivity in Atmosphere		
		Air	Argon	Hydrogen
Cr ₂ O ₃	870	1.0	1.1	5.6
Cr ₂ O ₃	870	1.0	1.0	3.6
1% UO ₂	760	1.0	2.2	4.9
1% CuO	1200	1.0	1.1	2.1
1% MnO ₂	870	1.0	1.6	2.3

TABLE J-4
EFFECT OF MIXTURES OF ADDITIVES ON THE SEEBECK VOLTAGE
AND RESISTIVITY OF Cr₂O₃

Additive	Seebeck Voltage ($\mu\text{V}/^\circ\text{C}$)	Resistivity (ohm-cm)
1% MnO ₂	480	110
1% Li ₂ O	390	10
1% MnO ₂ + Li ₂ O	330	38
1% CuO	345	0.9
1% CuO + Li ₂ O	365	4.2

TABLE J-5
SEEBECK VOLTAGE OF VARIOUS OXIDES AS A FUNCTION OF TEMPERATURE

Material	Seebeck Voltage ($\mu\text{V}/^\circ\text{C}$) at Temperature ($^\circ\text{C}$)						
	595	650	705	760	815	870	925
NiO	290	300	320	330	340	370	-
ZnO	-	-	30	130	190	-	-
Cu ₂ O	700	-	850	-	690	-	750
Fe ₂ O ₃	-	-	210	200	170	140	110
MoO ₃	-	-	700	-	-	-	-

TABLE J-6
FIGURE OF MERIT OF OXIDIC COMPOSITIONS

	Cr ₂ O ₃	Cr ₂ O ₃ + 1% NiO	Cr ₂ O ₃ + 5% NiO
T ₁ , hot junction temperature, $^\circ\text{K}$	1400	1400	1400
T ₂ , cold junction temperature, $^\circ\text{K}$	650	650	650
α , avg. $\mu\text{V}/^\circ\text{K}^*$	450	300	100
ρ , ohm-cm	15	1.7	0.7
K, watts/cm $^\circ\text{K}$ (assumed)	0.1	0.1	0.1
Z, $^\circ\text{K}^{-1}$	1.35×10^{-7}	5.3×10^{-7}	1.4×10^{-7}

*estimated above 1100 $^\circ\text{C}$

APPENDIX K - SUMMARY OF MEASUREMENTS OF RESISTIVITY AND SEEBECK COEFFICIENT OF FERRITES AND TITANATES AT TEMPERATURES UP TO 1000°C

Philipp H. Klein

July 1959

ABSTRACT

The electrical resistivities and Seebeck coefficients of a number of oxidic semiconductors are presented for the temperature range 25 - 1000°C. For the materials exhibiting the highest values of S^2/ρ , additional measurements were taken after the specimens were partially reduced. Specimens of strontium titanate, doped with niobium and with antimony, were examined for their stability to reduction by heating in a vacuum. Although none of the compounds investigated are currently suitable for application in thermoelectric devices, it is concluded that additional study of the effects of doping on the ferrite and titanate systems may lead to some promising materials for high-temperature uses.

INTRODUCTION

There can be little doubt of the virtue of precise measurements, as functions of temperature, of the electrical resistivity, the Seebeck coefficient, and the thermal conductivity of any material which is being considered for use in thermoelectric power generation. Given these three properties, it is possible to calculate the figure of merit, Z , which is defined by

$$Z = \frac{S^2}{\rho k}$$

where S is the Seebeck coefficient (sometimes called the thermoelectric power), ρ is the electrical resistivity, and k is the thermal conductivity. When Z is precisely known over a range of temperatures, the optimum performance of a thermoelectric generator operating within that temperature range can be predicted with accuracy.

Competing with the desire for precision in the measurement of the factors entering into the figure of merit is the frequent wish for a rapid method for their estimation. The gross effects of alteration of the composition of a material may be more important, for the moment, than a detailed knowledge of individual values. The investment in time and care entailed in precise measurements may be unwarranted by their practical value. It is therefore important that a method be devised which will enable the investigator to select the most promising of the materials at his disposal for careful scrutiny of their properties. If the technique can be so contrived that it yields data of moderate precision while also performing the function of rapid screening, both the academic and practical ends can be served.

The determination of the sign, magnitude, and temperature dependence of the Seebeck coefficient is relatively simple. Measurement of the magnitude of the electrical resistivity and its variation with temperature is also accomplished with relative ease. In the case of thermal conductivity, however, the measurement technique becomes quite complex at temperatures above 300°C, and may become an end in itself at 1000°C. Fortunately, the electrical properties can be evaluated consecutively in the same apparatus. Small changes in composition can be expected to

produce a larger change in these properties than in the thermal conductivity, in this temperature range. Therefore, when provided with the electrical behavior of his materials, the investigator may decide to undertake the measurement of thermal conductivity, or make a rough estimate of the figure of merit.

DESIGN OF EQUIPMENT

Two different sets of equipment have been employed, both of which permit the measurement of the resistivity and Seebeck coefficient of two or more specimens, from room temperature to 1000°C, in the course of an eight-hour day. The first apparatus constructed was a modification of a two-probe resistivity-measuring fixture. An improved equipment, in which the resistivity is determined by the more reliable four-probe method, was used for the later measurements. Both incorporate such desirable features as the rapid placement of samples, rapid changes in temperature, and easy establishment of the desired temperature difference across the sample (for measurement of the Seebeck coefficient). For simplicity, complicated thermal shielding has been eliminated. Finally, both devices employ standard electrode materials which are chemically inert, and both permit measurement in a controlled atmosphere or vacuum.

In the original equipment - dubbed a 'two-probe S- ρ meter' - rapid temperature changes were made possible by the use of a radio-frequency heater and a pair of graphite susceptors as the source of heat. As is shown in Figure K-1, a temperature difference of five to ten degrees could be maintained across the sample by vertical motion of the coil of the induction heater. To minimize the effects of convection in the residual gases in the bell-jar, the upper cylinder was always kept at the higher temperature. Although there was no thermal shielding, the use of flat plates or cylinders as the sample shapes reduced the effects of thermal radiation from the specimen.

Figure K-2 shows the sample and electrode assembly of the two-probe system in some detail. Platinum was sputtered over the entire sample, and carefully abraded from the edges. Sputtering was selected as the means of electrode application in preference to painting because of the possibility of contamination by the non-metallic portions of paints or pastes. The sputtered electrodes were placed in contact with the platinum foils indicated in Figures K-1 and K-2, to which thermocouples and voltage probes have been spot-welded. There results an electrical circuit consisting solely of the sample itself and platinum conductors. As a result, all Seebeck coefficients determined are directly referred to the standard material, platinum.

The measuring circuit employed with the two-probe model is shown schematically in Figure K-3. Seebeck voltages were determined with the switches in the position shown in the drawing. For this measurement, the potentiometer was connected to the sample by means of the wires '1' and '2'. The temperatures of the opposite faces of the specimen were measured within seconds of the Seebeck-voltage measurement, using the thermocouples shown in Figure K-2.

In order to measure the resistance of the specimen, the switch connecting the voltage source to the measuring circuit was closed, and the voltages developed across the sample and across the standard resistor were determined. Because of the limited range of the particular potentiometer used, neither of these voltages ever exceeded 15 millivolts.

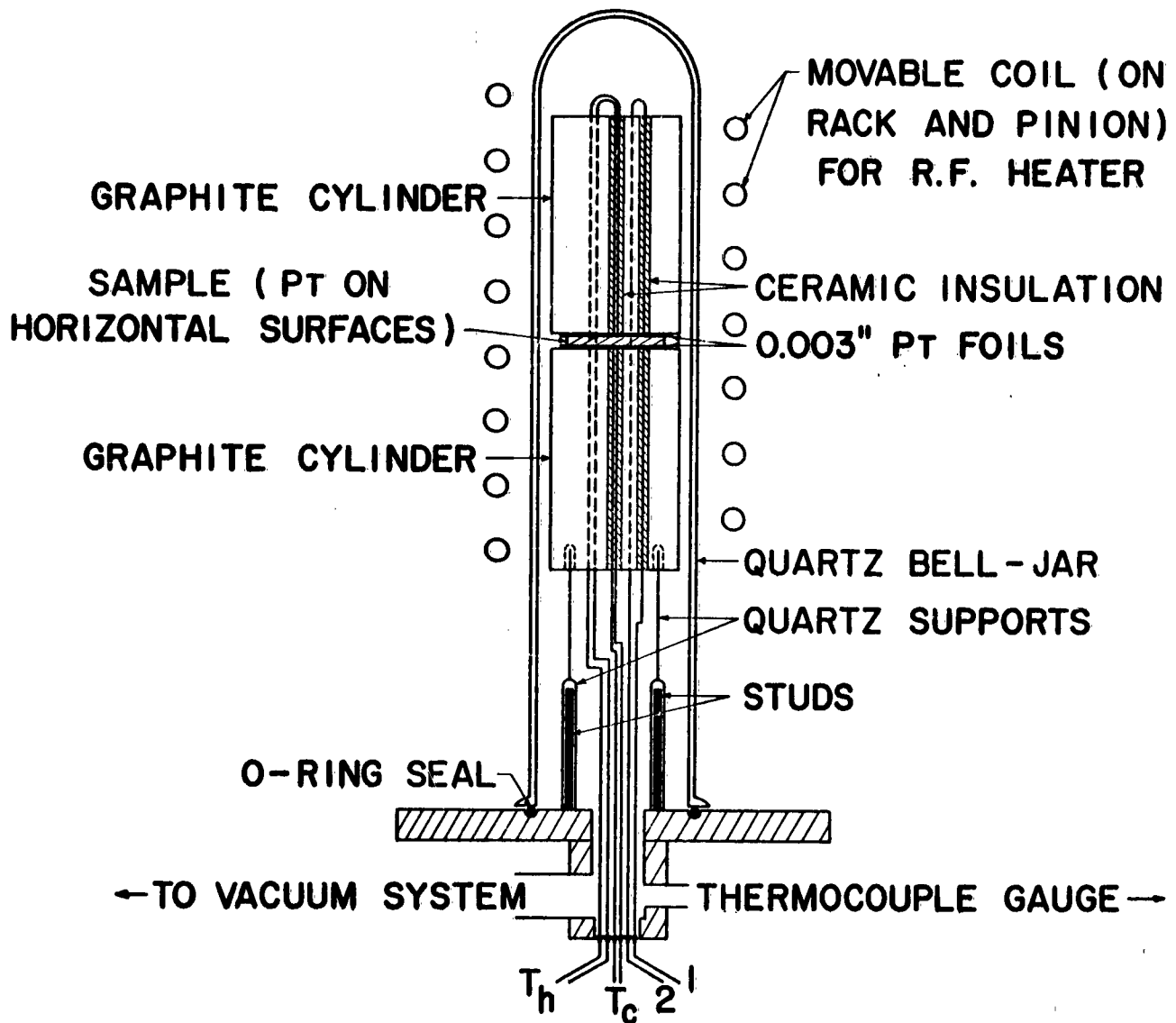


Figure K-1: Schematic Diagram of Two-probe $S-\rho$ Meter

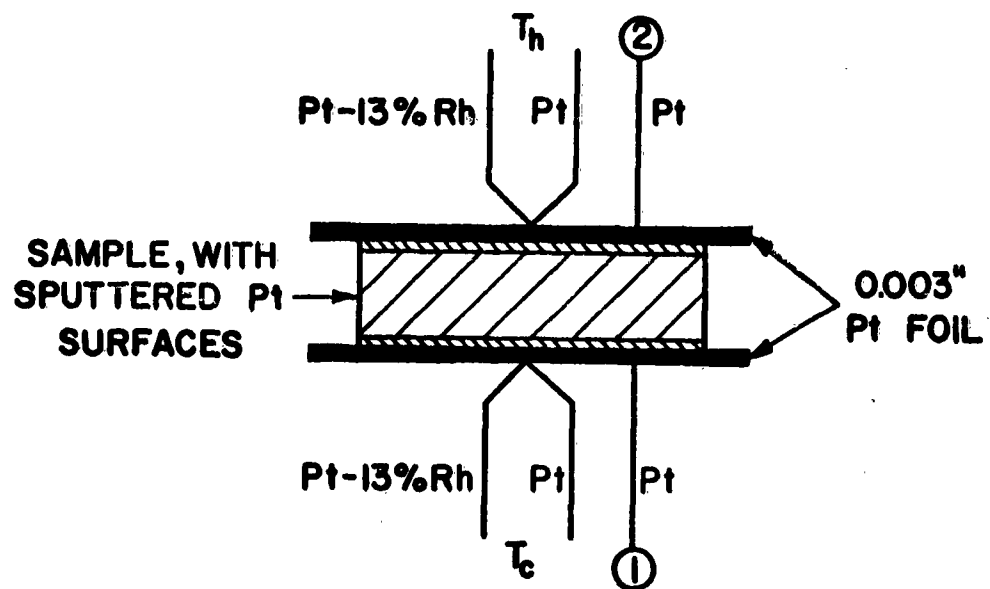


Figure K-2: Sample Placement in Two-probe $S-\rho$ Meter

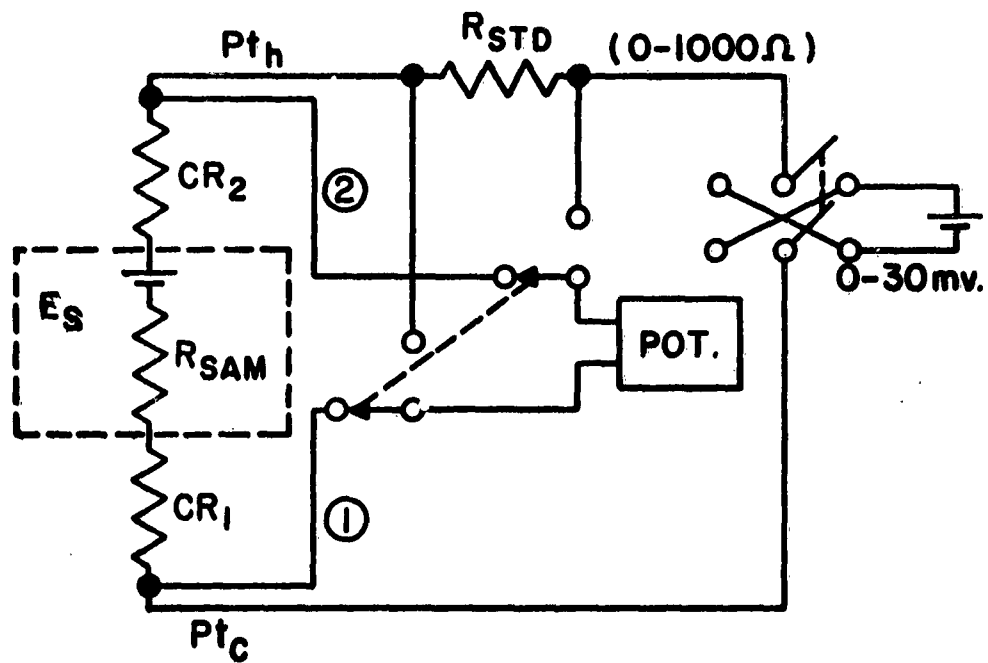


Figure K-3: Measuring Circuit for Two-probe Equipment

Since ionic migration may become appreciable at higher temperatures, there is always the possibility that the specimen may exhibit the properties of a galvanic cell. To avert misleading observations resulting from this phenomenon, the direction of current flow was reversed and a second set of data immediately taken. If the apparent resistance with the current reversed differed markedly from the initial value, and changed rapidly with time, electrolytic action was suspected. A difference in apparent resistance which is not subject to a time-variation is indicative of a rectifying contact either between the sputtered electrodes and the specimen or between the platinum foil and the sputtered contacts.

An obvious failing of any two-probe method for the measurement of resistance is the introduction of contact resistances (shown in Figure K-3 as CR_1 and CR_2). Because of this, the resistance and resistivity data derived by its application must be considered as maxima. Experiments on pieces of different thicknesses and of identical composition and cross-section have shown that, for the systems investigated, the contact resistances were less than five per cent of the observed resistance of the thinnest sample. It should be pointed out, in addition, that the method was conceived as a means of determining the value of making more accurate measurements on a given material. When viewed in this light, it can be seen that the unlikely presence of excessive contact resistances can only cause rejection of the material for further study, and cannot result in over-optimistic estimates of its worth for thermoelectric applications.

In order to permit more complete interpretation of the data obtained with the S-P meter, a four-probe model was constructed. The principle of its design is shown in Figure K-4. The sample was a flat, oblong plate, on which four dots of platinum were sputtered (through a mask) to serve as electrodes. Four thermocouples make contact with the electrodes, the platinum leads also serving as portions of the electrical measuring circuit. For measurement of the resistivity, the two outer leads were used as current leads, the inner pair being the voltage probes. Despite the fact that the current leads are placed on a side of the plate, Smits^(K-1), following the calculations of Uhlir^(K-2), has shown that proper selection of the dimensions produces results which can readily be corrected to give excellent agreement with measurements made by more conventional methods. If the dimensions indicated in Figure K-5 are so selected that $t:wd::1:2.5:10$, the correction is less than one per cent. It can be readily seen that only a small error results from the use of the circular electrode spots, provided that their diameter is kept to less than $0.1w$. It was found quite feasible to prepare samples which meet these geometric requirements, when t , the thickness, is 0.5 cm, or less.

To simplify placement of samples in the four-probe assembly, the schematic location of the thermocouples in Figure K-4 was inverted, so that the specimen rests on the thermocouple beads, as is shown in Figure K-5. A chief advantage of this inversion is the fact that it is not necessary to disturb the thermocouple leads when changing samples. The dimensions of the Lavite heater-core are such that samples are automatically placed in contact with the thermocouples when placed inside the core.

It will be noted that resistance heating was used in the four-probe device, rather than induction heating. The change was made because of several factors. First, measurements made in the original equipment gave indications that chemical reduction was effected by the presence of hot graphite in the bell-jar. Second, the size of the specimens requires that more stringent precautions against temperature

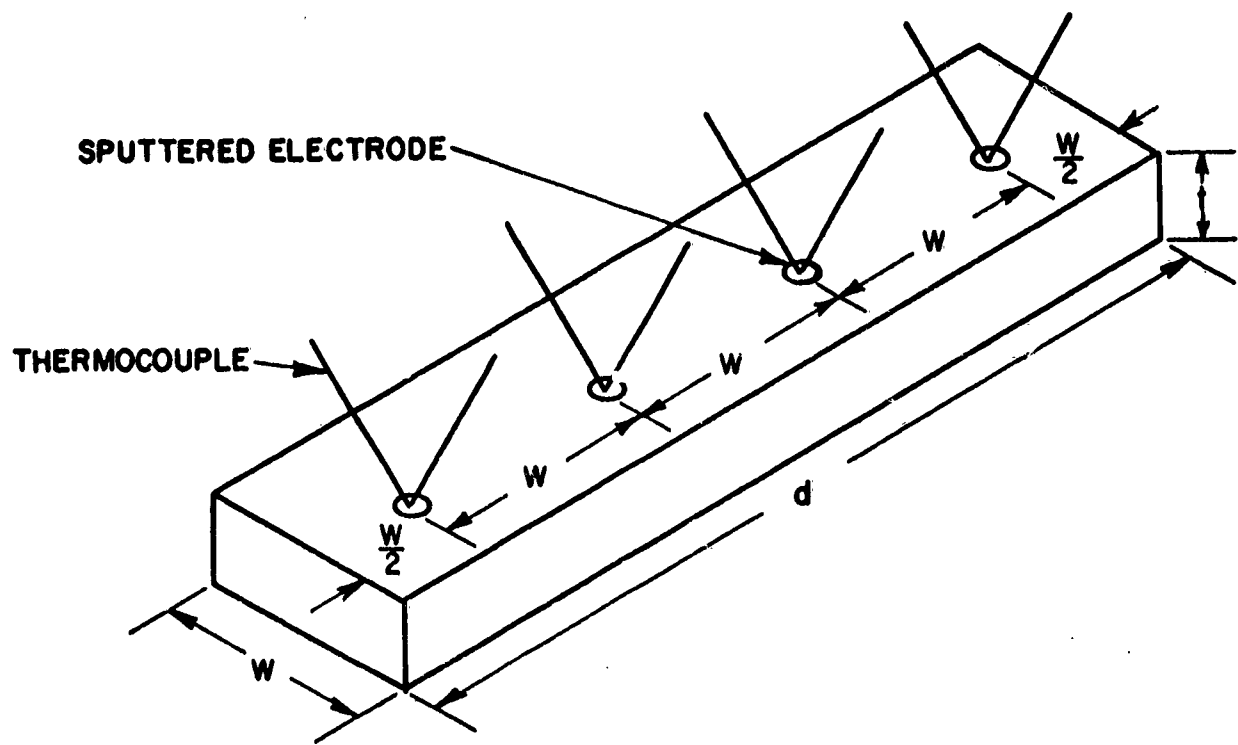


Figure K-4: Sample Placement in Four-probe S- ρ Meter

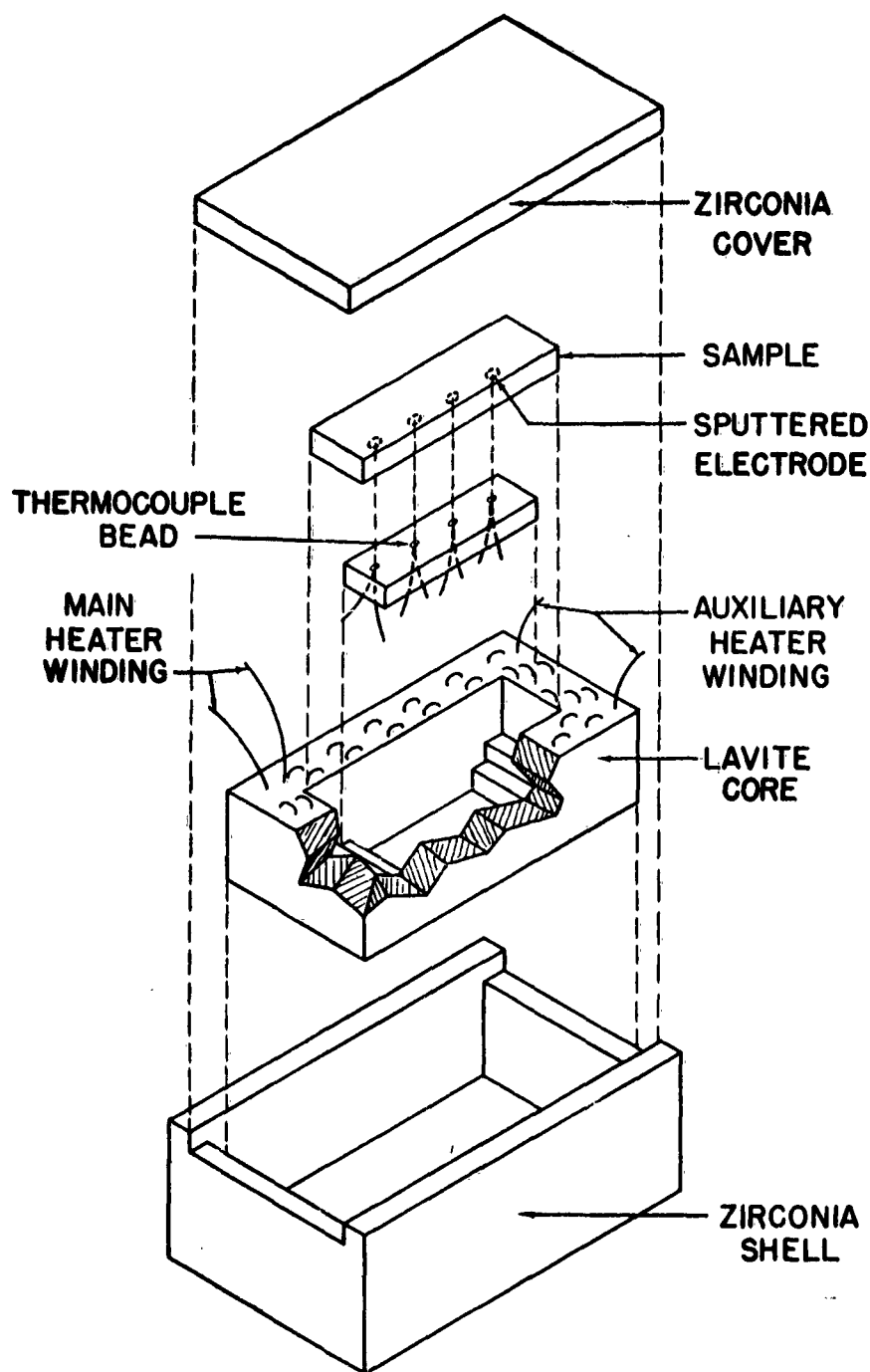


Figure K-5: Exploded View of Four-probe Apparatus

inhomogeneities be taken. By surrounding the specimen with a heater, and placing both heater and sample in an insulating container, greater control over local variations in temperature could be obtained. Finally, decreasing the thermal inertia of the system was highly desirable. The rate of cooling of the resistance-heated device was found to be about twice that of the system employing the large graphite susceptors.

At one end of the Lavite heater core, in Figure K-5, can be seen an auxiliary heater winding. The purpose of this winding was to introduce a temperature difference between the outermost electrodes, in order to measure the Seebeck coefficient. It was possible to maintain the temperatures of all four electrode spots within one degree of one another, at 1000°C, using only the main heater. With the auxiliary heater, temperature differences of between five and ten degrees could be produced across the electrodes with the widest separation. It thereby became possible to measure the resistivity of the sample under isothermal conditions, while yet being able to impress small temperature differences for determination of the Seebeck coefficient. This degree of versatility was not available with the two-probe equipment.

DISCUSSION OF TYPICAL RESULTS

In order that a material be considered for thermoelectric applications, it is almost essential that the quotient, S^2/ρ , be at least 10^{-5} - 10^{-6} watt/cm-°K². To meet this criterion, a material with a resistivity of 1 ohm-cm must exhibit a Seebeck coefficient of 1000 microvolts/°K. To satisfy the requirement with a material whose resistivity is 0.01 ohm-cm, the Seebeck coefficient need be only 100 microvolts per degree. Materials currently employed in thermoelectric devices have Seebeck coefficients of about 100-200 microvolts/°K and resistivities of the order of 10^{-3} ohm-cm, throughout the temperature range of their use. This corresponds to an S^2/ρ ratio of 10^{-5} to 4×10^{-5} watt/cm-°K².

With these criteria in mind, it can be seen that the materials whose properties are depicted in Figures K-6 and K-7* are clearly not suitable for utilization of their thermoelectric properties. Although the electrical resistivity of the iron titanate tends toward the useful range at high temperature, the Seebeck coefficient is too low to lend promise to the material. The shape of the $\log \rho - 1/T$ curve obtained with 95% BaTiO₃ + 5% BaFeO₃ is an apparent contradiction to an empirical rule established by Parker(K-3). He found that semi-metallic behavior in a low temperature range and semiconducting properties at elevated temperatures are found only in materials whose resistivity is less than 4 ohm-cm at the temperature of transition from semi-metallic to semiconducting behavior.

The seventy-fold exaltation of the apparent resistivity at the transition point is not completely ascribable to contact resistances. Flaschen and van Uitert(K-4), in a series of room-temperature measurements, showed that the apparent resistivity with evaporated-gold electrodes was less than one order of magnitude greater than the 'true' value. Sputtered platinum electrodes may be expected to have an effect similar to that of evaporated gold films, at room temperature. At elevated temperatures, one would expect the effect to be diminished, if slight diffusion of the

*All of the data displayed in Figures K-6 and K-7 were obtained with the two-probe S- ρ Meter.

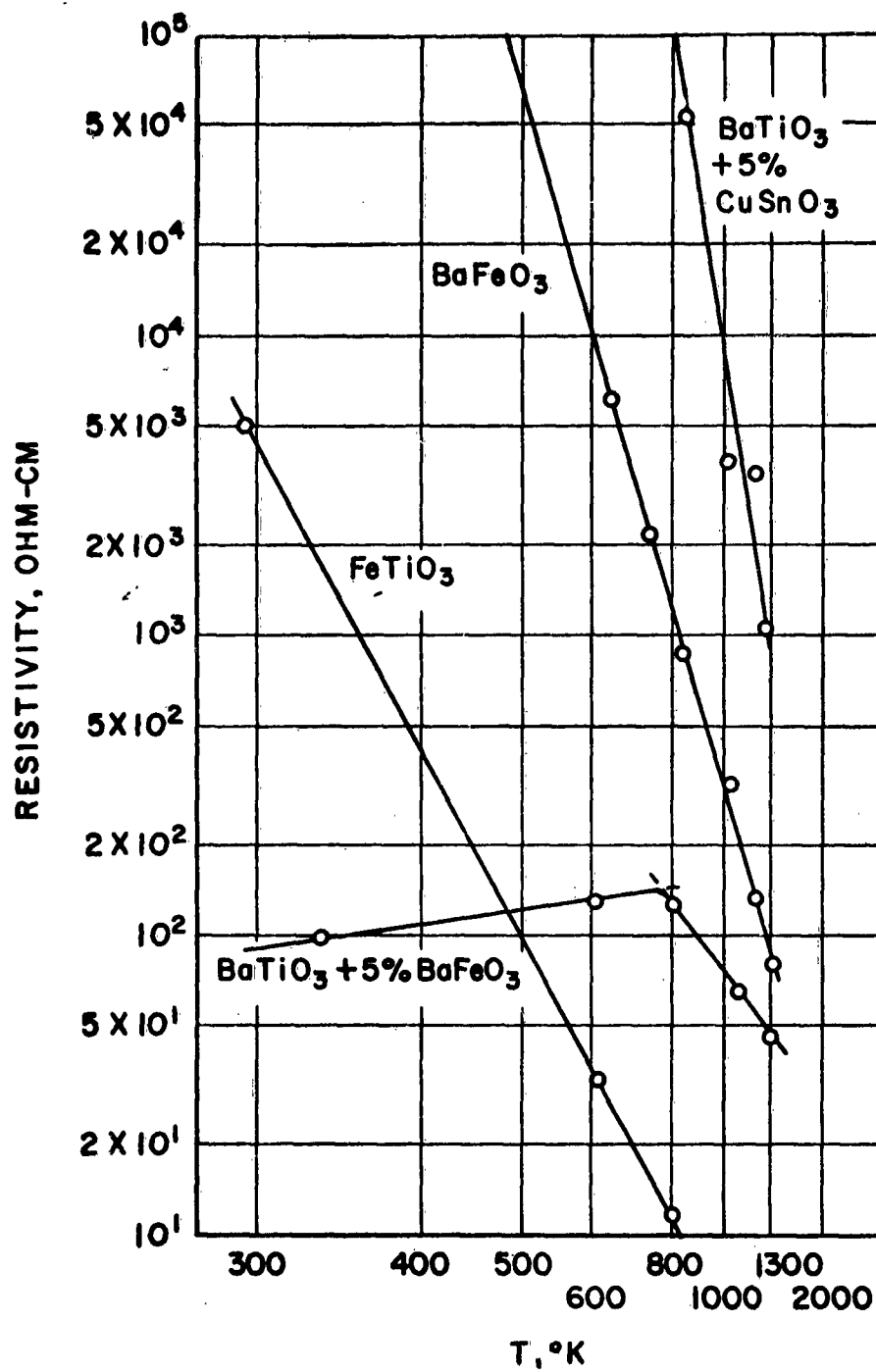


Figure K-6: Resistivity Data for a Group of Titanates

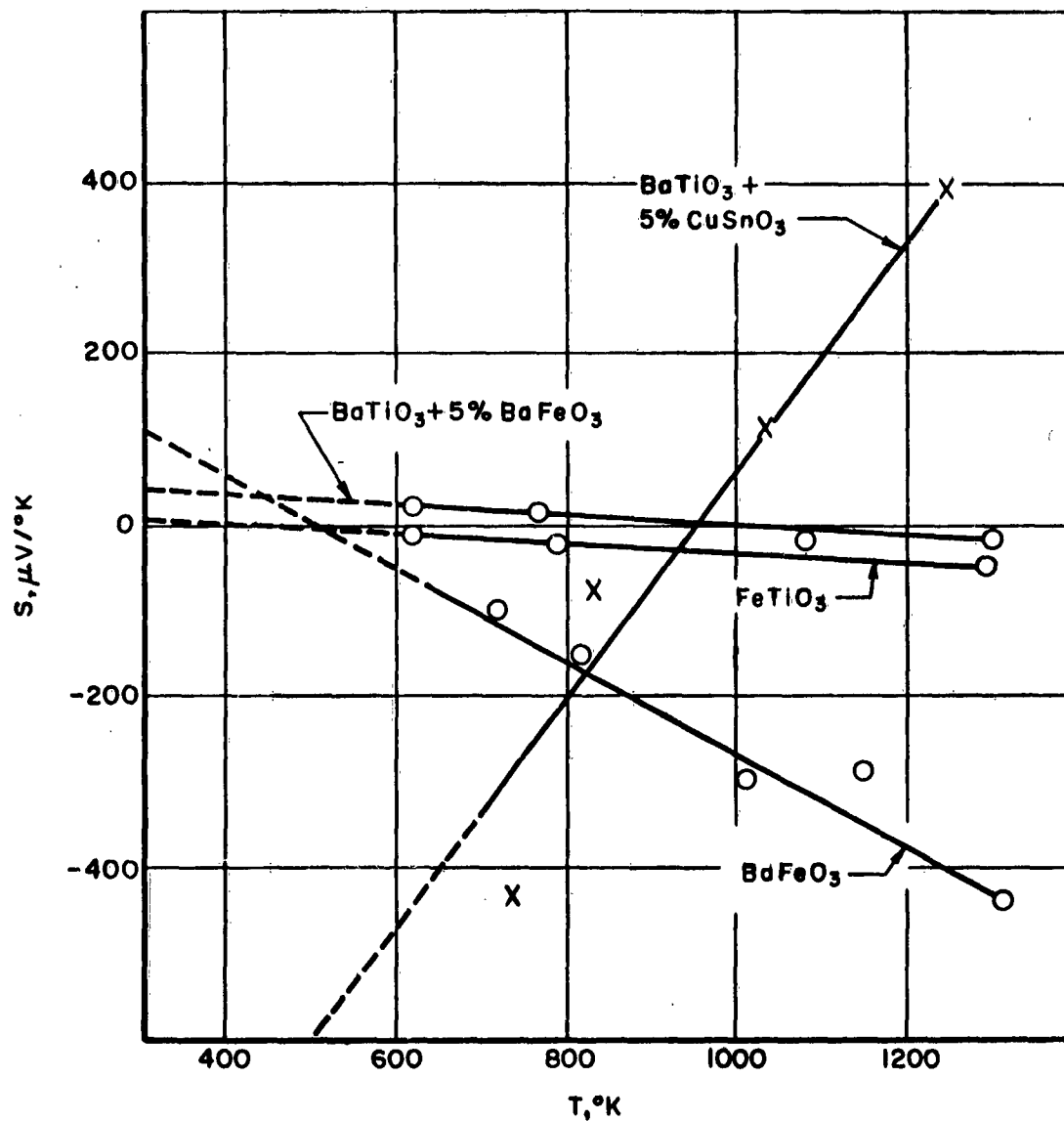


Figure K-7: Seebeck Coefficients of a Variety of Titanates

electrode metal into the surface layers of the ceramic were to take place. This ambiguity is absent from data obtained with the four-probe equipment.

Some of the ferrites whose properties are displayed in Figures K-8 and K-9 come slightly closer to meeting the criteria for thermoelectric utility. It is interesting to note that the discontinuity in the $\log \rho - 1/T$ curve for the undoped nickel-zinc ferrite takes place at the temperature of transition from p-type to n-type conduction. A similar phenomenon was observed by Volger (K-5) in his study of a series of ferromagnetic oxides. In the p-type region, the pure nickel-zinc ferrite has an activation energy for conduction of 0.31 eV, which agrees with the observations of Parker (K-6). Van Uitert (K-7) found that negative carriers predominate in nickel-zinc ferrites when the Fe:O ratio is greater than 2:4. Since the present work involved the heating of the samples in a vacuum, it is likely that this stoichiometric ratio would be somewhat greater than 0.5. The well-known difficulty of reduction of manganese-bearing ferrites makes its positive Seebeck coefficient seem consistent with this picture.

The Curie temperature of the undoped nickel-zinc ferrite was determined prior to the present measurements, and found to be about 515°C (793°K). This corresponds quite closely to the temperature at which the slope of the $\log \rho - 1/T$ curve and the sign of the predominant carriers change. This observation would seem to contradict the observation of Parker (K-3, K-6) that, in nickel-zinc ferrites, the discontinuities in the $\log \rho - 1/T$ curves do not take place at the magnetic transformation temperature. However, Parker found that all his materials were p-type, which fact suggests differences in oxygen content between his samples and those of the present investigation.

The data presented in Figures K-8 and K-9 indicate that doping of ferrites - either by addition of specific doping agents or by slight reduction - significantly improve the prospect of utilizing the materials for thermoelectric applications. Additional study of the stability of the reduced and doped compounds would be necessary before any other conclusions can be drawn.

Figures K-10 and K-11 portray results obtained on some oxidic compounds of barium, cobalt, chromium, and titanium. Their high resistivities and low Seebeck coefficients eliminate them from consideration for further study. The curves are presented here mainly for their academic value.

Both models of the S- ρ meter are ideally suitable for the study of the effects of vacuum-reduction without physically disturbing the specimen or exposing it to the atmosphere. Taking advantage of this feature, the effects of initial purity on the properties of reduced strontium titanate were investigated. Weise and Lesk (K-8) found that the resistivity of strontium titanate decreases by as much as seven orders of magnitude, upon reduction in hydrogen. Losses in weight accompanying this great change in electrical resistivity amounted only to 0.23 per cent. Using an optical technique and working with single crystals of extremely pure strontium titanate, Gandy (K-9) has obtained evidence of marked enhancement of the reversible rate of oxygen diffusion in this material over that in chemically-pure strontium titanate. The effects of vacuum-reduction on the electrical resistivity and Seebeck coefficient of the ultra-pure materials had not been measured, however.

The two-probe S- ρ meter was used to compare the resistivities and Seebeck coefficients of ceramic bodies prepared from chemically-pure strontium titanate (TAM, Inc., CP grade) and ultra-pure material (obtained from the research laboratories of

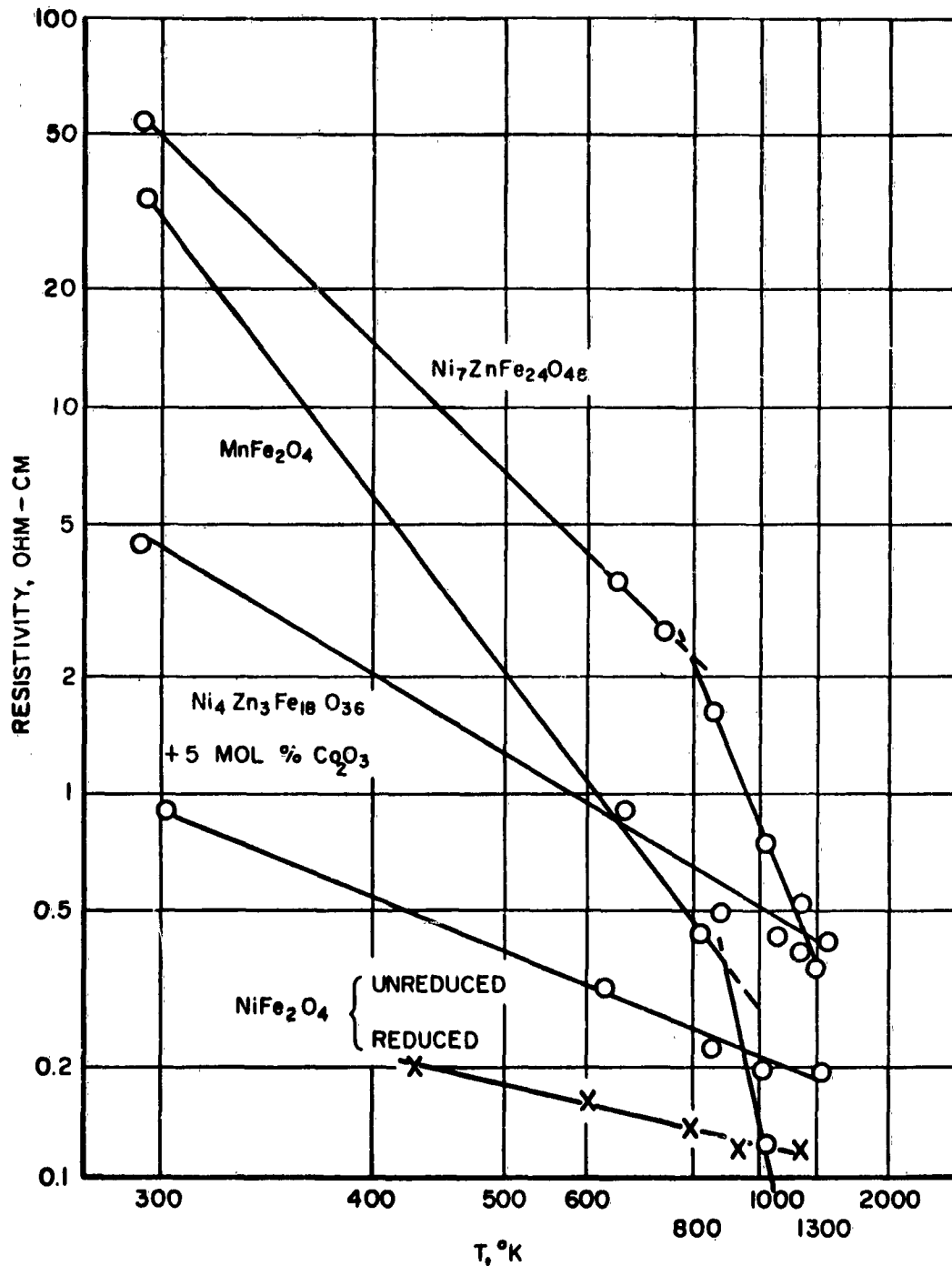


Figure K-8: Variation of Resistivity of a Number of Ferrites as a Function of Temperature

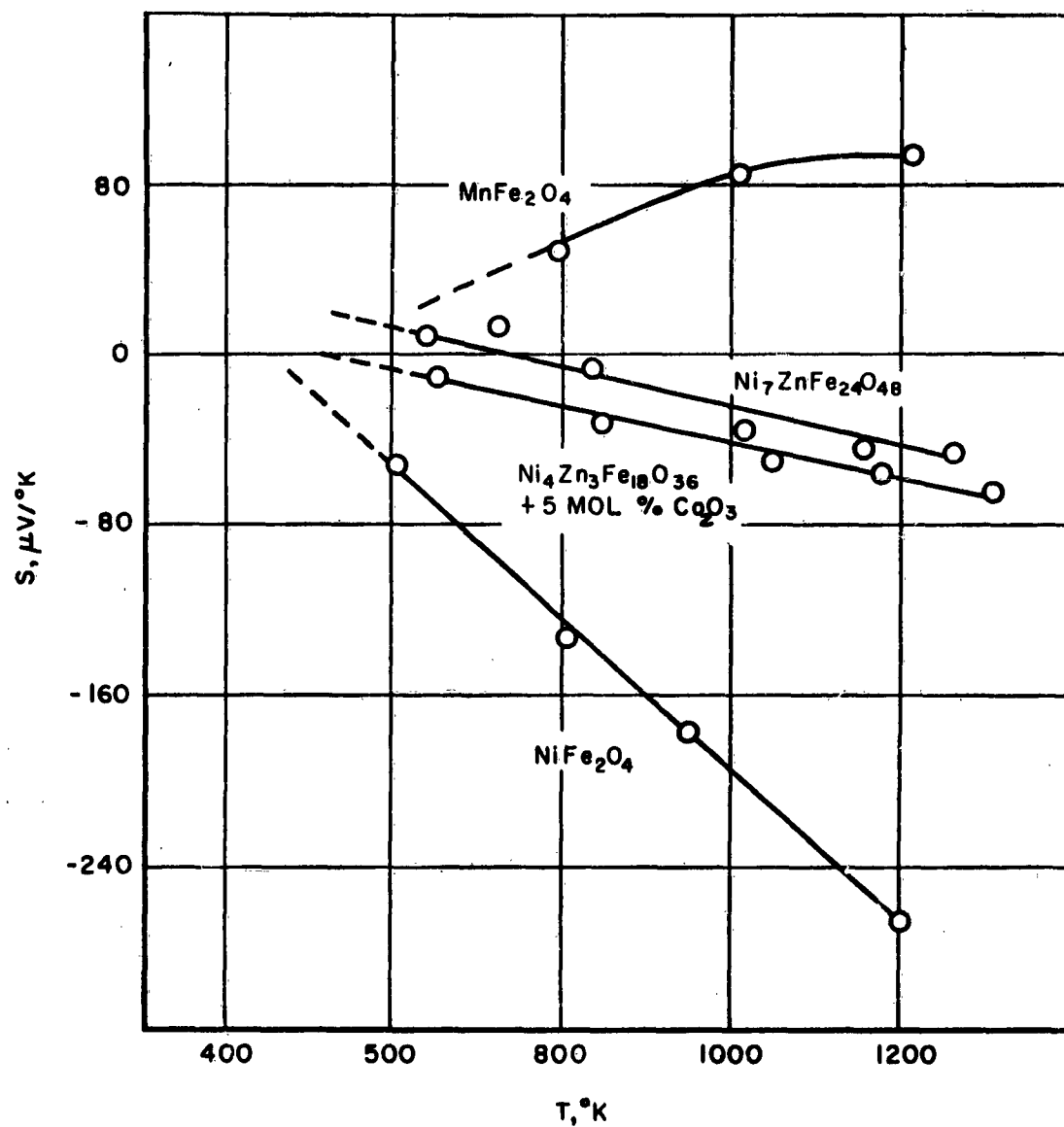


Figure K-9: Seebeck Coefficients of the Ferrites Whose Resistivities are Shown in Figure K-8

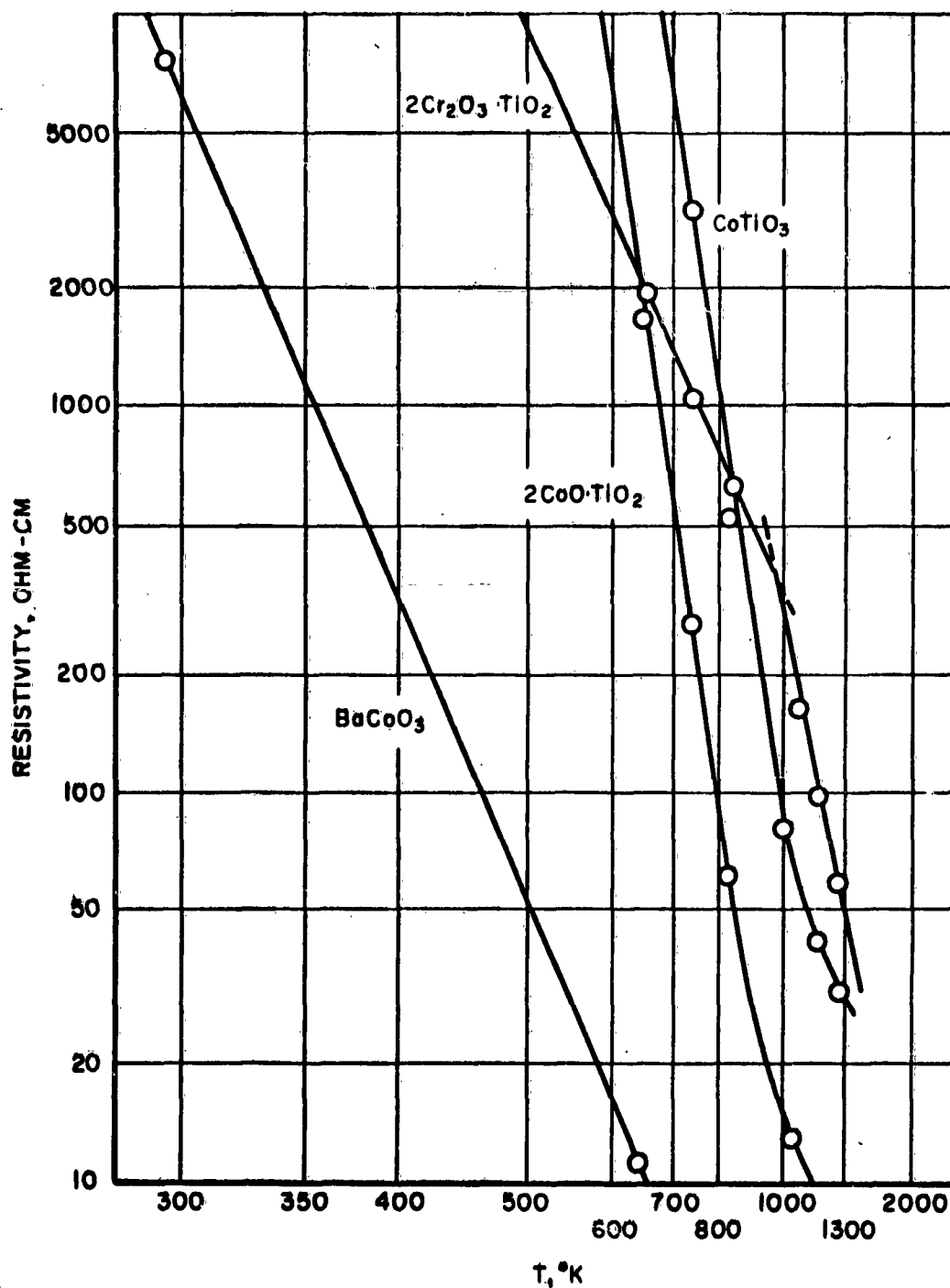


Figure K-10: Effect of Temperature on the Resistivities of a Number of Compounds of Mainly Academic Interest

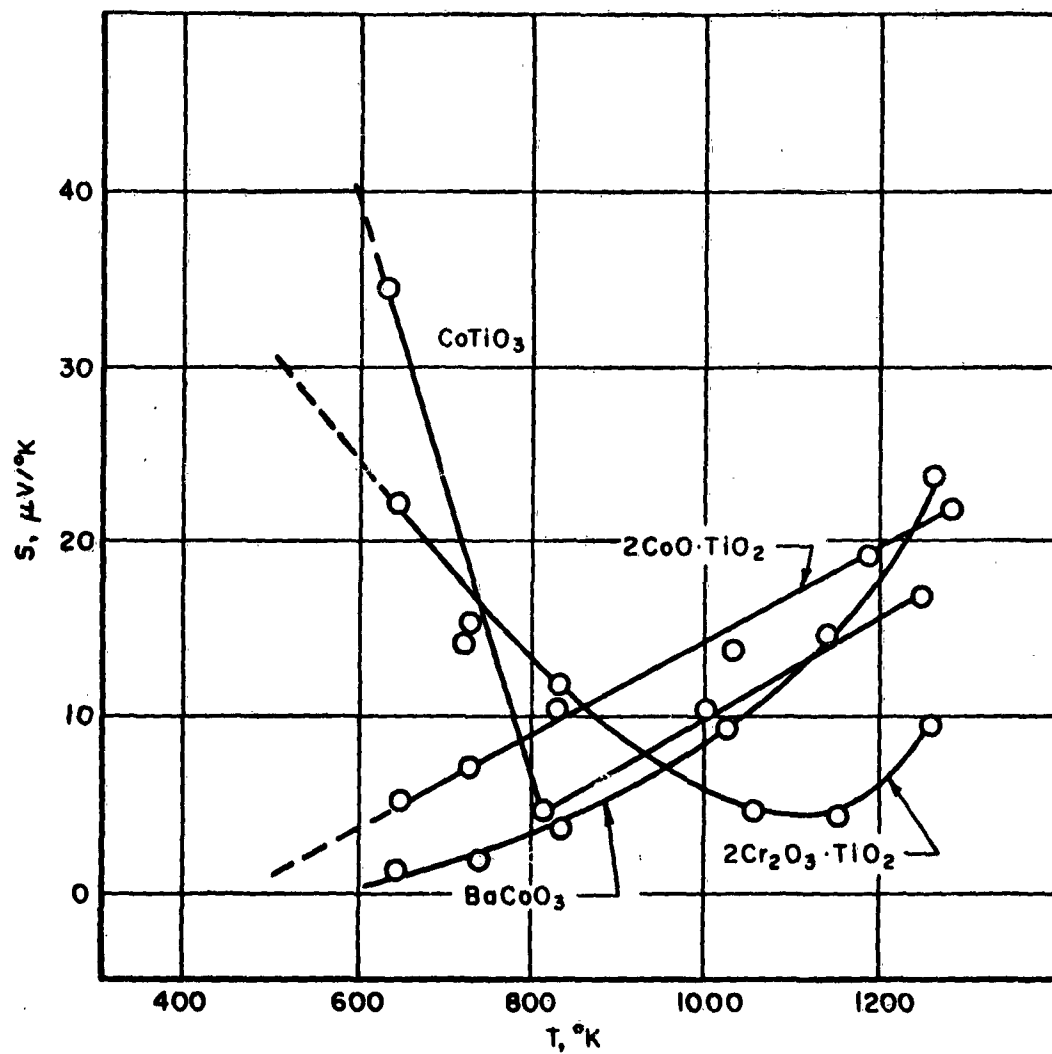


Figure K-11: Seebeck Coefficients of Materials Whose Resistivities are Shown in Figure K-10

the National Lead Company). Ceramic bars of both degrees of purity were pressed and fired at 1450°C, the CP bars in air, the ultra-pure bars in oxygen. All fired specimens exhibited a density which was 94-96% of the theoretical value (5.12 g/cm³). Reduction took place in the measuring equipment, and was effected by heating to 1050-1080°C and pumping with the diffusion pump. At the end of the reduction period, the sample was allowed to come to equilibrium with its gaseous environment and the series of measurements taken. The results are shown in Figures K-12 and K-13.

It is evident, from the resistivity data in Figure K-12, that the reduction of ultra-pure strontium titanate takes place more readily than does that of CP material. Despite the fact that there was no attempt made to reduce it during the initial measurements on the ultra-pure specimen, its resistivity is one or two orders of magnitude lower than that of the CP sample after more extensive reduction. As can be seen from Table K-1, the CP sample, after only half an hour of vacuum-reduction, showed a discontinuity in its $\log \rho - 1/T$ curve. At 1000°K, its resistivity was nearly equal to that of Weise and Lesk's specimen after its first reduction in hydrogen (K-8). Its low-temperature activation energy was only one-tenth that of the Weise and Lesk specimen after its first reduction. In accordance with the observations of Gandy (K-9), the activation energies and resistivities in the impurity-conduction region are appreciably lower for the strontium titanate of higher purity. The resistivity is not quite so nearly constant, however, as the values obtained from measurement of a CP specimen which had been extensively reduced in a hydrogen atmosphere.

Examination of the Seebeck coefficient data (Figure K-13 and Table K-1) shows that that property is increased by reduction, particularly at higher temperatures. The reason for the larger values exhibited by the vacuum-reduced material is not obvious. Nor does any explanation come to mind for the low Seebeck coefficient of the hydrogen-reduced CP strontium titanate.

From Figure K-12 and Table K-1, it is evident that, as vacuum-reduction proceeds, the resistivity of the ultra-pure strontium titanate approaches a limiting low value. If this observation is correct, the limiting value could be taken as the lowest resistivity attainable by introduction of oxygen vacancies into the material. Since it would be necessary to diminish the resistivity by two or three orders of magnitude for strontium titanate to become interesting for thermoelectric purposes, it does not appear that vacuum-reduction alone is a suitable method.

On the other hand, if sufficient amounts of a known impurity were introduced, it might be possible to lower the resistivity to the desired range. With this in mind, samples of ultra-pure strontium titanate were prepared, in which one per cent additions of niobium and of antimony were incorporated. These impurities were selected on the basis of their radii, as well as because of their known tendency toward the pentavalent state. If pentavalent ions are substituted for the normally tetravalent titanium ions, it was thought, some of the titanium ions would have to adopt the trivalent state, in order to preserve electrical neutrality. This situation would lead to a greater tendency toward "super-exchange", with a consequent decrease in the resistivity.

Figure K-14 shows the results obtained for the two doped samples, and compares them with the CP, ultra-pure, and hydrogen-reduced specimens which had been examined previously. Evidently, the two impurities behave in different fashions. The antimony behaves in the manner expected: the carriers introduced by its incorporation

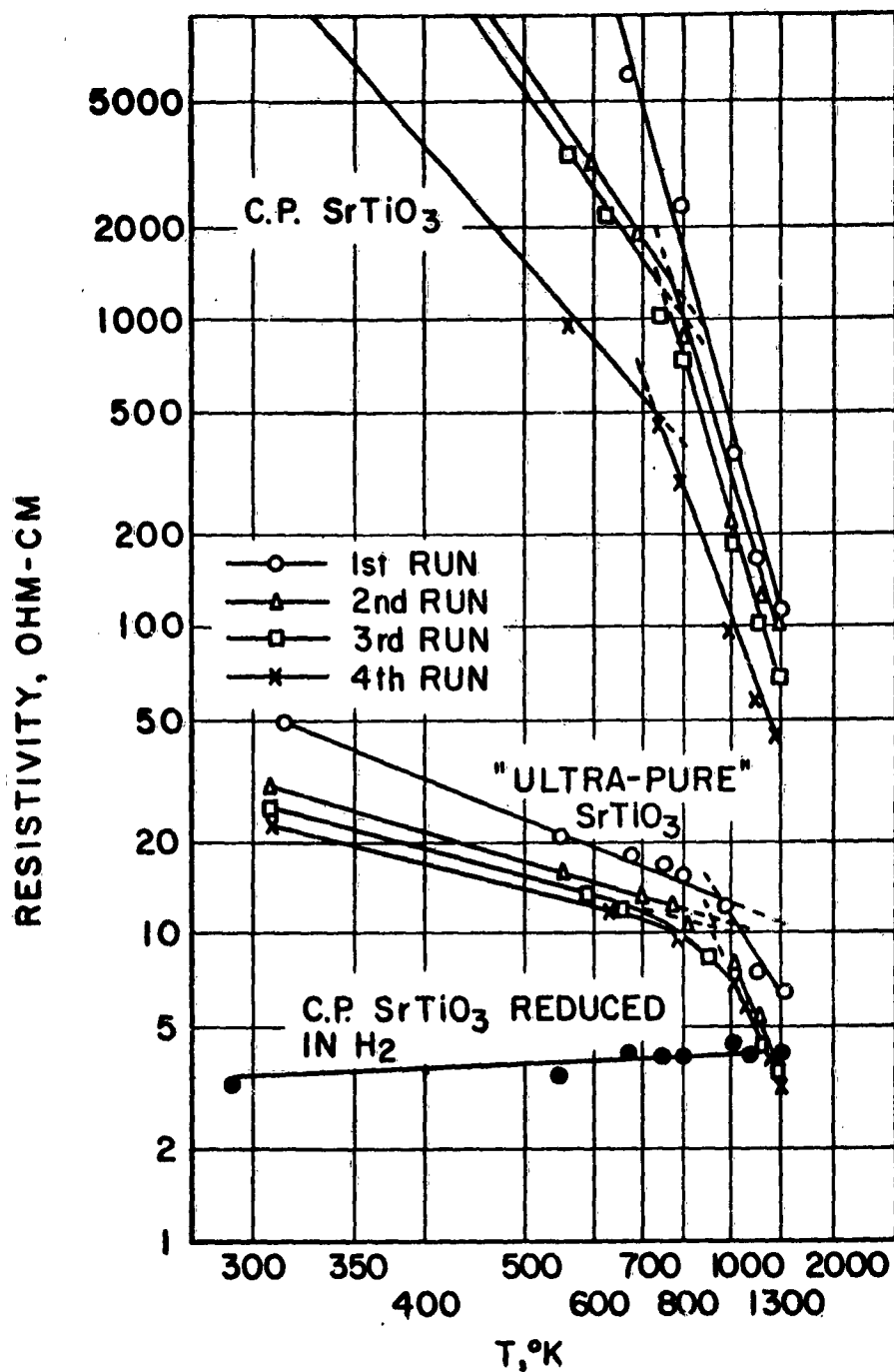


Figure K-12: Effect of Reduction in a Vacuum on Strontium Titanate of Two Initial Degrees of Purity. In Each Case, the Circles Represent the Lowest Degree of Reduction, the Crosses the Highest Degree of Reduction.

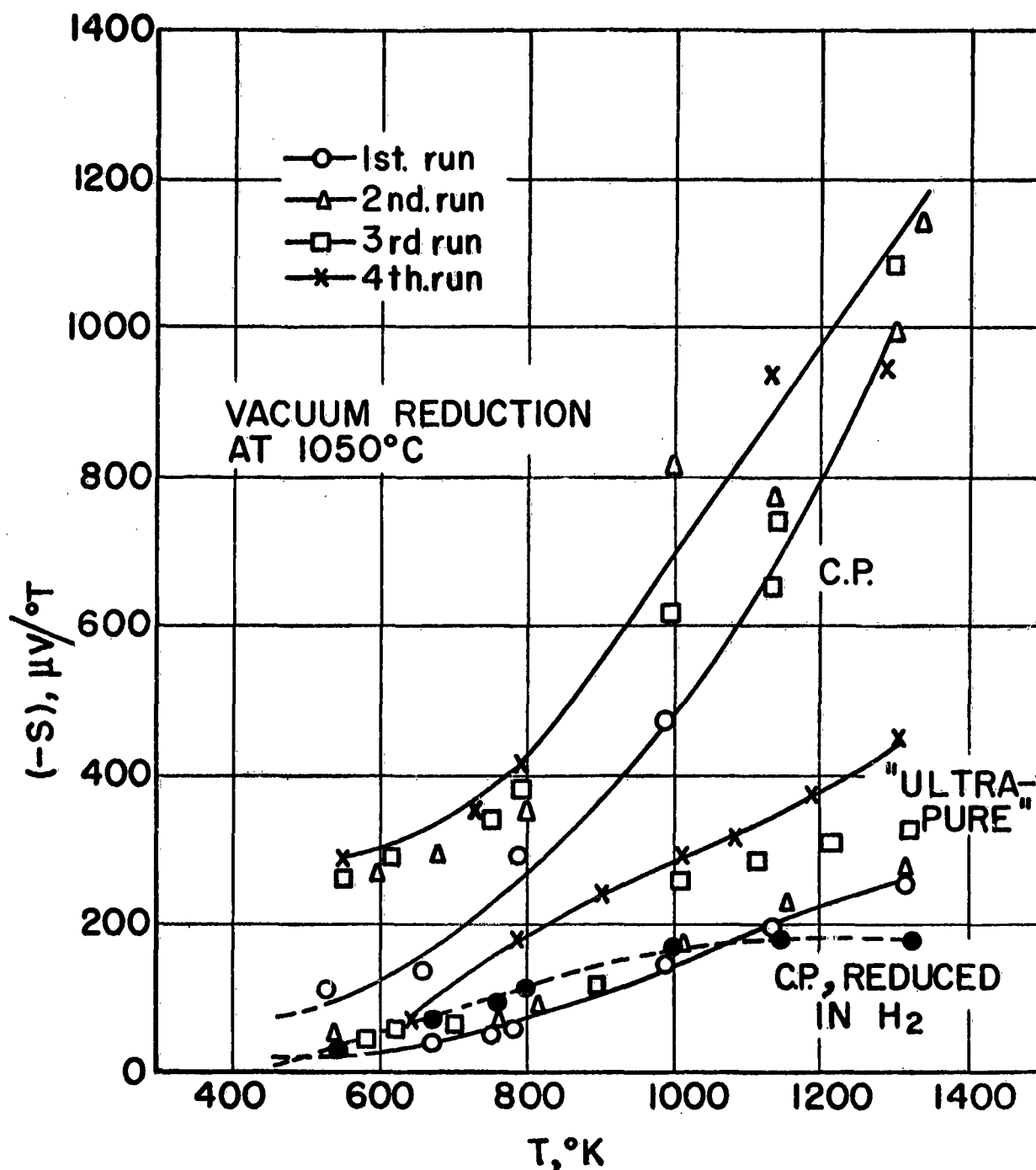


Figure K-13: Seebeck Coefficients of Strontium Titanates Whose Resistivities are Shown in Figure K-12. For Clarity, Curves are Drawn Only Through Data for Lowest and Highest Degrees of Reduction. Graph Symbols having the same Significance as in Figure K-12. See Table K-1 and Text for Details of Reduction Procedure.

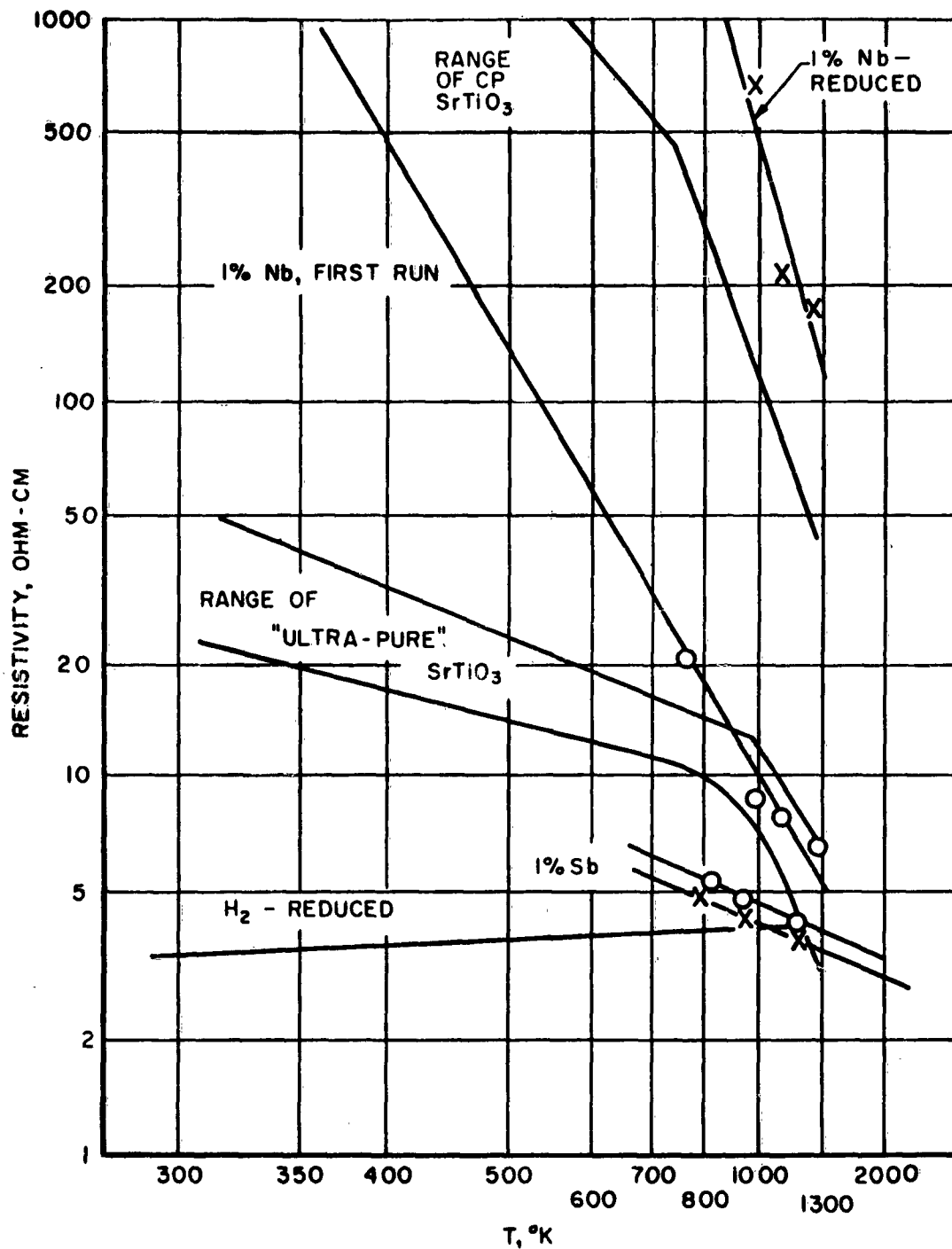


Figure K-14: Resistivities of Doped, Ultra-pure Strontium Titanate Compared with Undoped Samples. Circles: Unreduced Material; Crosses: After Vacuum Reduction at 1080°C for One Hour.

TABLE K-1

THE DEPENDENCE OF THE ACTIVATION ENERGY FOR CONDUCTION
ON TIME OF REDUCTION OF STRONTIUM TITANATE

<u>Reduction Time at 1050°C, Hours</u>	<u>Activation Energy, ev</u>	<u>Applicable Temperature Range, °K</u>	<u>Resistivity at Discontinuity, ohm-cm</u>
<u>C.P. Strontium Titanate</u>			
0.5	0.12	288 - 630	10,700
	0.49	630 - 1300	
1.5	0.18	287 - 738	1,450
	0.44	738 - 1300	
2.5	0.18	285 - 785	1,350
	0.43	785 - 1300	
4.5	0.25	292 - 748	410
	0.35	748 - 1300	
Hydrogen- Reduced	-0.014	291 - 1300	4.0 at 740°K
<u>Ultra Pure Strontium Titanate</u>			
0.	0.045	307 - 760	15.8
	0.14	760 - 1300	
1.	0.041	307 - 940	11.0
	0.32	940 - 1300	
2.	0.034	307 - 920	9.8
	0.29	920 - 1310	
3.	0.034	310 - 925	9.6
	0.28	925 - 1300	

do not prevent the vacuum-reduction of the strontium titanate, and there is an additional decrease in the resistivity. Niobium, on the other hand, results in a material intermediate in its resistivity between the CP and the ultra-pure material. On attempting to reduce it by heating in a vacuum, the niobium-doped sample increased in resistivity to values which were indistinguishable from those of the unreduced CP strontium titanate.

No immediate explanation comes to mind for the behavior of the niobium-doped specimen. From the curves of Figure K-12, it appears that the "locking-in" of oxygen by the presence of impurities (as reported by Gandy^(K-9)) takes place in the Nb-doped sample to an extraordinary extent. It would require further experimentation to ascertain the mechanism of the process. Regardless of the mechanism of the process, it is evident that these few experiments on doping of strontium titanate have not produced materials meeting the requirements for application to thermoelectric devices.

None of the materials investigated can be classed as immediately useful for thermoelectric generator applications. (See Tables K-2 and K-3). However, with additional study and modifications of the composition, it may be possible to effect sufficient improvements in the properties of some classes of compounds to make it worthwhile to determine the thermal conductivity. Doped nickel-bearing ferrites would be likely materials in which such improvements could be wrought, as might antimony-doped strontium titanate.

The equipment developed in the course of this investigation appears adequate both for the purposes of screening materials and for studying small changes in resistivity and Seebeck coefficient. The speed of the four-probe S- ρ meter is sufficient to permit three samples to be studied with ease in a day. With slight modification of the holders for the electrical leads, sample placement can be simplified and reliability of performance increased.

ACKNOWLEDGEMENTS

The author is indebted to Dr. Harold W. Gandy for many stimulating discussions, and for making available his data on ultra-pure strontium titanate prior to their publication; and to Drs. Edward C. Henry, Herbert C. Rothenberg, and Alexis V. Illyin for supplying him with specimens. The collaboration of David J. Leestma in the design and construction of the four-probe equipment is acknowledged with thanks. The extreme gratitude of the author is due Harry C. Hinman, whose patience and diligence are largely responsible for the data contained in this paper.

REFERENCES

- K-1. F.M. Smits, Bell System Tech. J. 37, 711 (1958)
- K-2. A. Uhlig, Jr., Bell System Tech. J. 34, 105 (1955)
- K-3. R. Parker, Phil. Mag. (8) 3, 853 (1958)
- K-4. S.S. Flaschen and L.G. van Uitert, J. App. Phys. 27, 190 (1956)
- K-5. J. Volger, Physica, 20, 49 (1954)
- K-6. R. Parker, Proc. Phys. Soc. B 70, 531 (1957)
- K-7. L.G. van Uitert, J. Chem. Phys. 23, 1883 (1955)
- K-8. E.K. Weise and I.A. Lesk, J. Chem. Phys. 21, 801 (1953)
- K-9. H.W. Gandy, Phys. Rev. 113, 795 (1959)

TABLE K-2

ELECTRICAL RESISTIVITIES AND SEEBECK COEFFICIENTS OF THE OXIDIC SEMICONDUCTORS STUDIES
AT THREE SELECTED TEMPERATURES
(Resistivities in ohm-cm, Seebeck coefficients in microvolts/°K)

Composition	600°K		900°K		1200°K				
	s	ρ	s	ρ	s	ρ			
BaFe ₁₂ O ₁₉	-0.8	20.4	3.1 x 10 ⁻¹⁴	-3.7	16.6	0.82 x 10 ⁻¹²	-10.	10.5	0.95 x 10 ⁻¹¹
BaFe ₁₂ O ₁₉ + 50 mol% BaTiO ₃	+0.4	8.8	1.9 x 10 ⁻¹⁴	-0.3	1.7	5.3 x 10 ⁻¹⁴	-10.	0.62	1.6 x 10 ⁻¹⁰
95 mol% BaTiO ₃ + 5 mol% BaFeO ₃	+22	17.0	2.8 x 10 ⁻¹¹	+7	18.0	2.7 x 10 ⁻¹²	-13	32.5	5.2 x 10 ⁻¹²
FeTiO ₃	+10	800	1.2 x 10 ⁻¹³	+25	37	3.9 x 10 ⁻¹³	+40	7.9	2.0 x 10 ⁻¹⁰
95 mol% BaTiO ₃ +5 mol% CuSnO ₃	-465	2.35 x 10 ⁶	9.15 x 10 ⁻¹⁴	-75	1.8	3.1 x 10 ⁻¹³	+325	1.48 x 10 ³	7.13 x 10 ⁻¹¹
2CoO·TiO ₂	+3.8	7000	2.0 x 10 ⁻¹⁵	+12	23.5	6.2 x 10 ⁻¹²	+20	8.8	4.5 x 10 ⁻¹¹
2Cr ₂ O ₃ ·TiO ₂	+24.5	2.8 x 10 ³	2.1 x 10 ⁻¹³	+6.8	380	1.2 x 10 ⁻¹³	+6.3	74	5.3 x 10 ⁻¹³
CoTiO ₃	+40	80000	2.0 x 10 ⁻¹⁴	+7.2	225	2.3 x 10 ⁻¹³	+16	36.5	7.0 x 10 ⁻¹²
BaCoO ₃	+1.0	17	5.9 x 10 ⁻¹⁴	+5.8	2.3	1.4 x 10 ⁻¹¹	+18.0	0.76	4.26 x 10 ⁻¹⁰
Ni ₇ ZnFe ₂₄ O ₄₈	+2.	4.8	8.3 x 10 ⁻¹³	+20	1.4	2.9 x 10 ⁻¹⁰	+48	0.45	5.1 x 10 ⁻⁹
2BaO·Fe ₂ O ₃	-52	11250	2.4 x 10 ⁻¹³	-215	510	9.02 x 10 ⁻¹¹	-370	115	1.18 x 10 ⁻⁹
Ni ₄ Zn ₃ Fe ₁₈ O ₃₆ + 5 mol% Co ₂ O ₃	-8.0	0.88	7.3 x 10 ⁻¹¹	-32	0.52	2.0 x 10 ⁻⁹	-59	0.40	8.6 x 10 ⁻⁹
MnFe ₂ O ₄	+40	1.1	1.4 x 10 ⁻⁹	+71	0.20	2.4 x 10 ⁻⁸	+92	0.035	2.4 x 10 ⁻⁷

TABLE K-2 (continued)

Composition	600°K		900°K		1200°K	
	S	ρ	S	ρ	S	ρ
NiFe_2O_4	-53	0.17	1.6×10^{-8}	-162	0.134×10^{-7}	0.13×10^{-7}
SrTiO_3						
CP, first run	-130	11500	1.48×10^{-12}	-400	2.7×10^{-10}	4.38×10^{-9}
CP, fourth run	-305	780	1.19×10^{-10}	-600	2.18×10^{-9}	1.7×10^{-8}
Ultra-pure, first run	-33	18.5	5.9×10^{-11}	-120	1.07×10^{-9}	6.5×10^{-9}
Ultra-pure fourth run	-90	13.0	6.2×10^{-10}	-230	6.6×10^{-9}	3.6×10^{-8}
CP, H_2 -reduced	-40	3.9	4.1×10^{-10}	-140	4.8×10^{-9}	6.8×10^{-9}
1% Sb added, first run	*	(6.8)	*	*	5.2	4.2
1% Sb, 2nd run	*	(6.3)	*	*	4.4	3.5
1% Nb added, first run	*	61	*	*	13.5	6.2
1% Nb, 2nd run	*	--	---	*	900	290

* Unreliable performance of the measuring equipment during these measurements renders Seebeck coefficient data doubtful.

TABLE K-3
ACTIVATION ENERGIES FOR CONDUCTION OF MATERIALS STUDIED

<u>Composition</u>	<u>Activation Energy, ev</u>	<u>Applicable Temperature Range, °K</u>	<u>Resistivity at Discontinuity, ohm-cm</u>	<u>Resistivity at 1000°K</u>
BaFe ₁₂ O ₁₉	--- 1.33	300 - 1100 1100 - 1300	15	16
BaFe ₁₂ O ₁₉ + 50 mol %	0.245	300 - 1300	---	1.25
BaTiO ₃				
FeTiO ₃	0.988	650 - 1260	---	20
95 mol% BaTiO ₃ + 5 mol% CuSnO ₃	0.705	736 - 1260	---	7000
2CoO·TiO ₂	0.86	300 - 850	---	14
2Cr ₂ O ₃ ·TiO ₂	0.40 0.44	300 - 950 950 - 1300	300 ---	--- 255
CoTiO ₃	1.01	300 - 835	---	80.0
BaCoO ₃	0.31	300 - 1100	---	1.6
Ni ₇ ZnFe ₂₄ O ₄₈	0.13 0.31	300 - 700 770 - 1300	2.5 ---	--- 0.9
2BaO·Fe ₂ O ₃	0.45	300 - 1300	---	305
Ni ₄ Zn ₃ Fe ₁₈ O ₃₆ + 5 mol% Co ₂ O ₃	0.07	300 - 1300	---	0.52
MnFe ₂ O ₄	0.176 0.536	300 - 840 840 - 1250	0.395 ---	--- 0.107
NiFe ₂ O ₄ first run	0.008	400 - 1100	---	0.220
NiFe ₂ O ₄ , 2nd run	0.005	300 - 1100	---	0.135
SrTiO ₃ : *				
with 1% Sb, 1st	0.006	700 - 1100	---	4.6
with 1% Sb, 2nd	0.006	700 - 1100	---	4.0

TABLE K-3 (continued)

<u>Composition</u>	<u>Activation Energy, ev</u>	<u>Applicable Temperature Range, °K</u>	<u>Resistivity at Discontinuity, ohm-cm</u>	<u>Resistivity at 1000°K</u>
with 1% Nb, 1st	0.223	300 - 1200	---	9.9
with 1% Nb, 2nd	0.49	630 - 1200	---	500

* The data on un-doped SrTiO_3 will be found in Table K-1.

APPENDIX L - SUMMARY OF THERMOELECTRIC INVESTIGATIONS OF ENCAPSULATED INTERMETALLIC AND LIQUID SEMICONDUCTORS

E. Fischer-Colbrie

May, 1959

ABSTRACT

The development of an encapsulation technique allowing the production of thermoelectric cells operable up to 1450°K has been described. Furthermore, the synthesis and encapsulation of intermetallic and liquid semiconductors and alloys has been reported. Measured data on Seebeck coefficients, electrical resistivities, and calculated figures of merit versus temperature have been presented. PbTe and Zn-Sb show performance characteristics extended to considerably higher temperatures than shown in the state of the art. Pb-Sb and InSb exhibit interesting properties at high temperature in the liquid phase. Measurements have been carried beyond the melting point of the encapsulated material; thus numerous novel data have been obtained.

INTRODUCTION

The tasks

- 1.5 - Intermetallic Semiconductors and
- 1.6 - Liquid Semiconductors

have been treated in a combined form since most of the work is common for both tasks.

The investigation on this study program has been concerned with materials and enclosures to be used in the temperature range of 300°C to 1000°C . Intermetallic semiconductors have been known as potential thermoelectric generator materials for some time. However, progress in solid state physics in recent years had led to better knowledge of the laws governing the transport processes inside a solid state body. Although a method for the "engineering" of optimized properties of thermoelectric materials still is not available, guidelines for the selection of materials have been established. As guidelines, the following may be considered:

1. A band gap of the order of 0.2 - 1.0 electron volt, or a band gap which adjusts itself to such values at the operating temperature due to its T-dependence.
2. A carrier concentration of the order of 10^{19} carriers per cubic centimeter which is still below, but close to, degeneracy.
3. A thermal conductivity of suitably low values which may be adjusted or tailored by any possible means which do not affect seriously the other established properties.

These guidelines, however, become more and more uncertain if it is desired to predict the thermoelectric properties of alloys or materials at high temperatures in the liquid phase or materials which are possibly liquid at the hot end of a generator cell and solid at its cold end.

Since more thermoelectric materials appear to be available for the temperatures from 300°-650°C (which represents the lower half of the established temperature range), it seemed reasonable to be more concerned with the selection and investigation of materials suitable for 600°-1000°C temperatures. These temperatures represent the upper and less explored portion of the temperature range. The encapsulation, specially developed for this contract, introduces a new set of requirements on the selection of materials, and some deviation from originally selected materials appeared necessary since vapor pressures, melting points, and corrosion problems enter the picture.

PROPOSED WORK ON INTERMETALLIC AND LIQUID SEMICONDUCTORS

In the original proposal dated April 4, 1958, and in Exhibit A of the Technical Management Report No. 8 of September 3, 1958, the following tentative list of solid compound semiconductors was selected for their potential high temperature performance:

<u>Compound</u>	<u>Melting Point</u>
Lead sulfide	1114°C
Cadmium sulfide	1750°C
Cadmium telluride	1041°C
Gallium antimonide	706°C
Gallium arsenide	1240°C
Indium phosphide	1017°C
Lead telluride	917°C

It is fully expected that encapsulation will be a necessary prerequisite for successful experimentation with these compounds at high temperatures. It had been planned to select three compounds from this list and to synthesize, dope, seal, and measure them. It is also expected that synthesis of new materials with improved properties will be directed by results obtained.

The encapsulation is an obvious prerequisite for the liquid semiconductors. For this portion of the contract, it had been proposed that the initial phases of the study would consist also of the synthesis, doping, sealing, and measuring of liquid materials. It has been suggested that mercuric selenide, an alkali metal chalcogenide, or some other compound shall be studied. The results again should direct synthesis of new and improved materials.

EXPERIMENTAL WORK

Encapsulation and Sealing Techniques

The temperature requirement of 1000°C as the upper operating temperature limit for intermetallic and liquid semiconductor materials and cells introduces

a considerable amount of stability problems. The encapsulation of all the materials which shall be operated above their melting point is unavoidable. The encapsulation may be useful for materials which are not to be used in the liquid phase but which tend to change their properties if not encapsulated and exposed to high temperatures for a longer period of time. Such property changes may occur by diffusion, dissociation, oxidation, evaporation, or the like. As long as the vapor pressure of the compound investigated is below atmospheric pressure at 1000°C, no special provisions have to be considered in regard to the mechanical strength of the cell.

It is our firm belief that an encapsulation for intermetallic semiconductor materials is a potential advantage and that the investigation of the thermoelectric behavior of selected materials in the encapsulated state may yield valuable results. In a well designed enclosure, the tendency toward deterioration of the thermoelectric properties due to instabilities appears suppressed. Because of this, it may be expected that the encapsulated material may be useful to higher temperatures than the material without enclosure.

Any enclosure must reduce the over-all efficiency of a thermoelectric generator because the heat conduction in the enclosure material allows heat to bypass the thermoelectric material. By choosing optimum geometry for each cell, however, this heat loss can be kept or brought down to a few per cent, (for example 3% to 5%) of the total heat. This optimization has been disregarded in the experimental program up to the present time since the main objective has been the basic enclosure development and study of the behavior of enclosed materials.

The first type of enclosure pursued in our development is a quartz glass vessel or a quartz glass tubing provided with molybdenum electrodes. Both molybdenum and quartz withstand the upper temperature requirements of 1000°C. Regular quartz-to-metal seals require graded glasses to match differences of expansion coefficients between the electrode metal and the quartz. The low softening points of such graded glasses (below 1000°C) inhibit the high temperature application.

Molybdenum foils or ribbons of the order of 0.0025 cm thickness lend themselves to non-graded seals to quartz. Molybdenum wires have been hammered down to such ribbons and sealed directly to quartz. Two cells of this kind are shown in Figure L-1, one provided with two electrodes and one with four electrodes. Although many useful data have been obtained from such cells, their design has many disadvantages, especially if they are to be used as cells for a thermopile generator. Accurate temperature measurements which are extremely important for exact thermoelectric data, especially for Seebeck coefficient measurements, are very hard to make on such a design.

Furthermore, only molybdenum can be employed as electrode material, whereas a variety of electrode materials appears desirable. The low expansion quartz glass also contributes a certain risk in view of the generally higher expansion coefficients of the core materials added to the inherent danger of breakage of glass enclosures.

Most of the disadvantages of the quartz-molybdenum cell have been overcome by the development of the metal-ceramic enclosure. This type of cell consists



Figure L-1: Encapsulation in Quartz Glass Vessel.

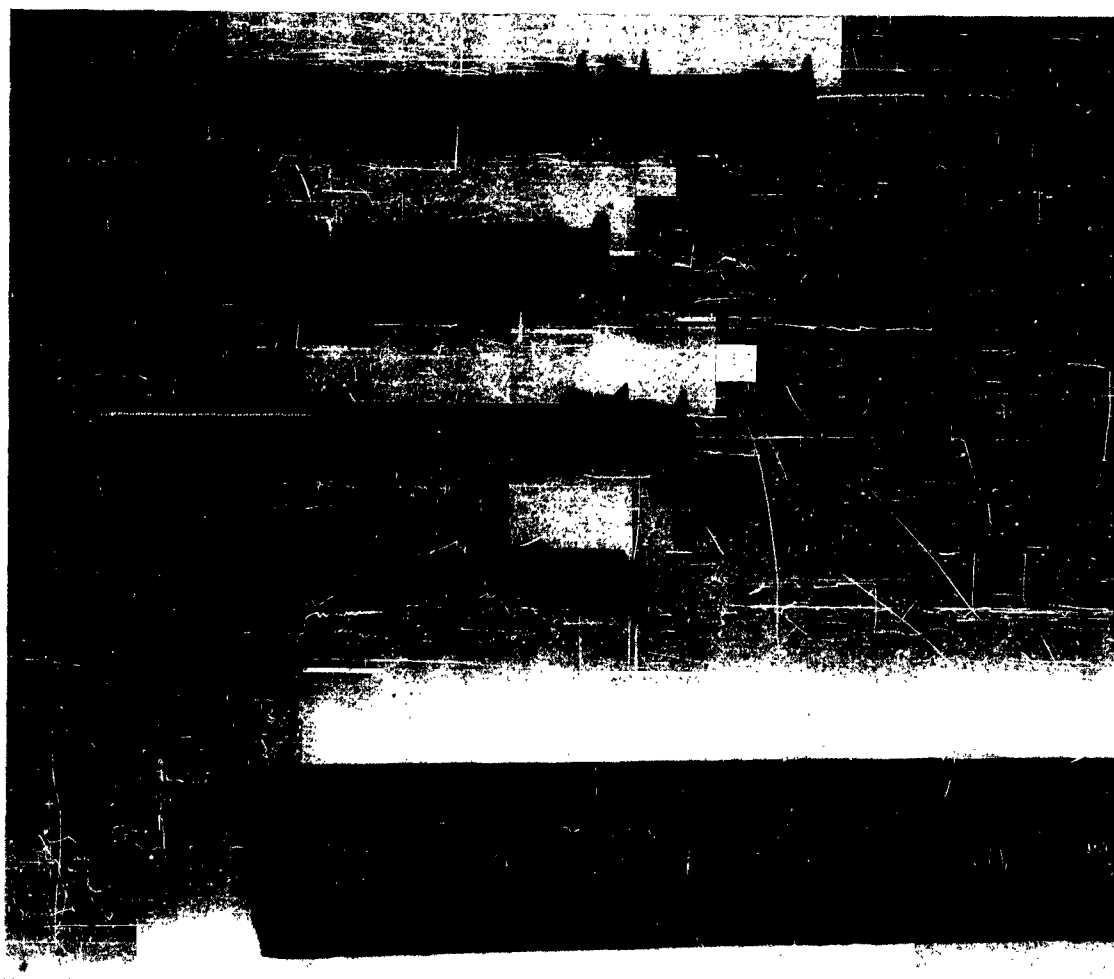


Figure L-2: Encapsulation by Sealing to Ceramics.

of a ceramic tubing such as Forsterite or alumina provided with sealed-on metal electrodes. The basic sealing technique developed for vacuum tubes by Beggs* has been modified to permit the encapsulation of thermoelectric materials. Certain metals like titanium and copper, or titanium and nickel, titanium and iron, or nickel and zirconium form alloys which are reactive with the ceramic part. Thus, a bond can be produced by locally creating eutectic proportions of the two metals. The sealing temperature depends upon the eutectic points of the two metals. Since 1000°C has been established as the upper temperature limit for this investigation, the titanium-iron combination which forms a eutectic at 1055°C has been favored.

This sealing technique has been used successfully to produce most of the cells investigated. In a further development, this technique can be extended to higher sealing temperatures and therefore to higher operating temperatures of the sealed cell, if so desired. High melting metals, such as molybdenum or tungsten, also can be sealed to ceramics although they form alloys with the active metals only at extremely high temperatures. In order to seal high melting metals to ceramic, it is necessary to sandwich two shims between the high melting metal and the ceramic. The two shims or foils can be, for example, a titanium and a nickel shim or a titanium and an iron shim which form their eutectic alloys at around 1000°C and thus provide a solder between the high melting metal and the ceramic.

It can be seen that a large variety of electrode materials can be sealed to ceramics using this technique. Hence, a variety of problems introduced by the intermetallic or liquid semiconductor in contact with the electrode material can be solved.

Figure L-2 shows several such cells, provided with two or more electrodes and produced as described. The multielectrode cells are made by sealing sets of washers to the ceramic tubings or by sawing slots into the tubing and inserting and sealing an electrode into these slots. The cell geometry chosen for the material investigation is different from the geometry of cells to be used in a thermopile. It is quite certain, however, that such changes in geometry will not require any basic change in the sealing technique. The following are several advantages of this enclosure technique.

The contact area between the active material and the electrodes can be made large, thus providing good electrical and thermal contacts. This advantage, in turn, leads to a higher accuracy of temperature measurements and, therefore, to more accurate Seebeck coefficient data than in the quartz molybdenum design initially described. The expansion coefficients of the electrodes and the ceramic body can now be brought to a much better match. Furthermore, the expansion coefficient values of the cell match now better the values of expansion coefficient of the material investigated. The expansion coefficient of pure iron and the expansion coefficient of commercially available Forsterite** lie just within the

*J. E. Beggs, IRE Transactions of the PGCP, Volume CP-4, No. 1, March, 1957.

**For example, Alsimag 243, American Lava Company.

tolerances determined by the geometry chosen for the experimental cell. For other geometries, however, a better match may be necessary. In this event, Forsterite bodies of higher expansion coefficient will have to be used. Such Forsterites have been developed by the General Electric Company*.

This type of cell can be used to encapsulate a variety of intermetallic materials, especially if their expansion coefficients are not too different from that of iron. For low expansion materials, low expansion ceramics must be used in connection with low expansion electrode materials. Examples of this are the alumina containers provided with molybdenum electrodes sealed to the container by means of nickel and titanium foils or shims. Ways of circumventing expansion problems, however, can be considered here.

To obtain information on the upper temperature limit at which a Forsterite iron type cell can be operated, a mechanical stability test has been performed for 30 minutes which showed that mechanical destruction occurs at temperatures higher than 1220°C at which temperature the seals proved to be stable.

Electrode Corrosion Tests

Another requirement imposed on the ceramic and electrode materials is their stability in contact with the solid or liquid thermoelectric material. The electrode and the active material should wet well but still should exhibit only slight solubility which means that hardly any electrode material should diffuse into the thermoelectric material.

One of the basic requirements for a satisfactory encapsulation is the selection of an electrode material which is sufficiently stable in contact with the thermoelectric material even if the latter one is in the liquid state. At the same time, this electrode material must lend itself to the adopted metal ceramic sealing technique. An experimental search was undertaken to find suitable contact materials. A small amount of each of the compounds selected previously was vacuum sealed in small quartz phials together with samples of potential contact material and then heated above the melting point for three to five hours. After cooling, the phials were opened and the electrode material inspected as to its corrosion status, electric surface resistance, and change of weight.

A list of electrode materials is given here which have been considered in these tests:

Chromel A	Palladium
Chromel P	Platinum
Chromium	Platinum + 13% Rhodium
Gold	Stainless Steel 304
Inconel	Steel (cold rolled)
Iron + 40% Cr	Tantalum
Iron (pure) (Armco)	Titanium
Kovar	Tungsten
Molybdenum	Zirconium

*C. G. Childs and E. Duderstadt - G.E. Receiving Tube Department - GE Report #R-57 ETR-6.

It should not be assumed that each compound has been tested in contact with each electrode material since certain predictions and published data permitted the elimination of a considerable number of combinations.

In Table L-1 the results of the stability experiments are given. Listed are the compound, its melting point, and three choices of electrode materials. It must, of course, be recognized that there is no guarantee that those materials which passed this type of test will also stand up for long-time operations. They merely indicate that these combinations appear to be sufficiently stable for the measurements in mind.

TABLE L-1

List of High Temperature
Contact Materials to Thermoelectric Materials

Compound (alloy)	Melting Point °C	Choice of Contact Material		
		1st	2nd	3rd
CdTe	1041	Mo	Fe	---
GaSb	706	Mo	Ta	---
GaAs	1240	Mo	W	---
PbTe	917	Mo	Fe	Ti
HgSe	sublimes	Cr	Cr-Fe	---
Sb ₂ Se ₃	611	Mo	Fe	---
As ₂ Se ₃	360	Fe	Mo	---
Bi-Sb	390	Fe	Mo	Ti
Ge + 5% Te	929	W	---	---
GeTe	725	W	---	---
HgTe	650	Mo	Ta	W
InSb	530	Fe	Mo	---
Pb-Sb	290	Mo	---	---
ZnSb	565	Mo	Fe	Ti

Materials

The materials originally proposed to be investigated in Tasks 1.5 and 1.6 of our proposal have been listed in Column I of Table L-2 as #1-9. This selection has been performed prior to the development of the encapsulation technique and was because of this reason obviously subject to changes. Under numbers 10-18 either substitutes or "other" materials are listed which became important as the work on the contract went on; for example, by a shift of emphasis to high temperature materials. The possibility of such changes has been indicated and anticipated in the proposal.

In Column II the materials are listed which actually have been synthesized in our laboratory for the purpose of further investigation, whereas Column III shows the materials for which results on corrosion tests have been obtained. In Column IV the materials are listed which have been encapsulated at the closing date of the work.

Rough screening tests have been performed on the materials in Column V of the table, whereas in Column VI and VII the materials are listed for which either Seebeck coefficients or resistivity data versus temperature or both have been obtained in the encapsulated state.

Highly pure gallium and gallium arsenide have been received very recently and, since the deadline for this report had been advanced by three months, no time was left to investigate the two gallium compounds, i.e. gallium arsenide and gallium antimonide except for corrosion tests carried out in GaSb to determine the suitability of electrode materials.

TABLE L-2

Materials and Work Done

	I Materials Proposed	II Materials Synthesized	III Corrosion Tests	IV Materials Encapsulated	V Rough Screening	VI Seebeck Coefficient Measurement	VII Resistivity Measurement Taken
1.	PbS	PbS			PbS		
2.	CdS	CdS			CdS		
3.	CdTe	CdTe	CdTe	CdTe			
4.	GaSb	GaSb	GaSb				
5.	GaAs	GaAs*	GaAs				
6.	InP				InP		
7.	PbTe	PbTe	PbTe	PbTe	PbTe	PbTe	PbTe
8.	HgSe	HgSe	HgSe		HgSe		
9.	Alk. Chalc.						
10.		Sb ₂ Se ₃	Sb ₂ Se ₃	Sb ₂ Se ₃	Sb ₂ Se ₃		Sb ₂ Se ₃
11.		As ₂ Se ₃	As ₂ Se ₃	As ₂ Se ₃	As ₂ Se ₃		As ₂ Se ₃
12.		Bi-Sb	Bi-Sb	Bi-Sb	Bi-Sb	Bi-Sb	
13.		Ge + 5% Te	Ge + 5% Te				
14.		GeTe	GeTe				
15.		HgTe	HgTe				
16.		InSb	InSb	InSb	InSb	InSb	InSb
17.		Pb-Sb	Pb-Sb	Pb-Sb	Pb-Sb	Pb-Sb	Pb-Sb
18.		ZnSb	ZnSb	ZnSb	ZnSb	ZnSb	ZnSb

*Obtained from outside.

Since both gallium arsenide and gallium antimonide are of considerable interest, results of their investigation may be a valuable contribution to the over-all results on this contract.

To date no work has been done on indium phosphide.

Due to lack of time, also, no work has been done on any of the alkali chalcogenides.

At the time of the termination of our work, we carried the development of the encapsulation technique only to the point of using iron electrodes sealed to Forsterite. Although we do not anticipate serious problems, the further development of cells in which, for example, molybdenum or any other metal than iron is required in contact with the encapsulated material as electrode metal has not been carried out experimentally yet. Therefore, several materials such as Ge-Te or GeTe, HgTe or HgSe have not been encapsulated.

PbS, on the other hand, shows a limited chemical stability in vacuo at elevated temperatures. Its encapsulation would be again of a different type, the development of which was postponed.

In case of HgSe we hesitated to encapsulate this material in what we called a "regular" capsule since its vapor pressure may lead to undesired breakage at high temperatures. A specially reinforced capsule is indicated. Time was not available to produce such a capsule, and HgSe therefore has not been followed up further as of now.

In almost all cases, the compounds or alloys have been synthesized by enclosing the constituents in the desired proportion in evacuated and sealed quartz tubings and by heating the constituents above their melting point in a subsequent firing process. The materials have been handled in a so-called dry box in which an oxygen free atmosphere has been maintained, thus reducing the exposure to air and humidity to a minimum. After the firing step, the quartz enclosure has been opened and the material processed into a cell. This step again has been carried out in the oxygen-free atmosphere. The cell itself then has been sealed in vacuum. The purity of the constituents, although known, varies for the different materials and is dependent on the availability. The metals arsenic, bismuth, germanium, lead, tellurium, antimony, selenium, and zinc have been obtained as 99.999% pure whereas cadmium, gallium, mercury, indium, and sulphur have been obtained as either 99.99% pure or even less. The impurity introduced during processing may be impurities coming from quartz or Forsterite. There is also a possibility that some titanium or iron may be present in one or the other materials. Oxidation has been kept to a minimum since nitrogen has been used as an atmosphere for the handling processes. Impurities added are mentioned later during the discussions of the individual compounds.

Measurements

Of the data which characterize the over-all thermoelectric quality of a material, the Seebeck coefficient with respect to platinum and the resistivity have been measured versus temperature. In order to calculate the figure of merit, thermal conductivity data have been taken from publications or from reasonable extrapolations of such data. The measurements on the encapsulated

materials are made for the purpose of experimentally scanning a group of potential compounds or alloys in their solid and liquid phases.

In accordance with the philosophy of a scanning type of measurement, and in order to avoid duplications with other portions of this contract, it did not appear worthwhile to put excessive effort into setting up elaborate and expensive measuring equipment. It appeared useful to find a reasonable compromise between time and effort versus extreme accuracy. With the rather modest setup used, accuracies in the order of $\pm 12\%$ could be obtained for the Seebeck coefficient data and $\pm 7\%$ for the resistance data. Such accuracy is sufficient to draw conclusions for applications and for further work.

The measurements were taken in a tubular furnace provided with two separate heater systems, each of which had been controlled independently. Thus, a desired temperature difference could be established. This temperature difference could be reduced to zero or reversed, if so desired. For the sake of a simple and reliable setup, means for keeping the temperature perfectly constant while taking the readings have been omitted, and the readings have been corrected for the temperature change during the measuring process by interpolation. The setup has been tested by a standard cell which had the same physical and thermal properties as a regular cell but contained platinum instead of a material with unknown thermoelectric properties. The thermoelectric data of platinum are well known and therefore could be taken from tables and compared with the data obtained in the measuring setup. Correction factors have been established since small reproducible differences of the measured values and the catalogued values have been found for platinum.

These correction factors are temperature dependent and their existence and necessity can be explained by a small incorrectness of the temperature measurement inherent in the otherwise useful design of the cells since the thermocouples cannot be placed exactly at the most desirable points.

Since a small temperature difference of, for example, 10° between T_{cold} and T_{hot} is desirable to calculate the Seebeck coefficient, a temperature gradient from the point measured on the electrode and the inner portion of the cell of only 1° on each electrode will produce an error in the Seebeck coefficient of 20%.

In our case, we found the numerical values for the correction factor to be 1.07 at 300°C up to 1.17 at about 1000°C .

Furthermore, we produced a setup as shown in Figure L-3 in which the thermocouples have been placed on or very close to the desired points of the cell, thus being able to read true or very close to true temperature readings since the thermal requirements of the cell design appear pretty much fulfilled. Using this setup for measurements, we found the Seebeck coefficients measured to be in their expected ranges without applying correction factors.

Since the design of this type of arrangement, however, is not practical for the bulk of our work, we preferred to apply arithmetical corrections instead of complicating the run of our investigation unnecessarily.

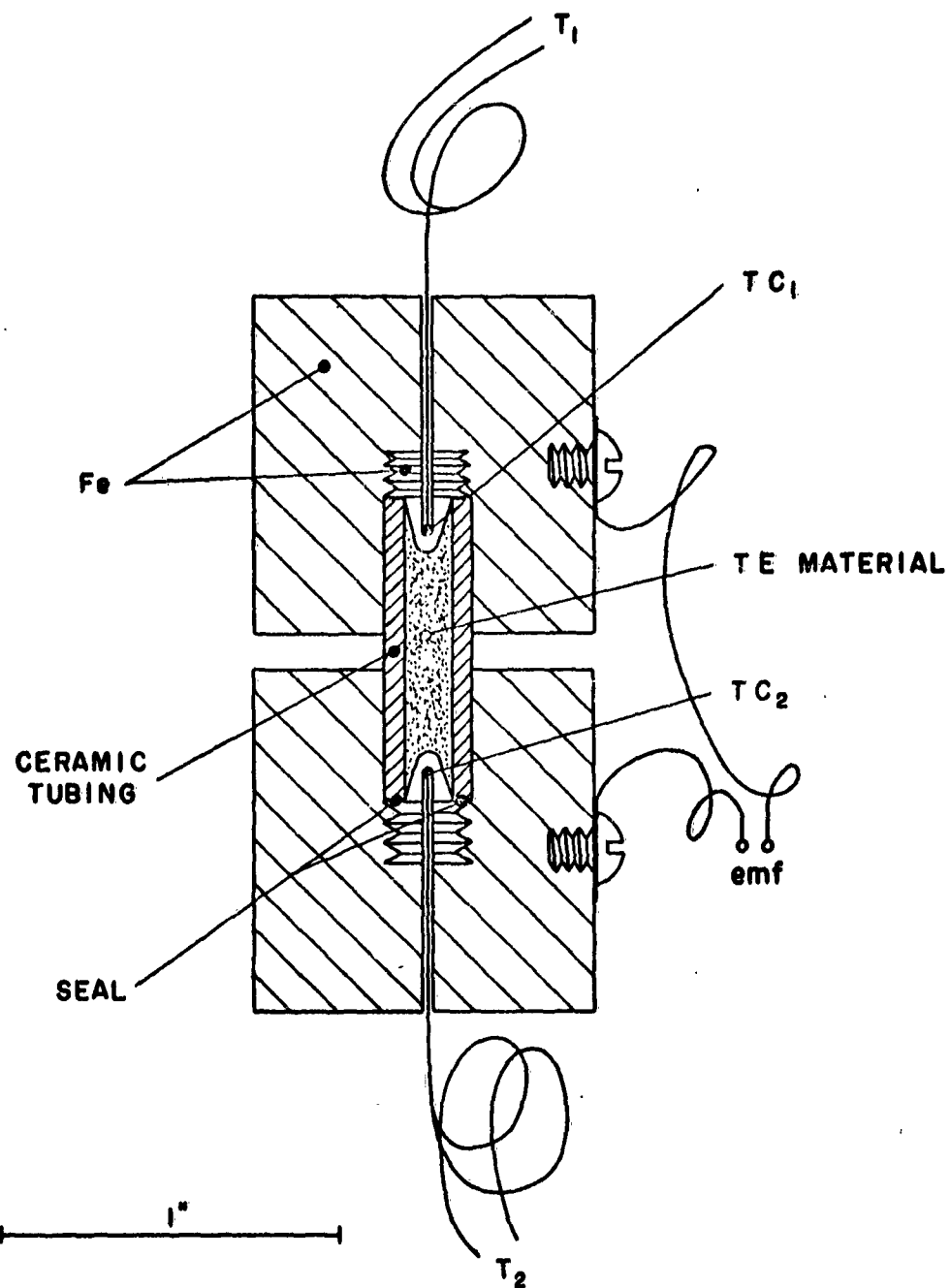


Figure L-3: TE Cell with Improved Conditions for Temperature Measurements.

Since during the preparation of the cells all the materials investigated were heated up to and above the melting point, good bonding was produced between the active and the electrode material. As a consequence very low contact resistances were obtained. The absolute values of the contact resistances were found to be so low that they were disregarded in the material resistivity data. The resistivity data therefore include two negligibly small contact resistance values, one on each end of the cell.

Material Data

Lead Sulfide

Processing of the synthesized lead sulfide, especially the attempt to encapsulate it into a cell, leads to dissociation of the lead sulfide material. It would not be stated that the material cannot be encapsulated, but certainly some modification of the technique appears necessary. To date, no further attempt has been made to modify the encapsulation process in order to make the enclosure of lead sulfide possible. The resistivity of lead sulfide is inherently high, and it may be rather difficult to reduce this value to limits useful in thermoelectric generator applications. Since the material does not readily meet present encapsulation requirements, the work on PbS has been placed on a list of tentative later work.

Cadmium Sulfide

The statement just made for lead sulfide holds also for cadmium sulfide. Cadmium sulfide has a melting point of 1750°C . A melt, however, can only be obtained if a pressure of 100 atmospheres or more is present; otherwise the compound dissociates and sublimates. A relatively large effort would be required to encapsulate cadmium sulfide in a cell. The requirements set by the cell techniques again are not met by cadmium sulfide. Cadmium sulfide is also a compound of very high resistivity. No further attempt, therefore, has been made as of now to produce cadmium sulfide capsules. Investigations of the compound in the state of sintered crystalline powder may be interesting and appears possible.

Cadmium Telluride

This compound has a rather high expansion coefficient and therefore causes some problems in the present Forsterite enclosure. Its resistivity is also high. Work on CdTe reached the study of encapsulation at the termination of this work.

Gallium Antimonide

Since the constituent gallium has been received just recently, no data can be presented now. From a small amount of gallium which was available at the beginning of this work, gallium antimonide has been synthesized and used for corrosion tests. These tests indicate that molybdenum appears to be a useful contact material. To introduce Mo, however, into the standard iron-Forsterite cell, certain cell development appears necessary such as double seals.

Gallium Arsenide

No work on gallium arsenide can be reported since gallium was received only a short time ago. Gallium arsenide as a compound has been obtained from outside the General Electric Company during the compilation of this report.

Indium Phosphide

Since the synthesis of this material is inherently more difficult than most of the other compounds, work has been postponed. It still is active on the list for further investigation.

Lead Telluride

This compound has been rather thoroughly investigated in the encapsulated state. The specific material used has been n-type doped with 0.1% bismuth. A total of six cells have been made. In Figure L-4 data on resistivity are presented and in Figure L-5, the Seebeck coefficient versus temperature. The resistivity first rises with increasing temperature up to 1050°K and then drops rapidly until the melting point is reached. The Seebeck coefficient-temperature relationship starts at surprisingly low values but rapidly reaches a maximum at 1000°K, then begins to drop rather rapidly to zero and becomes slightly positive beyond the melting point. In Figure 6 the figure of merit Z , equal to S^2/ρ K, is plotted versus temperature. The values for this curve were calculated using the resistivity and Seebeck coefficient data measured and using phonon conductivity data which were obtained by the extrapolation of published information. Whereas the electronic portion of the thermal conductivity can be calculated reasonably well, the estimate of the phonon conductivity appears to be not as simple, especially if the temperature of the material approaches the melting point or even is measured in the molten state. One can see in Figure L-6 that the figure of merit shows a rather broad maximum between 700° and 1000°K. On the same diagram, the figure of merit is plotted for what may be called the state of the art. Our results appear to be a considerable improvement on the state of the art in which the Z values drop above 450°K and measurements beyond 820°K cannot be made on lead telluride due to sublimation. The encapsulation, however, allowed measurements beyond 800°K and showed surprisingly good results above this temperature.

Mercury Selenide

This compound** has been selected as a potential material for the liquid semiconductor group. It has been synthesized, and corrosion tests have been run. An electrode material stable in contact with liquid mercury selenide is, for instance, tantalum. The introduction of tantalum, however, requires some further work on the Forsterite-metal enclosure. Changes in the enclosure technique are required to use this electrode material. Such work has been postponed in favor of work on materials which can be enclosed readily in what we call a standard iron Forsterite cell. A reinforced cell also may be necessary.

* For example, A. F. Ioffe: Semiconductor Thermoelements and Thermoelectric Cooling, Infosearch 1957.

** See, For example, A. I. Blum, N. P. Mokrovski and A. R. Regel; *Izv. Akad. Nauk*; Vol. XVI, No. 2, p. 139; 1952.

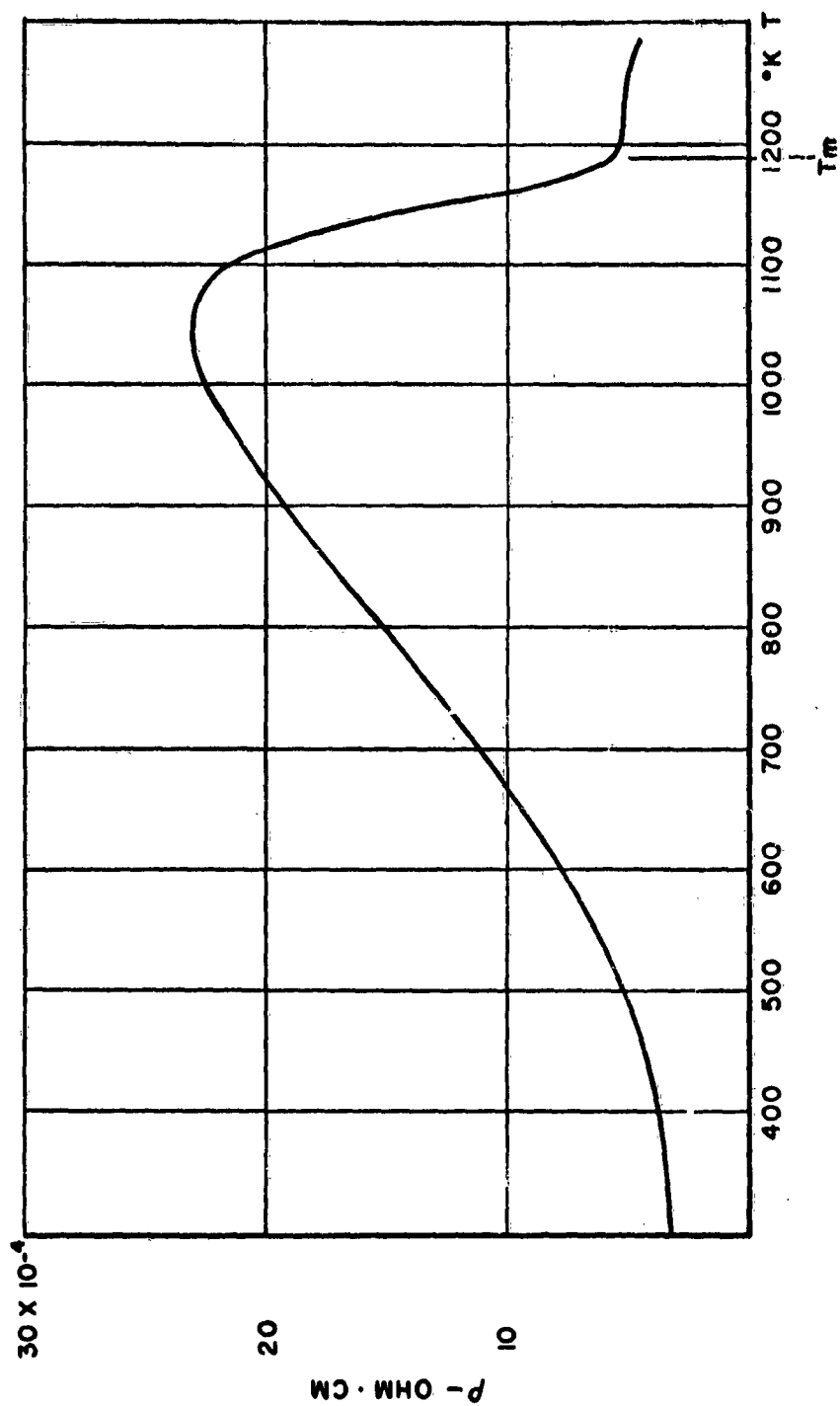


Figure L-4: Resistivity vs Temperature, Lead Telluride.

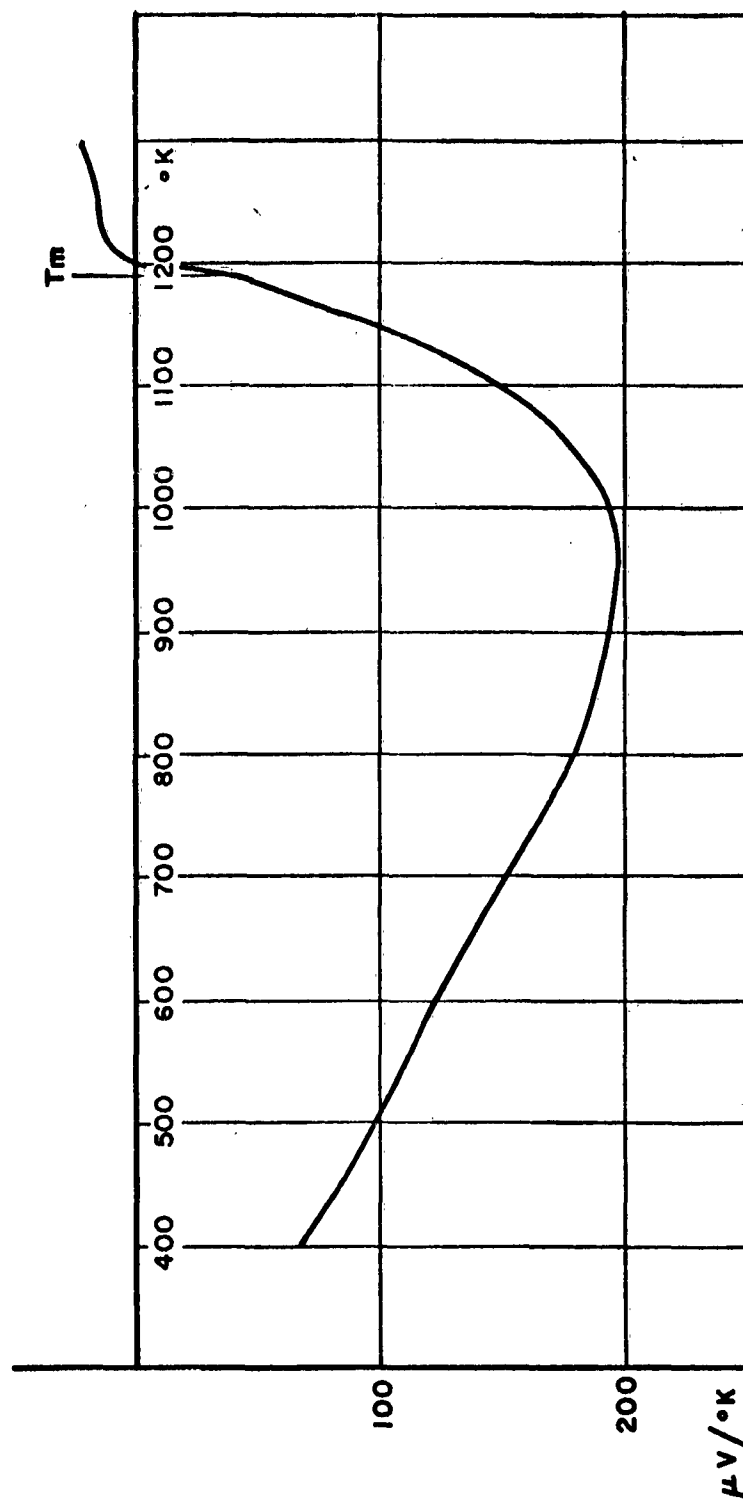


Figure L-5: Seebeck Coefficient vs Temperature, Lead Telluride.

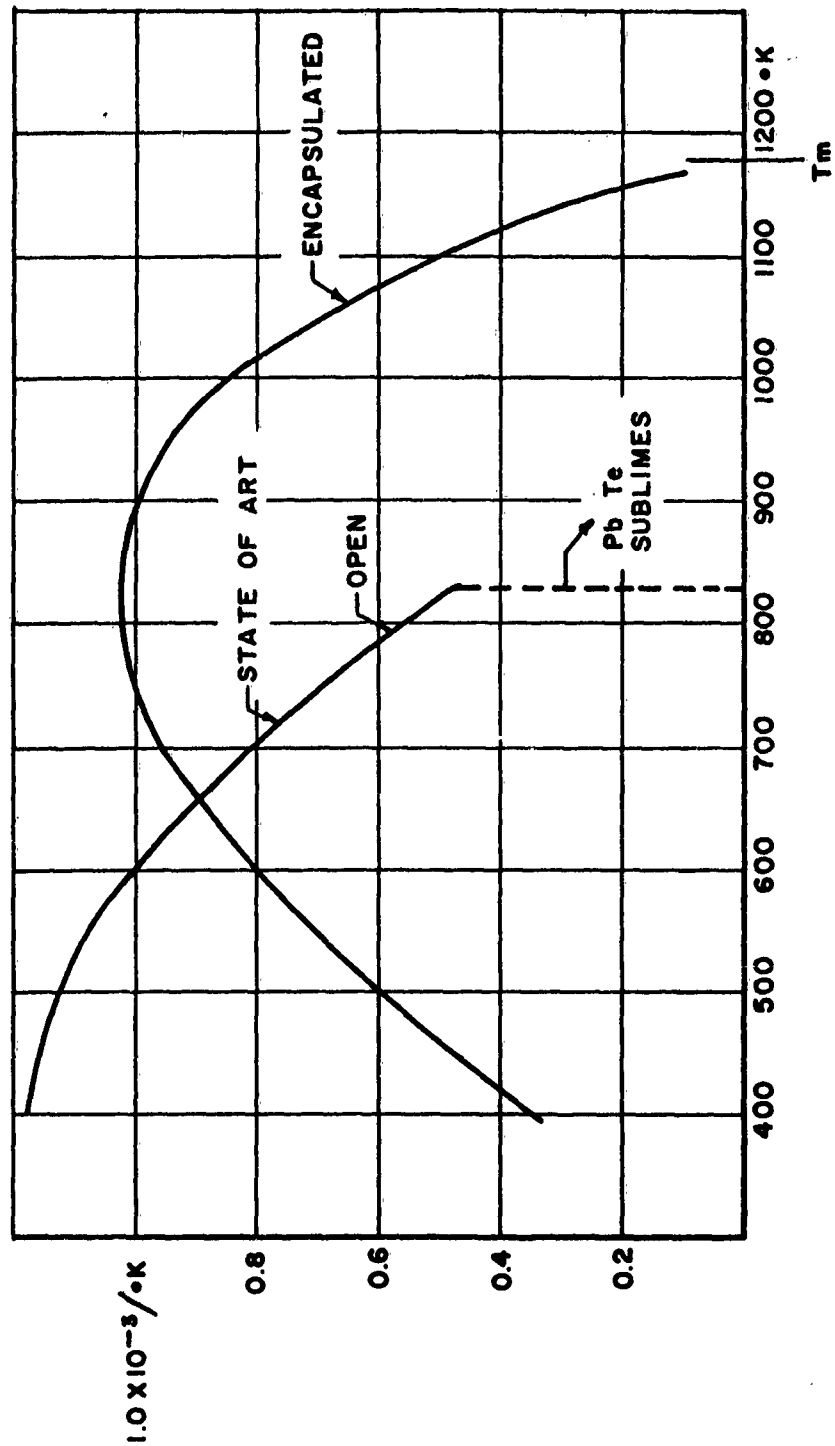


Figure L-6: Figure of Merit vs Temperature, Lead Telluride.

Alkali Chalcogenides

No work has been done on this group of materials as of now since more effort has been devoted to other compounds.

Note: The materials designated as #10 - #18 in Table L-2, which are reported on in the following, represent materials which have been selected additionally to the materials designated in the table as #1 - #9. These materials have been mentioned in the proposal and in later statements as possible "others". They either substitute for some of the first nine materials or have been selected as the work on the contract proceeded. The group #10 - #18 again falls into the solid as well as the liquid material category and therefore serves both tasks.

Antimony Selenide

This compound may, to a certain extent, be a substitute for PbS and CdS or the HgSe. Among the selenides, this compound is easy to synthesize and encapsulate. It is a V-VI compound. This selenide exhibits rather high electric resistivities. Figure L-7 shows the resistivity measured on the undoped compound Sb_2Se_3 versus reciprocal temperature. The antimony as well as the selenium were of the highest purity available, i.e. 99.999+. The resistivity drops from around 4000 ohm-cm at room temperature to 0.4 ohm-cm at the melting point which is at 880°K. The resistivity remains constant at 0.4 ohm-cm up to 980°K. No data above 980°K have been taken.

Arsenic Selenide

Arsenic selenide has a melting point of 360°C and, therefore, is a representative of the category of liquid materials in the 300° - 1000°C temperature range. It is a close relative to the previously treated antimony selenide. Thus, most of the statements made about Sb_2Se_3 are valid also for As_2Se_3 . Arsenic selenide has been synthesized, corrosion tests have been run, and it has been processed into a cell, although the low melting point caused difficulty to do so. In Figure L-8 the resistivity versus temperature is shown for the undoped arsenic selenide. The resistivity values are rather high even at the melting point. The resistivity drops further above the melting point, however, with a smaller slope.

Bismuth Antimony

Since bismuth antimony alloys are known to be rather efficient thermoelectric materials at temperatures below 300°C, it appeared to be a worthwhile experiment to encapsulate a typical representative of the bismuth antimony alloys and to investigate the properties in the liquid phase. A 76-24 atom percent bismuth antimony alloy, therefore, has been synthesized, and after securing the right electrode materials, the alloy has been encapsulated. Figure L-9 shows the results obtained on the Seebeck coefficient versus temperature for this alloy. It turned out that this material does not seem to be very useful at higher temperatures or, more precisely, in the liquid state since its Seebeck coefficient becomes practically zero around the melting point. It seems to stay low after liquification as measured against platinum.

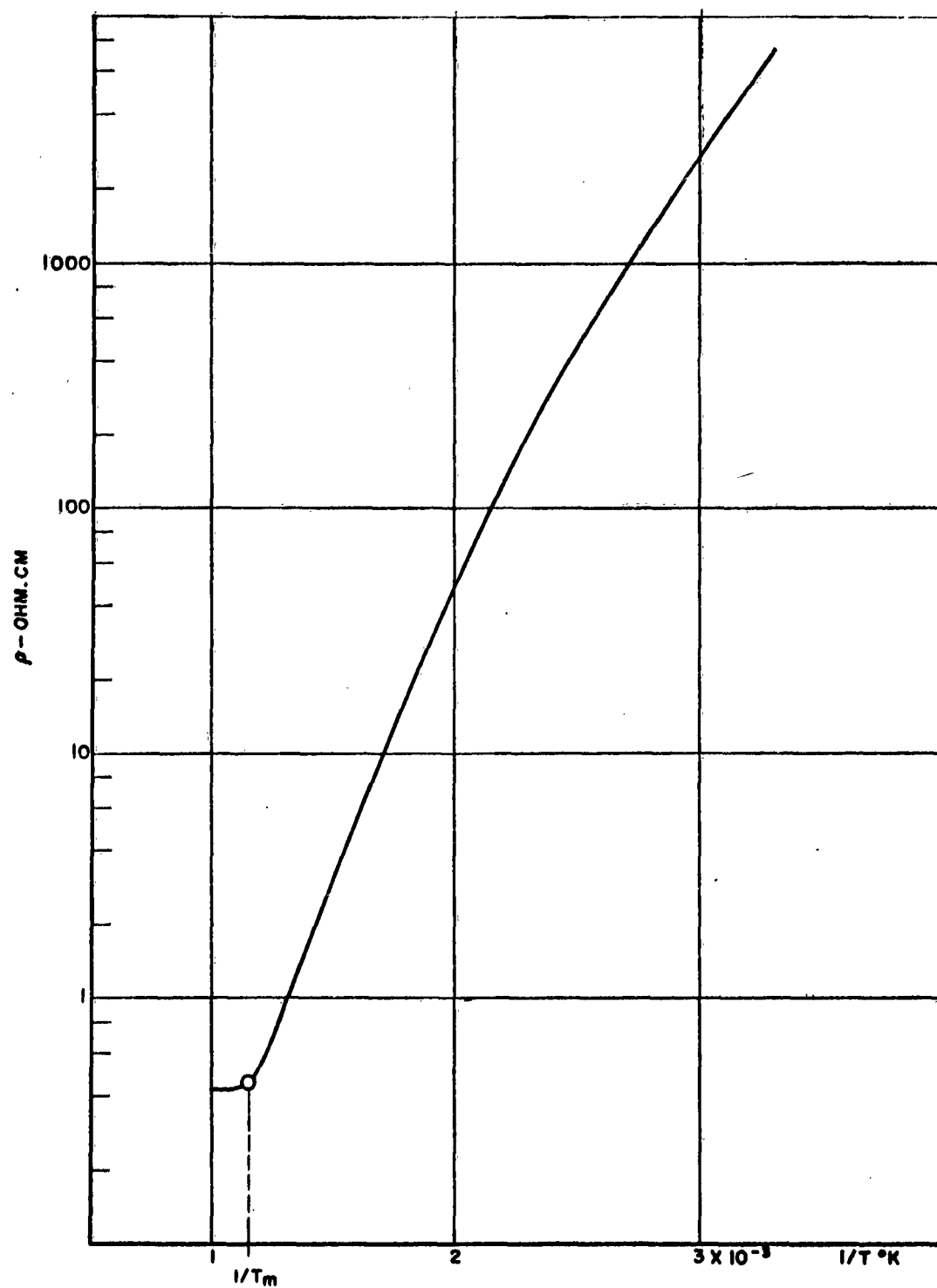


Figure L-7: Resistivity vs Reciprocal Temperature, Sb_2Se_3 .

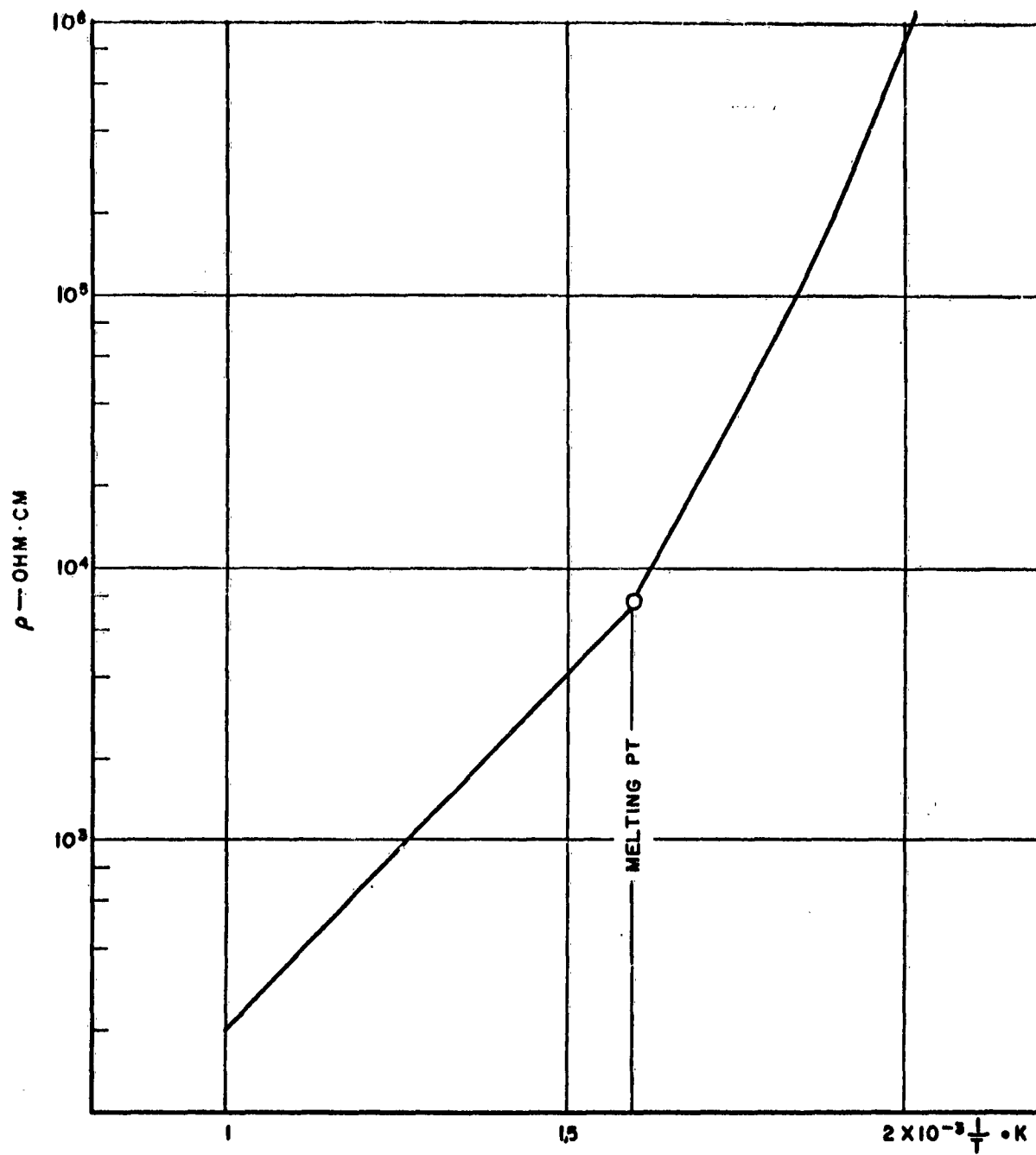


Figure L-8: Resistivity vs Reciprocal Temperature, As_2Se_3 .

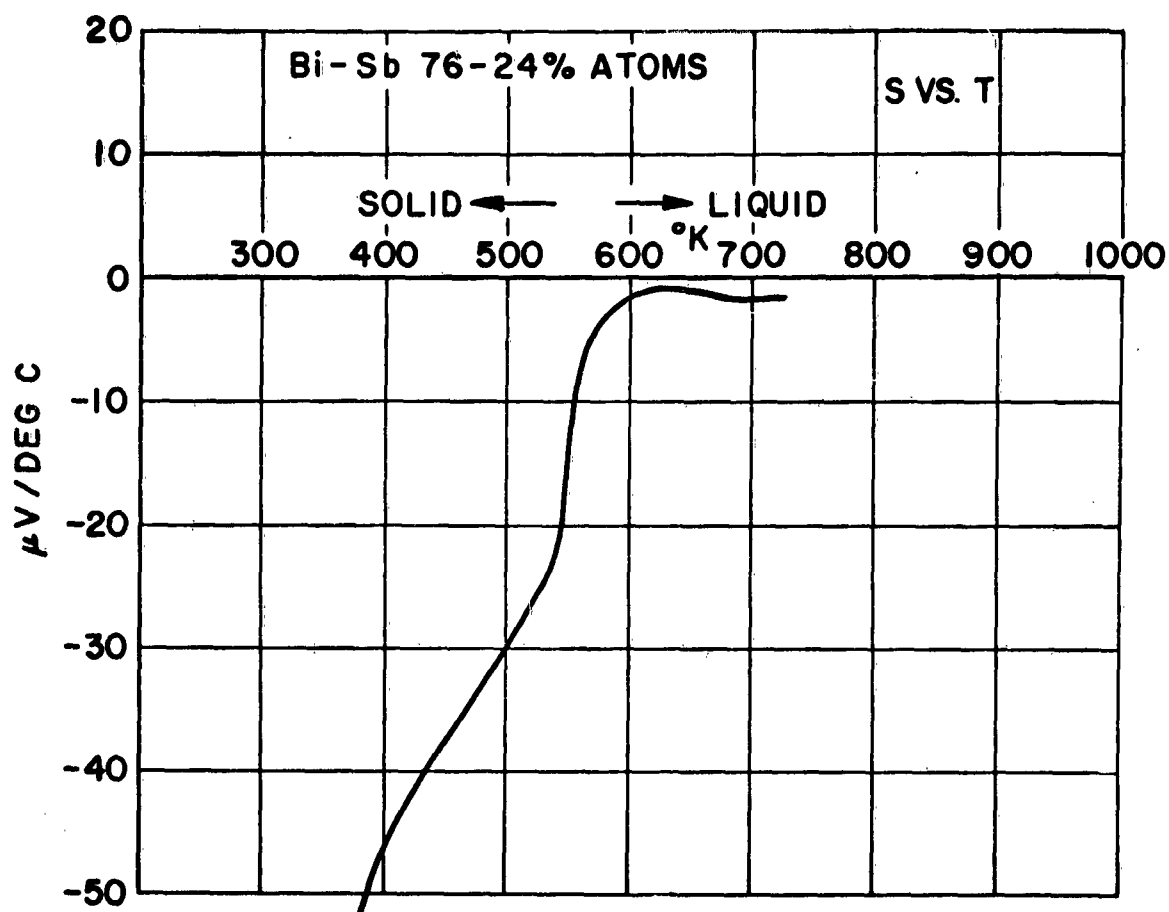


Figure L-9 Seebeck Coefficient vs Temperature, Bismuth - Antimony.

Germanium + Tellurium

The emphasis on the search for materials which exhibit useful thermoelectric properties in the upper half of the 300° to 1000° temperature range led to the interest in germanium tellurium alloys. Two materials have been synthesized; namely, germanium + 5% by atom tellurium and germanium + 50% by atom tellurium. The corrosion tests show that the standard iron Forsterite cell could not be used for encapsulation since so far only tungsten appeared to be useful contact material. At reporting time, we have been concerned with the question of incorporating tungsten into a ceramic cell.

Mercury Telluride

This compound has been synthesized for further investigations. It was planned to process it further in ceramic cells with molybdenum instead of iron contacts.

Indium Antimonide

The purity of the indium metal used for the synthesis of indium-antimonide is in the order of 99.99%. The compound has been synthesized and encapsulated. In Figures L-10 and L-11 the Seebeck coefficient versus temperature measurements and the resistivity versus temperature measurements are presented. The material is n-type in the solid state and becomes p-type in the liquid state. A maximum of the order of 60 microvolts per degree is reached in the n-type material at around 650° K. From then on the Seebeck coefficient goes rapidly toward zero near the melting point and the material becomes p-type (35 microvolts per degree at temperatures of 950° K).

The curve in the liquid phase does not show any tendency to flatten off at the high temperatures and, in further experiments, an attempt should be made to reach higher S-values in the liquid state by increasing the temperature still further. The resistivities are very low and they show little dependence on the temperature. The resistivity drops from 5×10^{-4} ohm-cm at 500° K to about 1.5×10^{-4} ohm-cm near 800° K. There is no rapid change in the resistivity when the material is carried from the solid to the liquid phase. Calculations of the figure of merit have not been carried out. Indium-antimonide was selected because of its high electron mobility at room temperature although its band gap is undesirably small. The measurements reported here refer only to a sample of unspecified impurity content. An analysis would have to be made to clarify the amount and kinds of impurities present.

Lead Antimony Alloys

In a rather recent publication*, indications have been found that lead antimony alloys may yield useful thermoelectric properties in the liquid phase. Two alloys, therefore, have been produced, having compositions of 50-50 and 76-24 atom percent. They were processed into cells.

*I. D. Konozenko and V. I. Ustianov, Soviet Physics-Technical Physics, Vol. 2, #8, pp. 1567, August, 1957.

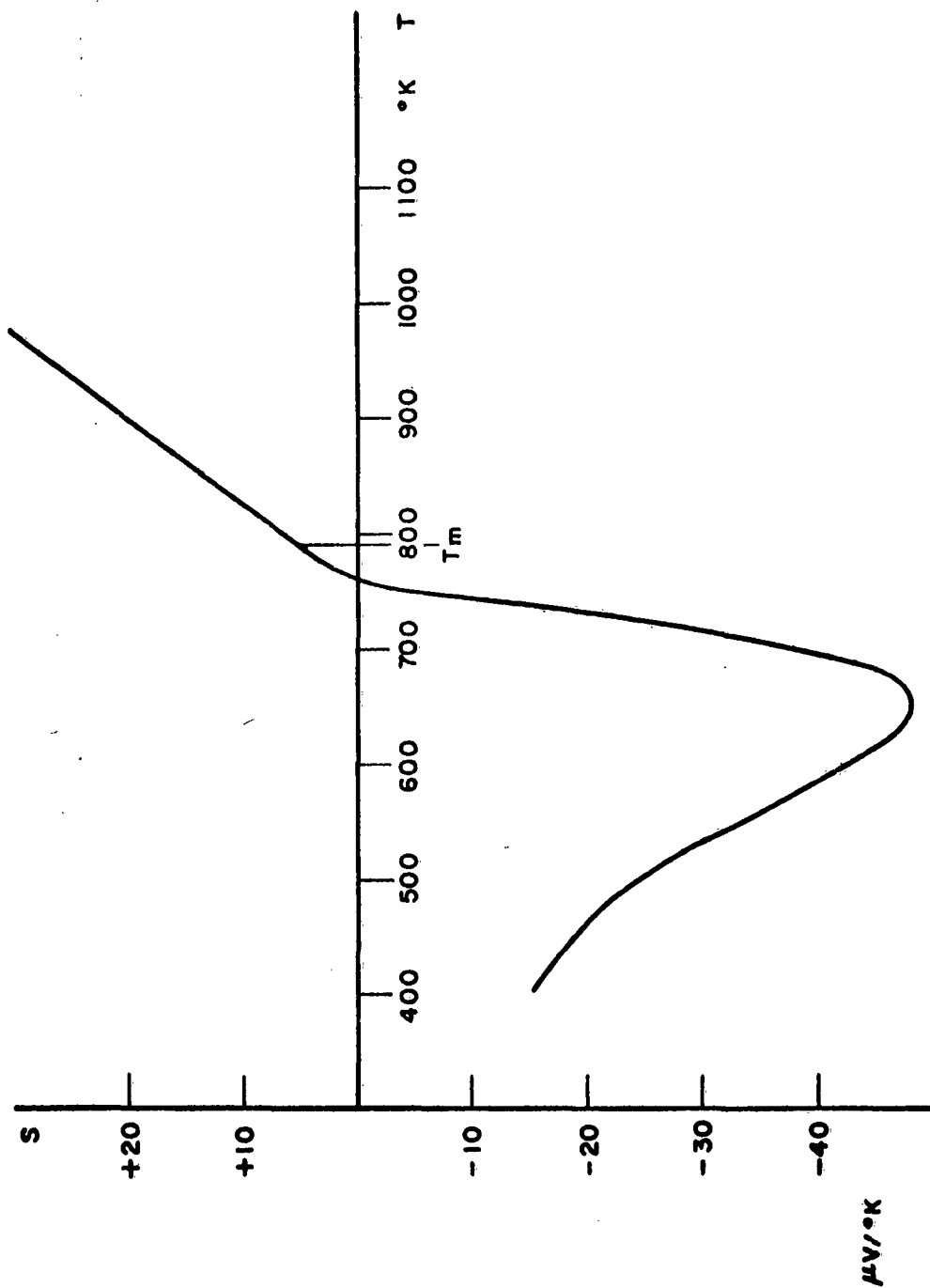


Figure L-10: Seebeck Coefficient vs Temperature, Indium - Antimonide.

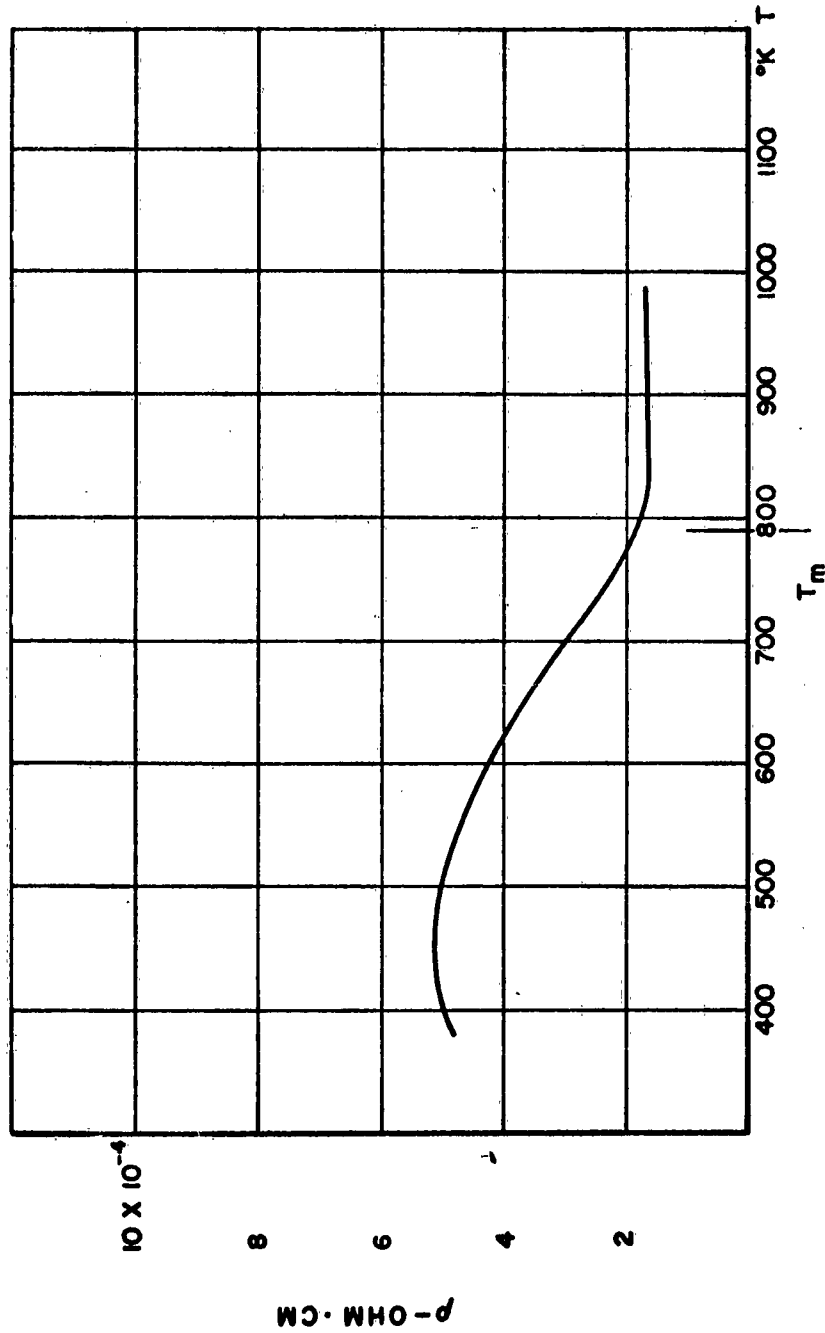


Figure L-11: Resistivity vs Temperature, Indium - Antimonide.

Figure L-12 shows the data obtained for the Seebeck coefficient for the two materials. Both alloys seem to change their carrier polarity, being n-type at lower and p-type at higher temperatures. The intersection for the 50-50 alloy with the x-axis occurs close to the melting point whereas the intersection for the 76-24 alloy may be estimated to be somewhat above 300°K. The absolute values of S, showing a maximum of 70 μ V, have to be considered as low; thus the indication found in the publication could not be verified by the total of four samples made. This maximum value has been found at the highest temperature. The curve, however, shows saturation tendencies in this area, thus the material has not been followed up further.

Using published data of thermal conductivity and resistivity, a maximum figure of merit of 0.1×10^{-3} can be found at 1000°K.

It is of interest to note that, of the materials which have been investigated on this program at temperatures up to and above the melting point, all but three have exhibited Seebeck coefficients in the liquid state which are practically zero. These three exceptions are InSb as previously noted and the two lead antimonide alloys of Figure L-12. All three show considerable thermoelectric properties at temperatures well in excess of the melting points.

Zinc Antimonide

The thermoelectric performance of this material has been rather thoroughly investigated and published data* are available for unencapsulated materials. It is of interest to study the performance in the encapsulated state since the evaporation of zinc becomes noticeable at 350 C. Several cells of ZnSb have been produced, with and without additives. The resistivity versus temperature has been plotted for these materials given in Figure L-13. It can be seen that the resistivity of the material without additives first rises with temperature up to about 600 K and then drops, reaching its lowest value at the melting point. Another, rather small, rise may be noted with further temperature increase. Measurements showed that the resistivity of the material with additives increases considerably during annealing, whereas the resistivity of the material without additives is hardly affected by annealing processes. Our measurements indicate the additives do increase the Seebeck coefficient but not so much as reported in the literature at the lower temperatures.

In Figure L-14 the Seebeck coefficient has been plotted versus temperature for materials with and without additives.

A slight rise is obtained with increasing T up to 750°K, and then a sharp drop occurs close to the melting point. The material remains p-type with small S values in the liquid state, if measured against platinum.

Although ZnSb has been investigated by many people, no final data on the thermal conductivity versus temperature are available to the author at the time of this writing. In order to get estimated values, the electronic portion of the thermal conductivity versus temperature has been calculated. This portion becomes important in the case of low resistivity.

*I. A. Joffe L.C.

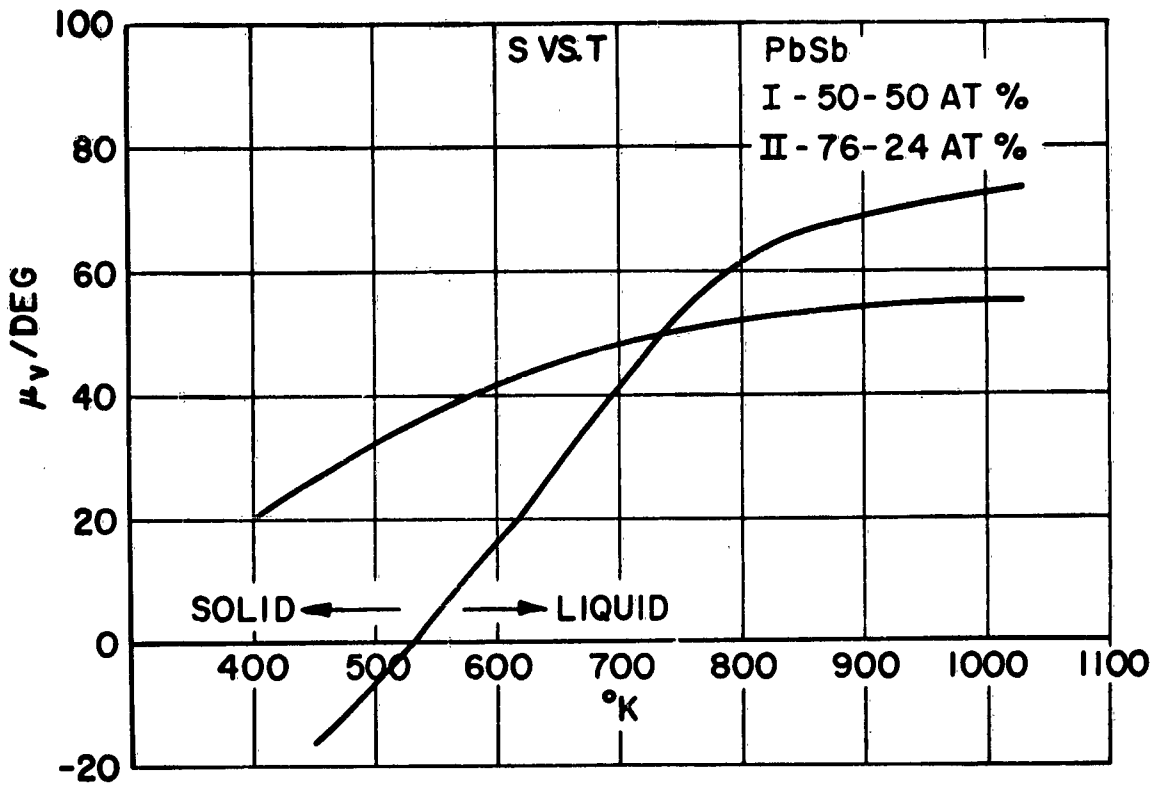


Figure L-12: Seebeck Coefficient vs Temperature,
Lead - Antimony Alloys.

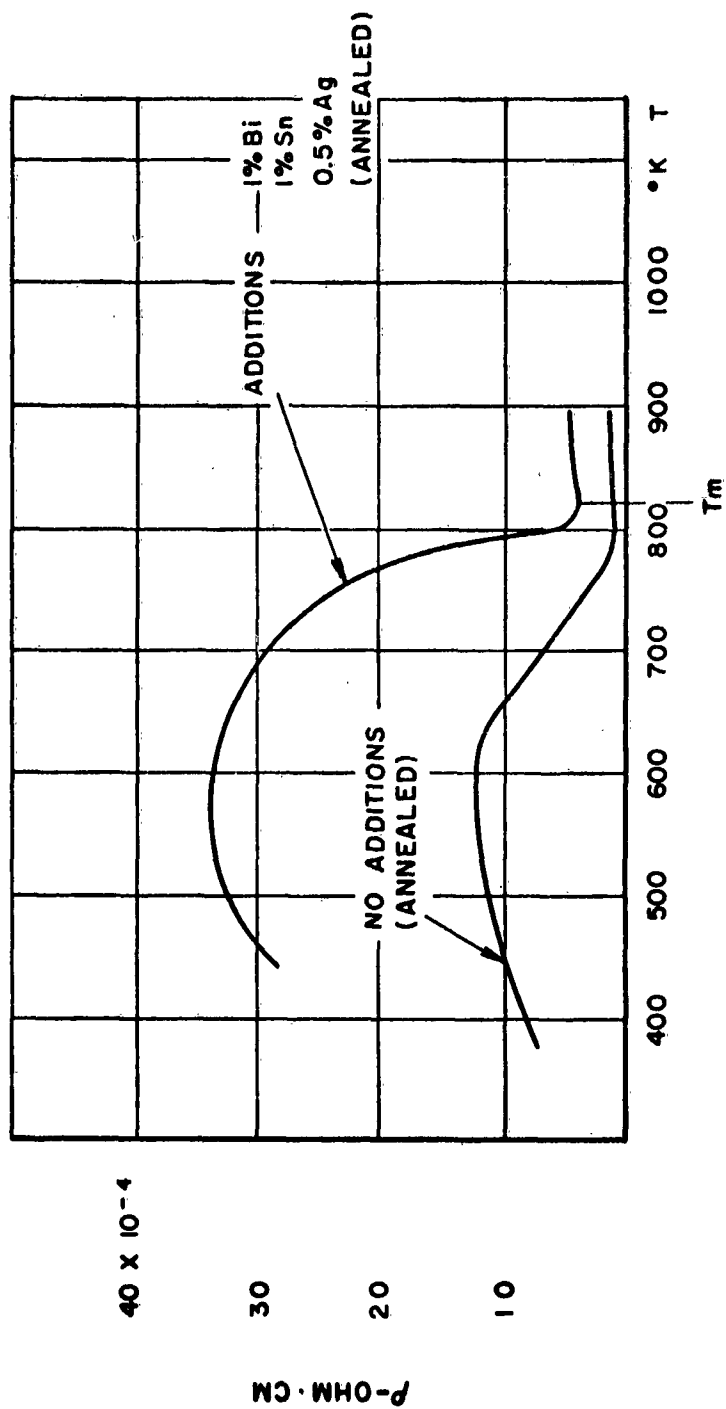


Figure L-13: Resistivity vs Temperature, Zinc - Antimonide.

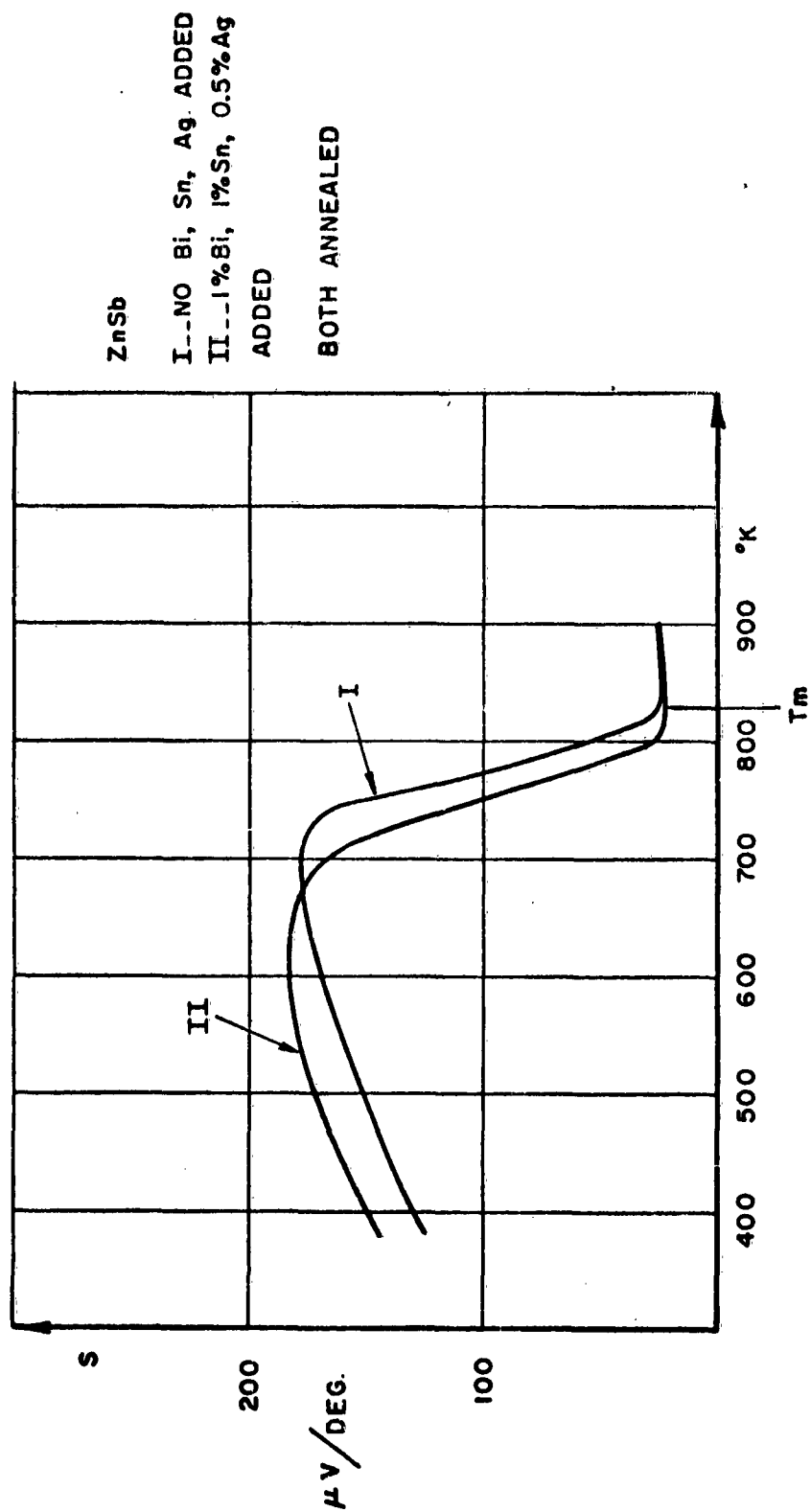


Figure L-14: Seebeck Coefficient vs Temperature, Zinc - Antimonide.

These data are presented in Table L-3 together with information on phonon conductivity taken from the literature. The data refer to the material without additives.

TABLE L-3

Thermal Conductivity of ZnSb
(Watts/cm² K)

	<u>Electronic Portion</u>	<u>Phonon Portion</u>	<u>Total</u>
400°K	8.6×10^{-3}	13.3×10^{-3}	21.9×10^{-3}
500°K	8.2×10^{-3}	12.2×10^{-3}	20.4×10^{-3}
600°K	8.6×10^{-3}	12.2×10^{-3}	20.8×10^{-3}
700°K	17.2×10^{-3}	12.1×10^{-3}	29.4×10^{-3}
800°K	136.0×10^{-3}	12.0×10^{-3}	148.0×10^{-3}

The figure of merit is plotted versus temperature in Figure L-15 for the material without additives. Measured S and ρ values and K data of Table L-3 were used to calculate the values for Z . In the same diagram, the figure of merit is plotted as published recently*. One can see readily that the data on Z for the encapsulated material cover a temperature range extending to higher temperatures than the unenclosed. Whether this effect truly results from the encapsulation or results from differences in composition or doping remains to be seen.

The third curve for Z in Figure L-15 represents ZnSb with additives which is surprisingly low compared with the other two graphs.

DISCUSSION AND CONCLUSIONS

The philosophy of the work on this portion of the contract has been one of rapid material scanning and searching. The organization of such a program therefore obviously led into numerous avenues in order to increase the probability of success.

At the termination of the work, the line drawn naturally cuts through branches of the work which have not been explored entirely and the exploration of which may be desirable.

*Westinghouse Progress Report #12 on Thermoelectricity (BuShips).

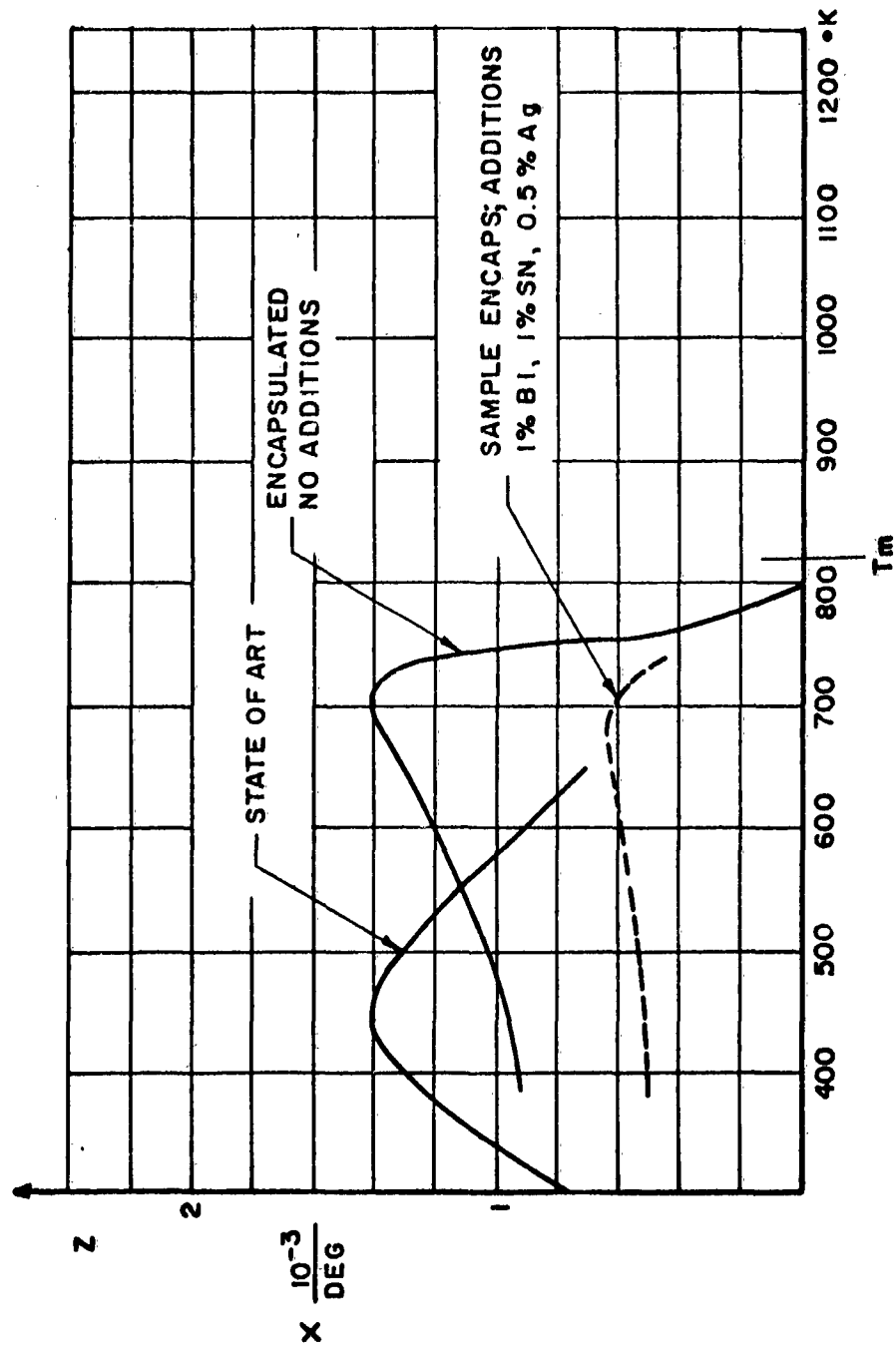


Figure L-15: Figure of Merit vs Temperature, Zinc - Antimonide.

A review of the achievements at the time of termination, however, shows that three major and striking contributions can be reported from the completed portion of the work:

1. The encapsulation
2. The data obtained on encapsulated lead telluride and on
3. Zinc antimonide.

Encapsulation

The first of our major contributions to the over-all program undoubtedly has been the rapid adaptation of ceramic to metal seals, previously developed at the G.E. Research Laboratory. The word "adaptation" obviously stands for a further development and has been chosen to give credit to the originators.

Here is a summary of the advantages and disadvantages of encapsulation of thermoelectric cells:

Advantages of Encapsulation

1. Extension of the useable temperature interval toward higher temperatures. Demonstrations of this effect have been given by the reported results.
2. Increasing the operating lifetime at all temperatures.
3. Improvement of the figure of merit at high temperatures. However, no time has been available to ascertain whether or not these improvements are truly a characteristic of encapsulations per se.
4. Facilitation of the fabrication of stable, low contact resistance junctions.
5. Improvement of the mechanical strength of the TE components. (TE materials are, in general, very brittle.)
6. Improvement of the reliability of the TE components.
7. Permitting operation close to the melting point. Demonstrations of (occasionally) exceeding the melting points of TE materials without impeding performance are given.
8. Facilitation of the segmentation of materials by inserting metallic membranes into the capsules or by stacking individual cells.
9. Making experimental miniaturization feasible. Laboratory cells have effective diameters of only 1/8".

Disadvantages of Encapsulation

1. Efficiency lowering heat losses through the capsule. As stated, we expect to be able to keep these losses within reasonable limits.
2. Increased cost.

The capsules themselves are designed for a higher operating temperature than requested in this contract. They have been provided with large area contacts to minimize contact resistance and thermal impedances. Various metals can be placed in contact with the thermoelectric materials. Due to the limited effort, however, only iron electrodes sealed to Forsterite have been used.

Materials and Data

The second and the third major contributions are the results obtained on the performance of encapsulated ZnSb and PbTe in the solid state.

In Figure L-16 we listed the best n- and p-type thermoelectric materials known to us as of April/May, 1959, within their optimum temperature ranges. These optimum temperature ranges have been found by the intersection of Z versus T curves of the individual materials. In the figure, furthermore, the average Z value over the respective temperature range is given as well as the value of the maximum Z value plus the temperature at which this maximum value has been found.

Any firm statement on the specific use of given compounds is inadvisable, however, because the list of best performers is being revised frequently. Furthermore, the problems to be encountered in matching TE compounds to electrode materials requires some flexibility of choice.

It has been, however, the result of this work that in the n-type branch encapsulated PbTe could be listed as the best material known between 380° and 800° C.*

It proved to be considerably superior to the indium arsenide-phosphide alloy + InAs_{1-x}P_x which has been published rather recently** and which has been believed to be the best material in the same range of the n-type branch.

Furthermore, encapsulated ZnSb could take first place in the p-type branch from about 280° to 470° C which again is an important achievement.

According to the data obtained on n-type PbTe and p-type ZnSb, both encapsulated, it has been demonstrated that both materials not only can be used up to higher temperatures but additionally show unexpectedly improved performances at these temperatures.

Although the results obtained on liquid semiconductors or on materials measured up and beyond the melting point are not as striking as the results obtained on the solids, there are several indications as to the direction of further experiments. So, for example, the rising Seebeck coefficient curves observed in liquid InSb and in the lead antimony alloys will require further high temperature investigations.

*Information received just prior to publication of this Appendix indicates that more recent data on unencapsulated lead telluride produced by the Minnesota Mining and Mfg. Co. makes it necessary to modify this statement to read between 530° and 800° C instead of between 380° and 800° C.

**R. Bowers, J. E. Bauerle and A. J. Cornish; Westinghouse Scientific Paper 431FD405-PL.

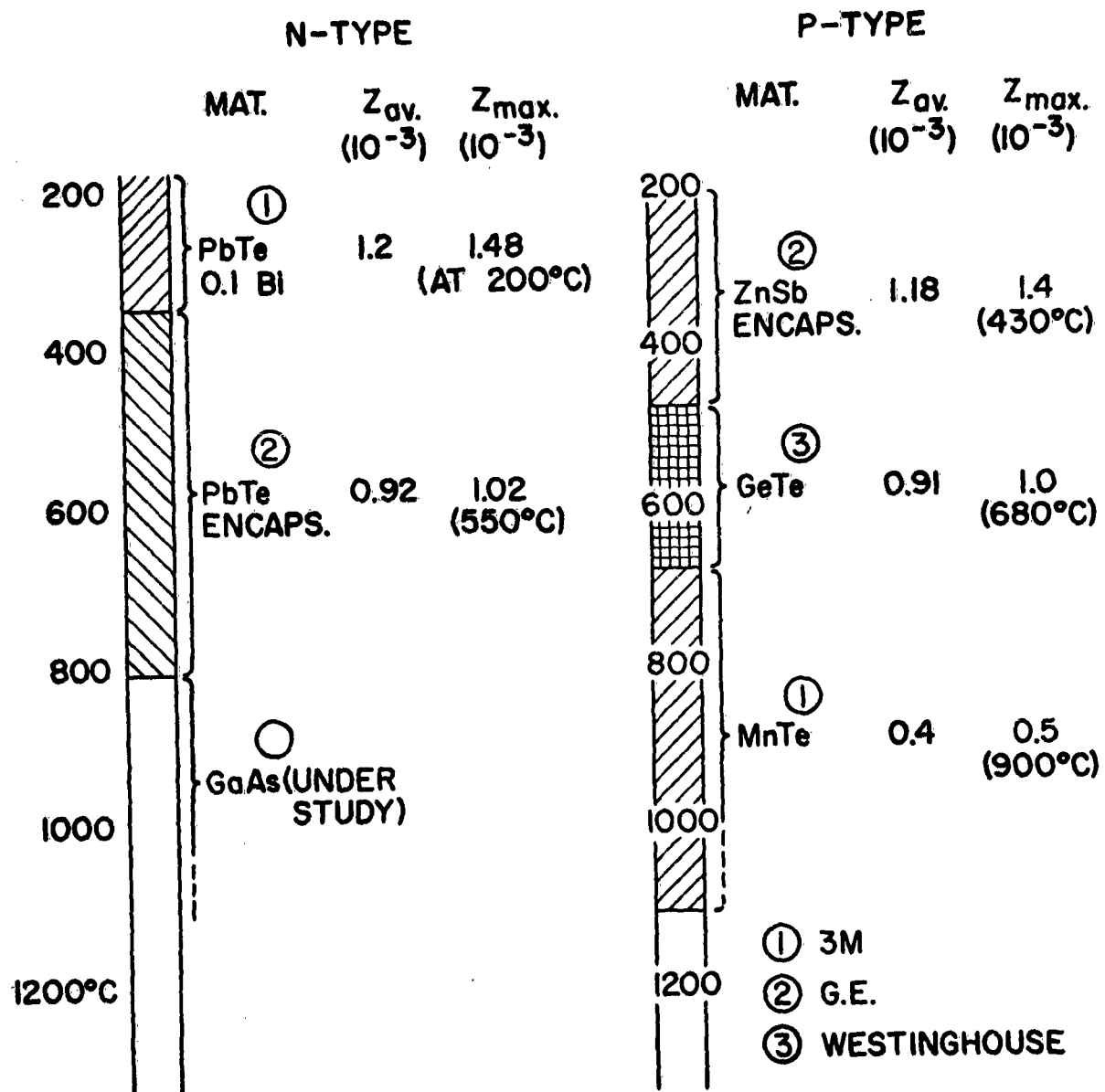


Figure L-16: Best Performing TE Materials - April 1959.

GENERAL REMARKS

At the termination of the work on tasks 1.5 and 1.6, no refinement work has been carried out on the material development such as optimum doping or the reduction of the thermal conductivity.

It is possible, therefore, that such work may improve further the thermoelectric properties of the materials reported.

The experimental work done seems to prove and support wholly or partly the following assumptions:

1. Optimum performance of a single material cannot be expected to cover a wide temperature interval.
2. The narrow temperature interval of best performance is likely to fall close to the melting point T_m if the material is truly optimized.
3. The Z-plateaus of a series ($i = 1 \rightarrow i = n$) of optimized TE materials are likely to follow the relationship

$$Z_i = \frac{1}{T_{ih}}$$

(the proportionality constant has tentatively been taken equal to one, in order to approximate the experimental values of Figure L-17.)

It can be seen that the potential efficiencies of segmented elements are excellent for low values of T_c even if no further improvement in the relationship

$$Z_i = \frac{1}{T_{ih}}$$

should be forthcoming.

4. Reliable operation near the melting point requires adequate encapsulation.
5. Furthermore, it proved that the basic assumptions made initially on guidelines concerning, for example, the band gap and carrier concentration have proven to be useful.

The work reported and the data presented fulfill the requirements as proposed and outlined in the portions 1.5 and 1.6 of the contract since the search led to top performance high temperature materials which can be highly recommended for the design of thermoelectric generators.

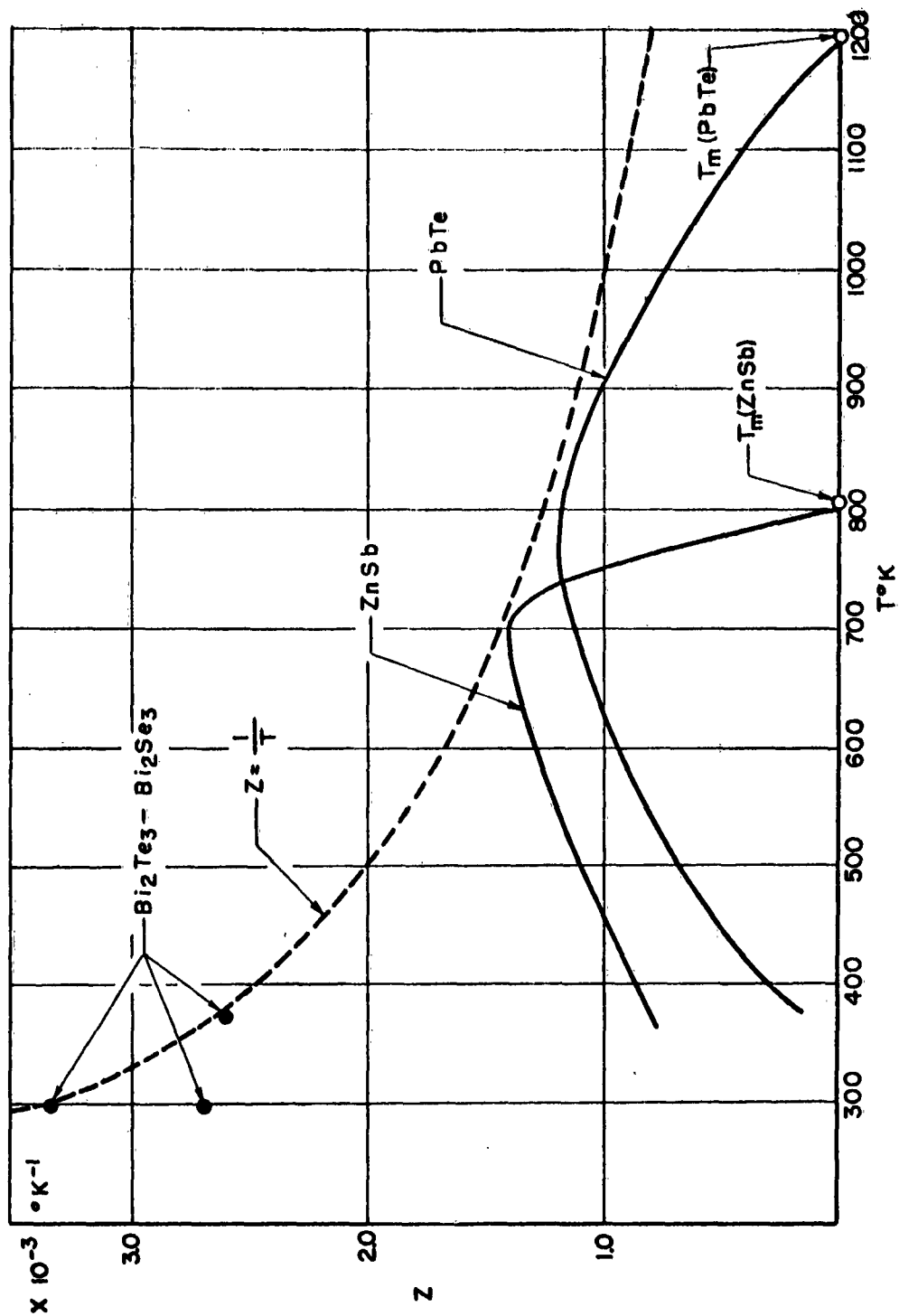


Figure L-17: Temperature Dependence of Some Figures of Merit.

APPENDIX M - GROWTH OF SINGLE CRYSTALS OF TRANSITION METAL OXIDES AND MEASUREMENT OF THEIR THERMAL CONDUCTIVITY

F. H. Horn
R. Newman
G. A. Slack

May, 1959

GROWTH OF SINGLE CRYSTAL OXIDES

Roger Newman

For both the thermal conductivity and optical absorption measurements single crystals were employed. These were prepared by either the Verneuil (flame fusion) method or by halide decomposition as described below.

Verneuil Method

The apparatus used for the flame fusion method is shown schematically in Figure M-1. It is similar to devices that have already been described in the literature.^{M-1} The powdered oxides used were obtained by pyrolyzing the appropriate reagent grade carbonates. Powder is introduced into the oxygen line at a controlled rate by adjusting the frequency and magnitude of the force applied to the hammer. Material is collected on the alumina rod which is retracted from the flame at a controlled rate. The operating procedure was to first collect a mound of flame sintered material on the alumina. Then, either by adjusting the flame, or the position of the rod in the flame, or both, a molten drop was formed at the top of the mound. When the situation was stabilized at the desired drop size the alumina rod was slowly lowered and crystal growth at the rate of between 1/8" and 1/4" per hour proceeded. The success of the operation was very much determined by the experience and judgment of the operator in determining when the proper combination of growth variables was achieved. In growing both NiO and CoO crystals it was necessary to use oxygen-rich flames in order to avoid the formation of the reduced metal. However, for MnO a hydrogen-rich flame was employed. The use of a very oxygen-rich mixture in this case resulted in the formation of Mn₃O₄. The best crystals grown were cylinders about 0.5 cm in diameter and 4 or 5 cm long. They showed good cleavage in 3 mutually perpendicular (100) directions. In this respect NiO was the easiest to cleave, CoO next, and MnO the most difficult to cleave. The cleavage faces showed evidence of a substructure (e.g. small angle grain boundaries) with regions usually about a mm in width running along the growth direction. Back reflection Laue photographs indicated, for the representative samples, that the crystals were single--that is to say the misorientations indicated by the substructure were not large (e.g. less than 1°).

In the growth of Li-doped NiO crystals Li₂CO₃ was added to the NiO powder in amounts up to 50 mol percent. However, in all cases as estimated from the resistivity only a small fraction of the Li remained in the grown crystal. The lowest resistivity single crystals were about 10 ohm cm. Using the data of Morin^{M-2} and Verwey^{M-3} taken with sintered powders, this indicates a composition of about 1 mol percent Li.

Some attempts were made to achieve higher doping levels by diffusion of the Li₂O into pure NiO crystals contained in sealed alumina tubes. At about 1000°C crystals having resistivities of about 10² ohm cm were obtained. This did not represent any improvement over crystals prepared by direct doping.

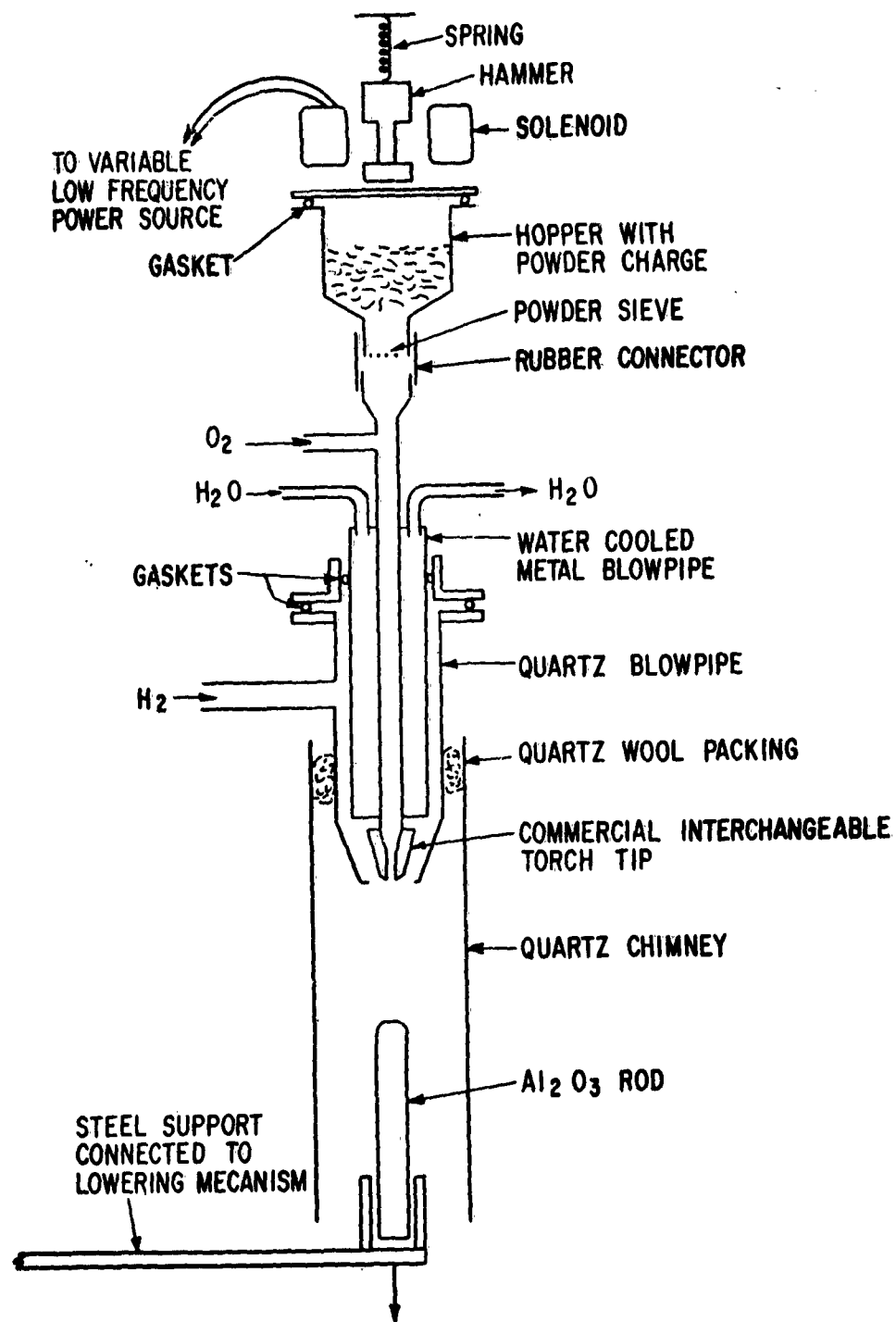


Figure M-1: Flame Fusion Apparatus.

Halide Decomposition

Here we employed a process essentially like that described by R. E. Cech.^{M-4} The apparatus is schematically shown in Figure M-2. The metal halide vaporizes and reacts with H₂O vapor at the MgO surface. This results in an epitaxial growth of metal oxide which in favorable circumstances is a single crystal having the same orientation as the MgO. A typical reaction for NiO is



The essential point is that the metal monoxide crystal structures and lattice constants are very close to that of MgO (4.20 AU), and coherent epitaxial growth is possible. Under the usual growth a film of NiO from 20 - 50 μ thick and 1 to 2 cm² in area could be grown in a few hours. This NiO film could be freed from its MgO backing by chemical dissolution of the MgO in hot H₂SO₄. It could then be used as a seed for growing either thick (i.e. 1 to 2 mm) crystals of NiO or for growing another oxide crystal, CoO for example. For preparing the thick NiO crystals the method using the unmounted film as a seed enabled the crystals to grow in thickness at twice the rate they obtained using a mounted film. This is simply because growth could be simultaneously achieved on both crystal surfaces of the unmounted film.

In contrast to NiO which is not noticeably attacked by any acid, CoO is readily attacked by all the strong acids. For this reason the procedure for growing thick NiO crystals could not be carried over directly for CoO, since there was no reliable way of freeing the CoO film. Instead thin (20 - 50 μ) NiO films were used as seeds for growing thick CoO crystals. For the thermal conductivity measurements the contribution to the total conductivity of the thin NiO film, which represented less than 1/20 of the cross section of the crystal, could be neglected.

Attempts were made to grow Li-doped NiO crystals by incorporating either LiBr or Li₂O in the NiBr₂ charge. Using resistivity as a measure of the amount of Li introduced, no evidence for Li in the NiO crystals was found.

OTHER METHODS FOR GROWING SINGLE CRYSTAL OXIDES

F. Hubbard Horn

Effort was directed toward attempting to grow crystals by a floating zone procedure starting with rods of pressed and sintered NiO and Li-doped NiO powders. NiO was not successfully melted by high frequency heating even when the NiO was heated to nearly its melting temperature. It was possible to melt Li-doped NiO by rf (450 kc) heating; however, in a short time the lithium oxide was lost by volatilization and the melt could not be maintained.

Several solvents for NiO were investigated with the aim of finding one from which NiO could be grown by a modified molten layer procedure. Small crystals of NiO could be obtained from borax-NiO solutions; however, the problems associated with seeded crystal growth were not solved. This method remains unproven. It is clear that the flame fusion or epitaxial growth methods are superior at present.

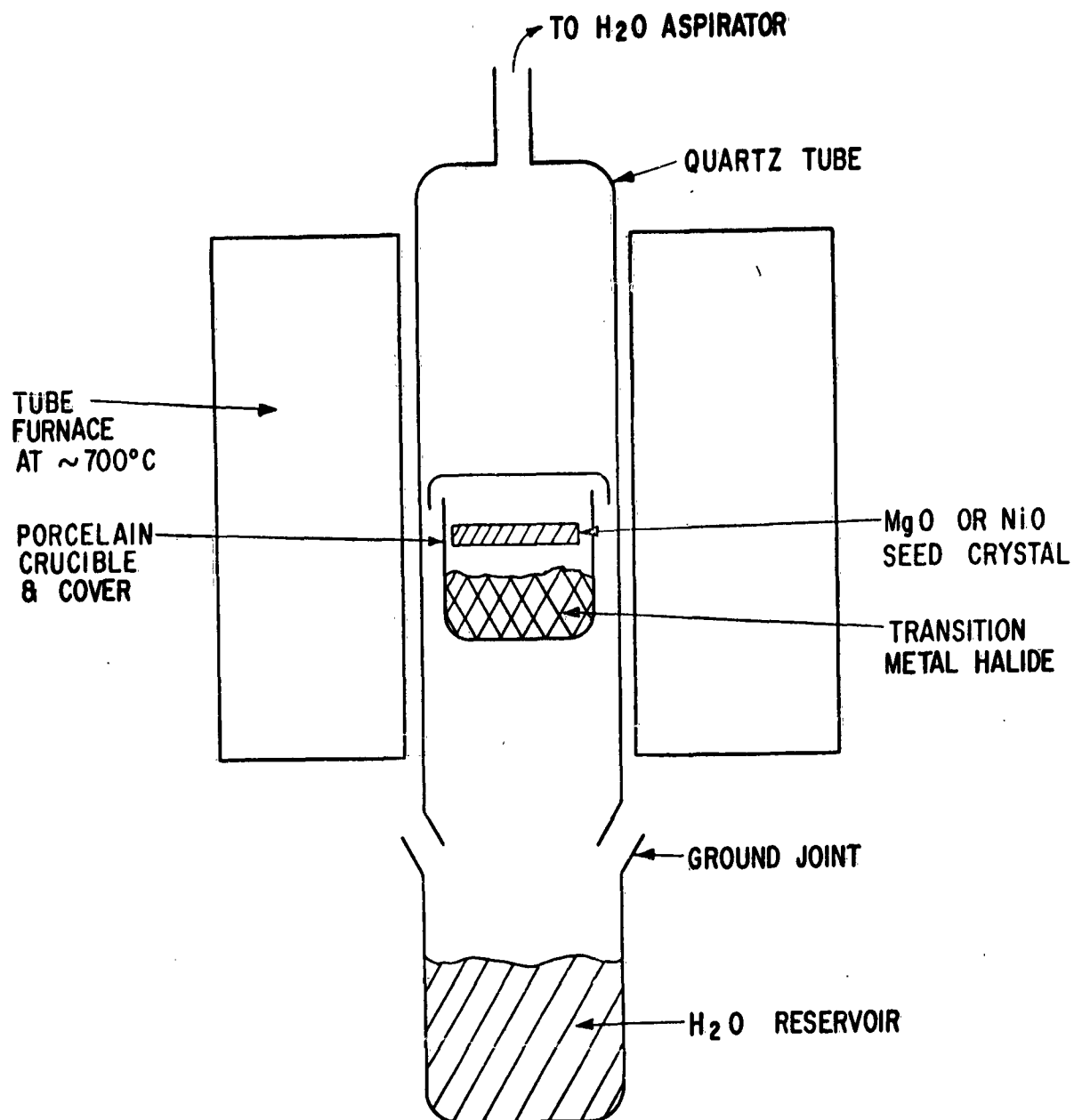


Figure M-2: Halide Decomposition Apparatus.

THE THERMAL CONDUCTIVITY OF TRANSITION METAL OXIDES

Glen A. Slack

Introduction

The thermal conductivity of a solid is an important parameter to know if the solid is being used or considered for use in a thermoelectric generator. The transition metal oxides are a class of solids which exhibit some promising characteristics for thermoelectric generators. Therefore a study of their thermal conductivity was initiated, since the available data^{M-5} in the literature on anything except samples consisting of loose powders was very meager.

The present study involved the measurement of the thermal conductivity of high purity, single crystals of MgO, MnO, CoO, and NiO over the temperature range from 3°K to 300°K. Measurements were also made on single crystals containing intentionally added impurities in order to gain a better understanding of the fundamental processes that determine the thermal conductivity. The crystals, except for MgO, were grown by Dr. R. Newman of this laboratory by either the flame fusion process or the halide decomposition process, as described elsewhere in this report. The MgO crystal was obtained from Mr. L. Schupp.

Method of Measurement

The apparatus used in making the thermal conductivity measurements is shown in Figure M-3. The crystal, as shown, is mounted on the bulb of a constant volume helium gas thermometer with a thin layer of an epoxy resin cement, Armstrong^{M-6} type A-2. A heater made of nichrome wire wound on a metal form is similarly cemented to the top of the crystal. A chain of differential thermocouples made of Au + 2.1 atom percent Co versus Manganin wire^{M-7} is used to measure the temperatures along the crystal. The lowest temperature thermocouple junction at a temperature T_4 is cemented to the gas thermometer bulb. The value of T_4 is measured with the gas thermometer. Two other thermocouple junctions at temperatures T_3 and T_2 provide the means of measuring the emfs corresponding to the temperature differences $T_2 - T_3$ and $T_3 - T_4$. The rate of heat input, Q , to the crystal is determined electrically by measuring the d.c. amperage flowing through the crystal heater and the d.c. voltage across it. The thermal conductivity of the crystal under steady state conditions at an average temperature of $1/2 (T_2 + T_3)$ is determined by

$$\lambda = \frac{Q}{T_2 - T_3} \frac{L}{A},$$

where L is the distance between the thermocouple junctions at T_2 and T_3 , and A is the cross-sectional area of the crystal.

The crystal is kept in the evacuated inner can at a gas pressure of always less than 10^{-4} mm Hg at 300°K, and less than 10^{-6} mm Hg at 3°K. The radiation shield around the sample was used for samples of low thermal conductivity in order to correct for the small (20 percent or less) effects of external thermal radiation. The post heaters, variable thermal resistors, exchange gas, and outer can were very seldom used. Their purpose is to provide control of the temperature T_4 , but this was readily

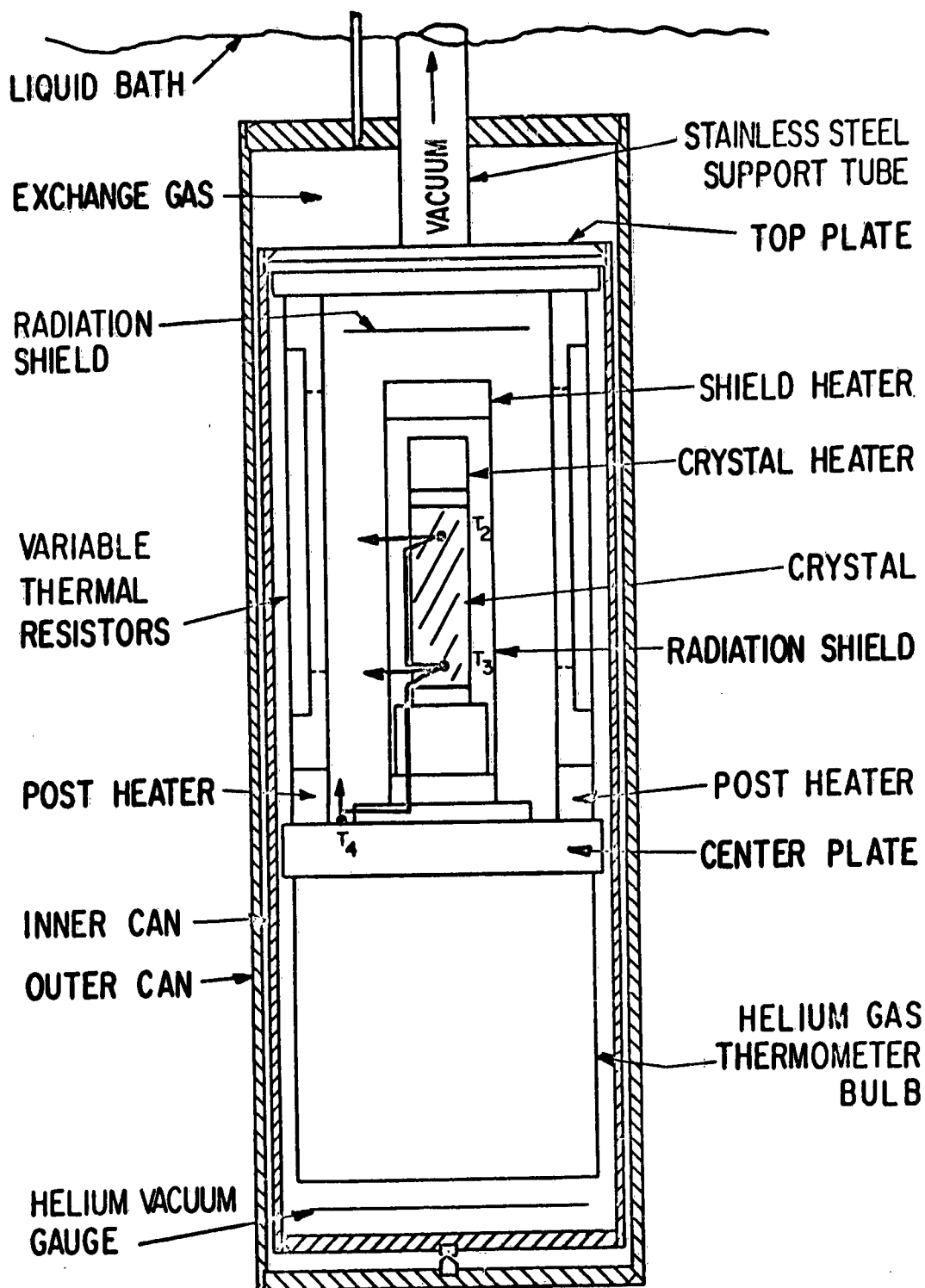


Figure M-3: Device for Measuring Thermocouple Conductivity.

achieved by immersing the inner can directly in successive liquid baths of helium, hydrogen, nitrogen, solid CO₂ plus ethyl alcohol, and then water.

Results on MgO

A small single crystal of MgO was obtained from Mr. Lewis Schupp at the General Electric Lamp Research Laboratory in Cleveland. Its designation was R58 and was grown in a carbon arc furnace. Its estimated impurity content is 8 ppm of Fe, 3 ppm of Cr, 5 ppm of Sr, and 3 ppm of Li. After cutting to size this crystal was annealed at 1485°C in argon and slowly cooled. The sample was a clear, transparent white and exhibited no strains under polarized lights. It was measured in Run No. 14, and a description of this crystal as well as other crystals measured is given in Table M-1. The results are shown in Figure M-4.

Crystals of MgO belong to the cubic system and have a NaCl structure. They are diamagnetic in contrast to the transition metal oxides studied here which are paramagnetic or antiferromagnetic. The only published measurements^{M-8, M-9} on single crystals of MgO are for temperatures above 300°K, and are also plotted in Figure M-4. The agreement between the present results and those in the literature at 300°K is considered good. The absolute accuracy of the present measurements on MgO and other crystals is about ± 5 percent, and the relative accuracy for points at different temperatures on the same sample is ± 3 percent.

TABLE M-1
TABLE OF CRYSTALS STUDIED

<u>Growth Process</u>	<u>Crystal</u>	<u>A₂ mm</u>	<u>L mm</u>	<u>Run No.</u>	<u>Annealed ?</u>	<u>Added Impurity</u>	<u>Comments</u>
carbon arc	MgO	13.3	55.	14	yes	none	
Verneuil	MnO	18.8	11.9	8	no	none	
Verneuil	MnO	18.8	11.9	16	yes	none	Same crystal as Run No. 8
halide	CoO	3.2	7.9	11	no	none	Small NiO core
Verneuil	NiO	15.5	11.0	7	no	none	
Verneuil	NiO	15.5	11.0	9	yes	none	Same crystal as Run No. 7
halide	NiO	6.5	6.0	10	no	none	
halide	NiO	6.5	5.3	15	yes	none	Same crystal as Run No. 10
Verneuil	MnO-CaO	24.2	10.6	26	yes	3 mole % CaO	
Verneuil	MnO-CoO	19.8	7.7	22	no	10 mole % CoO	
Verneuil	MiO-Li ₂ O	11.3	4.6	12	no	x = 1 % Li	

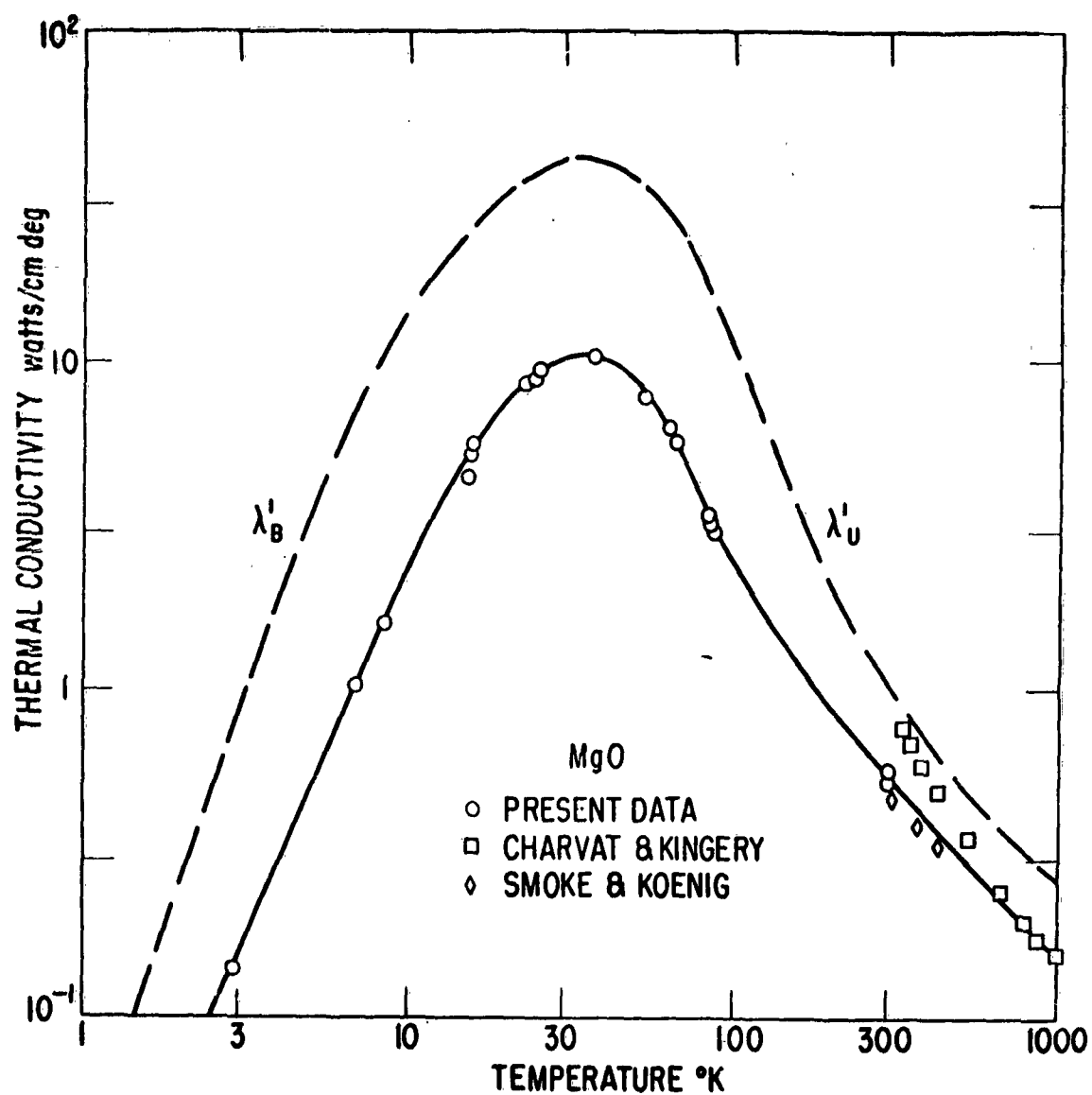


Figure M-4: Thermal Conductivity Versus Temperature for MgO.

TABLE M-1 (continued)

<u>Growth Process</u>	<u>Crystal</u>	<u>A₂ mm</u>	<u>L mm</u>	<u>Run No.</u>	<u>Annealed ?</u>	<u>Added Impurity</u>	<u>Comments</u>
Verneuil	NiO-CoO	21.6	6.6	13	no	5 mole % CoO	
Verneuil	NiO-CoO	29.7	7.0	17	yes	25 mole % CoO	

A = x sectional area

L = separation between thermocouples

As can be seen from Figure M-4 the thermal conductivity of MgO rises as the temperature falls to a maximum conductivity of about 10 watts/cm deg at 35°K and then decreases with a further drop in temperature. This type of behavior is very familiar in crystalline solids which possess no free electrons.^{M-10}

From theoretical considerations^{M-11, M-12} concerning phonon-phonon interactions it is possible to estimate the thermal conductivity at a temperature equal to the Debye temperature, Θ . This theoretically estimated value will be denoted by λ'_{Θ} , whereas the experimentally observed value is λ_{Θ} (no prime). The theoretical estimate is based on the assumption that phonons are the only important carriers of thermal energy in the solid, and also that their mean free path is limited only by being scattered by other phonons. The first of these assumptions appears to be justified for all of the crystals reported on here, but for some of the crystals additional scattering mechanisms are present. The equation for λ'_{Θ} is

$$\lambda'_{\Theta} = .572 M \Theta^2 V_0^{1/3} \gamma^{-2} \text{ deg}^{-3} \text{ sec}^{-3} \quad (\text{M-1})$$

where M is the average gram atomic mass of an atom in the crystal, V_0 is the average volume occupied by one atom in \AA^3 , and γ is Gruneisen's constant. Equation (M-1) gives reasonable values of λ'_{Θ} for many solids.^{M-13}

Furthermore it may be supposed^{M-11} that the experimental data on Al_2O_3 and solid helium, which are isotopically pure, should represent the variation of thermal conductivity, λ_U , with temperature when phonon-phonon scattering is the mechanism which limits the phonon mean free path. This means $\lambda_U/\lambda_{\Theta}$ is assumed to be characteristic function of reduced temperature T/Θ for all simple solids. Values of this function taken from smoothed experimental data^{M-8, M-14, M-15, M-16} are given in Table M-2.

TABLE M-2
RELATIVE THERMAL CONDUCTIVITY VERSUS REDUCED TEMPERATURE
FOR PHONON-PHONON SCATTERING

T/Θ	$\lambda_U'/\lambda_\Theta'$	T/Θ	λ'/λ_Θ'
1.00	1.0	0.067	300
0.39	3	0.053	1000
0.21	10	0.045	3000
0.13	30	0.039	10000
0.089	100		

Using this approach for MgO, and a value for the Debye Temperature at room temperature of $\Theta_{300} = 760^\circ\text{K}$ (see Table M-3), and $\gamma = 2$, the λ_U curve is drawn in Figure M-4.

At any temperature the general theory^{M-17} shows that the thermal conductivity is given by:

$$\lambda = \frac{1}{3} \ell v c \quad (\text{M-2})$$

where ℓ is the phonon mean free path, v is the average sound velocity, and C is the phonon contribution to the specific heat per unit volume of the solid. At temperatures below 35°K in MgO an upper limit to the thermal conductivity is set by the geometrical diameter of the crystal.^{M-8} This upper limit, λ_B , produced by boundary scattering is given by Equation M-2 with the substitutions: $\ell = d$, the average crystal diameter; and $C = 12RD(\Theta_0/T)$, where R is the universal gas constant, D is the Debye function, and Θ_0 is the Debye temperature at 0°K . The curve for λ_B in Figure M-4 was calculated in this manner.

It can be seen from Figure M-4 that the calculations from simple theory agree with the experimental results to within a factor of 3. This type of agreement is satisfactory at temperatures above the thermal conductivity maximum at 35°K . For temperatures below 35°K the agreement is expected to be better, and the experimental thermal conductivity is lower than λ_B probably due to the presence of a small number of dislocations,^{M-19} grain boundaries, or colloidal precipitates in the crystal. Thus MgO serves as a model of a simple oxide which can be used as a standard of comparison for the more complicated transition metal oxides.

Results on High Purity MnO, CoO, and NiO

A number of both high purity transition metal oxide crystals, and crystals containing intentionally added impurities were measured. First consider the high purity crystals which contain generally less than 0.2 percent of foreign impurities. These crystals were made from commercially available C.P. powder of the transition metal carbonate for the Verneuil process or metal bromide for the halide process. The results are shown in Figure M-5.

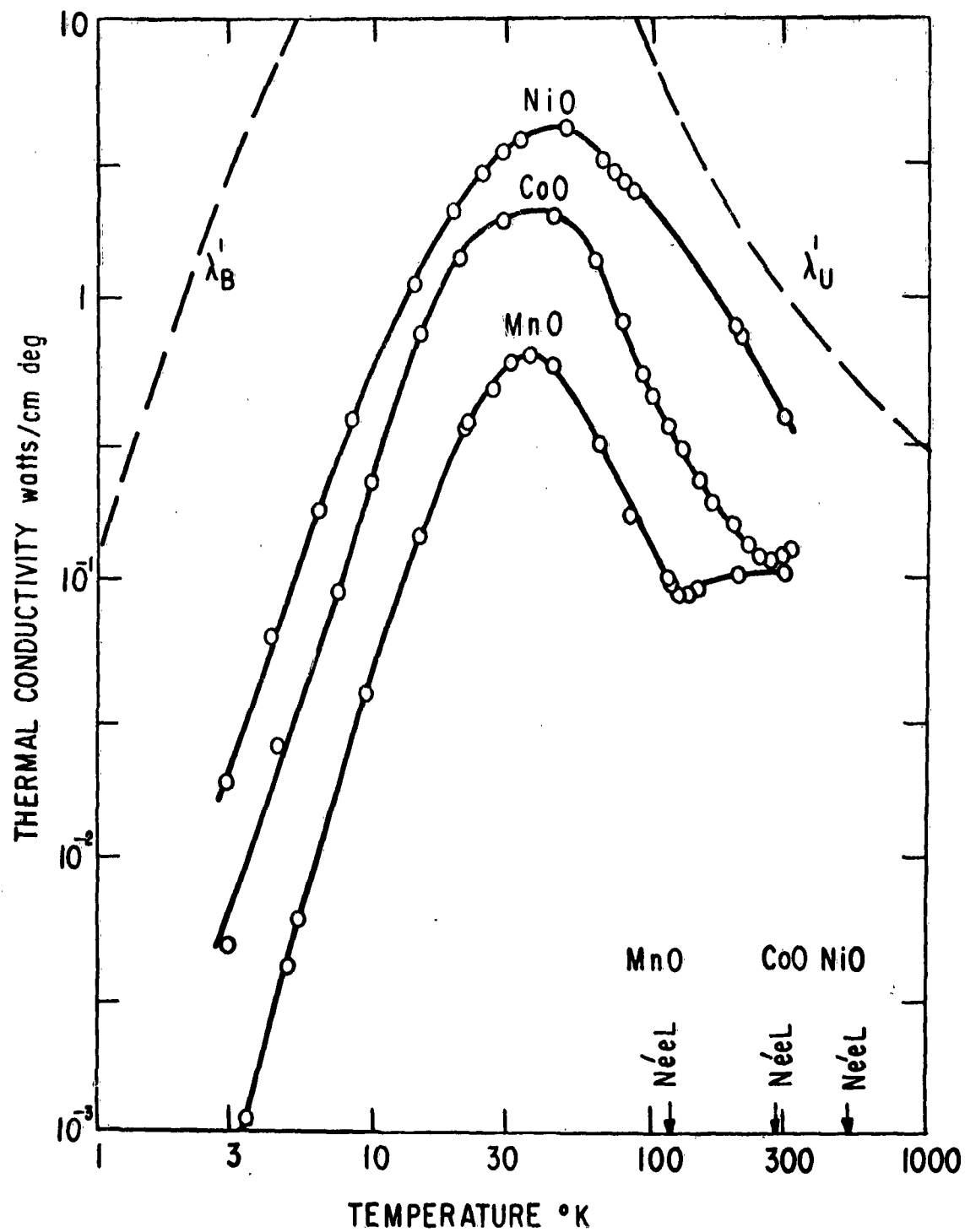


Figure M-5: Thermal Conductivity Versus Temperature for Various High-Purity Oxides.

In order to facilitate the analysis of these and subsequent results, Table M-3 has been drawn up from data in the literature. ZnO is included in this table for a comparison since it, like MgO, is diamagnetic and Zn lies to the right of Ni in the same row of the periodic table.

TABLE M-3
PHYSICAL CONSTANTS OF SOME OXIDE CRYSTALS

Crystal	ρ gm/cm ³	V_g Å ³	$\theta_{300^\circ\text{K}}$	$\theta_{0^\circ\text{K}}$	$10^5 v/\text{sec}$	T_N °K
MgO	3.58	9.25	760(a)	955(f)	7.00(f)	
MnO	5.41	10.9	520(b)	~420(g)	~3.1(h)	116(b)
CoO	6.53	9.50	590(c)	~480(g)	~3.4(h, i, j)	290(l)
NiO	6.85	9.08	630(d)	~510(g)	~3.3(h, k)	523(m)
ZnO	5.73	11.8	620(e)	~500(g)	~3.8(h)	

- a. G. S. Parks and K. K. Kelly, J. Phys. Chem. 30, 47 (1926). W. F. Giaque and R. C. Archibald, J. Am. Chem. Soc. 59, 561 (1937).
- b. R. W. Millar, J. Am. Chem. Soc. 50, 1875 (1928). Average restrahl energy of 0.042 ev determined by R. Chrenko.
- c. Estimated using an average restrahl energy of 0.051 ev for CoO determined by R. Newman.
- d. Seltz, Dewitt, McDonald, J. Am. Chem. Soc. 62, 88 (1940). Average restrahl energy of 0.055 ev determined by R. Newman.
- e. Maier, Parks, Anderson, J. Am. Chem. Soc. 48, 2564 (1926); R. W. Millar, J. Am. Chem. Soc. 50, 2653 (1928); K. Clusius and P. Harteck, Zeit. physik. Chem. 134, 243 (1928).
- f. M. A. Durand, Phys. Rev. 50, 449 (1936); J. deLaunay, J. Chem. Phys. 24, 1071 (1956).
- g. Crude estimate to \pm 30 percent.
- h. From θ_0 , F. Seitz "The Modern Theory of Solids", McGraw-Hill, New York, 1940, pg. 111.
- i. M. E. Fine, Phys. Rev. 87, 1143 (1952).
- j. R. Street and B. Lewis, Nature, 168, 1036 (1951).
- k. From reference j at 530°K.

l. G. Assayag and H. Bizette, Compt. rend. 239, 238 (1954).

m. Tomlinson, Domash, Hay, Montgomery, J. Am. Chem. Soc. 77, 909 (1955).

An analysis of the results in Figure M-5 is most conveniently carried out by calculating the phonon mean free path as a function of temperature from the experimental data on thermal conductivity. Rewrite Equation M-2 as

$$\ell = 3 \lambda / v C. \quad (M-3)$$

The velocity values are from Table M-3. The phonon contribution^{M-20} to the specific heat, C , for the transition oxides MnO, CoO, and NiO is taken to have the same value per mole as ZnO^{M-21} at the same reduced temperature T/θ . It is further assumed that θ versus T/θ is the same as for ZnO because of a lack of sufficient data on the transition oxides. There is a pronounced contribution to the specific heat from the energy which is supplied to crystal in the process of disordering the magnetic system. This specific heat is not, however, directly associated with the phonons and so does not enter in Equation M-3. In fact the total thermal conductivity of the crystal can be considered to be a sum of the contributions from lattice waves (phonons) and magnetic moment waves (magnons) acting independently.

$$\lambda_{TOT} = \lambda_{phonon} + \lambda_{magnon}$$

The λ_{magnon} term from Equation M-3 is

$$\lambda_{magnon} = \ell_m v_m C_m / 3,$$

where C_m is the magnetic contribution to the specific heat, v_m is the average magnetic wave velocity, and ℓ_m is the average mean free path of a magnon. The experimental results can be explained by considering only λ_{phonon} , so it is believed that λ_{magnon} is very small. Since C_m ^{M-20} and v_m ^{M-22} are comparable to C and v , it follows that in the present crystals $\ell_m \leq 0.1 \ell$ at all temperatures.

The mean free path, ℓ , of an average phonon as a function of reduced temperature T/θ for MgO is shown in Figure M-6. The experimental and theoretical curves are taken from Figure M-4. Note that near $T/\theta = 1$ the mean free path varies as T^{-1} . At lower temperatures it rises rapidly until it becomes temperature independent and limited by the size of the crystal for temperature below $\theta/100$. This sigmoid shaped curve is that predicted by simple theory. The value of ℓ as a function of T/θ is shown for MnO, CoO, and NiO in Figure M-7. The experimental data for λ as well as the theoretical curve for NiO are from Figure M-5. Using Equations M-1 and M-2 and the data in Table M-1 and in Table M-3 it can be seen that the ℓ versus T/θ curves from simple theory for MnO, CoO, and NiO should be nearly identical. However, no one of these three oxides agrees with this theory. The mean free path is always less than predicted. The agreement becomes progressively worse the lower the Neel temperature, T_N , of the oxide.

At temperatures above T_N the value of ℓ appears to be nearly temperature independent and equal to about 10 lattice constants for all three oxides. One lattice

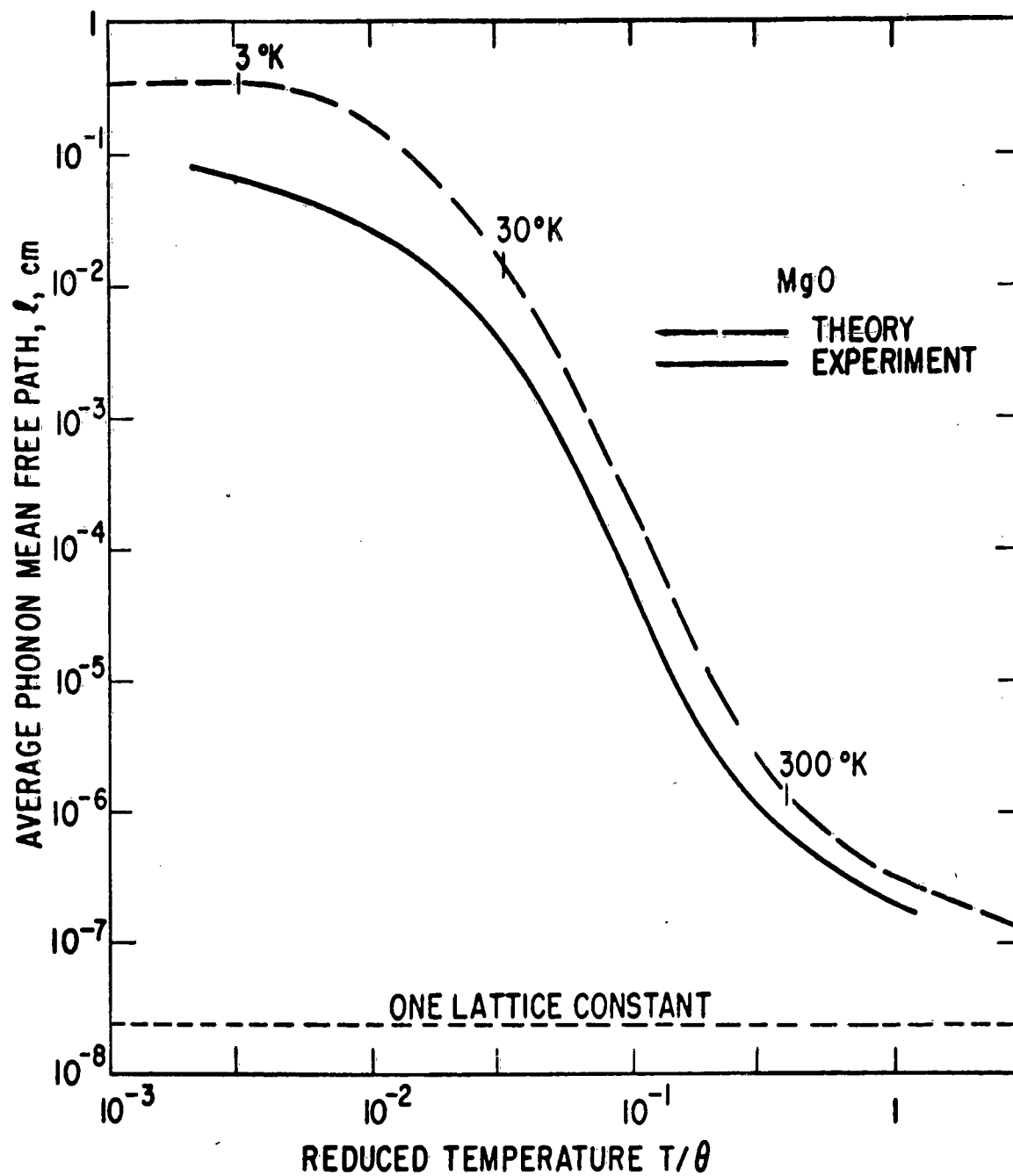


Figure M-6: Average Phonon Mean Free Path, (ℓ) Versus Reduced Temperature, (T/θ) for MgO.

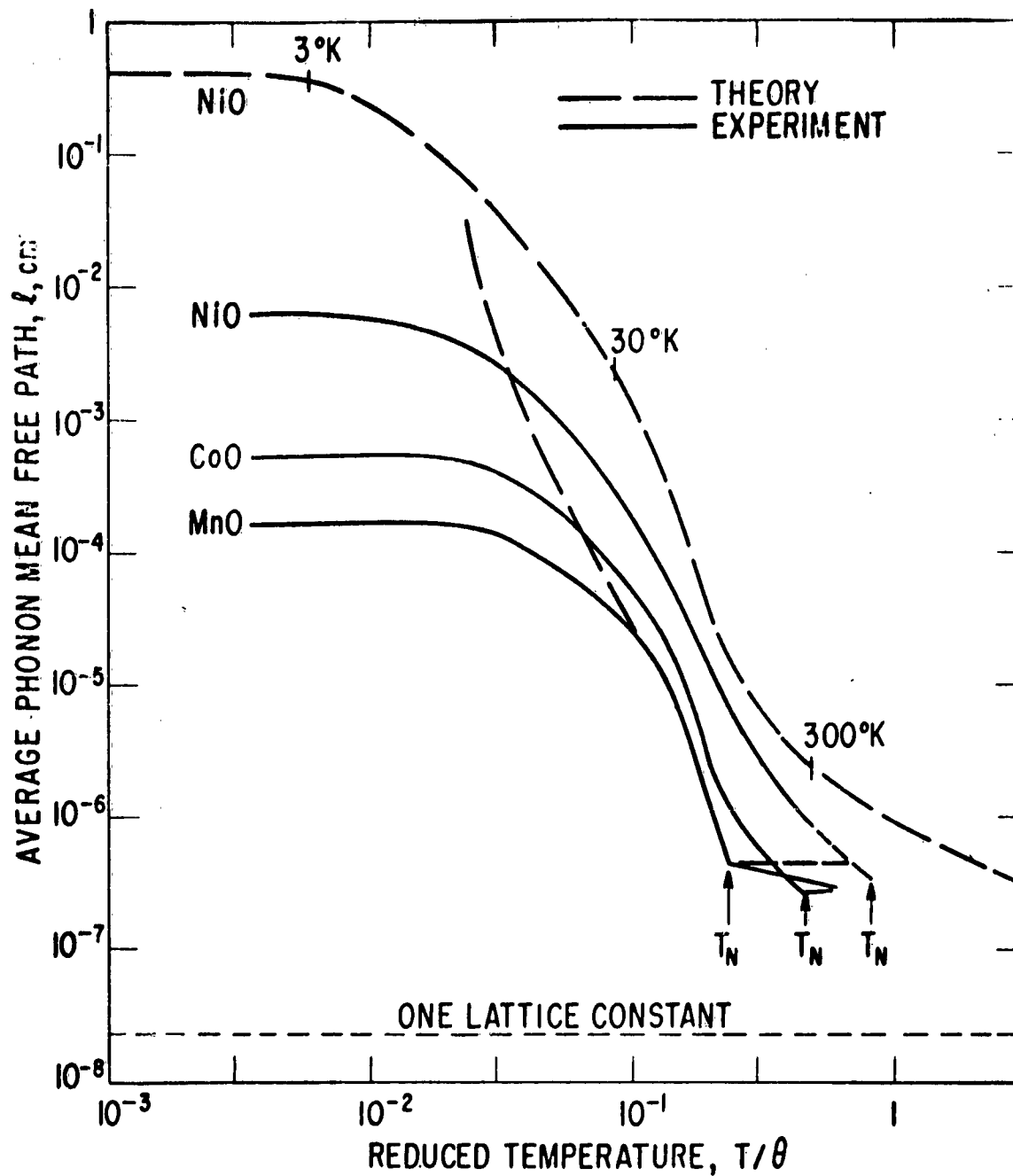


Figure M-7: Average Phonon Mean Free Path, (λ) Versus Reduced Temperature, (T/θ) for Various Oxides.

constant is the ultimate minimum for λ . It appears that above T_N the phonons are being scattered by interaction with the disordered electron magnetic moments on the magnetic ions. As the temperature is lowered below T_N the crystal becomes antiferromagnetic^{M-22} and the magnetic system becomes progressively better ordered. With increased ordering the phonon scattering decreases. For such a model the phonon-magnetic moment scattering disappears in a completely ordered magnetic system and λ is determined only by phonon-phonon or phonon-boundary scattering.

Some simple calculations can be made based on this model of phonons as carriers scattered only by interaction with the magnetic moments. Consider MnO in which the experimental λ is much less than simple theory. Let S be the scattering cross-section of a Mn atom which possesses an "unoriented" magnetic moment. Now S is assumed to be independent of the phonon wavelength and will be some fraction, f , of the geometrical cross-section of a Mn atom, i.e.

$$S = f V_0^{2/3}$$

The density, n , of "unoriented" moments per unit volume is defined as

$$n = \frac{1}{2V_0} \left[1 - \frac{M(T)}{M(0)} \right],$$

where $2V_0$ is the average volume of an MnO molecule, $M(T)$ is the spontaneous magnetization^{M-22} of one of the antiferromagnetic sub-lattices at a temperature T , and $M(0)$ is the saturation magnetization at $T = 0^\circ\text{K}$. Then the phonon mean free path is given by

$$\lambda'_s = n^{-1} S^{-1} = 2V_0^{1/3} f^{-1} \left[1 - \frac{M(T)}{M(0)} \right]^{-1} \quad (\text{M-4})$$

For temperatures above T_N the value of $M(T)$ is zero, and consequently λ is independent of temperature with a value of $2V_0^{1/3} f^{-1}$. This is nearly what is observed for MnO with $f = 0.1$ (see Figure M-7). Below T_N there is a rapid increase in λ as the magnetic moments become more ordered. In Table M-4 values of $1 - M(T)/M(0)$ are given versus T/T_N for MnO with $J = 5/2$. In MnO the magnetic moment is caused only by spins, and $J = 5/2$.^{M-22} The dashed theoretical curve in Figure M-7 lying over the experimental curve for MnO is the value of λ'_s from Equation M-4. The theory has been fitted to the experimental data only at T_N , which gives $f = 0.1$. The agreement extends over two decades of λ and one decade of T . At temperatures above 300°K in MnO phonon-phonon scattering is becoming as important as the phonon-magnetic moment scattering. At temperatures below 300°K domain scattering becomes important. The application of this simple theory to CoO and NiO becomes more complicated because phonon-phonon and phonon-magnetic moment scattering are both involved. The basic mechanisms are still the same, and the magnetic interaction has about the same strength since $f \approx 0.1$ for NiO and CoO as well as MnO.

TABLE M-4

FRACTION OF DISORDERED SPINS AS A FUNCTION OF TEMPERATURE FOR $J = 5/2$

T/T_N	$1 - \frac{M(T)}{M(0)}$	T/T_N	$1 - \frac{M(T)}{M(0)}$
> 1	1.00	0.30	2.4×10^{-2}
1.00	1.00	0.20	6.0×10^{-3}
0.95	0.67	0.15	1.3×10^{-3}
0.90	0.55	0.12	3.3×10^{-4}
0.80	0.38	0.10	7.6×10^{-5}
0.70	0.27	0.09	2.9×10^{-5}
0.60	0.18	0.08	8.6×10^{-6}
0.50	0.11	0.07	2.1×10^{-6}
0.40	0.063	0.06	4.0×10^{-7}

An additional complicating factor arises because of the crystallographic distortion which occurs in these transition metal oxides at T_N . Above T_N they all possess a cubic crystal structure. Below T_N both MnO and NiO become rhombohedral while CoO becomes tetragonal.^{M-23} This leads to the formation of antiferromagnetic domains.^{M-24, M-25} Phonons appear to be scattered at the domain boundaries leading to a phonon mean free path which is considerably less than the microscopic size of the crystal. If a single domain wall is a very efficient scatterer of phonons, then ℓ at $T \leq \theta/100$ is just equal to the average width of a domain. Providing a domain wall has a thickness ^{M-24} of 10 lattice constants or more, and that the spins within the wall are very disordered, then it appears that a wall should be a good scatterer of phonons. This conclusion is based on the fact that at temperatures above T_N phonons of all energies possess a mean free path of about 10 lattice constants in the disordered magnetic system and that S appears to be independent of the phonon wavelength. From Figure M-7 the limiting value of ℓ is taken as the domain size. It is 60 microns in NiO, 5 microns in CoO, and 1 micron in MnO. This value varies somewhat with annealing treatment (see Figures M-8 and M-10).

High Purity Crystals From Different Sources

High purity single crystals of NiO were prepared by the Verneuil process and by the halide decomposition process. These were measured in both the "as grown" state and a "well annealed" state. The annealing procedure for the NiO and all the other oxides studied here was to warm slowly, hold them at a temperature of 1500°C for about 30 minutes, and then cool slowly to room temperature (cooling rate $< 20^\circ\text{C}/\text{minute}$). During this entire procedure the crystals were kept under argon at a pressure of 1 atmosphere. The results are shown in Figure M-8. Note that the results for the halide process and Verneuil process crystals are quite similar, and that the annealing raises the thermal conductivity below 20°K by about a factor of 2. Neither the method

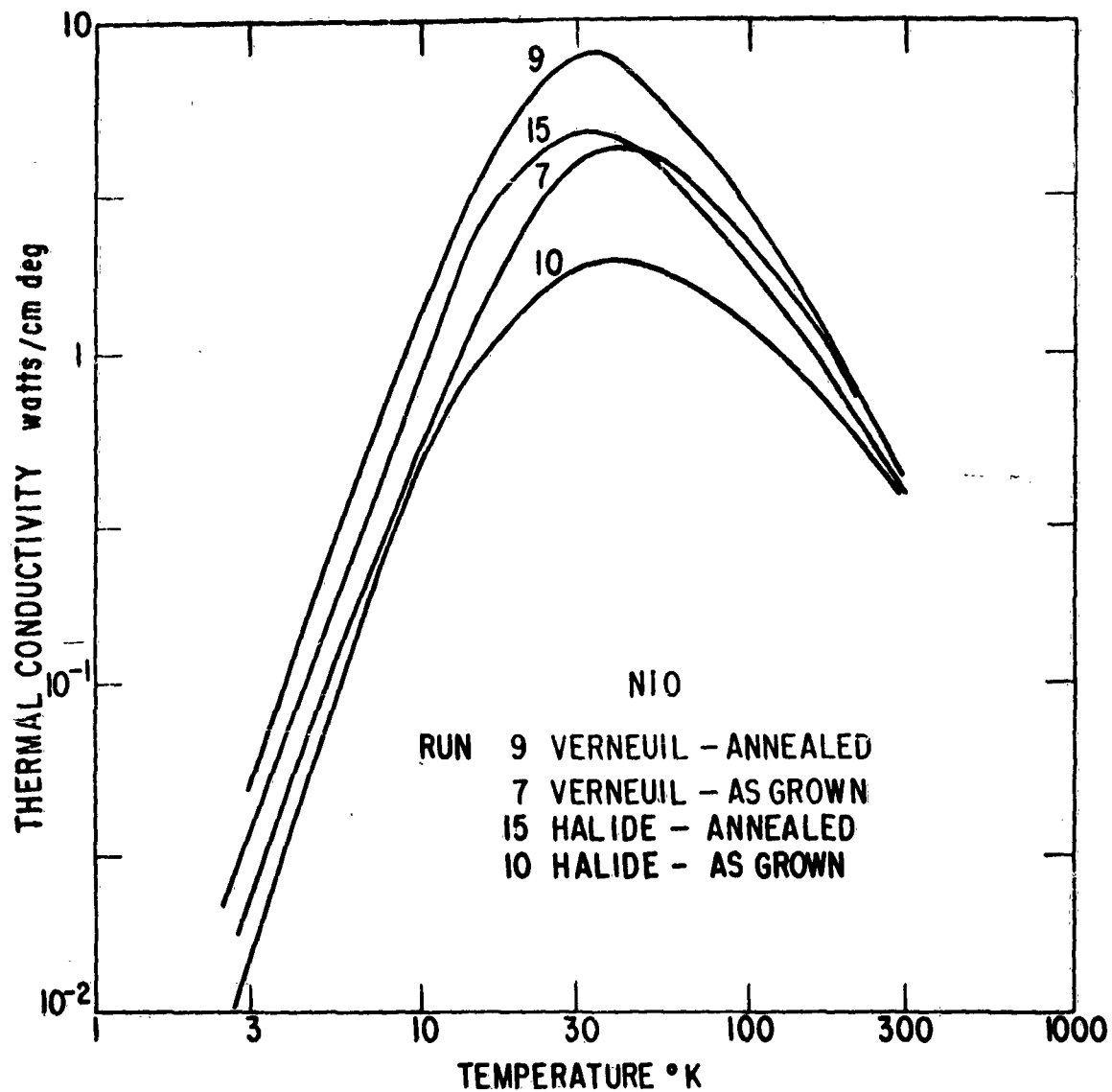


Figure M-8: Thermal Conductivity, (K) Versus Temperature, (T) for NiO.

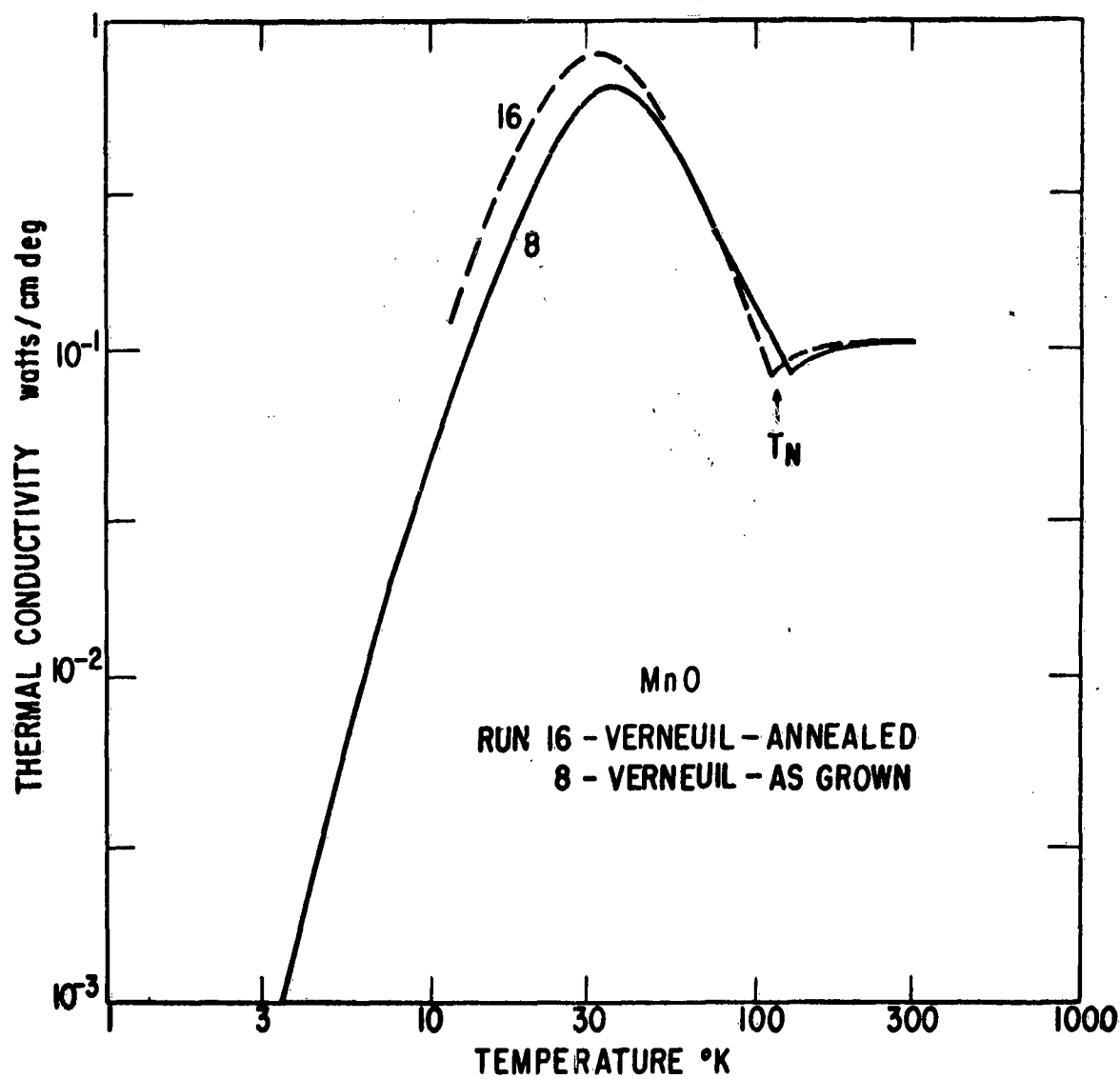


Figure M-9: Thermal Conductivity, (K) Versus Temperature, (T) for MnO.

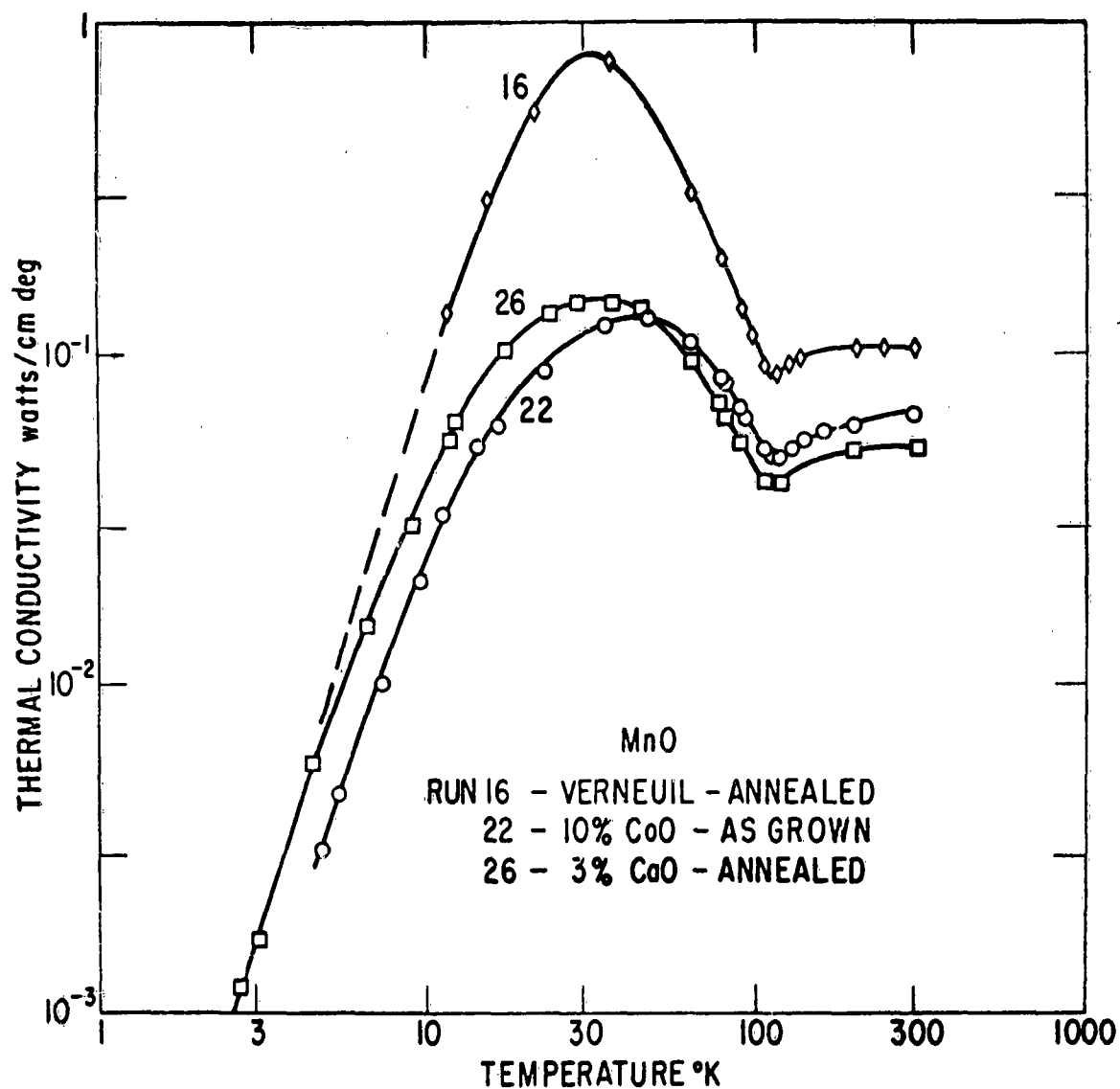


Figure M-10: Thermal Conductivity, (K) Versus Temperature, (T) for MnO with Various Additions.

of crystal growth nor the annealing treatment appreciably affect the thermal conductivity at 300°K. However, it is important to realize that some difference in thermal conductivity between a strained and an annealed NiO crystal is still observable even at 300°K.

A Verneuil process MnO crystal is shown in Figure M-9 before and after annealing. Note that the annealing raises the thermal conductivity at low temperatures by about a factor of 2, and that the temperature at the minimum shifts slightly. Only a single, unannealed halide process crystal of CoO was measured and the results have already been presented in Figure M-5.

The general conclusion to be drawn is that the measurements of thermal conductivity on a high purity, well annealed single crystal are reasonably reproducible, even on samples from different sources. The room temperature thermal conductivity values represent an intrinsic property of the sample while the low temperature results vary somewhat with the annealing treatment.

Crystals With Added Impurities

In order to study the effects of small amounts of impurities on the thermal conductivity, mixed crystals of MnO-CoO and MnO-CaO were made. Such mixed crystals of MnO-CoO crystals can be made over the whole composition range, M-26, M-27 while MnO-CaO crystals can be made with several mole percent of CaO in the MnO. M-28 The results for high purity, well annealed MnO (Run No. 16), a well annealed crystal of 97 mole percent MnO + 3 mole percent CaO (Run No. 26), and an unannealed crystal of 90 mole percent MnO + 10 mole percent CoO (Run No. 22) are shown in Figure M-10. Notice that these low impurity concentrations reduce the thermal conductivity of MnO at room temperature by a factor of at most two. Higher impurity concentrations would reduce it even more. Thus the conductivity results on high purity MnO crystal made from C. P. MnCO_3 which possessed residual chemical impurities such as other transition metals, alkalis, and alkaline earths of the order of 0.2 percent or less, should be only slightly affected by these trace impurities.

The occurrence of the minimum in the thermal conductivity versus temperature curve of MnO is not appreciably influenced by the addition of small amounts of impurities. The minimum is still quite pronounced and still occurs at about the same temperature as in high purity MnO. The lower thermal conductivity of the mixed crystal is the result of scattering of phonons by these point impurities (Co, Ca) which were not present in the original high purity crystals. There is no major difference between the effect of a magnetic (Co) and a non-magnetic (Ca) impurity. The thermal conductivity at temperatures below 10°K is altered very little by the added Co or Ca. The greatest effect is caused by annealing, as can be seen from Figure M-10.

Single mixed crystals of NiO-Li₂O and NiO-CoO were grown by the Verneuil process. The NiO-CoO system forms a complete series of solid solutions, M-26, M-29 and the NiO-Li₂O forms solid solutions M-30 of the form $\text{Ni}_{1-x}\text{Li}_x\text{O}$ up to $x = 0.3$. The results for $\text{Ni}_{1-x}\text{Li}_x\text{O}$ for $x = 0.01$ (Run No. 12), 95 m percent NiO - 5 m percent CoO (Run No. 13), 75 m percent NiO - 25 m percent CoO (Run No. 17), and for high purity NiO (Run No. 9) are shown in Figure M-11. The CoO concentrations were those of the powder from which the crystals were grown.

The excess Li in the NiO changes the valence of a fraction x of the Ni ions to

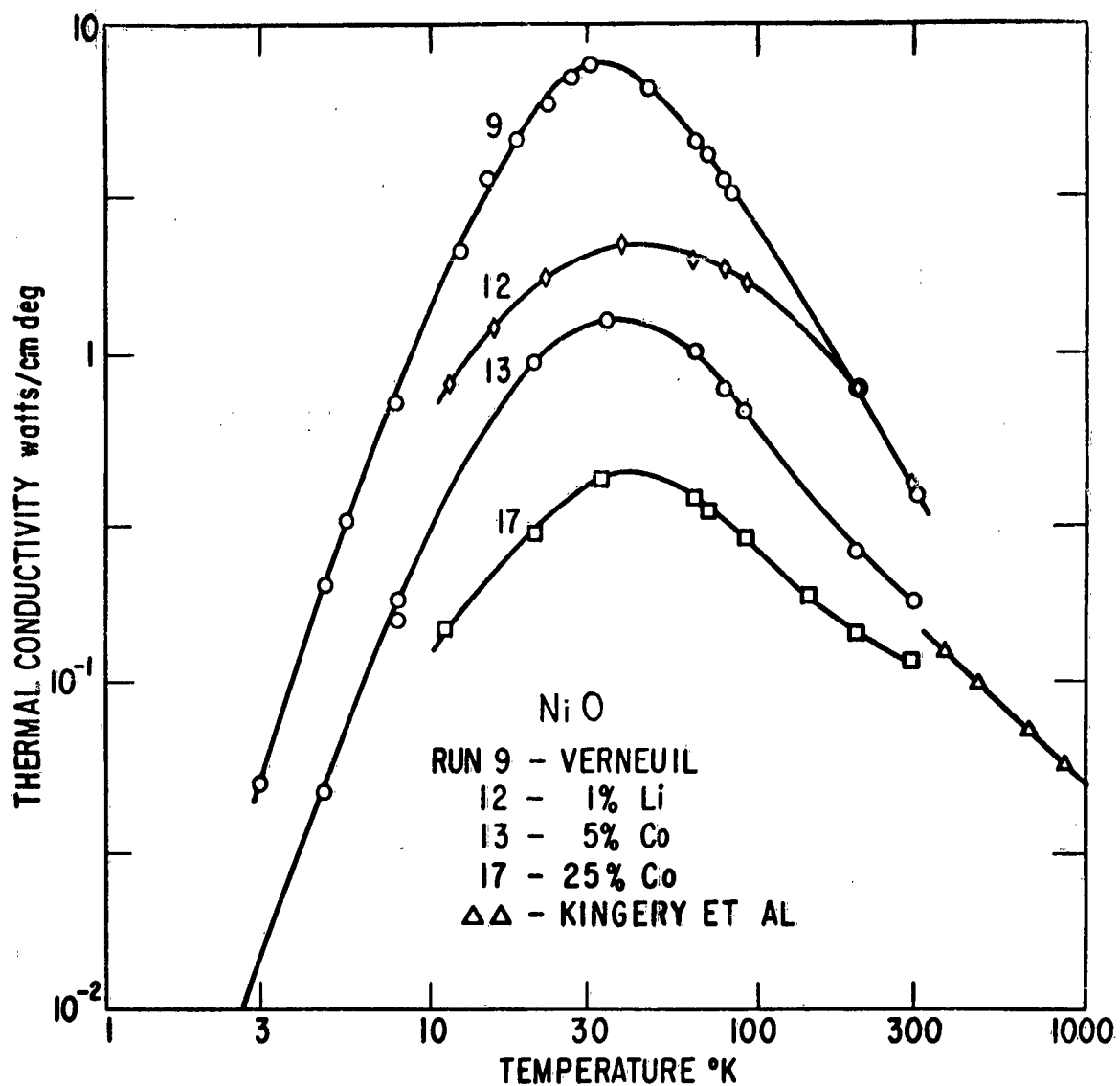


Figure M-11: Thermal Conductivity, (K) Versus Temperature, (T) for NiO with Various Additions.

Ni^{+++} , and thus makes NiO into a semiconductor. The sample in Run No. 12 had a room temperature electrical resistivity of 10 ohm-cm. The value of $x = 0.01$ was estimated from this resistivity^{M-31}. For comparison the electrical resistivity at room temperature of the high purity NiO is greater than 10^5 ohm-cm. With this tremendous increase in the electrical conductivity of NiO there is little if any noticeable change in the thermal conductivity. The results in Figure M-11 for the $\text{Ni}_{.99}\text{Li}_{.01}\text{O}$ crystals (Run No. 12) are quite similar to the high purity halide process NiO (Run No. 10) shown in Figure M-8. The thermal conductivity for both these unannealed crystals is less than that of the best annealed NiO (Run No. 9) primarily because of strains. The amount of thermal conductivity, λ_e , caused by the transport of thermal energy by the electrons can be estimated from the Weidemann-Franz law. This law states $\lambda_e = L \sigma T$, where $L = 1.48 \times 10^{-8}$ volt² deg⁻², σ is the electrical conductivity, and T the absolute temperature. For the NiO sample in Run No. 12 this contribution is $\lambda_e = 4 \times 10^{-7}$ watts/cm deg at 300°K. The value of λ_e is less at all lower temperatures since σ decreases exponentially^{M-32} with decreasing temperature. Such a small effect cannot be detected. So even with 1 percent of Li in the NiO the excess electrons neither noticeably increase the thermal conductivity by providing more carriers of thermal energy, nor do they decrease the thermal conductivity by scattering the other carriers, i.e. phonons.

The addition of CoO to the NiO does decrease the thermal conductivity at 300°K. The 25 mole percent CoO crystal has about 1/4 the thermal conductivity of the pure NiO at room temperature. From this data it is estimated that a crystal of about 50 mole percent CoO, would have the lowest thermal conductivity in the NiO-CoO system with a value of .08 watts/cm deg at 300°K, a lower conductivity than that of either pure NiO or CoO. At temperatures below 10°K the results on these mixed crystals are generally intermediate between those for high purity NiO and high purity CoO. This means that the size of the antiferromagnetic domains varies nearly monotonically with composition in going from NiO to CoO.

Conclusions

The thermal conductivity of the transition metal oxides MnO, CoO, and NiO at temperatures below 300°K is caused only by phonons, and is lower than would be expected from theoretical comparison of the results with measurements made on MgO. This difference is associated with the fact that these transition metal oxides possess magnetic moments with which the phonons can interact, in contrast to MgO which is diamagnetic and possesses no unpaired magnetic moments. At temperatures well above the Neel temperature, T_N , the thermal conductivity of the paramagnetic oxides will approach the theoretical values calculated for diamagnetic oxides. In the regions around T_N the phonons are strongly scattered by unoriented magnetic moments. Below 10°K the thermal conductivity appears to be limited by the presence of antiferromagnetic domains.

When either magnetic or non-magnetic impurities are incorporated substitutionally into the lattice the thermal conductivity below 10°K is changed very little, but above 10°K it is lowered by point impurity scattering. The presence of a minimum in the thermal conductivity versus temperature curve at the Neel temperature appears to be an intrinsic property of the solid associated with the presence of the magnetic moments of the electrons in the 3d shells of the metal ions.

REFERENCES

- M-1. A. Verneuil, Ann. chim. et phys. 3, 20 (1904).
- M-2. F. J. Morin, Phys. Rev. 93, 1199 (1954).
- M-3. Verwey et al, Philips Research Reports 5, 173 (1950).
- M-4. R. E. Cech and E. Alessandrini, Trans. Am. Soc. Metals 51 (1959).
- M-5. Kingery, Franci, Coble, Vasilos, J. Am. Ceram. Soc. 37, 107 (1954).
- M-6. Armstrong Products Co., Warsaw, Indiana.
- M-7a. Borelius, Keesom, Johansson, Linde, Commun. Kamerlingh Onnes Lab. Univ. Leiden, No. 217d (1932).
- M-7b. W. H. Keesom and C. J. Matthijs, Physica 2, 623 (1935).
- M-7c. Powell, Rogers, Coffin, J. Research Natl. Bur. Standards 59, 349 (1957).
- M-8. F. R. Charvat and W. D. Kingery, J. Am. Ceram. Soc. 40, 306 (1957).
- M-9. E. J. Smoke and J. H. Koenig, College of Engin. Res. Bulletin, No. 40, Rutgers, New Brunswick, N. J. (Jan. 1958).
- M-10. R. Berman, Advances in Physics 2, 103 (1953).
- M-11. G. Leibfried and E. Schlomann, Nachr. Akad. Wiss. Gottingen, Math. physik. Kl. 4, 71 (1954).
- M-12. G. K. White and S. B. Woods, Phil. Mag. 3, 785 (1958).
- M-13. P. G. Klemens, Solid State Physics, Vol. 7, pg. 47, Academic Press, New York, 1958.
- M-14. Webb, Wilkinson, Wilks, Proc. Roy. Soc. (London) A214, 546 (1952).
- M-15. Webb and Wilks, Phil. Mag. 44, 663 (1953).
- M-16. Berman, Foster, Ziman, Proc. Roy. Soc. (London) A231, 130 (1955).
- M-17. P. G. Klemens, Proc. Roy. Soc. (London) A208, 108 (1951).
- M-18. H. B. G. Casimir, Physica 5, 495 (1938).
- M-19. Sproull, Moss, Weinstock, J. Appl. Phys. 30, 334 (1959).
- M-20. J. W. Stout and E. Catalano, J. Chem. Phys. 23, 2013 (1955).
- M-21. Reference e. under Table M-3.
- M-22. Nagamiya, Yosida, Kubo, Advances in Physics 4, 1 (1955).

- M-23. H. P. Rooksby, Acta Cryst. 1, 226 (1948); N. C. Tombs and H. P. Rooksby, Nature 165, 442 (1950).
- M-24. Y. Y. Li, Phys. Rev. 101, 1450 (1956).
- M-25. Reference 1 under Table M-3.
- M-26. L. Passerini, Gazz. chim. ital. 59, 144 (1929).
- M-27. Bacon, Street, Tredgold, Proc. Roy. Soc. (London) A217, 252 (1953).
- M-28. G. Natta and L. Passerini, Gazz. chim. ital. 59, 139 (1929).
- M-29. N. Perkis and A. Serres, J. phys. radium 18, 47 (1957).
- M-30. Goodenough, Wickham, Croft, J. Phys. Chem. Solids 5, 107 (1958).
- M-31. Verwey, Haaijman, Romeijn, Oosterhout, Philips Research Reports 5, 173 (1950).
- M-32. F. J. Morin, Phys. Rev. 93, 1199 (1954).

APPENDIX O - THERMAL CONDUCTIVITY STUDIES WITH THE POWELL METHOD⁽¹⁾

A. I. Dahl

April, 1959

INTRODUCTION

Recent years have seen a substantial increase in the interest in, and the importance of thermal properties of materials. Such information aids in the search for materials to meet the needs of new and special engineering applications. These data also serve the design engineer in the analysis and evaluation of thermodynamic and transport phenomena associated with many processes involving heat generation, dissipation and flow. While there is available in the technical literature a considerable amount of data on the thermal conductivity of most of the common metals, such as copper, iron, aluminum, etc. there is a definite need for data on new and non-standard materials which are playing a prominent role in present day technology. Specifically, there is a need for a simple and rapid means for making thermal conductivity measurements on small test specimens. Such a system or device should be applicable to materials covering a wide range of conductivity values, and to be of most value, it should require a minimum of time for the preparation of the test specimens, and for obtaining and reducing the measurement data.

The technical literature presents many methods for measuring the thermal conductivity of solids. These methods may be classified into two basic categories, namely: 1) static and 2) dynamic. The static or steady-state method consists essentially in measuring the steady-state unidirectional temperature distribution between two parallel or coaxial surfaces of the body in which a temperature gradient is maintained perpendicular to the surfaces. In the dynamic method the temperature is varied suddenly or periodically for one portion of the sample, and the temperature change with time is measured to determine the thermal diffusivity, α , from which with a knowledge of specific heat, c , and the density, ρ , the conductivity is derived from the basic heat flow equation.

Thus it is seen that the determination of the thermal conductivity coefficient for any material involves essentially the measurement of heat flow through a given portion of a sample over a given temperature gradient. The greatest problem is the attainment of a heat flow pattern consistent with the theoretical relationships which form the basis for defining conductivity. Under the steady-state method of determining thermal conductivity, the measurements are made under equilibrium conditions which usually require several hours or even days to attain. Even when an equilibrium state is attained, extraneous heat losses must be either measured experimentally or reduced to insignificance. Reduction of the heat loss is generally accomplished by thermal lagging or by the use of guarding with compensating heaters.

R. W. Powell has described a method of measuring thermal conductivity which differs from any of the conventional methods. The attractiveness of the Powell system rests primarily on two factors:

1. The method is applicable to small samples having a simple geometry, for example, a 1/2" diameter (or 1/2" x 1/2" square) x 1/8" thick disc type specimen. Such a sample would usually be available without special fabrication.

(1) Journal of Scientific Instruments 34, 485 (1957).

2. The actual measurement can be made in the matter of minutes, thus the cost of conducting the test is low. The above factors are particularly significant when a number of materials are to be surveyed and when the materials are difficult or impossible to fabricate into the special shapes and sizes normally required for conventional thermal conductivity test procedures.

THE POWELL COMPARATOR SYSTEM

General Description

The Powell method cannot be uniquely specified as being either a static or a dynamic method of measuring thermal conductivity. As will be shown in the analysis which follows, a pseudo-static condition appears to exist following an initial transient of very short duration. If one touches a number of objects at normal ambient temperature the substance with the highest thermal conductivity will feel the coldest while the one of lowest conductivity will feel the warmest. If the objects are above body temperature, the reverse will be true, that is, the best conductor will feel the warmest, and the poorest thermal conductor will feel the coolest. The rate of heat transfer from the hand to the substance, or the reverse, is primarily a function of the thermal conductivity of the substance. Powell's device for measuring thermal conductivity essentially replaces the human sensation of warmth and cold with physical measuring techniques.

In Powell's apparatus, two similar metal spheres are mounted in a block of balsa wood such that one sphere is recessed just within the surface, while the other projects slightly beyond the surface, see Figure 0-1.

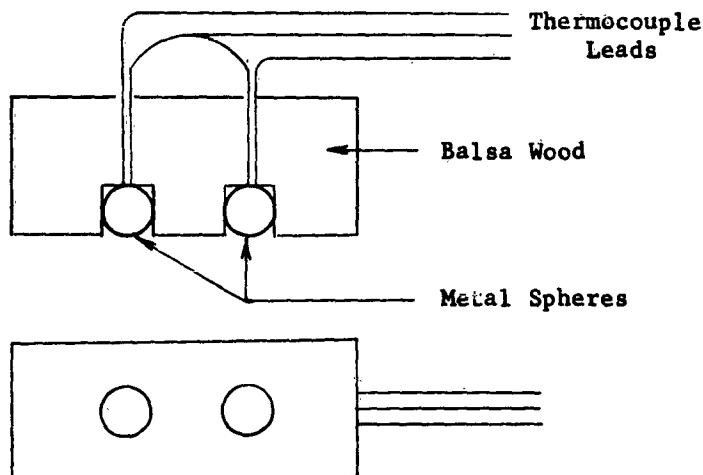


Figure 0-1: Schematic of Mounted Metal Spheres Showing Imbedded Thermocouples.

When the device is placed in contact with the material under test, one of the spheres makes contact while the other does not make physical contact with the material. Thermocouples are mounted within each of the spheres and arranged so as to measure separately or differentially, the temperature of the spheres. Powell observed

that when the assembly, initially at a uniform temperature above that of the material under test, was placed on the sample material, the rate of decrease in temperature of the contacting sphere, as compared to the non-contacting sphere, was a measure of the thermal conductivity of the test material. Thus, after having calibrated the device using materials of known thermal conductivity, it was possible to use it to measure the conductivity of other materials. His calibration data indicated that for materials within a given range of thermal conductivity, there was a linear relation between the rate of temperature change and the square root of the thermal conductivity.

Powell makes the statement that "by keeping the contact area small, it would seem that the variable state becomes of very short duration so that the experiment is conducted under relatively steady thermal conditions, when the thermal resistance governing the rate of heat transfer is primarily a function of the thermal conductivity of the material under test." His experimental data seem to bear this out. However, a sound basis and more positive explanation of the phenomena are needed.

Basic Concepts

A study of the heat transfer phenomena involved in the Powell system has indicated that the behavior does not lend itself to a rigorous theoretical treatment. Certain empirical relations among the various parameters do exist and are observed experimentally, but these cannot be deduced and expressed on the basis of strictly theoretical considerations of the thermal phenomena. Many inter-related factors are involved in the operation of the system. These include:

1. Size of detector sphere
2. Loading on detector sphere
3. Mechanical and thermal properties of the sphere and sample.
 - a. Young's modulus
 - b. Elastic limit
 - c. Poisson's ratio
 - d. Density
 - e. Specific heat
 - f. Surface emissivity
4. Surface Conditions
 - a. Roughness
 - b. Presence of films

As a means of analyzing the basic aspects of the heat flow phenomena involved in the Powell system, recourse was had to the closely analogous phenomena of electrical conduction. Because of the fundamental similarity between the flow of heat within a solid and that of electric charge in a non-inductive circuit, we can treat the problem of heat transfer by means of the electrical analogy. Ohm's law corresponds to Fourier's law. The concept of electrical resistance corresponds to thermal resistance; that of electrical capacity of a circuit component to thermal capacity of a mass. This method enables one to analyze many transient and steady-state heat flow problems which do not yield readily to direct theoretical solutions.

A detailed treatment of the application of the electrical analogy concept to the thermal phenomena in the Powell comparator system is presented in Appendix P of the Thermopile Generator Feasibility Study. The pertinent conclusion of the electrical analog study was that in the operation of the Powell system, the transient heat flow state, occurring at the instant the detector sphere is brought into contact with the test sample, is of such short duration that the heat flow proceeds under essentially steady-state conditions for a period of 10 to 20 seconds. Thus, the cooling rate of the detector sphere during this time interval is a measure of the thermal conductivity of the sample.

EXPERIMENTAL COMPARATOR STUDIES

Preliminary Comparator Models

The initial phase of the experimental work with the Powell system consisted of the fabrication of a number of simple laboratory models and a series of qualitative studies of their performance characteristics. In the first unit, the detector spheres, 3/8" diameter steel balls were mounted in transite block 2" x 1" x 3/4" thick. A number of turns of Nichrome heater element wire was wound about the block to serve in heating the assembly. A No. 30 gage chromel-alumel thermocouple was imbedded in each detector sphere. A sketch of the unit is shown in Figure O-2.

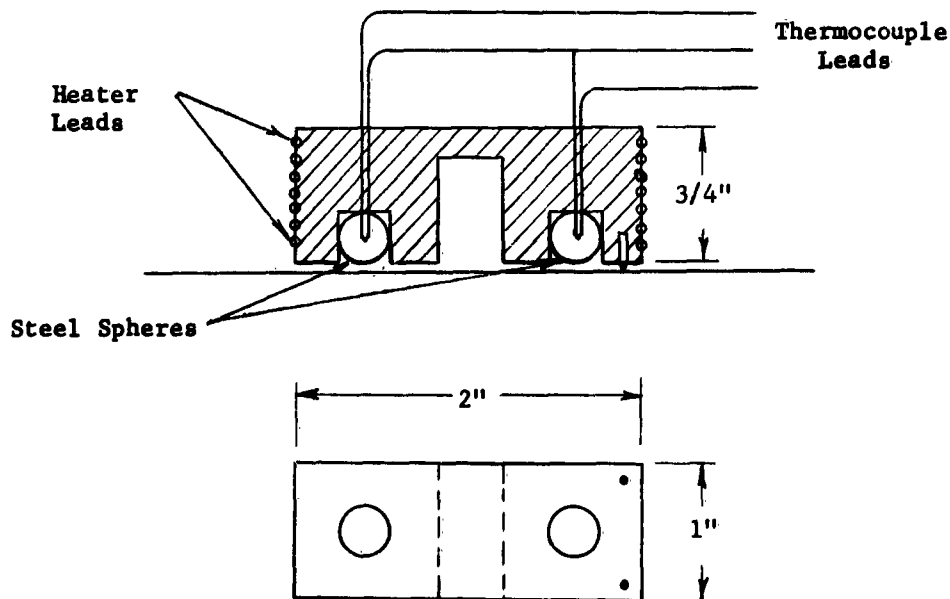


Figure O-2: Schematic of Mounted Metal Spheres Showing Imbedded Thermocouples.

Test samples used with the comparator were 2" x 3/4" x 1/4" thick. In the operation of the unit, the block containing the detector spheres was heated to about 95°C and then manually applied to the test sample at about 25°C. The differential output of the thermocouples imbedded in the spheres was observed with a potentiometer recorder. The change in indication over a 10 second period after contacting the sample was used as the response criterion.

The data obtained with the comparator described above, as well as with a second unit in which 1/4" diameter phosphor bronze spheres were used as detectors, were regarded as qualitative only and served to point out problem areas which would require study and analysis. The principal areas were:

1. Need for accurate control of the load on the contacting sphere.
2. Reduction of the flow of heat between the detector spheres through the supporting block during an observation.
3. General reduction of heat losses from the detector spheres to the surrounding structures.
4. Desirability of operating with smaller temperature differentials between detector spheres and sample.
5. Need for maintaining uniform and reproducible surface finish on sample.
6. Need for avoiding oxide or other foreign films on surface of detector or sample.

OPERATING MODEL OF COMPARATOR

Thermal Comparator Model No. 3

On the basis of the information acquired in the preliminary studies, a thermal comparator apparatus was designed and constructed for further evaluation of the Powell method of measuring thermal conductivity. A sketch of the apparatus, designated as comparator No. 3, is shown in Figure O-3. The detectors are 1/4" diameter spheres mounted in transite blocks. Each of the detector supports is provided with an individually controlled heater. Provision is made for varying the load on the assembly over a range from 5 to 200 grams. To minimize the effects of air currents and extraneous heat losses, a closed end cylinder is placed over the equipment when observations are being made.

Thermal comparator No. 3 was originally provided with phosphor bronze detector spheres. Experimental tests with this unit showed a considerable spread in the observed data. After a detailed analysis of the data and a number of exploratory tests, it was determined that a major cause of the wide variations was the formation of surface films on the phosphor bronze detectors. It was observed that experiments conducted immediately after cleaning the surface of the contacting sphere with crocus paper indicated a considerably greater response than when the sphere had been exposed to the atmosphere for as little as 10 minutes. In fact, successive observations showed an appreciable drift in indication.

Another unexpected effect which was consistently observed with comparator No. 3 using the phosphor bronze spheres, was what appeared to be an upper limit to the heat

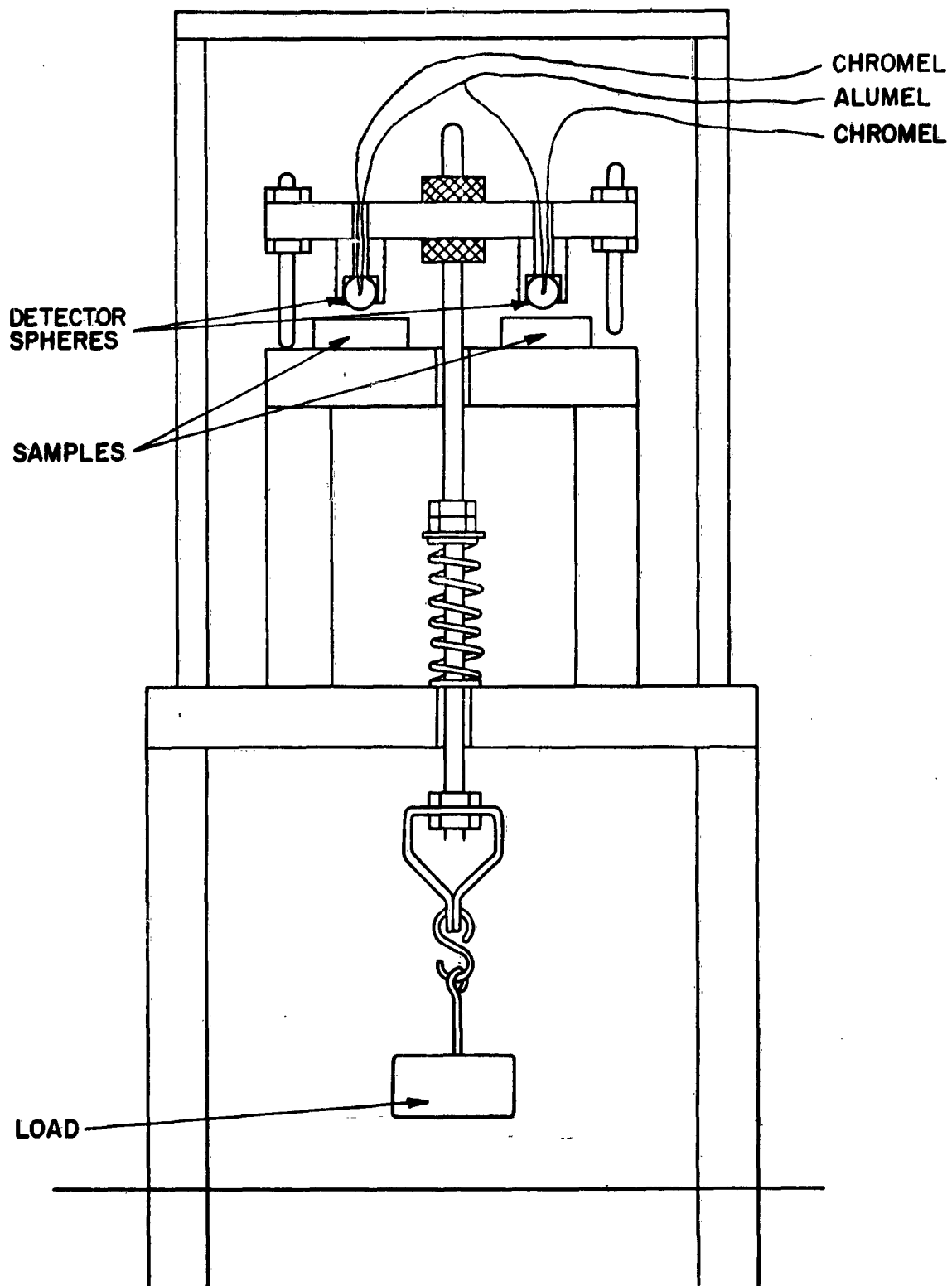


Figure 0-3: Comparator No. 3.

flow rate, as indicated by the comparator response, regardless of the thermal conductivity of the test sample. This upper limit appeared to be reached with zinc as the test specimen, and specimens with a higher thermal conductivity, such as aluminum and copper, indicated approximately the same heat flow rate as the zinc sample. It was first thought that the response of the instrumentation used in reading the comparator signal might be limiting the observed signal. However, the substitution of a recorder having a much higher rate of response demonstrated that the limiting value of the signal was inherent in the comparator itself.

An analysis of the conductance of heat through a small contact area, such as in the case of a sphere in contact with a flat slab, shows that the overall conductance will be determined predominantly by the material having the lowest conductance. For example, if a sphere of good conducting material is placed in contact with a slab of poorer conducting material, the heat flow through the contact area will be determined primarily by the conductivity of the slab whereas if the conditions are reversed, the sphere will predominate in determining the heat flow rate. Thus, if we apply this analysis to the Powell thermal comparator, the detector sphere should be of a higher thermal conductivity than any of the materials to be tested. It is believed that the limiting value of response observed when comparator No. 3 was used with zinc, aluminum and copper results from this situation.

Thermal Comparator Model No. 3A

The phosphor bronze detector spheres of comparator No. 3 were replaced by silver spheres. This modified version, designated as Model No. 3A, should be expected to yield a number of specific advantages over the original design.

Silver has a higher value of thermal conductivity and the comparator should therefore be applicable to materials over a higher range of conductivities.

The silver spheres should be less subject to the formation of surface films than phosphor bronze.

The surface emissivity of silver is lower than that of phosphor bronze; this reduces the radiation heat losses from the exposed surfaces of the spheres.

When a sphere is brought into contact with a flat plate, the area of contact between the two objects may be expressed by the formula:

$$a = 0.721 \sqrt[3]{PD \frac{1 - \nu_1^2}{E_1} + \frac{1 - \nu_2^2}{E_2}} \quad (0-1)*$$

where a = radius of contact, inches
P = load in pounds
D = diameter of sphere, inches
 ν = Poisson's ratio
E = Young's modulus

Subscripts 1 and 2 refer to sphere and plate respectively.

* R. J. Roark, Formulas for Stress & Strain, McGraw Hill, 1943, P. 275.

Formula (O-1) applies for the case of elastic stresses only. If the elastic limit of either of the materials is exceeded, equation (O-1) is no longer available.

A series of tests were conducted to determine the effect of loading on the response of thermal comparator No. 3A. The test specimens included three steels, zinc and aluminum in the form of discs 3/4" in diameter and 1/4" thick. The surface of each specimen was lapped to a uniform condition. The loading on the assembly was varied from 20 to 200 grams. It should be pointed out that the loading values do not represent the actual load on the contacting sphere since the sphere is one of three points of support, and in addition, the force required to overcome the spring resistance is also included in the loading values. The test data are summarized in Figure O-4. It will be noted from the graphs in Figure O-4 that with the exception of the zinc specimen, the response of the comparator becomes relatively insensitive to loading in the range 150 to 200 grams. The cause for the behavior of the zinc sample is not apparent.

Thermal comparator No. 3A was used to intercompare the thermal conductivity of eight metallic materials covering a range in conductivity of 0.15 to 2.4 watts/cm°C. The specimens were prepared in disc or rectangular form, 1/4" thick. Surfaces were lapped and cleaned prior to test. A loading of 200 grams was used throughout the tests. The observed data are summarized in Table O-1 and shown graphically in Figure O-5.

TABLE O-1
DATA OBTAINED WITH THERMAL COMPARATOR NO. 3A

Loading 200 grams, Sample Temperature 28°C, T = 12°C

	Conductivity watts/cm °C	Deflection μv/10 sec.
B11G25H (CuCoBe alloy)	2.36*	217.
Aluminum	2.2	190.
Zinc	1.13	172.
B4A2C (cold rolled steel)	0.61	133.
B50A8D (steel)	0.46*	110.
416SS	0.25	86.
304SS	0.16	60.
ML1700 (special steel alloy)	0.15*	48.
Quartz		22.

* The asterisk refers to measured values of thermal conductivity. All others are "book values" from the technical literature.

The solid line in Figure O-5 represents the calibration of the comparator established on the basis of the three materials of known conductivity. The dashed lines indicate a deviation $\pm 10\%$ from the calibration line.

The data in Figure O-5 indicate reasonably consistent results for all but the aluminum specimen. However, this may be fortuitous since the "book values" of thermal conductivity available in the technical literature show a considerable spread.

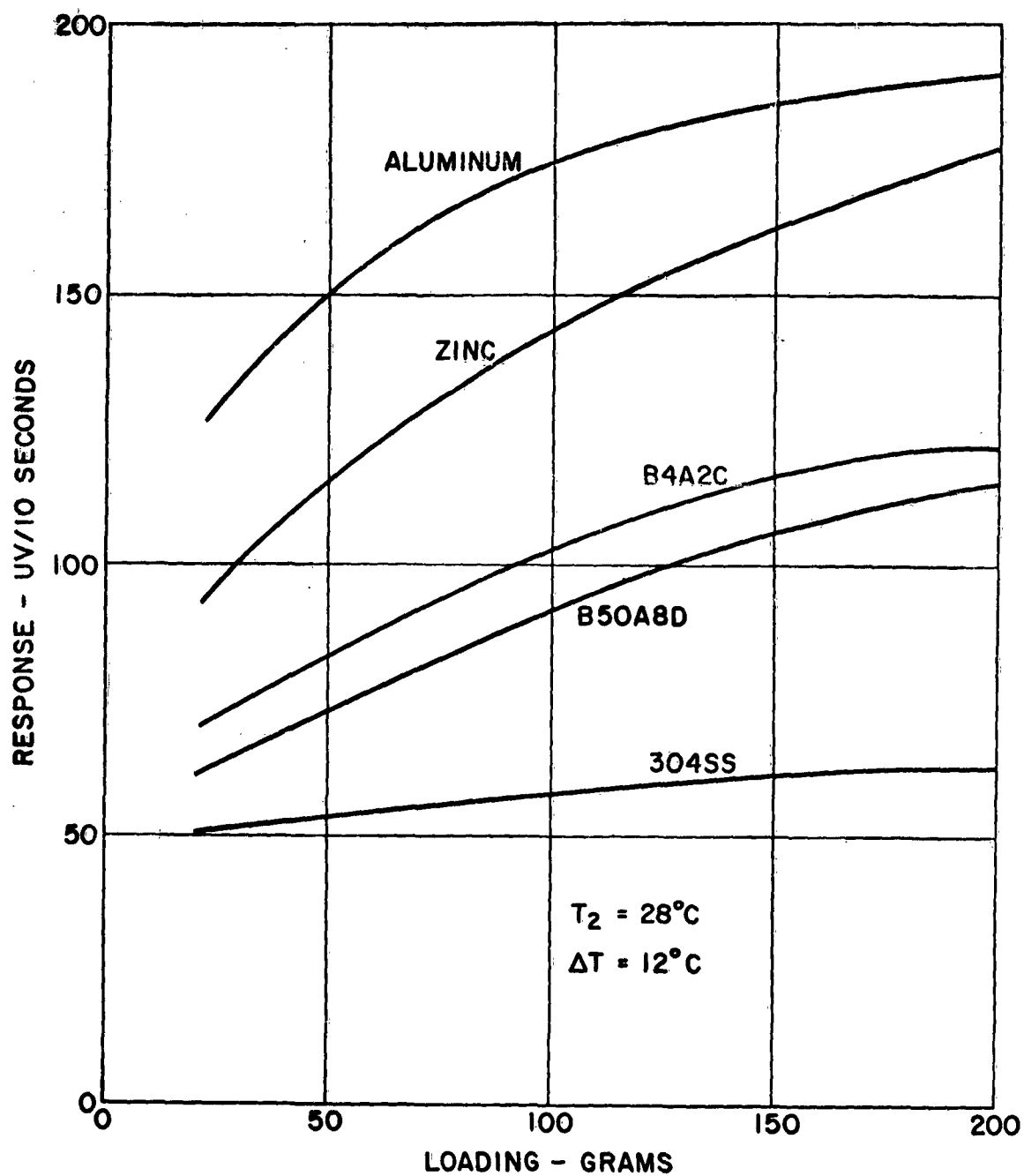


Figure O-4: Comparator No. 3A, Loading vs Response.

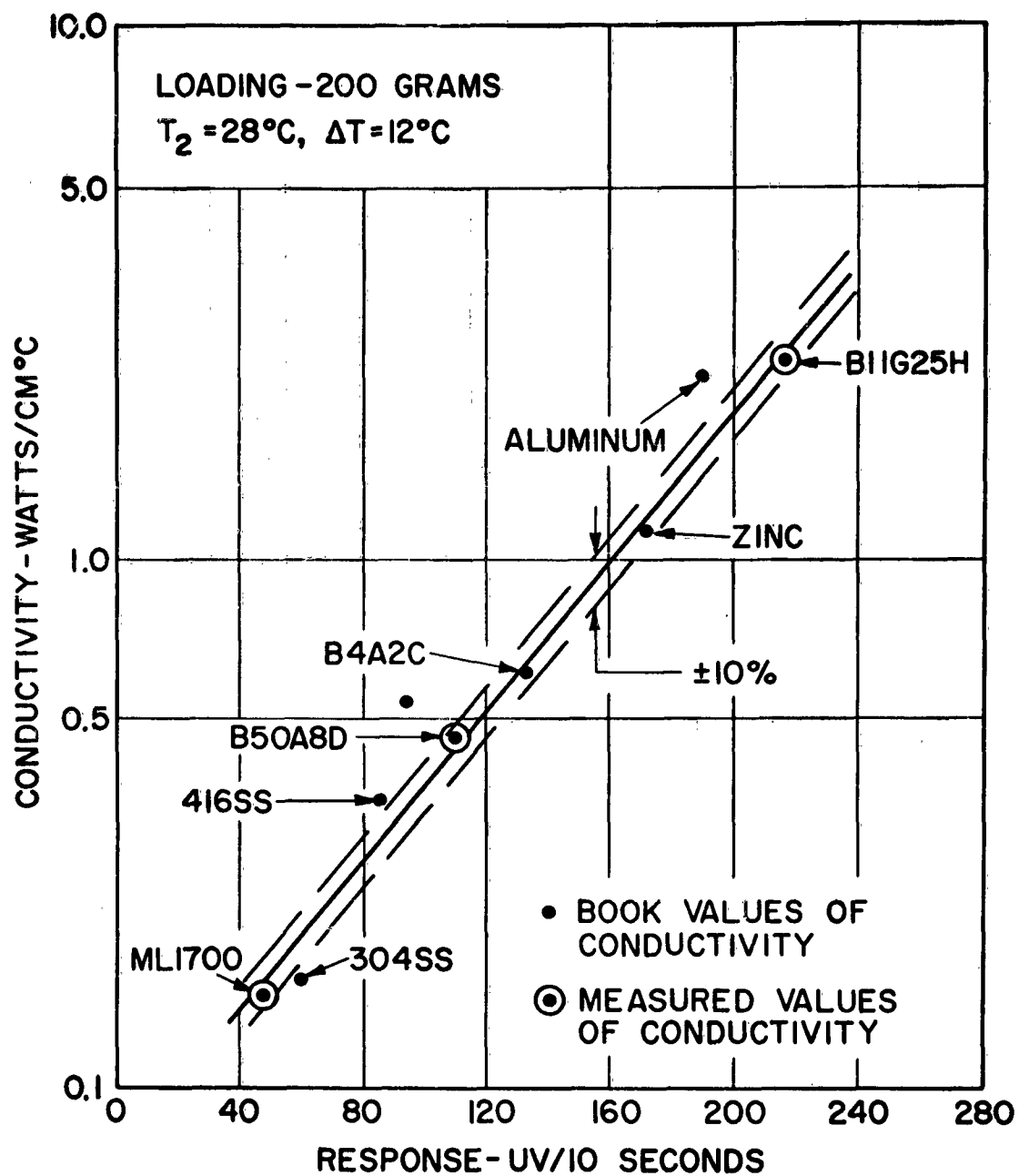


Figure O-5: Comparator No. 3A, Response vs Conductivity.

Furthermore, the accuracy of the measured values of thermal conductivity on which the calibration curve is based, is estimated to be between 5 and 10%.

It would appear, however, that for these metallic materials having thermal conductivities in the range of 0.16 to 2.4 watts/cm°C, the comparator is capable of giving reasonably consistent test data. The need for additional materials with known values of thermal conductivity to serve as standards is evident.

The experimental studies with the Powell system up to this point have been concerned with metals having thermal conductivities in the range of 0.15 to 2.4 watts/cm°C. One of the primary areas of interest in the thermoelectric generator program is in materials of low thermal conductivity, namely 0.01 to 0.15 watts/cm°C. These materials are largely in the category of semi-conductors or insulators. The physical properties of these materials generally differ considerably from those of the metals class. Furthermore, several of the materials included in this study were available only in small irregular shaped samples. These factors necessitated some modifications in the techniques of applying the Powell method.

The arrangement for applying the load on the contacting sphere was changed so as to provide a means of obtaining a value of the force which the sphere exerted on the test sample. This was accomplished by applying the load along the vertical axis through the center of the sphere and correcting for the load required to cause the sphere to just make contact with the test specimen. By this means the actual net load on the sample could be obtained. The comparator with this modification was designated as No. 3B.

In the case of a number of the materials, only a single small irregular shaped piece was available for the conductivity studies. In those instances the surface on which the detector sphere was to make contact was ground flat and lapped to the final finish. An alternate material having as nearly as possible the same surface radiating characteristics as the test specimen was placed below the non-contacting silver sphere.

The initial test with the low-conductivity materials was to study the effect of load on the response of the comparator for each of the test materials. These data are summarized in Figure O-6. Since the thickness of the individual samples varied in thickness from about 0.08" to about 0.25", the load on the detector sphere which was required to cause the sphere to just make contact with the sample was subtracted from the total load on the sphere to obtain the true loading on the test specimen. The data in Figure O-6 indicate a relatively low sensitivity of comparator response to loading of 5 to 15 grams. A net loading of 12 grams was selected as being appropriate for this class of materials.

A cross plot of the data in Figure O-6 for a net loading of 12 grams is shown in Figure O-7. It is unfortunate that additional data on the thermal conductivity of these materials is not available so as to obtain a measure of the effectiveness of the comparator system for this class of materials.

Thermal Comparator Model No. 4

The information and experience gained in the study of the Powell comparator system as presented above led to the design and construction of a unit embodying those features which would make for a practical thermal conductivity device capable of oper-

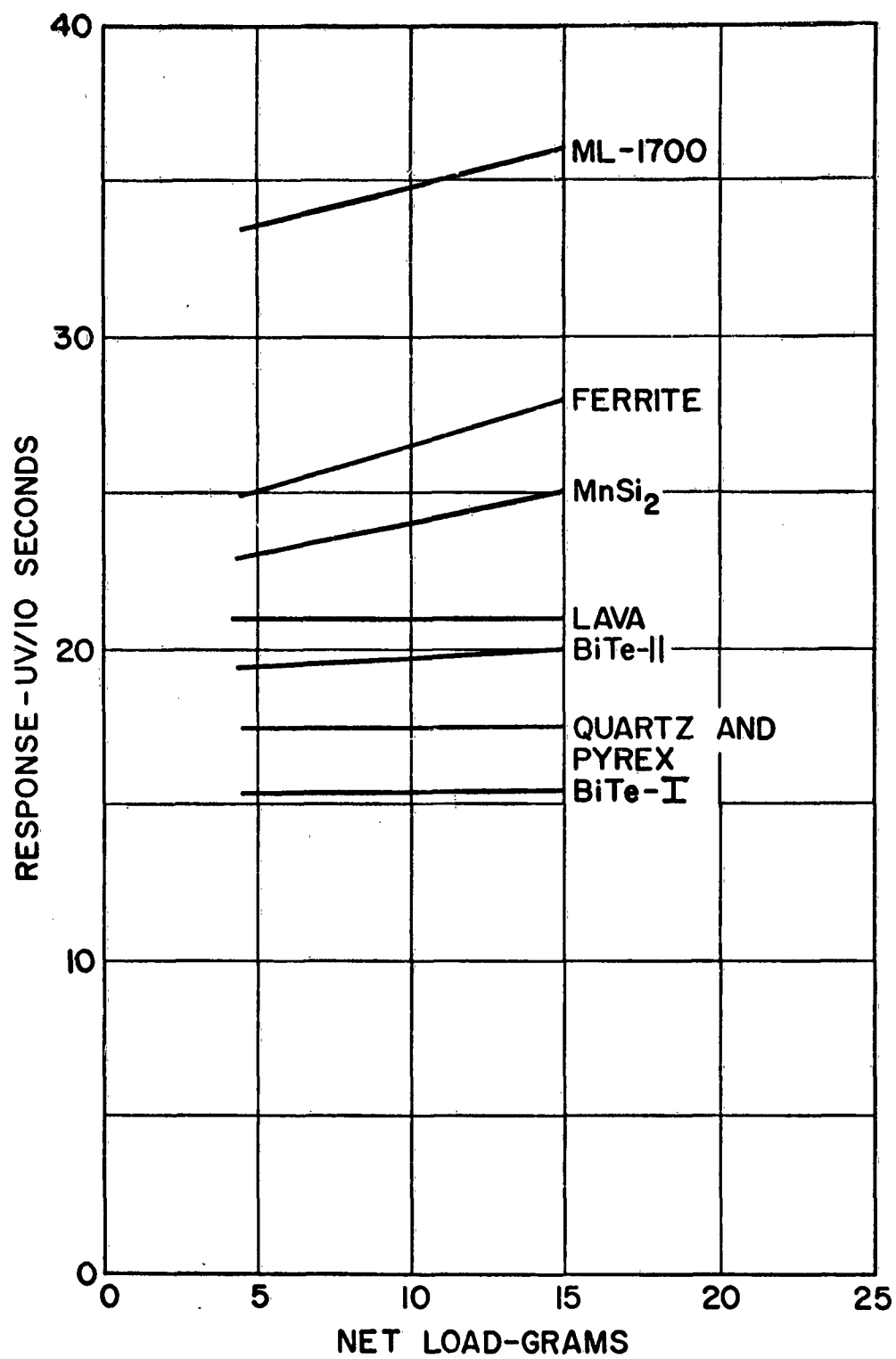


Figure O-6: Comparator No. 3B, Loading vs Response.

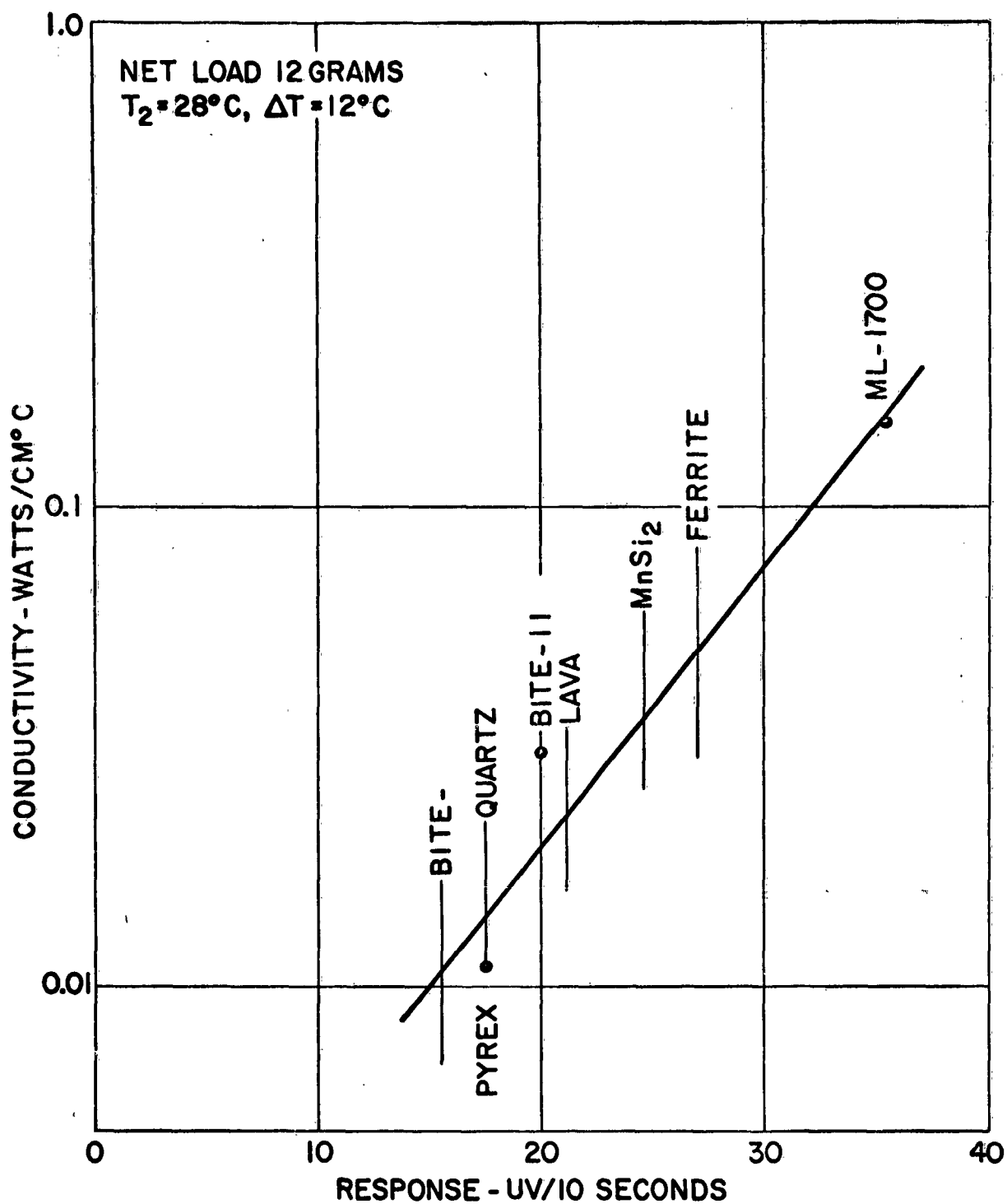


Figure O-7 : Comparator No. 3B, Response vs Conductivity.

ation at temperatures up to about 500°C. A photograph of the unit, designated as Comparator No. 4, is shown in Figure O-8.

The detector spheres, 1/4" diameter silver balls, are mounted in lava supports. No. 30 gage chromel alumel thermocouples are located at the center of each sphere. An electric heater element is wound on each support and imbedded in alundum cement. The normal position of each of the detector spheres relative to the test specimen is adjusted by means of a counter weight and adjusting screw. The test specimens, either 1/4" x 1/4" square or 1/4" round sections of 1/8" to 1/4" in thickness, are mounted on individual pedestals. Provision is made to heat the test samples within the supporting pedestals by means of individual heaters surrounding the pedestals. The load on the contacting sphere is located directly above the sphere and can be applied remotely by means of an air operated bellows. All components of the comparator are capable of withstanding temperatures of 500°C.

Because of a time and cost limitation on the thermal conductivity program, only a limited amount of experimental testing was possible with thermal comparator No. 4. All tests were conducted with the samples at ambient temperature, namely 28°C and with the detector spheres at 40°C. An initial test to determine the effect of loading on the comparator response was conducted on five materials covering a wide range of conductivity. The results are shown in Figure O-9. The response versus loading shows an approximately linear change with loads in the range 50 to 200 grams. This is in contrast to the observations on comparator No. 3A where the response tended to level off for the higher loads. On the basis of these data, a load of 200 grams was selected for all subsequent tests.

Response tests with comparator No. 4 were conducted with nine materials. These data are summarized in Table O-2 and shown graphically in Figure O-10. Unfortunately measured values of conductivity are available for only four of the materials. For the remaining materials, quoted values found in the literature are shown. Such values are not necessarily applicable for the samples used in the tests.

TABLE O-2
CALIBRATION RESPONSE - COMPARATOR NO. 4

<u>Material</u>	<u>k</u> <u>watts/cm°C</u>	<u>Deflection</u> <u>μv/10 sec.</u>
B11G25H (CuCoBe Alloy)	2.36*	90
B4A2C (CR Steel)	0.61	69
B50A8D (Steel)	0.46*	58
304SS	0.16	29
ML-1700 (Special Steel Alloy)	0.15*	39
MnSi ₂		20
PbTe	0.031	14
Fused Quartz	0.012	12
Pyrex	0.011*	11

* Measured values of conductivity

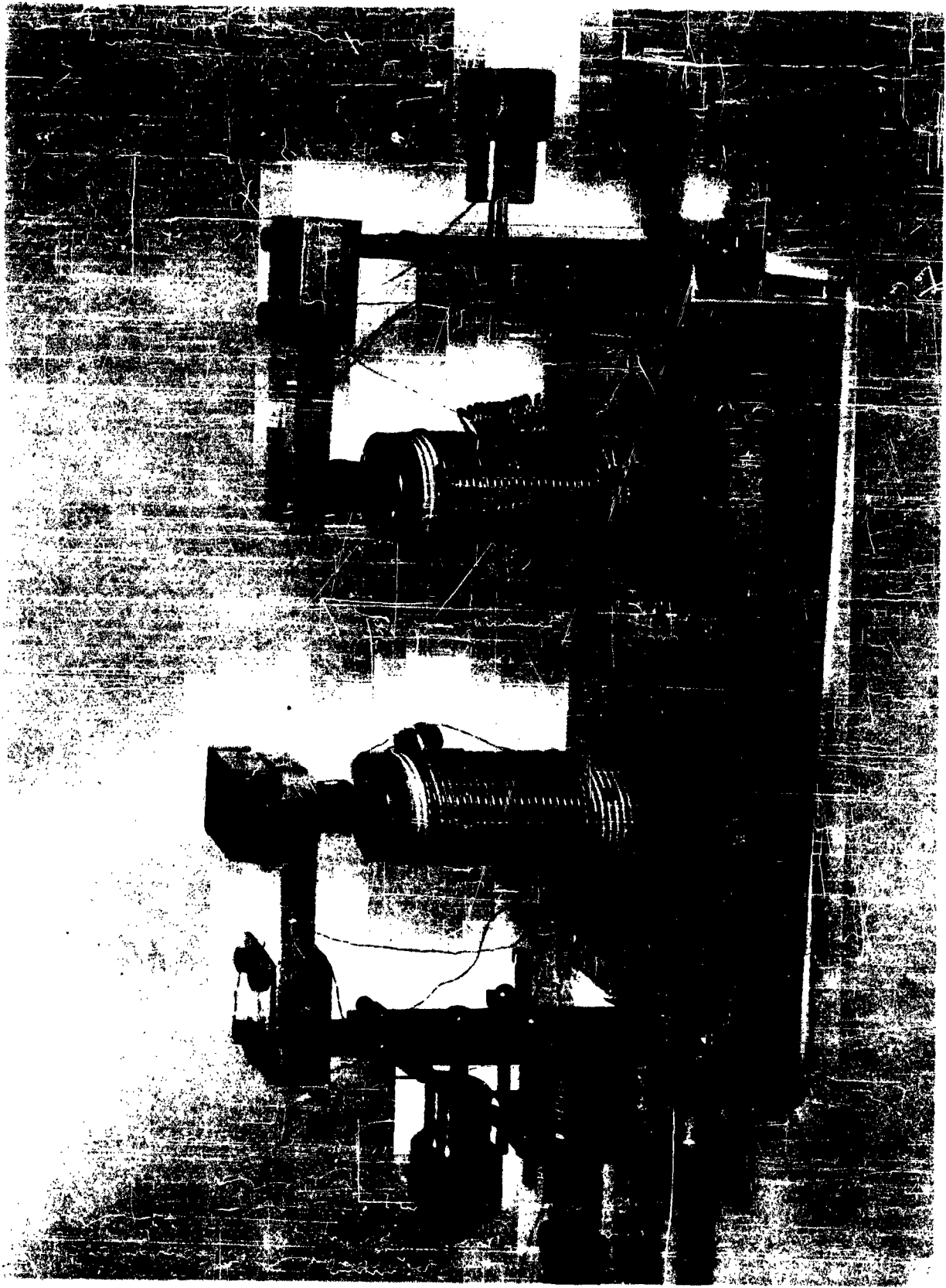


Figure 0-8: Photograph of Comparator No. 4.

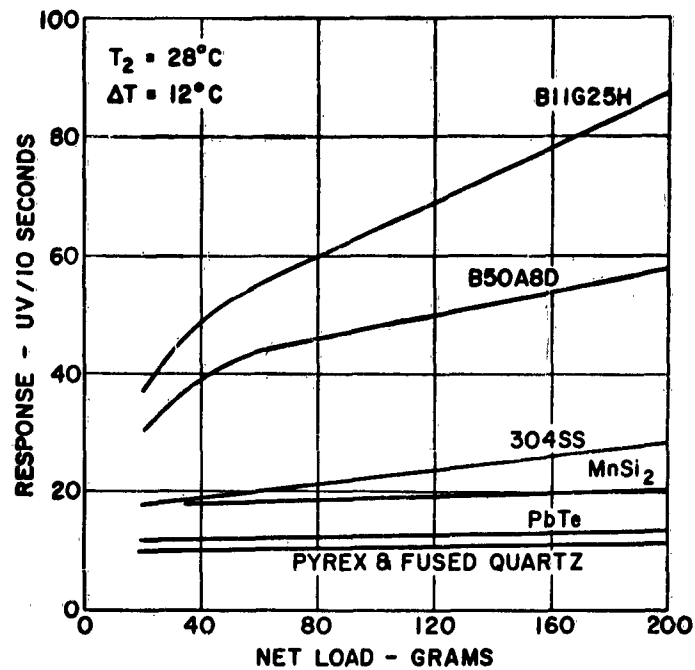


Figure 0-9: Comparator No. 4, Loading vs Response

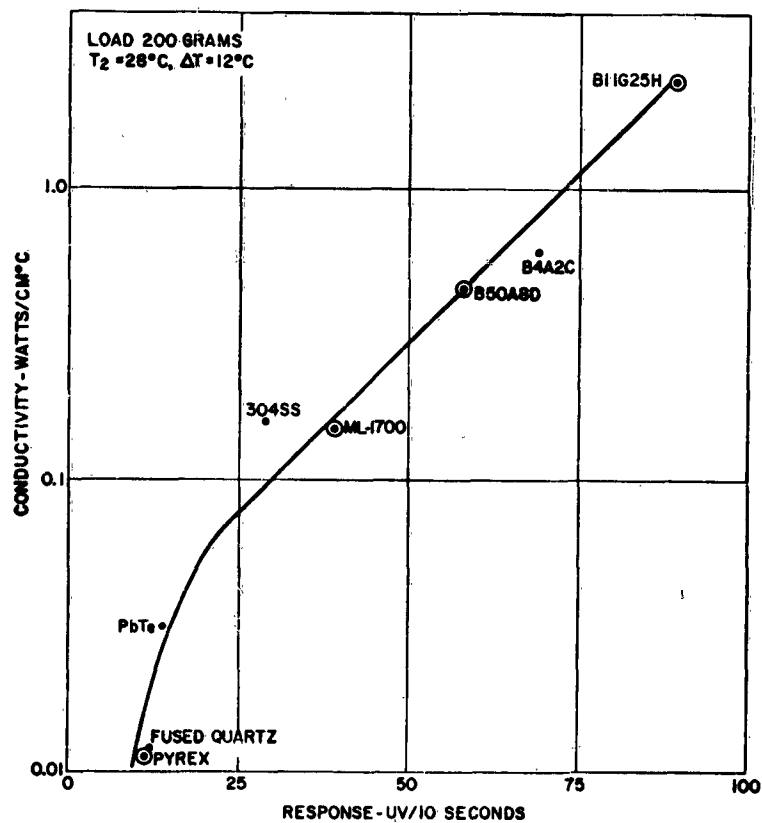


Figure 0-10: Comparator No. 4, Response vs Conductivity.

APPLICATION OF POWELL SYSTEM AT HIGHER TEMPERATURES

Most materials exhibit a significant variation of thermal conductivity with temperature. For this reason it is important to be able to make conductivity measurements over a range of temperatures. This is particularly true for the newer thermoelectric materials which are being developed under the Thermopile Generator Study program. The problems associated with making thermal conductivity measurements increase in complexity and difficulty as the temperatures are increased.

In the operation of the Powell system, the basic assumption is that the heat transfer from the detector spheres to the surroundings by processes other than conduction through the contact area is the same for the two spheres, thus making the response solely a function of the conduction heat flow through the contacting area. If this balance of heat exchange between the individual spheres and their surroundings is upset, the difference will be included in the response signal and interpreted as heat flow through the contact area. Thus, it is essential that the balance conditions be maintained for all operating temperatures.

Radiation Effects

Because of the Stefan-Boltzmann fourth power radiation law, radiation plays a much greater part in the heat transfer between objects at high temperatures than at ambient temperatures. Thus, while it may be permissible to neglect the radiation exchange between the detector spheres and the samples in the operation of the Powell comparator under ambient temperature conditions, this may not be the case for tests at higher temperatures. To obtain a better appreciation of the magnitude of the radiation effect let us calculate the rate of heat exchange between the detector sphere and the test sample for a range of temperatures and compare this radiation heat transfer with the heat flow from the detector sphere to the sample through the contact area.

From the experimental data obtained with Comparator No. 3A as listed in Table O-1 for the condition of a 12°C differential between sample and detectors, we can obtain the conduction heat transfer, q_c , from the contacting sphere to the sample. This can be computed using the equation:

$$q_c = \rho v c \frac{\Delta T}{\Delta t} \quad (O-2)$$

where ρ , v and c are the density, volume and specific heat, respectively, of the contacting sphere and $\frac{\Delta T}{\Delta t}$ is the rate of temperature change, °C/sec.

For comparator No. 3A with 1/4" diameter silver detector spheres,

$$\begin{aligned} \rho &= 10.5 \text{ g/cm}^3 \\ v &= 0.134 \text{ cm}^3 \\ c &= 0.056 \text{ cal/g.}^\circ\text{C} \end{aligned}$$

Converting μv deflection (in Table O-1) to temperature, °C, $1^\circ\text{C} = 41 \mu\text{v}$.

Selecting four materials listed in Table O-1, we can calculate q_c through the contact area.

TABLE 0-3
CALCULATION DATA

<u>Material</u>	<u>Deflection</u> <u>μv/10 sec.</u>	<u>T/Δt</u> <u>°C/sec.</u>	<u>cal/sec.</u> \dot{q}_c	<u>watts</u>
Aluminum	190	4.6	.0362	.151
B50A8D	110	2.7	.0213	.089
304SS	60	1.5	.0118	.049
Quartz	22	0.5	.0039	.016

For the present purpose we shall assume that \dot{q}_c does not vary with temperature. This is not strictly true but may be considered so in comparison to radiation heat transfer.

For the case of heat transfer from the sphere to the sample by radiation, \dot{q}_r , let us make the simplifying assumption that the radiation from the exposed hemispherical surface of the sphere is equivalent to that from the surface of a disc of the same diameter as the sphere. Thus the radiation heat exchange will be that between two flat surfaces, 1/4" in diameter. This may be expressed by the Stefan-Boltzmann equation:

$$\dot{Q}_r = \sigma A (T_1^4 - T_2^4) \quad (0-3)$$

where $\sigma = 5.67 \times 10^{-12} \frac{\text{watts}}{\text{cm}^2 \text{ } ^\circ\text{K}}$

$A = 0.317 \text{ cm}^2$

T_1 and T_2 are the temperatures, K, of sphere and sample, respectively

For our case $T_1 - T_2 = 12^\circ\text{K}$. Substituting in equation (0-3):

<u>T₁</u> <u>°K</u>	<u>T₂</u> <u>°K</u>	<u>\dot{q}_r</u> <u>watts</u>
300	288	0.0022
400	388	0.0052
600	588	.0181
800	788	.0431
1000	988	.0846
1200	1188	.1467
1400	1388	.233

The variation of the radiation heat transfer rate, \dot{q}_r , with temperature is shown graphically in Figure 0-11. Shown on the same graph is the conduction heat transfer rate, \dot{q}_c , through the contact area for aluminum, B50A8D (steel), 304SS and quartz.

In the application of the Powell comparator system, the purpose of the non-contacting sphere is to enable the heat losses from the contacting sphere, except that conducted to the sample through the contact area, to be balanced out, so that the comparator response will indicate only that conducted to the sample. At low temperatures when the extraneous heat losses from the spheres are low in comparison to that conducted

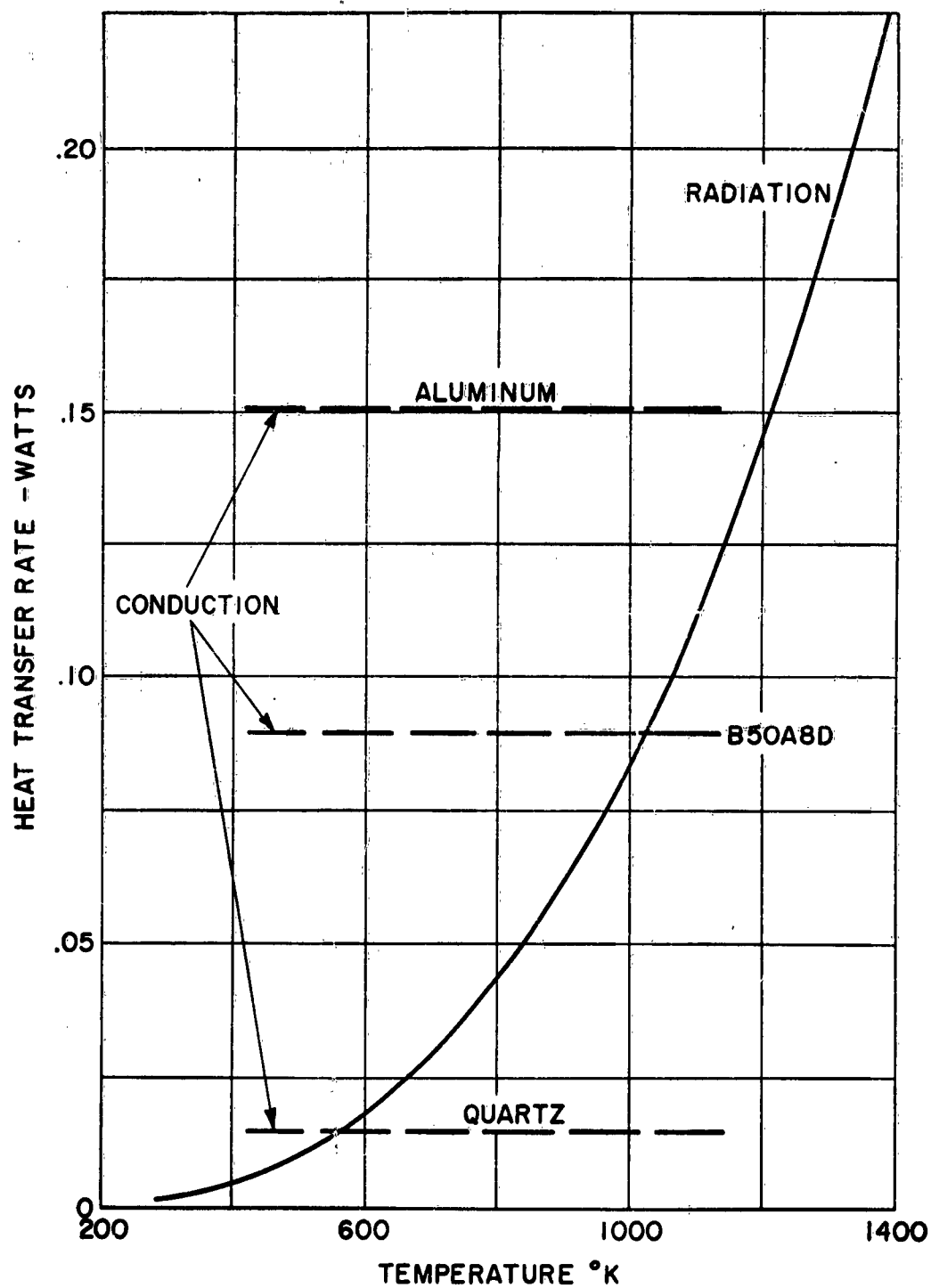


Figure O-11: Comparison of Conduction and Radiation Heat Transfer Rates, Contacting Sphere to Test Sample.

through the contact, the balancing can readily be accomplished. However, at the higher temperatures, where the radiation losses increase while the conduction through the contact remains approximately constant for any given material, the balancing of the heat losses from the two spheres becomes more difficult and must be made to an increasing degree of precision. Let us assume that we are able to accomplish the radiation balance to within 5% of the total radiation heat exchange.

From the curve, Figure O-11, we obtain the radiation heat transfer rate for selected temperatures:

TABLE O-4
RADIATION DATA

Sample Temperature		Radiation Heat Transfer Rate	5% of Radiation Heat Transfer Rate
°C	°K	Watts	Watts
50	323	0.002	0.0001
300	573	.015	.0007
600	873	.057	.0028
1000	1273	.175	.0088

From the values in the last columns of Tables O-3 and O-4 we obtain the following data:

TABLE O-5
COMPILED VALUES

Sample Temperature °C	$.05\dot{q}_r/\dot{q}_c$			
	Aluminum	B50A8D	304SS	Quartz
50	.001	.001	.001	.006
300	.001	.01	.014	.044
600	.019	.028	.057	.175
1000	.058	.099	.18	.55

From the data in Table O-5 the percentage error due to a 5% out-of-balance in radiation is indicated. It is apparent that the low conductivity samples would require better than a 95% radiation balance if satisfactory measurements with the Powell method are to be made.

It should be pointed out that in the radiation calculations above a surface emissivity of unity has been used whereas the value for silver is of the order of 5%. However, due to geometry considerations, the effective emissivity of the radiating spheres would be considerably higher. It is believed that the values in Table O-5 are on the conservative side.

Sample Protection

In the application of the Powell system the surface condition of the test samples is an important consideration. The presence of an oxide film or other foreign matter on the surface of the sample will seriously affect the comparator response. The same holds true for the detector spheres.

For observations under ambient temperature conditions, the surface condition of most materials would be expected to be sufficiently stable to allow measurements to be made within a reasonable time period without surface alterations. However, for higher temperature studies, particularly above about 200°C, most base metals will develop an oxide coating when exposed to air for minutes. To prevent this from occurring, it is suggested that the Powell comparator be operated in vacuum. This can be done with a bell jar placed over the apparatus. For some materials a high vacuum would be required to prevent surface oxidation.

Another advantage of operating the comparator in a vacuum would be the elimination of convection currents which should improve the temperature stability throughout the apparatus.

DISCUSSION OF RESULTS

The study of the Powell method for measuring thermal conductivity of solids has evoked considerable thought and discussion on the basic heat transport phenomena involved. The attractiveness of the method from its applicability to small test samples and the time required to conduct a test have stimulated efforts toward finding a sound basis for its acceptance and a full realization of its capabilities. Although it has not been possible to carry out a rigorous theoretical analysis of the heat transfer phenomena involved, the results of the electrical analog study indicate that a condition of steady state heat flow exists in the contact area between the detector sphere and the sample. This leads to the conclusion that the response of the comparator is a measure of the conductivity of the sample and not the diffusivity. The analysis also shows that the contact area must be small, of the order of a few mils, if this condition is to prevail.

The results of the tests with metals having conductivities in the range of 0.15 to 2.4 watts/cm°C, as presented in Figure O-5, indicate a promising degree of success of this method, at least for the ambient temperature conditions. The analysis of the effects of radiation heat transfer between the detector spheres and the sample for metals in this conductivity range indicate that for materials with conductivities higher than about 0.5 watts/cm°C the Powell method should be applicable to at least 600°C. For temperatures above 600°C and for material of lower conductivity, a better than a 95% control of the radiation balance would be required. This may be feasible by closer attention to the emissivity factor and temperature measurement and control factors.

The materials of major interest to the Thermopile Generator Study program fall in the conductivity range 0.01 to 0.15 watts/cm°C. The experimental tests with materials in this class have been seriously limited by the lack of reference standards of known conductivity. A sample of pyrex with a measured value of $k = 0.011$ watts/cm°C was obtained from the National Bureau of Standards. This was the only suitable reference standard available. However, the comparators used with the low conductivity materials indicated adequate response signals, and it is believed that with proper reference standards the Powell system would yield satisfactory conductivity data. The effects of radiation are more severe with the low conductivity materials as in Table O-5. However, operation at temperatures up to 300°C are believed possible.

For conductivity measurements with the Powell system above 100°C it is believed that enclosing the comparator in a vacuum would be required to prevent extraneous surface films. Even ambient temperature operation would be improved by a vacuum enclosure.

As a final conclusion of the study of the Powell system, we believe that the method offers a practical means of obtaining relative thermal conductivity data on a wide range of materials. With the availability of reference standards over the range of conductivities covered, absolute values of conductivity could be determined. For materials with conductivities above 0.5 watts/cm°C, measurements at temperatures up to 600°C are believed possible. For the insulator type materials with conductivities in the range 0.01 to 0.10, operation may be feasible up to about 300°C.

APPENDIX P - THE POWELL METHOD OF MEASURING THE THERMAL CONDUCTIVITY OF SOLIDS

A. I. Dahl

February, 1959

ABSTRACT

Powell's method* for determining the thermal conductivity of solids is analyzed from the viewpoint of the basic heat transfer concepts involved. Since the method does not appear to lend itself to a rigorous theoretical analysis of the thermal phenomena involved, it has been attacked by a consideration of an equivalent electrical analog. This approach rests on the fundamental similarity between the flow of heat within a rigid body and that of charge in a non-inductive electric circuit.

The analysis indicates a justification for the contention that in the application of Powell's thermal comparator method, the thermal resistance governing the rate of heat transfer is very predominately a function of the thermal conductivity of the material under test. This establishes the validity of regarding the comparator indications as true measurements of thermal conductivity.

INTRODUCTION

The need for a simple, inexpensive method of measuring the thermal conductivity of solids has long been recognized. To be generally useful such a method should be applicable to samples of such a size and shape as would be readily available without special fabrication. Powell's method is an approach toward meeting the above criteria.

If one touches a number of objects at normal ambient temperature, the substance with the highest thermal conductivity will feel the coldest while the one of the lowest thermal conductivity will feel the warmest. If the objects are above body temperature, the reverse will be true, that is, the best conductor will feel the warmest and the poorest thermal conductor will feel the coolest. The rate of heat transfer from the hand to the substance, or the reverse, is primarily a function of the thermal conductivity of the substance. Powell's device for measuring thermal conductivity essentially replaces the human sensation of warmth and cold with physical measuring techniques.

In Powell's apparatus, two similar metal spheres are mounted in a block of balsa wood such that one sphere is recessed just within the surface while the other projects slightly beyond the surface, see Figure P-1.

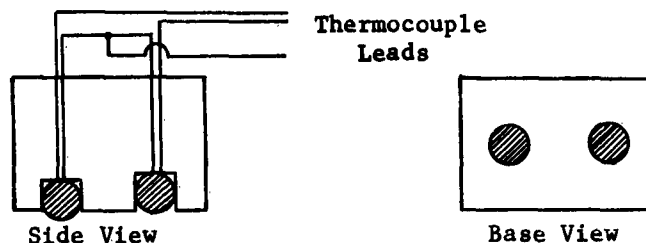


Figure P-1: Schematic of Mounted Metal Spheres.

* R.W. Powell, Journal of Scientific Instruments, V. 34, p. 485, Dec. 1957

When the device is placed in contact with the material under test, one of the spheres makes contact while the other does not make physical contact with the material. Thermocouples are mounted within each of the spheres and arranged so as to measure separately or differentially, the temperature of the spheres. Powell observed that when the assembly, initially at a uniform temperature above that of the material under test, was placed on the sample material, the rate of decrease in temperature of the contacting sphere, as compared to the non-contacting sphere, was a measure of the thermal conductivity of the test material. Thus, after having calibrated the device using materials of known thermal conductivity, it was possible to use it to measure the conductivity of other materials. His calibration data indicated that for materials within a given range of thermal conductivity, there was a linear relation between the rate of temperature change and the square root of the thermal conductivity.

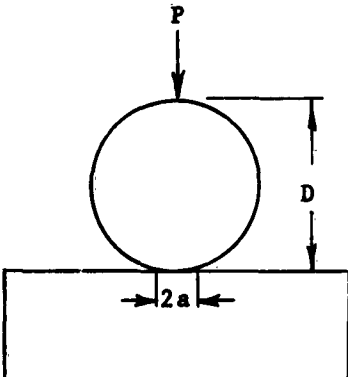
Powell makes the statement that "by keeping the contact area small, it would seem that the variable state becomes of very short duration so that the experiment is conducted under relatively steady thermal conditions, when the thermal resistance governing the rate of heat transfer is primarily a function of the thermal conductivity of the material under test." His experimental data seem to bear this out. However, a firmer basis and explanation of the phenomena are needed.

ELECTRICAL ANALOGY STUDIES

A study of the heat transfer concepts involved in the Powell device has indicated that the behavior does not lend itself to a rigorous theoretical treatment. Certain empirical relations do exist as is evident from the experimental results, but these cannot be deduced from strictly theoretical considerations of thermal phenomena. As a means of investigating the basic physical aspects of the problem, recourse was had to the closely analogous problem of electrical conduction on which some basic theoretical information may be obtained by the consideration of electrical contacts. Credit is due D. W. Jones, G.E.L., for this phase of the work.

Contact Area

When a sphere is brought in contact with a flat slab, the radius, a , of the contact area which is formed (providing the elastic limit of the materials is not exceeded) is given by the expression:



$$a = 0.721 \sqrt[3]{PD \frac{1 - \nu_1^2}{E_1} + \frac{1 - \nu_2^2}{E_2}} \quad (P-1)$$

where P = total load, pounds

D = Diameter of sphere, inches

ν = Poisson's ratio

E = Modulus of elasticity psi

Subscripts 1 and 2 refer to sphere and slab.

The contact area is, thus, a function of the load, sphere diameter, and of the sphere and slab material properties.

It may be of interest to note the variations in those mechanical properties of materials which would influence the contact area.

TABLE P-1
MECHANICAL PROPERTIES

<u>Material</u>	<u>Young's Modulus</u> <u>psi x 10⁻⁶</u>	<u>Poisson's</u> <u>Ratio</u>
Aluminum	10	0.33
Copper	16	.33
Nickel	30	.28
Tin	4	.33
Silver	11	.37
Zinc	12	.3 *
Tungsten	51	.17
304SS	29	.3 *
Phosphor Bronze	16	.35
Brass	15	.3 *
Silica Glass	10	

*Estimated Values

Calculations have been made of the contact radius, a , with 1/4" diameter phosphor bronze and silver spheres on various materials:

TABLE P-2
CONTACT DIMENSIONS

Phosphor Bronze Sphere, 1/4" diameter

<u>Plate</u> <u>Material</u>	<u>Contact Radius, a - inches</u>			<u>a/a</u> <u>Stainless</u> <u>Steel</u>
	<u>P = 10g</u>	<u>P = 50g</u>	<u>P = 100g</u>	
Aluminum	0.00067	0.00114	0.00144	1.22
Copper	.00061	0.00105	0.00132	1.12
304SS	.00055	0.00094	0.00118	1.00
Zinc	.00064	0.00110	0.00139	1.18

Silver Sphere, 1/4" diameter

Aluminum	0.00070	0.00120	0.00151	1.16
Copper	.00065	0.00112	0.00141	1.08
304SS	.00060	0.00103	0.00130	1.00
Zinc	.00067	0.00114	0.00144	1.11

The radius of the contact area formed when a sphere is brought in contact with each of the materials as compared with the radius of the contact area of the sphere on stainless steel, as given in the last column of Table P-2, indicates a very significant variation for the different materials. Furthermore, there are significant variations in the values of the modulus for a given material depending upon its mechanical condition, whether in a hardened or annealed state.

Contact Resistance

It can be shown that when two objects, such as a sphere and a slab, are brought into contact, the electrical resistance (neglecting the resistance of any surface films that may be present) through the two contact members is given by the equation:*

$$R = R_1 + R_2 = \frac{1}{4k_1 a} + \frac{1}{4k_2 a} \quad (P-2)$$

where k = conductivity

a = radius of contact area

subscripts 1 and 2 refer to the two bodies.

Let us confine our attention to a single contact member, the slab.

On the basis of theory of current flow through electrical contacts as developed by Holm, the equipotential surfaces in the vicinity of a circular contact area of radius a will be represented by semi-ellipsoids with the equation:

$$\frac{x^2}{a^2 + u} + \frac{y^2}{a^2 + u} + \frac{z^2}{u} = 1 \quad (P-3)$$

where u is a parameter and the coordinate axes coincide with the directions x and y . From equation (P-3) we see that the height of a semi-ellipsoid (normal to the xy -plane) is \sqrt{u} and that $\sqrt{a^2 + u}$ is its axis in the x and y directions.

The resistance from the contact area to an equipotential plane in terms of the parameter u is given by the equation:

$$R_u = \frac{1}{4\pi k} \int_0^u \frac{du}{(a^2 + u) \sqrt{u}} = \frac{1}{2k} \int_0^{\sqrt{u}} \frac{dz}{a^2 + z^2} = \frac{1}{2\pi k a} \tan^{-1} \left[\frac{\sqrt{u}}{a} \right] \quad (P-4)$$

The total resistance is obtained by setting $u = \infty$

$$R_{\text{total}} = \frac{1}{4ka} \quad (P-5)$$

This value of resistance corresponds to that given by equation (P-2) for each of the contact members.

* Ragnar Holm, Electric Contacts, Hugo Gebers Forlag, Stockholm, 1946.

Let us divide the contact member into volume meshes of equal resistance such that, beginning at the contact area, the boundaries of the meshes are equipotential surfaces. It can be shown that the equipotential surfaces will be ellipsoids given by equation (P-3) where

$$u = (0.072, 0.333, 1, 3, 13.9) a^2$$

Figure P-2 represents such a series of equipotential surfaces with the resistance between two consecutive surfaces equal to $R/6$. The sections drawn are ellipses with their focal points at the extremities of the contact diameter. Thus having defined the boundaries of the meshes, we can calculate the volume of each.

Electric Network

Let us now represent the case of an electric discharge through a contact between a sphere and a slab with an R-C network. We will arbitrarily divide each contact member into six meshes of equal resistance with the boundaries of the meshes as equipotential surfaces corresponding to those shown in Figure P-2. Such a network is indicated by Figure P-3. In the network representation:

R_1 and R_2 refer to the resistances of the individual meshes of the slab and sphere respectively. The c 's refer to the capacitances of the individual meshes, the first subscript designating the contact member and the second the particular mesh.

R_f refers to the film resistance.

Because of the fundamental similarity between the flow of heat within a solid and that of charge in a non-inductive circuit, we can treat the problem of heat transfer by means of an electrical analogy. Ohm's law corresponds to Fourier's law. The concept of electrical resistance corresponds to thermal resistance; that of electrical capacity of a conductor to thermal capacity of a mass. This method enables one to solve many transient and steady-state heat flow problems which do not yield readily to direct theoretical solutions.

APPLICATION OF ELECTRICAL ANALOGY TECHNIQUE TO POWELL'S COMPARATOR

We shall now employ the method of electrical analogy to describe the heat transfer phenomena in the measurement of thermal conductivity with Powell's comparator.

Detector Sphere - Silver, 1/4" Diameter

Conductivity Sample - ML-1700 Stainless Steel Slab, 1/4" Thick

TABLE P-3

THERMAL PROPERTIES

<u>Property</u>	<u>Material</u>	
	<u>Ag</u>	<u>SS ML-1700</u>
$k \left(\frac{\text{Btu}}{\text{hr ft}^2 \text{F}} \right)$	242	8.7

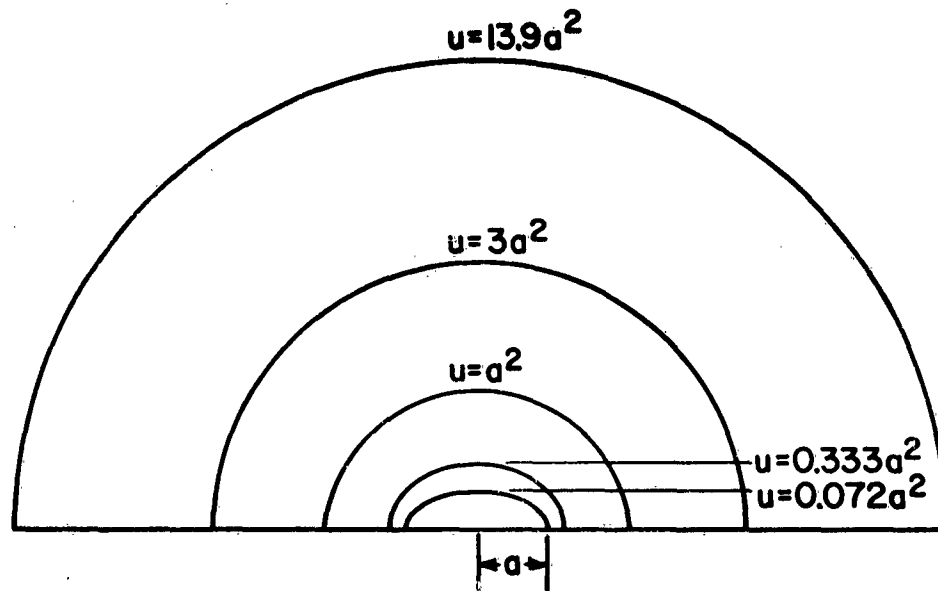


Figure P-2: The Resistance Between Two Consecutive Equipotential Surfaces of the Figure is $1/6$ of the Total Construction Resistance in One Contact Member.

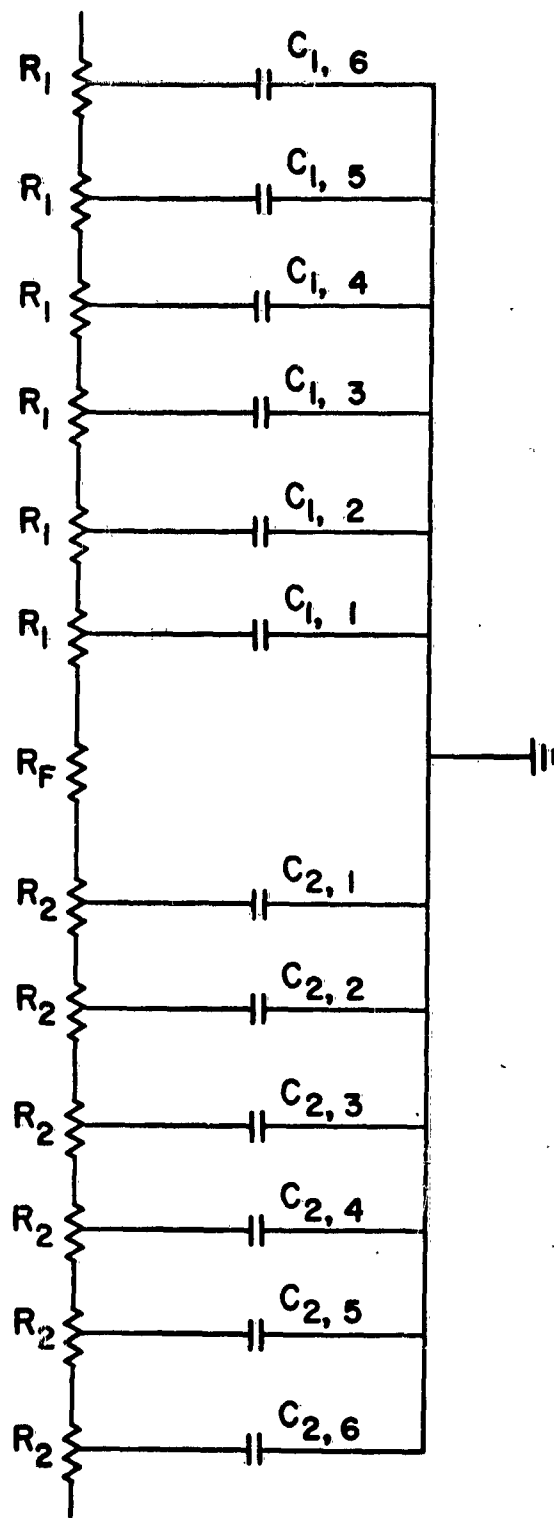


Figure P-3: Equivalent Electric Contact Network.

<u>Property</u>	<u>Material</u>	
	<u>Ag</u>	<u>SS ML-1700</u>
$\rho \left(\frac{\text{lb}}{\text{ft}^3} \right)$	650	500
$c \left(\frac{\text{Btu}}{\text{lb } ^\circ\text{F}} \right)$	0.10	0.12
$c \left(\frac{\text{Btu}}{\text{ft}^3 ^\circ\text{F}} \right)$	65	60

With a 10 gram load, the contact will be a disc 0.00060" in radius (see Table P-2).

Dividing each of the contact members into 6 meshes of equal resistance, we can calculate R_1 and R_2 using equation (P-4). The volumes of the meshes may be calculated from the data in figure P-2. From the volumes and the thermal properties, Table P-3, the capacities of the meshes are obtained.

The calculations are summarized in Table P-4. The data are given in the equivalent electrical units.

TABLE P-4
SILVER SPHERE - SS SLAB, 0.0006" RADIUS CONTACT

<u>Mesh No.</u>	<u>Stainless Steel Slab</u>		<u>Silver Sphere</u>	
	<u>Resistance Ohms</u>	<u>Capacitance uuf</u>	<u>Resistance Ohms</u>	<u>Capacitance μuf</u>
1	95.7	4.5	3.44	5.
2	95.7	7.5	3.44	8.
3	95.7	19.	3.44	21.
4	95.7	77.	3.44	84.
5	95.7	768.	3.44	830.
6	95.7	*1134 x 10 ⁶	3.44	**305 x 10 ⁶

* volume - hemisphere 1/4" radius

** volume - sphere 1/4" diameter

From the data in Table P-4 we can substitute for the R 's and c 's in Figure P-3. This has been done in Figure P-4.

From the data in Table P-4 we can compute the charging time, τ , (τ = time constant) for the various meshes in the circuit. These are given in Table P-5.

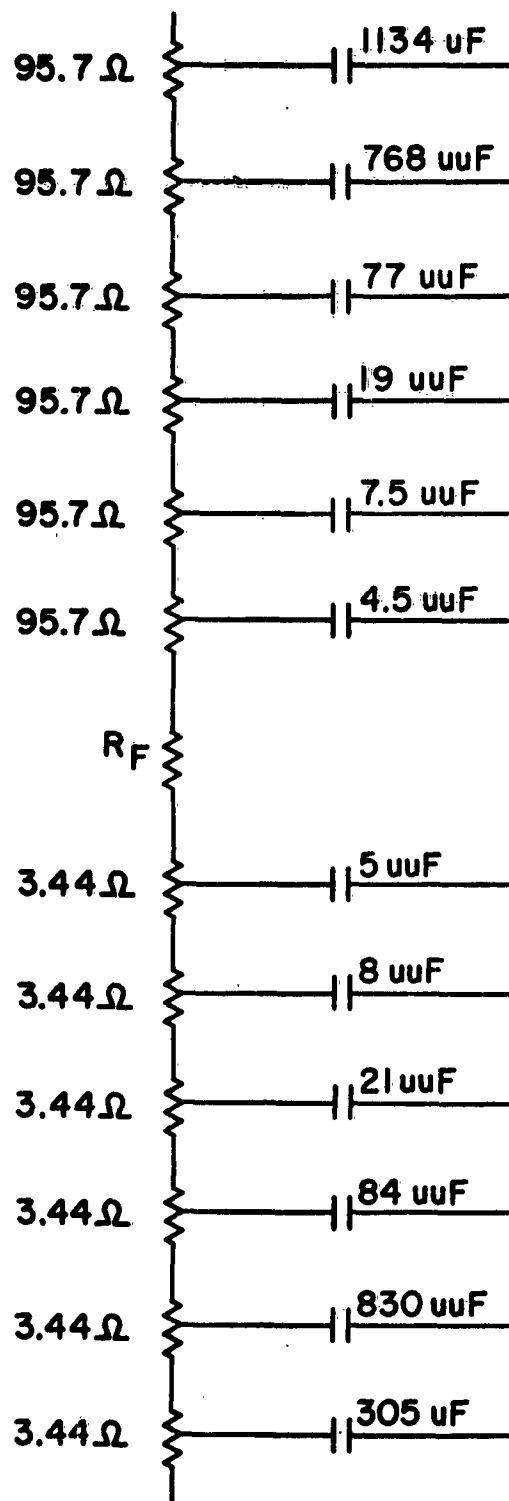


Figure P-4: Equivalent Electrical Circuit, 1/4" Silver Sphere, Stainless Steel Slab.

TABLE P-5
CHARGING TIMES SILVER SPHERE - SS SLAB, 0.0006" RADIUS CONTACT

<u>R-C Circuit</u>	<u>Resistance Megohms</u>	<u>Capacitance μf</u>	<u>τ-Seconds (RC x 3600)*</u>	<u>5τ Seconds</u>
$R_1 + R_2$; $C_{1,1} + C_{2,1}$	99×10^{-6}	9.5×10^{-6}	0.0034×10^{-3}	0.017×10^{-3}
$2(R_1 + R_2)$; $C_{1,2} + C_{2,2}$	198×10^{-6}	15.5×10^{-6}	0.011×10^{-3}	0.052×10^{-3}
$3(R_1 + R_2)$; $C_{1,3} + C_{2,3}$	297×10^{-6}	$40. \times 10^{-6}$	0.043×10^{-3}	0.22×10^{-3}
$4(R_1 + R_2)$; $C_{1,4} + C_{2,4}$	396×10^{-6}	$161. \times 10^{-6}$	0.240×10^{-3}	1.2×10^{-3}
$5(R_1 + R_2)$; $C_{1,5} + C_{2,5}$	495×10^{-6}	$1760. \times 10^{-6}$	3.14×10^{-3}	15.7×10^{-3}
$6(R_1 + R_2)$; $C_{1,6} + C_{2,6}$	594×10^{-6}	$1439. \times 10^0$	$3.1 \times 10^{+3}$	$15.4 \times 10^{+3}$

*Transfers equivalent electrical units from hours to seconds time base.

CONCLUSIONS

An examination of the data in Table P-5 indicates that the time required to bring the volume of material corresponding to as much as 5/6 of the total contact resistance to essentially a fully charged state amounts to about 16 milliseconds. Thereafter the only impedance to the flow of charge is the resistance of the contact. Thus the basic premise of Powell's method, that the variable state is of such short duration that the experiment is conducted under relatively steady thermal conditions, appears to be valid. In Powell's experimental technique, as well as our own, the rate of cooling of the detector sphere was observed to be essentially constant over a 10 second interval. Thus the initial transient, occurring in early stages of the experiment can be considered to have a negligible effect on the measured cooling rate. The cooling rate is therefore a measure of the thermal conductivity of the sample.

The data in Table P-5 were calculated for stainless steel as the sample material. Similar calculations have been carried out for aluminum and quartz, materials which differ widely in thermal conductivity. These data indicate that, so long as the contact area is small (corresponding to a 10 gram load on a 1/4" diameter silver sphere), the charging time is of such short duration as to have a relatively insignificant effect on the cooling rate.

It can be shown that the time constant, τ , is inversely proportional to the conductivity of the sample and directly proportional to the square of the contact radius. This emphasizes the desirability of maintaining a small contact area.

APPENDIX Q - ANALYSIS OF RADIATION HEAT LOSSES IN MEASUREMENT APPARATUS

S. B. Dunham

September, 1958

INTRODUCTION

An analysis has been made of the effect of radiant heat loss on the accuracy of the measurement technique developed by Harman and Logan for the measurement of the absolute values of the thermoelectric power and thermal conductivity. The method is fully outlined in their report. (Q-1) The method involves the use of the Peltier heat to maintain a temperature gradient across the specimen. The measurement of this gradient, the voltage across the specimen, and the ac resistivity allows the calculation of the absolute value of the thermoelectric power and the thermal conductivity.

The purpose of the analysis was to determine what the temperature generated by thermoelectricity at the ends of the specimen would be in terms of that with no radiant heat loss. The radiant heat loss will tend to drop the temperature difference. At the operating temperatures involved in this project, this radiant heat loss was considered to be a problem.

In order to make an analysis, certain assumptions were made as to the manner in which the radiant heat energy flowed. The equations were developed for two different situations. In the first the sample is located on the axis of a cylindrical oven. In the second a platinum shield is interposed between the oven and the sample.

The problem becomes one of heat radiation between surfaces, one of which does not have a uniform distribution of temperature. Since the distribution of temperature was considered to be uniform about any perimeter, a cylindrical geometry was assumed.

UNSHIELDED SAMPLE

In the first situation, where the sample is unshielded from the oven, a cross-section would have a square sample located in the middle of a circular oven. It is now assumed that the net heat flow by radiation is only radial, while that by conduction is only axial. The amount of net radiation transfer is then held to follow the Christiansen equation.*

$$\frac{\epsilon_1 \sigma A_1 (\theta_1^4 - \theta_2^4)}{1 + \epsilon_1 \left[\frac{1}{\epsilon_2} - 1 \right] \frac{A_1}{A_2}} = q \quad (Q-1)$$

where in this case the emissivities ϵ_1 and ϵ_2 are considered as unity so that this becomes for the sample section

(Q-1) T. C. Harman and M. J. Logan; Technical Report No. 1 on Special Measurement Techniques for Thermoelectric Materials with Results for Bi_2Te_3 and Alloys with Bi_2 and Se_3 . Battelle Memorial Institute. June 1, 1958.

* Symbols are defined below.

$$dq_r = q_r dx = \sigma p_{sa} (4\theta_o^3 \theta_{sa}) dx \quad (Q-2)$$

The heat flow out of the differential element of the sample by radiation will be equal to the difference in the thermal conduction heat due to the temperature gradient.

$$dq_c = K_{sa} A_{sa} \frac{d^2 \theta_{sa}}{dx^2} dx \quad (Q-3)$$

We can set these two heat flows as equal so that

$$\frac{d^2 \theta_{sa}}{dx^2} - \frac{4\sigma p_{sa} \theta_o^3 \theta_{sa}}{K_{sa} A_{sa}} = 0 \quad (Q-4)$$

In a complete solution of this equation we need a boundary condition. At either end of the sample the heat output will be equal to that produced in the junction by thermoelectric forces. This can be written in terms of the temperature drop along the sample expected due to the Peltier effect if there were no other heat transfer occurring except by conduction along the sample. The thermal gradient at either end would become

$$\frac{d\theta_{sa}}{dx} = \frac{\theta_p}{l} \quad \text{when } x = 0 \text{ or } l \quad (Q-5)$$

The solution of these equations becomes

$$\theta_{sa} = \frac{\theta_p}{l_c} \frac{e^{-lc} e^{cx} - e^{-cx}}{1 + e^{-lc}} \quad (Q-6)$$

where

$$c = \sqrt{\frac{4\sigma p_{sa} \theta_o^3}{K_{sa} A_{sa}}} \quad (Q-7)$$

These equations indicate that temperature distribution will be linear when the radiant heat loss is low and will be exponential near the ends when the radiant heat loss is high.

In practice the sample will be at a different average temperature than the oven. It will be generally lower due to conduction down the leads and radiation out the ends of the oven. However, if the losses of this sort are symmetrical, and there is no rapid change in the value of the thermal and thermoelectric coefficients of the material, this method of measurement will cancel them out. The temperature of the sam-

ple is of importance, and this is measured, not that of the oven. It would be necessary to look at the design of the experiment more precisely to see how large the unsymmetry will be; until a particular experiment is designed it would be unprofitable to set up any general rules.

Based on a preliminary design for a device which can operate in an oven presently available, the constants in equations (Q-6) and (Q-7) are as follows:

$$\begin{aligned}\sigma &= \text{Stefan Boltzmann Constant} = 5.7 \times 10^{-12} \text{ watts cm}^{-2} \text{ deg}^{-4} \\ p_{sa} &= \text{perimeter of sample} = 2.54 \text{ cm} \\ A_{sa} &= \text{cross section area of sample} = 0.403 \text{ cm}^2 \\ K_{sa} &= 2 \times 10^{-2} \text{ watts cm}^{-1} \text{ deg}^{-1} \text{ (thermal conductivity of sample)} \\ l &= 3.8 \text{ cm (length of sample)}\end{aligned}$$

The values of the ratio of the temperature at the ends of the sample compared with that for the normal Peltier temperature of $\theta_p/2$ are given in Table Q-1.

EFFECT OF SHIELD

When a shield is introduced, the equations become much more complicated. In this case we must take into account the fact that the emissivity of the shield is not unity. For platinum the value of 0.15 is taken as representative at all temperatures. The equation of balance of radiant heat flow radially must be made with the conduction heat flow axially both for the shield and the sample. In this case at the end of shield we must have no axial heat flow. The equations of heat balance are

$$1.2\pi\sigma r_{sh}\theta_o^3\theta_{sh} + \frac{16\sigma_w\theta_o^3}{34w_{sa}}(\theta_{sh} - \theta_{sa}) = K_{sh}A_{sh}\frac{d^2\theta_{sh}}{dx^2} \quad (Q-8)$$

$$1 + \frac{34w_{sa}}{3\pi r_{sh}}$$

$$\frac{16\sigma_w\theta_o^3}{34w_{sa}}(\theta_{sa} - \theta_{sh}) = K_{sa}A_{sa}\frac{d^2\theta_{sa}}{dx^2} \quad (Q-9)$$

$$1 + \frac{34w_{sa}}{3\pi r_{sh}}$$

These equations can be solved for the temperature distribution in the sample θ_{sa} by the ordinary means of differential equations and substitution of the values for the ends given above. When this is done, the resulting equation is of the form

$$\theta_{sa} = \frac{v_1}{1 + e^{\rho_1 l}} \left[e^{\rho_1 x} - e^{\rho_1 l} e^{-\rho_1 x} \right] + \frac{v_2}{1 + e^{\rho_2 l}} \left[e^{\rho_2 x} - e^{\rho_2 l} e^{-\rho_2 x} \right] \quad (Q-10)$$

where
$$v_2 = \frac{\beta_2 - (\rho_1)^2}{(\rho_2)^2 - (\rho_1)^2} \frac{\theta_p}{2\rho_2}, \quad v_1 = \frac{\beta_2 - (\rho_2)^2}{(\rho_1)^2 - (\rho_2)^2} \frac{\theta_p}{2\rho_1} \quad (Q-11)$$

$$(\rho_1)^2 = 1/2 \left[\beta_1 (1 + \gamma) + \beta_2 + \sqrt{[\beta_1 (1 + \gamma) + \beta_2]^2 - 4 \beta_1 \beta_2} \right] \quad (Q-12)$$

$$(\rho_2)^2 = 1/2 \left[\beta_1 (1 + \gamma) + \beta_2 - \sqrt{[\beta_1 (1 + \gamma) + \beta_2]^2 - 4 \beta_1 \beta_2} \right] \quad (Q-13)$$

$$\beta_1 = \frac{1.2\pi \sigma r_{sh} \theta_o^3}{K_{sh} A_{sh}} \quad (Q-14)$$

$$\beta_2 = \frac{16\sigma W_{sa} \theta_o^3}{1 + \frac{34 W_{sa}}{3\pi r_{sh}} K_{sa} W_{sa}^2} \quad (Q-15)$$

$$\gamma = \frac{40/3 \frac{W_{sa}}{\pi r_{sh}}}{1 + 34/3 \frac{W_{sa}}{\pi r_{sh}}} \quad (Q-16)$$

In addition to the specifications of the sample, we now add those of the shield (taking two different sizes):

$$\begin{aligned} r_{sh} &= 1.59 \text{ cm, or } 2.54 \text{ cm} \\ W_{sh} &= 0.025 \text{ cm} \\ K_{sh} &= 0.71 \text{ watt cm}^{-1} \text{ deg}^{-1} \end{aligned}$$

The effect of the two shields is thus shown in the final table.

TABLE Q-1

SUMMARY OF RESULTS

Temperature difference across specimen with radiation heat losses taken into account for various temperatures. In each column the units are normalized so that the temperature difference in the absence of radiation heat losses would be equal to 100. Note that the units are thus different in different columns.

<u>TYPE OF SHIELD</u>	<u>300K</u>	<u>500K</u>	<u>800K</u>	<u>1000K</u>	<u>1300K</u>
None	82.0	53.0	27.7	19.8	13.3
5/8" radius	96.0	74.8	45.8	34.4	24.0
1" radius	89.0	66.6	39.0	28.9	19.9

LIST OF SYMBOLS USED

ϵ_1	= Emissivity of inner surface
ϵ_2	= Emissivity of outer surface
σ^2	= Stefan Boltzmann Constant, 5.7×10^{-12} watts $\text{cm}^{-2} \text{deg}^{-4}$
θ_1	= Temperature of inner surface
θ_2	= Temperature of outer surface
θ_o	= Temperature of oven (average of sample)
θ_{sa}	= Temperature of sample (difference from oven temperature)
θ_{sh}	= Temperature of shield (difference from oven temperature)
θ_p	= Temperature of sample due to Peltier effect only
A_1	= Area of inner surface
A_2	= Area of outer surface
A_{sa}	= Area of sample (cross section)
A_{sh}	= Area of shield (cross section)
K_{sa}	= Thermal conductivity of sample
K_{sh}	= Thermal conductivity of shield
q_r	= Radiation heat flow
q_c	= Conduction heat flow
P_{sa}	= Perimeter of sample
w_{sa}	= Width of sample
w_{sh}	= Thickness of shield
r_{sh}	= Radius of shield
l	= Length of shield and sample
x	= Distance along axis of sample and shield

Defined by equations are:

c - (Q-7)

v_1 and v_2 - (Q-11)

SymbolDefining Equation

ρ_1
 ρ_2
 β_1
 β_2
 δ

(Q-12)
(Q-13)
(Q-14)
(Q-15)
(Q-16)

APPENDIX R - MEASUREMENTS - Z METER

F. A. Ludewig, Jr.

May, 1959

SECTION I: EXPERIMENTAL WORK

OBJECTIVE

The objective of this phase of the program was to design, construct and evaluate an apparatus to measure certain characteristics of thermoelectric materials. The parameters of interest and target accuracies were as follows:

- s - Seebeck coefficient - microvolts per degree C $\pm 3\%$
- ρ - Electrical resistivity - ohm-cm $\pm 5\%$
- Z - Figure of merit - $\frac{s^2}{\rho K}$ $\pm 10\%$
- K - Thermal Conductivity - milliwatts per degree C $\pm 10\%$
- T - Temperature - degrees C $\pm 5\%$

All of the above listed measurements were to be made over a temperature range of 20 to 1000°C. The determination of K will be by the "Z meter" method.* The determination of s, ρ , k, and Z are to be made on the same sample in rapid succession; i.e. no significant changes in temperature, time or other environmental conditions.

Special preparation of the sample should be held to a minimum and a rapid (in terms of hours) measurement system would be desirable. Certain samples are expected to be difficult to prepare, therefore the smallest practical sample size consistent with measurement accuracies is desirable.

Most of the measurements are to be made under vacuum, however provisions should be made for the introduction of a specified gas.

MEASUREMENT CONSIDERATION

The objectives outlined above were established as desirable goals, however recognizing that certain compromises would be necessary. The following discussion describes certain practical problems and possible compromises.

"Z Meter"

The above referenced report of work done at Battelle Memorial Institute describes a measurement technique which enables calculation of thermal conductivity from a group of voltage measurements provided the measurements are performed under certain thermal

* T. C. Harmon and M. J. Logan - Technical Report No. 1 on Special Measurement Techniques for Thermoelectric Materials with Results for Bi₂Te₃ and alloys with Bi₂Se₃. Battelle Memorial Institute, June 1, 1958.

conditions. The basic heat flow assumptions are as follows. When a direct current is passed through an active thermoelectric material, heat is transferred from one junction to the other, and the defining equation is $q_p = sIT$ where s is the Seebeck coefficient, I is the current in amperes and T is the temperature in degrees K.

It is assumed that all of the heat transferred by the current flow is transferred in the opposite direction, by thermal conduction, and the defining equation is $q_c = K\Delta T \frac{A}{l}$ where K is coefficient of thermal conductivity, ΔT is the temperature difference in degrees C, A is cross sectional area in square centimeters and l is the distance between junctions in centimeters. If this assumption can be considered valid q_p can be equated to q_c . s , I , T , ΔT , A and l can be independently measured, therefore the equation can be solved for the only unknown, K .

In any practical case q_c will rarely equal q_p . If leads are attached to the sample there will be errors due to heat conduction in the leads. Unless special shielding is used there will be radiation heat losses from all surfaces. Under certain conditions these losses can be made small such that effects are within the accuracy tolerance. In other cases the heat losses can be determined and appropriate corrections applied which will reduce the effect of losses to something less than accuracy tolerance. Under other conditions neither of the above conditions can be achieved. It should be noted the thermal conditions regarding the "Z meter" are the same conditions that must be met in most devices used for the direct measurement of thermal conductivity; i.e. the magnitudes and directions of heat flow must be accounted for.

A more rigorous analysis of the heat flow problems is presented in a report by T. C. Harmon, J. H. Cahn, and M. J. Logan of Battelle Memorial Institute entitled - Measurement of Thermal Conductivity by Utilization of the Peltier Effect.

Measurement of Electrical Resistivity

The measurement of electrical resistivity of samples of material with a low length to cross sectional area ratio is best accomplished by a 4 terminal type measurement. In the case of measurements on thermoelectric materials it is desirable to make the measurement on alternating current. Since low resistance a-c bridges are generally not available, the voltmeter ammeter method is commonly used. The accuracies obtainable with normal instruments are within the target specification. The four probe measurement is independent of contacting resistances, provided a high resistance voltmeter is used; however the drop probes should be located in a region of uniform current distribution. However, if the current distribution is not uniform the correction can be calculated.

In general the current and voltage will be low level, therefore provisions are needed for adequate shielding or filtering to eliminate errors due to extraneous pick-up.

It was mentioned above that contact resistance of the probes is not of prime consideration, however these contacts and sources of heat conduction losses must be factored into the "Z meter" heat flow equation.

Measurement of Seebeck Coefficient

The Seebeck coefficient is in terms of microvolts per degree which means that it is the voltage existing across a thermoelectric material when a temperature difference

also exists. The measurement of s requires the creation of a temperature difference across the sample, measurement of this temperature difference and measurement of the d-c voltage across the sample. In the Z meter this temperature difference is created by passing a d-c current thru the sample. The temperature difference is measured by means of thermocouples attached to the ends of the sample. The d-c voltage drop is measured on the same type thermocouple lead on each end. For good temperature measurements the thermocouple junctions should be bonded via a good thermal path to the sample. Size and means of attaching the thermocouples should be such that the junction is not cooled by conduction thru the leads.

Problems of Combined Measurements

The use of the "Z meter" system of measurement results in determination of the pertinent characteristics of a material; i. e. s , ρ , K and Z . However several compromises must be made in order to obtain satisfactory overall measurements. However under certain conditions satisfactory compromises are impractical. For example, the accurate measurement of sample temperature requires a good thermal bond between the sample and thermocouple junction, however, bonding techniques are unknown for the materials under consideration. Second best to bonding is high pressure contact. To provide the high pressure a substantial support is needed. The conductivity of this support then becomes too large to be ignored. The support temperature can be servoed to the sample temperature, however radiation is still a problem, particularly at the higher temperatures. Also the "Z meter" operates on small values of ΔT which requires high servo accuracy.

The lack of bonding techniques is probably the largest single factor affecting the limitation of the "Z meter" at higher temperatures. As is shown in the above mentioned reports, if a sample could be suspended via fine lead wires in a container of known temperature the losses could readily be calculated and are inherently small. Also at room temperature, support material with sufficiently low thermal conductivity could be used so that adequate contact pressure could be obtained.

Another conflicting interest arises between the sample configuration most suitable for electrical resistivity measurement and the most suitable configuration to minimize the significance of thermal losses. A large A ratio is desirable for electrical resistivity measurement. A large A ratio is desirable so that sample conductance is high in comparison to conduction losses and also to minimize radiation losses for the measurement of thermal conductivity.

DESIGN OF MEASUREMENT DEVICES

The complete inter-relationship of the measurement problems was not fully appreciated in the early stages of the program; also it was difficult to predict the measurement accuracies attainable of each parameter. Therefore a design was evolved which would evaluate the seriousness of each problem at room temperature on known materials. Concurrently a theoretical analysis of the design was conducted to anticipate the problems to be encountered at high temperature where radiation losses become important. Other designs evolved from experience gained during these tests.

Initial Design

The initial testing was planned for room temperature only, however the major portions of the apparatus were designed for higher temperature use. Figure R-1 shows a

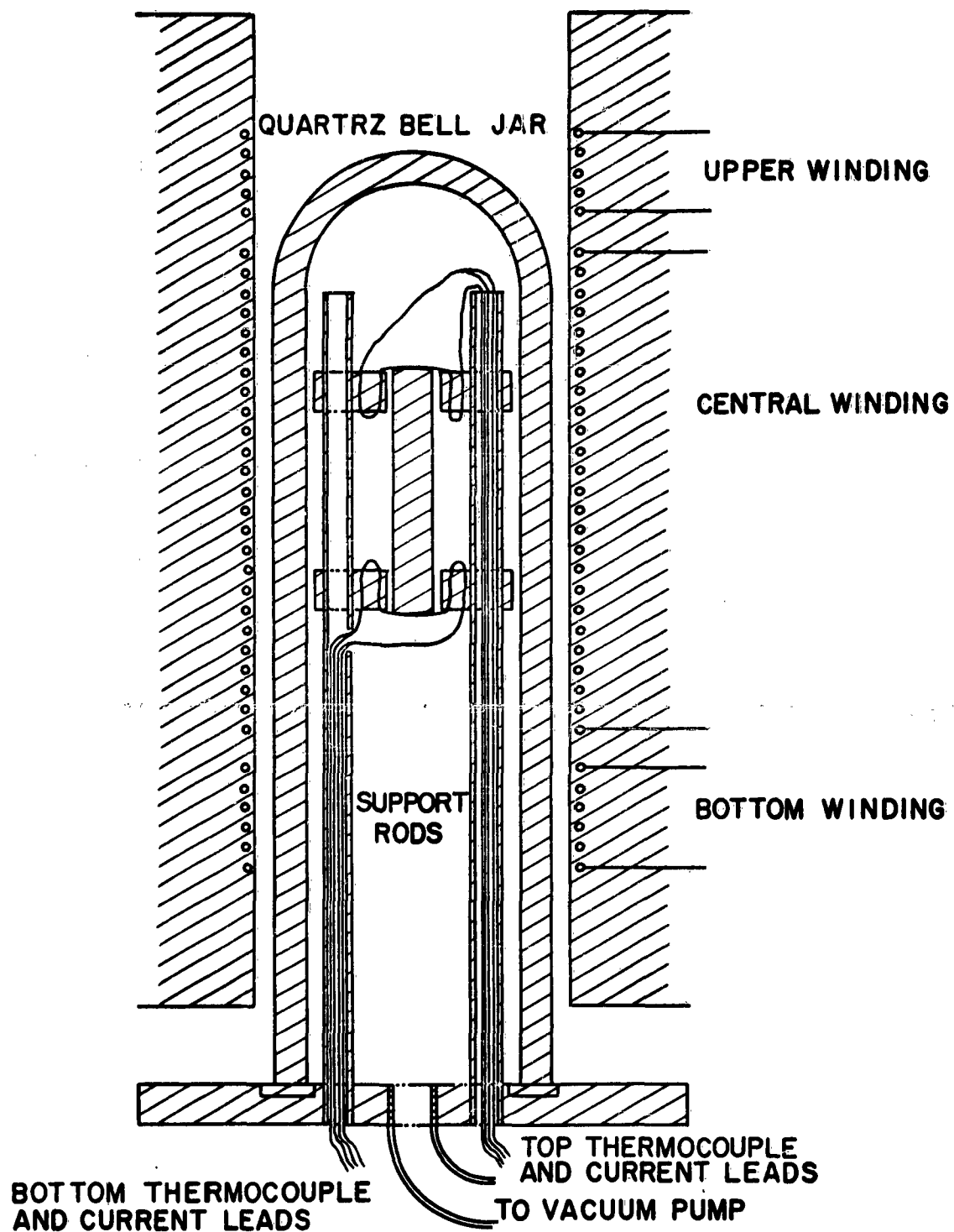


Figure R-1: Z Meter Apparatus.

sketch of the furnace, vacuum chamber and sample holder. The quartz bell jar is approximately 2 inches in diameter and 18 inches long. The furnace is an M-2718 three winding type manufactured by the Hevi-Duty Electric Company. The furnace was mounted on rails for easy removal of sample. The auxiliary equipment such as vacuum pump, vacuum gage, Variac controls for the furnace winding, etc. were standard laboratory items and are not shown.

The details of the sample holder are shown in Figure R-2. Only the top assembly is detailed, however the lower assembly was identical and consisted of a ceramic support plate which served as a terminal board and support for the sample and leads. The sample was supported by the three 2 x 6 mil contact strips. The two outer strips were platinum and the center strip was a butt welded Platinum-Platinum 10% Rhodium thermocouple. All joints were welded without the addition of a filler material. The leads connecting the sample holder to the main lead wire (20 mil dia.) were 15 x 40 mil. Provision was made so that the contact strip pressure could be increased by loading with dead weights. The sample size selected for these tests was approximately one quarter inch square by one and one half inches long.

Certain problems were expected with this design; for example the resistance measurement was made via the three leads on the end. The two outside strips were used as current probes and the thermocouple strip was used as the drop lead. The current distribution at the end of the sample was not uniform, however the error due to this was calculated. The radiation loss from the exposed side of the thermocouple strip would cause the sensed temperature to be lower, particularly under conditions of high thermal contact resistance between the sample and thermocouple strip.

The large $\frac{l}{A}$ ratio of the sample would be desirable for the resistance measurement, however the thermal conductance of the sample was low and would be affected by the conduction in the contact strips.

Results of Initial Design

A sample of Bi_2Te_3 was obtained to evaluate the effects described above. The effects of these factors proved more detrimental than anticipated. The thermocouples did not adequately sense the sample temperature, therefore S and K measurements were unsatisfactory. This was attributable to high thermal resistance between the sample and thermocouple contact strips.

The electrical resistivity measurements were difficult to make because of the excess amount of pickup. Shielding was deemed impractical because at elevated temperatures the furnace winding would also produce pickup which could not be shielded against. Therefore the circuitry shown in Figure R-3 was employed.

The measuring equipment consists of a supply of AC power to pass current through the sample. The voltage drop developed in the sample is then applied to a stable amplifier. The output of the amplifier supplies current to the field coil of a dynamometer wattmeter. The moving coil of the wattmeter is supplied with 400 cps sine wave of constant amplitude (20 volts). Provisions are made to vary the phase of the voltage signal so that the two currents of the wattmeter are in phase. Full scale deflection on the wattmeter corresponded to 2.0 millivolts of input to the amplifier. The basic characteristic of a dynamometer instrument makes it an excellent electrical filter; i.e., if a pure sinusoidal signal is applied to one coil (in this case 400 cycles on the moving coil) of a wattmeter and a signal containing 400 cycles plus other frequency signals is applied to the other coil, the wattmeter deflection will be propor-

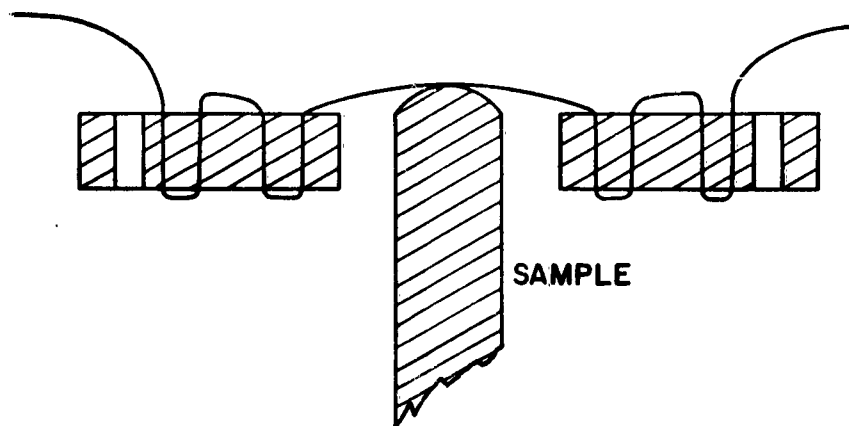
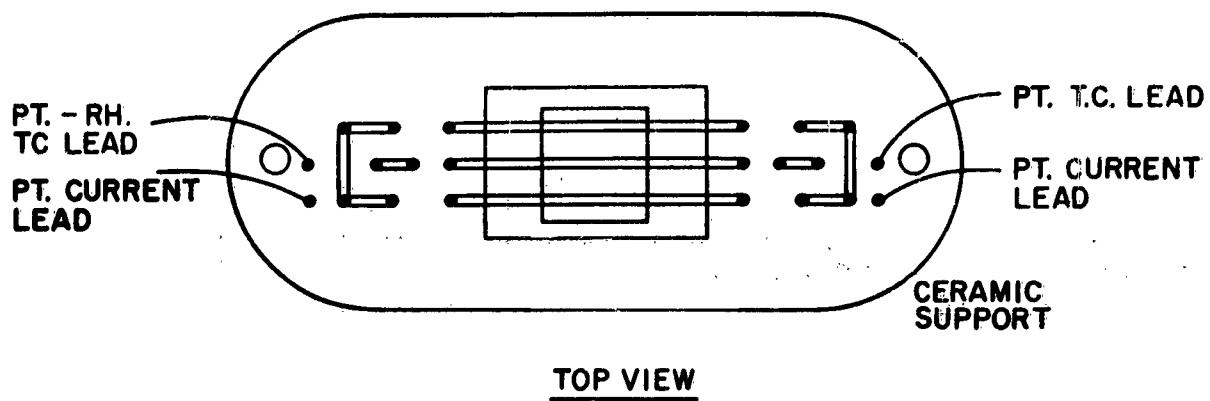


Figure R-2: Sample Holder.

tional to the products of only the two 400 cycles. Therefore the wattmeter can be considered a perfect filter.

Other experimenters have used screened cages for these low level AC measurements at room temperature. The results of the measurement of resistivity of materials by this method appears to be completely satisfactory. Once the circuitry is set up and adjusted, the measurement can be made almost as easily as with a conventional voltmeter.

Modification of Initial Design

Experience with the initial setup pointed up the contact resistance problems. Therefore the thermocouple strips were removed and replaced with a three mil conventional beaded thermocouple which was inbedded in a 1/16 inch hole in the end of the sample. The resultant measurements indicated that satisfactory measurement of ΔT could be obtained and the resultant values of s were satisfactory. However the value of K and Z did not agree with other methods. The conductance of the contact strip is approximately 20% of the sample conductance.

Conclusions based on Test Experience

The above tests indicated that the resistance measuring circuitry was adequate and could be modified to measure lower resistances. Therefore based on the experience with conduction losses, a sample with a smaller A ratio would be desirable. Also the analysis of the radiation losses (described in Appendix A) indicated that the present A ratio would be unsatisfactory. The radiation loss would be less for a cylindrical sample. The compromise between thermal and electrical considerations resulted in a suggested sample configuration such that the length to diameter ratio was between 0.5 and 1. However no satisfactory contacting means was obtained. Bonding techniques are not necessarily known for the materials to be measured. Pressure contacts would necessitate a support structure with resulting heat flow. Since the normal ΔT using the "Z meter" approach is of the order of one degree it did not appear practical to servo the support temperature to the temperature at the ends of the sample.

Z Meter Design for Room Temperature

A limited amount of information could be gained by making measurements at room temperatures. At room temperatures two of the major limitations are greatly reduced, i.e. radiation and material for the support structure. At room temperature material such as polystyrene could be employed in the support structure without the need for a temperature servo. The thermal conductivity of polystyrene is approximately an order of magnitude lower than the thermal conductivity of thermoelectric materials of interest. Figure R-4 is a sketch of a possible design. Since this program was mainly concerned with high temperature materials, no further effort was applied to this room temperature device.

High Temperature Apparatus for Measuring s , ρ , K

The experience and investigations of the "Z meter" technique for measuring thermoelectric materials parameters indicated that the main problems were the age old problems existing in the measurement of thermal conductivity. The small ΔT obtained in the "Z meter" was an additional hardship. Therefore attention was turned to the design of a device to measure thermal conductivity with modifications such that s and ρ could also be measured. The details of this design investigation are given in Appendix B.

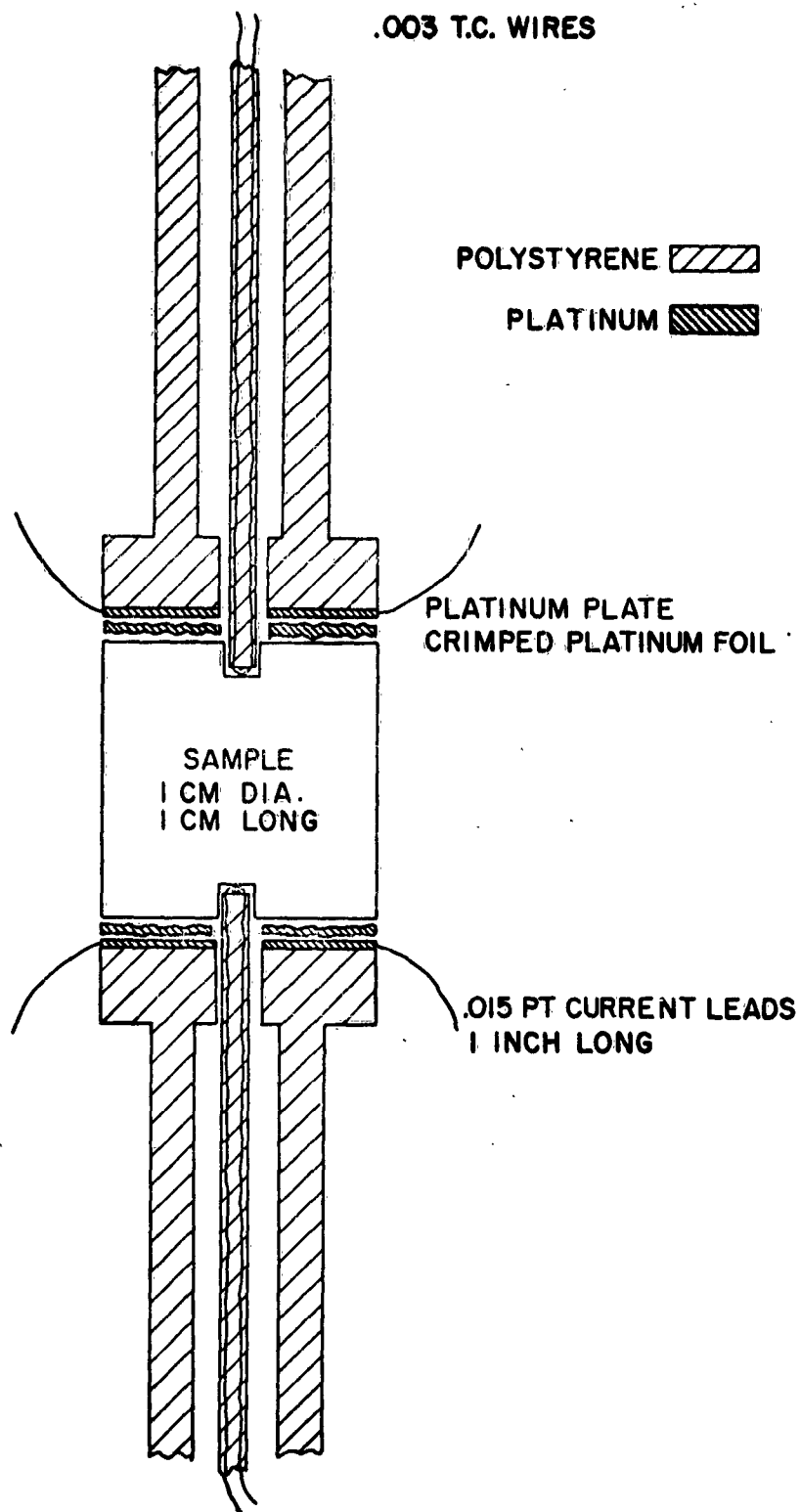


Figure R-4: Room Temperature Sample Holder Design.
WADD TR60-22, Pt. II 295

CONCLUSIONS

The results of this phase of the program indicate that it is not practical to build a "Z meter" for higher temperatures (above 100°C) unless the material to be measured can be bonded. The bond should make good electrical and thermal contact. The analysis of the thermal conductivity apparatus, described in Appendix B, indicates that measurements of s , ρ , K and Z are feasible at high temperature.

The expected accuracies are as follows:

K - Thermal conductivity	$\pm 13\%$
ρ - Electrical resistivity	$\pm 5\%$
s - Seebeck coefficient	$\pm 5\%$
T - Absolute temperature	$\pm 5\%$

It is to be noted that the above accuracies are estimated on the basis of the sample size described in Section III and based on the expected ranges of the parameters which would be useful for high temperature thermoelectric generators.

SECTION II: ANALYSIS OF RADIATION HEAT LOSSES

An analysis has been made of the effect of radiant heat loss on the accuracy of the measurement technique developed by Harman and Logan for the measurement of the absolute values of the thermoelectric power and thermal conductivity. The method is fully outlined in their report. (R-1) The method involves the use of the Peltier heat to maintain a temperature gradient across the specimen. The measurement of this gradient, the voltage across the specimen, and the ac resistivity allows the calculation of the absolute value of the thermoelectric power and the thermal conductivity.

The purpose of the analysis was to determine what the temperature generated by thermoelectricity at the ends of the specimen would be in terms of that with no radiant heat loss. The radiant heat loss will tend to lower the temperature difference. At the operating temperatures involved in this project, this radiant heat loss was considered to be a problem.

Only the effect of the heat radiated radially on the accuracy is considered here. The analysis of Harman, Cahn & Logan in a forthcoming article in the Journal of Applied Physics includes the radiant heats from the ends of the sample as well as the radial thermal conductivity drop. Another cause for lower accuracy lies in the asymmetry of the parameters of the conduction paths leading away from the sample. Symmetrical design should reduce this error. This error could also be reduced by reversing the direction of current in the sample, and taking an average of the two readings.

Ordinarily the radiant heat losses at normal room temperatures will barely affect the accuracy of measurement. If the sample is long and thin, the accuracy is impaired. As the temperature is raised the problem of reduced accuracy becomes important. Radiation shielding reduces the problem.

Radiation shielding is used to cut down the radiation loss between bodies of different temperatures. Since we have one body at a different temperature at the two ends, the thermal conductance of the shield is of importance. For instance, take as one extreme a shield with zero conductance. In this case there will be no flow of heat along the shield, and the heat will leave the shield on the outer side. At equilibrium the heat leaving will equal that entering at every point on the shield, so that it will be maintained at some intermediate temperature. In the other extreme the shield has infinite conductance. Now the temperature along the shield will be uniform. Since all the radiation heat entering or leaving from the non-uniform sample will be conducted along the shield it will assume the average temperature of the sample. Since there is a uniform temperature distribution along the oven on the far side of the shield, no radiant heat will flow out. An infinite conductance shield will thus effectively short circuit the heat flow and any other shields outside it will have no added effect in reducing the radiation loss.

A straight silver shield only one mil thick is effectively one of infinite conductance, so that only one such shield will be needed. Much the same is true of any metallic shield. It is thus of importance that it be chosen of as low emissivity as possible.

(R-1) T.C. Harman & M.J. Logan; Technical Report No. 1 on Special Measurement Techniques for Thermoelectric Materials with Results for Bi_2Te_3 and Alloys with Bi_2Se_3 . Battelle Memorial Institute. June 1, 1958.

The problem of infinite conductance may be met by using either an extremely thin coating of metal on a low conductivity material or by winding the metal in a spiral so that its effective conductance is reduced. It will probably have to be supported on some low conductivity material, such as quartz or a ceramic. Just changing the thermal conductance of the shield will result in cutting the loss due to radiation almost as much as the introduction of the conducting thermal shield.

The thermal shield should be as near the sample as possible. In deriving the equations it has been assumed that radiation only flows radially and the Christiansen equation holds. This equation indicates that radiation to an outer surface is reduced when that surface is close and of less than unity emissivity. When the lengthwise component of radiation is taken into account, it is found that this is even more true. The temperature difference at any point on the shield will be reduced by this sidewise flow of radiation as it will then see points on the sample that are of less temperature difference on the average. As the shield is moved closer to the sample, any point on it will not be able to see the other places on the sample, so that the lengthwise component of radiation is lower, and the temperature difference resulting will not be reduced as much. Since a temperature difference will occur only when the conductance of the shield is low, this effect of proximity will be of large importance only when the special shield structure is used.

Balancing Shield

A shield can be built that will be theoretically perfect if heat were supplied to one end while it was extracted from the other, so that each point on the sample could only radiate to a point on the shield of the same temperature. In fact it would be necessary only to have the same temperature gradient along the shield as along the sample. The constant difference in temperature between the shield and sample would be supplied by the conduction of heat along the symmetrical input leads, which would result in no change in the junction temperatures. The uniform temperature distribution in the shield can be supplied by a heater at one end. In this case it would be desirable to have as thick a shield as possible, so that any radiation from the shield to the oven wall would be of little effect.

In order to determine what temperature gradient the shield would be held at, its temperature at the points just opposite the ends of the sample should be measured, while the overall length of the shield is longer than that of the sample. In order to eliminate any tendency for "bootstrapping", the heat introduced should only be enough to bring the shield temperature gradient to a point just below that of the sample. Otherwise one would not be sure that the shield itself were supplying the gradient in the sample by radiation.

The loss of heat by radiation between the sample and the surrounding oven is of importance in the application of the "Z" meter technique to the high temperature (1000°C) measurement of the figure of merit of thermoelectric materials. The effect of this radiation is to lower the temperature difference produced in the thermoelectric material by the current flow.

The first situation analyzed is that where the sample radiates directly to the oven along its length. A cross-sectional view of the sample and oven is given in Figure R-5.

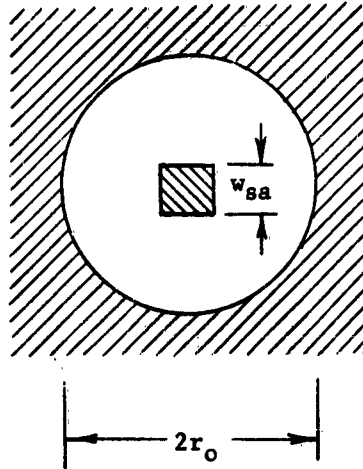


Figure R-5
Cross Section of Oven and Sample

In any differential length of the sample there will be three heat flows. There will be the flow of heat in one direction along the axis of the sample due to thermal conduction. There will be the flow of heat in the opposite direction set up by the thermoelectric forces at the junctions. Finally there will be the outward flow due to the radiation. End effects or radiation from the ends of the sample will be neglected. We assume equilibrium conditions are established.

The thermoelectric heat in the sample at point $x = -l/2$ or $x = l/2$ will be

$$q_p = I \Theta \alpha \quad (R-1)$$

and will be zero elsewhere.

The thermal conduction heat flow will be different leaving the section dx than that entering, and we have

$$q_c = K_{sa} A_{sa} \frac{d\Theta}{dx} \quad (R-2)$$

$$q_c + dq_c = -K_{sa} A_{sa} \left[\frac{d\Theta}{dx} + \frac{d^2\Theta}{dx^2} dx \right] \quad (R-3)$$

This difference dq_c will be balanced by the radiation loss dq_r so that

$$dq_r = dq_c = K_{sa} A_{sa} \frac{d^2\Theta}{dx^2} dx \quad (R-4)$$

Now some assumptions must be made to get the radiation loss in a simple form. Most of the work in this line has been with two bodies which have uniform temperature throughout. In this case the oven can be assumed to have a uniform temperature θ_o , but the sample will have an as yet unknown temperature that differs from this by the value $\theta(x)$ at any point x .

The equation of the net radiation of heat transferred from an inner body to one that surrounds it is given by the Christiansen equation

$$q_r = \frac{\epsilon_1 \sigma A_1 (\theta_1^4 - \theta_2^4)}{1 + \epsilon_1 \left[\frac{1}{\epsilon_2} - 1 \right] \frac{A_1}{A_2}} \quad (R-5)$$

If we take any cross-section of the sample and shield dx thick, and assume that this equation holds between the inner sample and the outer oven, and the sidewise flow of radiation is neglected, then

$$dq_r = \frac{\epsilon_{sa} P_{sa} [(\theta_o + \theta)^4 - \theta_o^4]}{1 + \epsilon_{sa} \left[\frac{1}{\epsilon_o} - 1 \right] \frac{P_{sa}}{P_o}} dx \quad (R-6)$$

Since $\theta \ll \theta_o$, then

$$dq_r = \frac{4 \epsilon_{sa} \sigma P_{sa} \theta \theta_o^3}{1 + \frac{P_{sa} \epsilon_{sa}}{P_o} \left[\frac{1}{\epsilon_o} - 1 \right]} dx \quad (R-7)$$

Comparing equations (R-4) and (R-7) gives

$$K_{sa} A_{sa} \frac{d^2 \theta}{dx^2} = \frac{4 \sigma P_{sa} (\theta \theta_o^3)}{\frac{1}{\epsilon_{sa}} + \frac{P_{sa}}{P_o} \left[\frac{1}{\epsilon_o} - 1 \right]} \quad (R-8)$$

The solution of this differential equation is of the form

$$\theta = A \sinh p\alpha + B \cosh p\alpha \quad (R-9)$$

where

$$\rho = \sqrt{\frac{4 \sigma P_{sa} \theta_o^3}{K_{sa} A_{sa} \left[\frac{1}{\epsilon_{sa}} + \frac{P_{sa}}{P_o} \left[\frac{1}{\epsilon_o} - 1 \right] \right]}} \quad (R-10)$$

For the boundary conditions we return to the value of the thermoelectric heat generated at the junctions and equate it to the conduction heat.

$$\begin{aligned} I \theta_o \alpha &= K_{sa} A_{sa} \frac{d\theta}{dx} \\ &= K_{sa} A_{sa} \left[\rho A \cosh \rho x + \rho B \sinh \rho x \right] \end{aligned} \quad (R-11)$$

when $x = -l/2, l/2$

From this we find

$$\begin{aligned} B &= 0 \\ A &= \frac{I \theta_o \alpha}{\rho K_{sa} A_{sa} \cosh \rho l/2} \end{aligned} \quad (R-12)$$

then

$$\theta = \frac{I \theta_o \alpha}{\rho K_{sa} A_{sa}} \frac{\sinh \rho x}{\cosh \rho l/2} \quad (R-13)$$

If the radiation losses approach zero, $\rho \rightarrow 0$, and the temperature at the ends would be that expected from the thermoelectric effect

$$\begin{aligned} \theta_p &= \frac{I \theta_o \alpha}{K_{sa} A_{sa}} \frac{\tanh \rho l/2}{\rho} \\ &= \frac{I \theta_o \alpha}{K_{sa} A_{sa}} \frac{\rho l/2}{\rho} \\ &= \frac{I \theta_o \alpha l}{2 K_{sa} A_{sa}} \end{aligned} \quad (R-14)$$

Substituting this value into (R-13) gives

$$\theta = \frac{2 \theta_p}{\rho l} \frac{\sinh \rho x}{\cosh \rho l/2} \quad (R-15)$$

and the end temperature would be

$$\theta_e = \frac{2\theta_p}{\rho l} \tanh \rho l / 2 \quad (R-16)$$

The ratio of the resulting end temperature to that without radiation becomes

$$R = \frac{\theta_e}{\theta_p} = \frac{\tanh \rho l / 2}{\rho l / 2} \quad (R-17)$$

Shield Effects

When a shield is interposed between the sample and the oven, we must not only account for the reradiation of heat from this shield, but also for the conduction of the heat along the shield. The shield is considered as floating, attaining some equilibrium temperature with respect to radiation. The radiation between the shield and the oven is

$$dq_{sh} = \frac{-\sigma P_{sh} (4\theta_o^3 \theta_{sh})}{\frac{1}{\epsilon_{sh}} \frac{P_{sh}}{P_o} \frac{1}{\epsilon_o}} dx \quad (R-18)$$

while between the sample and the shield

$$dq_{sa} = \frac{\sigma P_{sa} 4\theta_o^3 [\theta_{sh} - \theta_{sa}]}{\frac{1}{\epsilon_{sa}} + \frac{P_{sa}}{P_{sh}} \left[\frac{1}{\epsilon_{sh}} - 1 \right]} dx \quad (R-19)$$

The differential conduction along the shield is

$$dq_{ish} = -K_{sh} (2\pi r_{sh} w_{sh}) \frac{d^2 \theta_{sh}}{dx^2} dx \quad (R-20)$$

while that along the sample is

$$dq_{isa} = -K_{sa} w_{sa}^2 \frac{d^2 \theta_{sa}}{dx^2} dx \quad (R-21)$$

if we let

$$\phi_1 = \frac{\sigma P_{sh} (4\theta_o^3)}{\frac{1}{\epsilon_{sh}} + \frac{P_{sh}}{P_o} \left[\frac{1}{\epsilon_o} - 1 \right]} \quad (R-22)$$

$$\theta_2 = \frac{\sigma P_{sa} (4\theta_o^3)}{\frac{1}{\epsilon_{sa}} + \frac{P_{sa}}{P_{sh}} \left[\frac{1}{\epsilon_{sh}} - 1 \right]} \quad (R-23)$$

then

$$dq_{sh} = -\theta_1 \Theta_{sh} dx \quad (R-24)$$

$$dq_{sa} = \theta_2 (\Theta_{sh} - \Theta_{sa}) dx \quad (R-25)$$

The heat balance equations become

$$\theta_1 \Theta_{sh} + \theta_2 (\Theta_{sh} - \Theta_{sa}) = K_{sh} A_{sh} \frac{d^2 \Theta_{sh}}{dx^2} \quad (R-26)$$

$$\theta_2 (\Theta_{sa} - \Theta_{sh}) = K_{sa} A_{sa} \frac{d^2 \Theta_{sa}}{dx^2} \quad (R-27)$$

from (R-27)

$$\Theta_{sh} = \Theta_{sa} - \frac{K_{sa} A_{sa}}{\theta_2} \frac{d^2 \Theta_{sa}}{dx^2} \quad (R-28)$$

Now let

$$\beta_1 = \theta_1 / K_{sh} A_{sh} \quad (R-29)$$

$$\beta_2 = \theta_2 / K_{sa} A_{sa} \quad (R-30)$$

$$\gamma = \theta_2 / \theta_1 \quad (R-31)$$

then

$$\frac{d^4 \Theta_{sa}}{dx^4} - (\beta_1 + \gamma \beta_1 + \beta_2) \frac{d^2 \Theta_{sa}}{dx^2} + \beta_1 \beta_2 \Theta_{sa} = 0 \quad (R-32)$$

The roots of the auxiliary equation are

$$p^2 = 1/2 \left[\beta_1(1+\gamma) + \beta_2 \pm \sqrt{(\beta_1(1+\gamma) + \beta_2)^2 - 4\beta_1\beta_2} \right] \quad (R-33)$$

let

$$p_1 = 1/2 \left[\beta_1(1+\gamma) + \beta_2 + \sqrt{(\beta_1(1+\gamma) + \beta_2)^2 - 4\beta_1\beta_2} \right] \quad (R-34)$$

$$p_2 = 1/2 \left[\beta_1(1+\gamma) + \beta_2 - \sqrt{(\beta_1(1+\gamma) + \beta_2)^2 - 4\beta_1\beta_2} \right] \quad (R-35)$$

The form of the solution is then

$$\theta_{sa} = A \sinh p_1 x + A_c \cosh p_1 x + B \sinh p_2 x + B_c \cosh p_2 x \quad (R-36)$$

We can prove that, similarly to the no shield case, $A_c = B_c = 0$, and therefore

$$\theta_{sa} = A \sinh p_1 x + B \sinh p_2 x \quad (R-37)$$

The boundary condition in the sample is the same as before for the no shield case

$$\frac{d\theta_{sa}}{dx} = \frac{2\theta_p}{l} \quad \text{when } x = l/2 \quad (R-38)$$

In the shield the difference between the heat radiated from the sample to the shield and that radiated from the shield to the oven over the hot half of the sample is equal to the heat conducted along the shield at its center. Thus

$$\int_{-l/2}^0 \left[\epsilon_2 (\theta_{sa} - \theta_{sh}) - \epsilon_1 \theta_{sh} \right] dx = -K_{sh} A_{sh} \left. \frac{d\theta_{sh}}{dx} \right|_{x=0} \quad (R-39)$$

which can be rewritten as

$$\int_{-l/2}^0 \left[\gamma \beta_1 (\theta_{sa} - \theta_{sh}) \beta_1 \theta_{sh} \right] dx = \left. \frac{d\theta_{sh}}{dx} \right|_{x=0} \quad (R-40)$$

Substituting

$$\begin{aligned} & \int_{-l/2}^0 \left\{ \gamma \left[\frac{p_1^2}{\beta_2} A \sinh p_1 x + \frac{p_2^2}{\beta_2} B \sinh p_2 x \right] \right. \\ & \left. - \left[1 - \frac{p_1^2}{\beta_2} \right] A \sinh p_1 x + \left[1 - \frac{p_2^2}{\beta_2} \right] B \sinh p_2 x \beta_1 \right\} dx = \end{aligned} \quad (R-41)$$

$$- \left[\left[1 - \frac{\rho_1^2}{\beta_2} \right] A \rho_1 \cosh \rho_1 x + \left[1 - \frac{\rho_2^2}{\beta_2} \right] B \rho_2 \cosh \rho_1 x \right]_{x=0}$$

Let

$$r_1 = \beta_2 - \rho_1^2 \quad (R-42)$$

$$r_2 = \beta_2 - \rho_2^2 \quad (R-43)$$

Then

$$\int_{-l/2}^0 \left[(\rho_1^2 - r_1) A \sinh \rho_1 x + (\rho_2^2 - r_2) B \sinh \rho_2 x \right] \beta_1 dx =$$

$$- r_1 \rho_1 A - r_2 \rho_2 B \quad (R-44)$$

$$\beta_1 \left[\frac{\rho_1^2 - r_1}{\rho_1} A \cosh \rho_1 x + \frac{\rho_2^2 - r_2}{\rho_2} B \cosh \rho_2 x \right]_{-l/2}^0 =$$

$$r_1 \rho_1 A - r_2 \rho_2 B \quad (R-45)$$

$$\beta_1 A \frac{(\rho_1^2 - r_1)}{\rho_1} [1 - \cosh \rho_1 l/2] + \beta_1 B \frac{(\rho_2^2 - r_2)}{\rho_2}$$

$$[1 - \cosh \rho_2 l/2] = r_1 \rho_1 A - r_2 \rho_2 B \quad (R-46)$$

$$\frac{A}{B} = - \frac{\rho_1}{\rho_2} \cdot \frac{r_2 \rho_2^2 + \beta_1 [\rho_2^2 - r_2] (1 - w_2)}{r_1 \rho_1^2 + \beta_1 [\rho_1^2 - r_1] (1 - w_1)} \quad (R-47)$$

where

$$w_1 = \cosh \rho_1 l/2$$

$$w_2 = \cosh \rho_2 l/2 \quad (R-48)$$

If we let this expression be equal to D, then we can return to the other boundary condition expressed by equation (R-38) and substitute the value of the derivative obtained from equation (R-37) so that

$$[\rho_1 w_1 D + \rho_2 w_2] B = 2\theta_p / \ell \quad (R-49)$$

This expression can be solved for B, and the value of A can be solved from equation (R-48). The ratio of the resulting end temperature to that without radiation becomes

$$R = \frac{\theta_e}{\theta_p} = \frac{D \sinh \rho_1 \ell/2 + \sinh \rho_2 \ell/2}{\ell/2 (\rho_1 w_1 D + \rho_2 w_2)} \quad (R-50)$$

This is also the ratio of the actual thermal conductivity to indicated thermal conductivity. It can be seen that the solution of this formula from the physical parameters is rather involved with the substitution of several intermediate terms. Some simplification can be made in this intermediate work if the terms involving temperature were first removed from these terms. We then would have the following expressions.

$$\phi_{10} = \frac{4 \sigma P_{sh}}{\frac{1}{\epsilon_{sh}} + \frac{P_{sh}}{P_o} \left[\frac{1}{\epsilon_o} - 1 \right]} \quad (R-51)$$

$$\phi_{20} = \frac{4 \sigma P_{sa}}{\frac{1}{\epsilon_{sa}} + \frac{P_{sa}}{P_{sh}} \left[\frac{1}{\epsilon_{sh}} - 1 \right]} \quad (R-52)$$

$$\beta_{10} = \phi_{10} / K_{sh} A_{sh} \quad (R-53)$$

$$\beta_{20} = \phi_{20} / K_{sa} A_{sa} \quad (R-54)$$

$$\gamma = \phi_{20} / \phi_{10} \quad (R-55)$$

$$\rho_{10}^2 = 1/2 \left[\beta_{10}(1 + \gamma) + \beta_{20} + \sqrt{\beta_{10}(1 + \gamma) + \beta_{20}^2 - 4\beta_{10}\beta_{20}} \right] \quad (R-56)$$

$$\rho_{20}^2 = 1/2 \left[\beta_{10}(1 + \gamma) + \beta_{20} - \sqrt{\beta_{10}(1 + \gamma) + \beta_{20}^2 - 4\beta_{10}\beta_{20}} \right] \quad (R-57)$$

$$r_{10} = \beta_{20} - \rho_{10}^2 \quad (R-58)$$

$$r_{20} = \beta_{20} - \rho_{20}^2 \quad (R-59)$$

The relationship between these terms and their counterparts are

$$\begin{array}{ll} \varnothing_1 = \varnothing_{10} \theta_o^3 & P_1 = P_{10} \theta_o^{3/2} \\ \varnothing_2 = \varnothing_{20} \theta_o^3 & P_2 = P_{20} \theta_o^{3/2} \\ \beta_1 = \beta_{10} \theta_o^3 & r_1 = r_{10} \theta_o^3 \\ \beta_2 = \beta_{20} \theta_o^3 & r_2 = r_{20} \theta_o^3 \end{array} \quad (R-60)$$

Results Based on Formulas

Based on the above formulas, the ratio of actual to indicated thermal conductivity was calculated for several cases. They were based on use of a sample which had the following characteristics. It is rectangular with a square cross-section 1/4 inch on a side and 2 inches long. The thermal conductivity is assumed to be 1×10^{-2} watts $\text{cm}^{-1} \text{deg}^{-1}$. The oven wall is assumed to have unity thermal emissivity.

The results of varying the emissivity of the sample and the shield location, material and thickness are shown in Figure R-1. Several results stand out in the figure. At room temperatures the radiation loss is only of importance when there is no shield with a sample of unity emissivity. Unfortunately, most materials will have nearly this high an emissivity. When the thermal conductivity is as low as considered here, shielding should be used even at room temperatures. If it is possible to lower emissivity by polishing, or coating in any way that does not limit the other properties, it should be done.

The help due to low emissivity of the shield is of importance. This is especially true when the experiment is to be done with a high emissivity sample. Clean silver is better than platinum and since it is possible to carry out the experiment in a non-corrosive atmosphere, it is the best to use.

It was found by comparing thickness of the silver shield that there was very little change in efficiency when the shield thickness was changed from 1 mil to 100 mils. However when the shield was reduced in thickness to 0.1 mils or 0.001 mils, there was an increase in efficiency. In practice such a thin shield could not be made as it would be transparent and would probably not have the low emissivity of a thicker and smoother shield. However one way to approach it would be to wrap a silver ribbon around a tube that did not have good thermal contact between windings. In this way a lower thermal conductivity would result. The fact that the thickness of the shield is of importance is a consequence of the fact that the surface of the bodies involved are not of uniform temperature.

Table of Symbols

A_1	Area of inner surface
A_2	Area of outer surface
A_{sa}	Cross sectional area of sample
D	Ratio A/B

Table of Symbols - (continued)

I	Current in sample
K_{sa}	Thermal conductivity of sample
K_{sh}	Thermal conductivity of shield
l	Length of sample
P_o	Perimeter of oven
P_{sa}	Perimeter of sample
P_{sh}	Perimeter of shield
q_c	Thermal conduction heat
q_r	Thermal radiation loss
q_{sa}	Thermal radiation from sample to shield
q_{sh}	Thermal radiation from shield to oven
R	Ratio of temperature
r_1	Defined by equation (R-42)
r_2	Defined by equation (R-43)
r_{10}	Defined by equation (R-58)
r_{20}	Defined by equation (R-59)
r_{sh}	Radius of shield
w_1	Defined by equation (R-48)
w_2	Defined by equation (R-48)
w_{sa}	Thickness of sample
w_{sh}	Radial thickness of shield
x	Distance along sample
dq_{isa}	Differential thermal conduction along sample
dq_{ish}	Differential thermal conduction along shield
α	Thermoelectric power
β_1	Defined by equation (R-29)

Table of Symbols - (continued)

β_2	Defined by equation (R-30)
β_{10}	Defined by equation (R-53)
β_{20}	Defined by equation (R-54)
γ	Defined by equation (R-31)
ϵ_o	Emissivity of oven
ϵ_1	Emissivity of inner surface
ϵ_2	Emissivity of outer surface
ϵ_{sa}	Emissivity of sample
ϵ_{sh}	Emissivity of shield
ρ	Defined by equation (R-10)
ρ_1	Defined by equation (R-34)
ρ_2	Defined by equation (R-35)
ρ_{20}	Defined by equation (R-57)
ρ_{10}	Defined by equation (R-56)
ϕ_1	Defined by equation (R-22)
ϕ_2	Defined by equation (R-23)
ϕ_{10}	Defined by equation (R-51)
ϕ_{20}	Defined by equation (R-52)
σ	Stefan Boltzmann constant
θ	Temperature
θ_o	Temperature of oven
θ_1	Temperature of inner surface
θ_2	Temperature of outer surface
θ_e	Temperature at end of surface
θ_p	Defined in equation (R-14)
θ_{sa}	Differential Temperature of sample

Table of Symbols - (continued)

Θ_{sh} Differential Temperature of shield

Since the results of the analysis of Jules Cahn have been available, a calculation has been made of the loss in a sample having a configuration of radius to length similar to that in the Battelle experiments and with silver shielding and taking into account radiation from the ends. The results are shown in Figure R-6 for several values of thermal conductivity.

The analysis by Cahn in the forthcoming article mentioned above is more complete in that it takes into account several additional effects. However, this work points out some facts about radiation shielding not covered by that analysis. Due to the high thermal conductivity of most materials suitable as low emissivity shields, they will act as thermal short circuits for the different temperature set up. Thus there will be no advantage of having multiple shields.

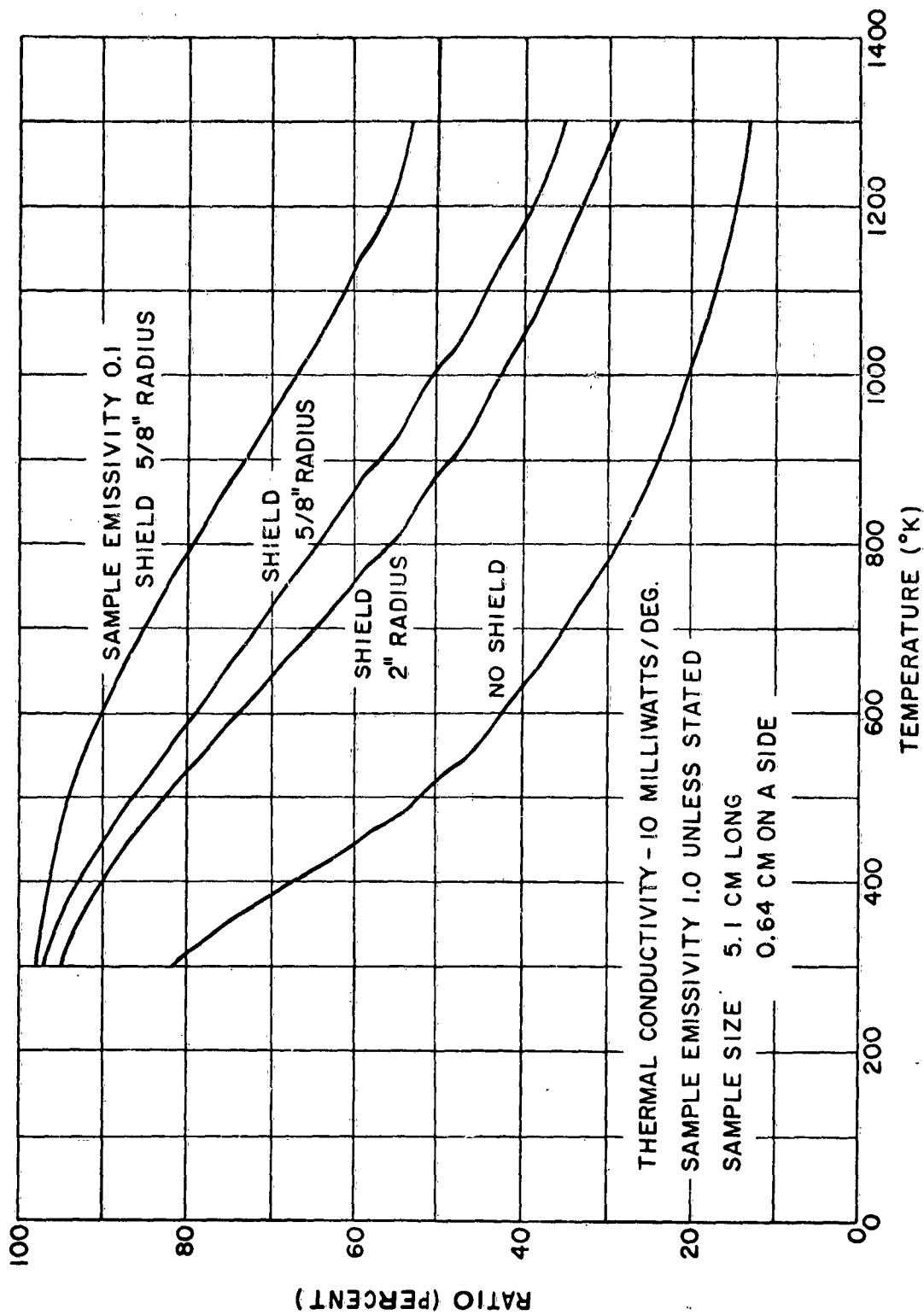


Figure R-6: Ratio Actual Thermal Conductivity to Indicated Thermal Conductivity for Various Conditions.

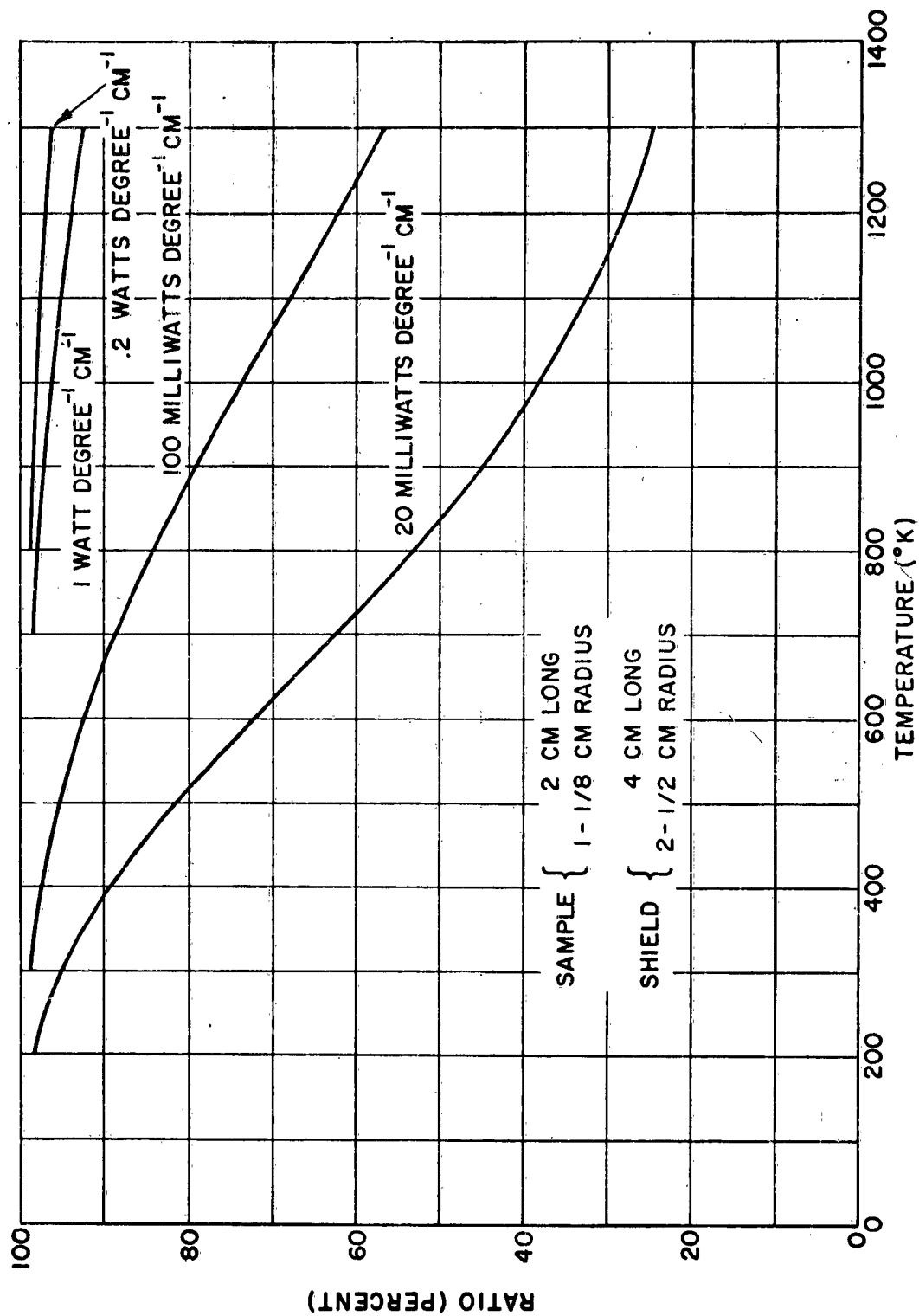


Figure R-7: Ratio Actual Thermal Conductivity to Indicated Thermal Conductivity for Various Thermal Conductivities.

SECTION III: HIGH TEMPERATURE FACILITY FOR MEASUREMENT OF ρ , K AND S

INTRODUCTION

It is desired that the equipment be designed to accommodate a single sample in such a manner that all data can be obtained during one temperature cycle from room temperature up to a maximum of 1000°C. As some of the materials to be tested are not suited to the imbedding of temperature and potential probes and to prevent the possibility of any contamination from welding, sparking or metallizing, it is preferred that the measurements be obtained thru pressure contacts applied to the end faces of the test specimen.

The measurement of the Seebeck thermoelectric effect, S, does not affect the design requirements as much as the wide range of electrical resistivities, ρ , and thermal conductivities, K, to be covered, that is:

ρ = Electrical Resistivity, 10×10^{-6} to 10 ohm-CM

K = Thermal Conductivity, 0.005 to 0.3 Watt-CM²/CM-°C

ASSUMPTIONS

It is assumed that in general the same instrumentation and techniques applied in the measurements at normal room temperature are sufficiently accurate and applicable, therefore, we are concerned here only with those factors directly relating to high temperature and its associated heat losses. A review of the subject revealed the limitations of various possible methods and indicated that in order to realize the practicability of a high temperature facility a compromise must be made between the accuracies obtainable in the electrical resistivity and thermal conductivity measurements and that certain assumed conditions prevail. This study therefore is being made with the following assumptions:

- a. That all test specimens will be to a given size within reasonable tolerance.
- b. Dimensional stability will be obtained from measurements made at room temperature before and after the temperature cycle.
- c. End faces will be smooth and samples suitable to withstand pressure contacts.
- d. That measurements will be made in vacuum so that heat transfer by conduction and radiation only need be considered.
- e. Data compiled from steady state conditions at successive increasing increments of temperature will provide the desired information on efficiency and characteristics of the material.

ANALYSIS

Electrical Resistivity (ρ)

The factors involved here are current distribution, application of potential probes and dimensional measurements. The only one of these which is directly related

to temperature is that of dimensional measurement and for which no means is provided for determining the temperature coefficient of expansion.

As shown in Figure R-8, provision is made for resistance measurement using the four lead method so that contact resistance does not enter directly into the measurement. The a-c bridge current can be supplied to the platinum contact end plates by using the thermocouple elements T₁ and T₃. Small platinum faced pressure contact potential probes P₁ and P₂ are also shown which make contact only at the center of the face of the test specimen.

The resistivity, ρ_{T_2} , at temperature T₂ is obtained from:

$$\rho_{T_2} = R_{T_2} \frac{A}{L}$$

where

R_{T₂} = resistance at temperature T₂

A = cross sectional area of sample

L = length of sample between points P₁ and P₂

T = mean sample temperature, $\frac{T_1 + T_3}{2}$

Current distribution is a function of pressure and surface contact resistance, the relation for which is shown in Figure R-9.

In determining a convenient sample size the above indicates that $\frac{A}{L}$ should be as small as practical. This is not in accord with the requirements for the measurement of thermal conductivity so, as a compromise, $\frac{A}{L} = 2$ was chosen and is the scale to which Figure R-8 is drawn.

Thermal Conductivity (K)

Time Response

The time required to attain a temperature and establish temperature equilibrium at a point becomes a major factor in determining the accuracy obtainable, allowable drift and number of temperature intervals that can be obtained on a sample within a reasonable period of time.

When a temperature has been attained the electrical resistivity measurement can be made as soon as the temperature is reasonably well stabilized. For the thermal conductivity measurement it is then required that a temperature difference be set up across the test specimen and the heat flow measured by means of the reference unit. This can be done by means of the heater built in the reference unit as shown in Figure R-8 and by adjustment of the center tapped furnace winding. The time required to establish equilibrium conditions will depend primarily upon the properties of the material of the test specimen and upon its dimensions.

Materials having a low thermal conductivity will respond more slowly so, based on the lower limit of 0.005 watt-cm²/cm-°C gives from

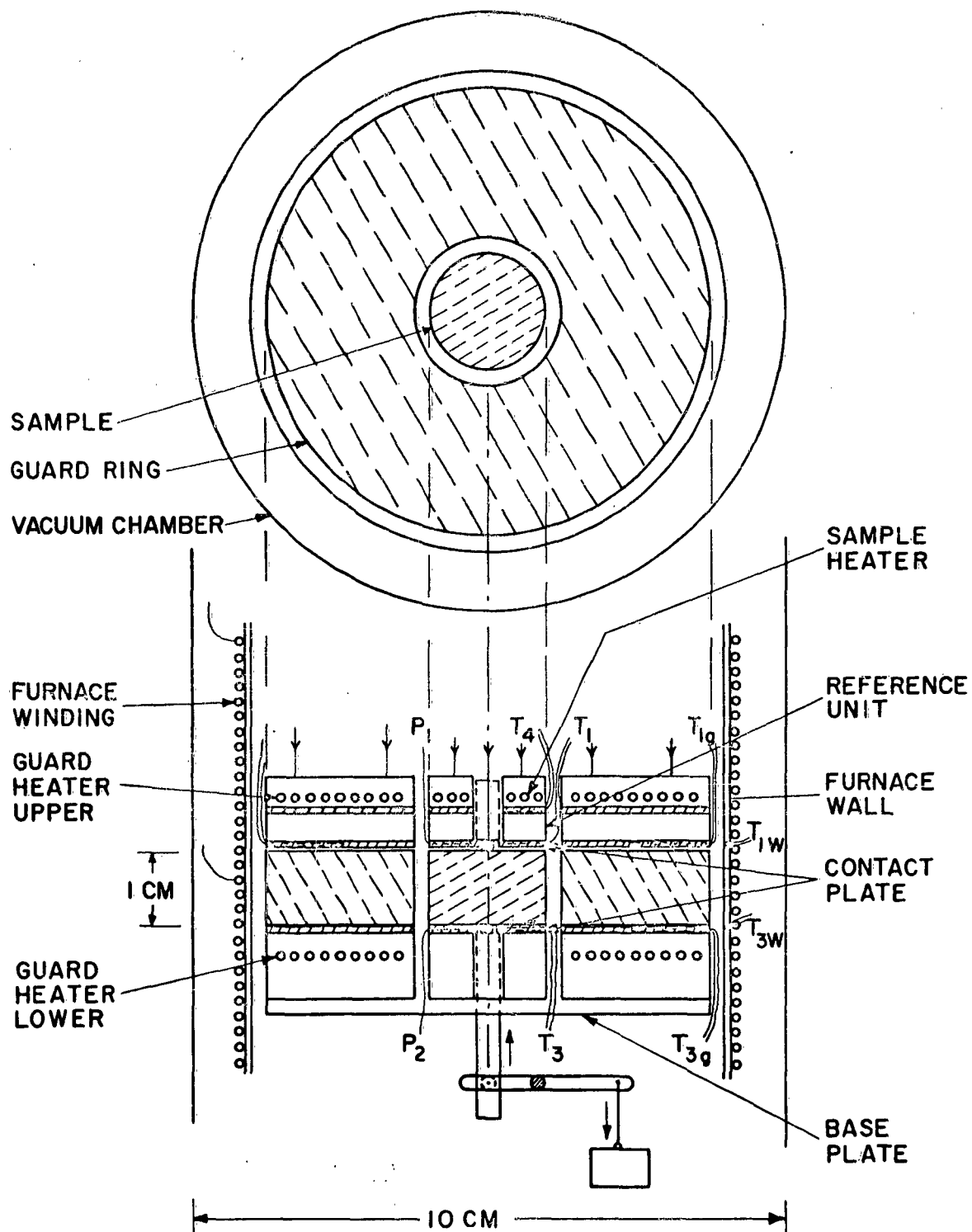


Figure R-8: Electrical Resistivity Measuring Device Excluding Contact Resistance Measurement.

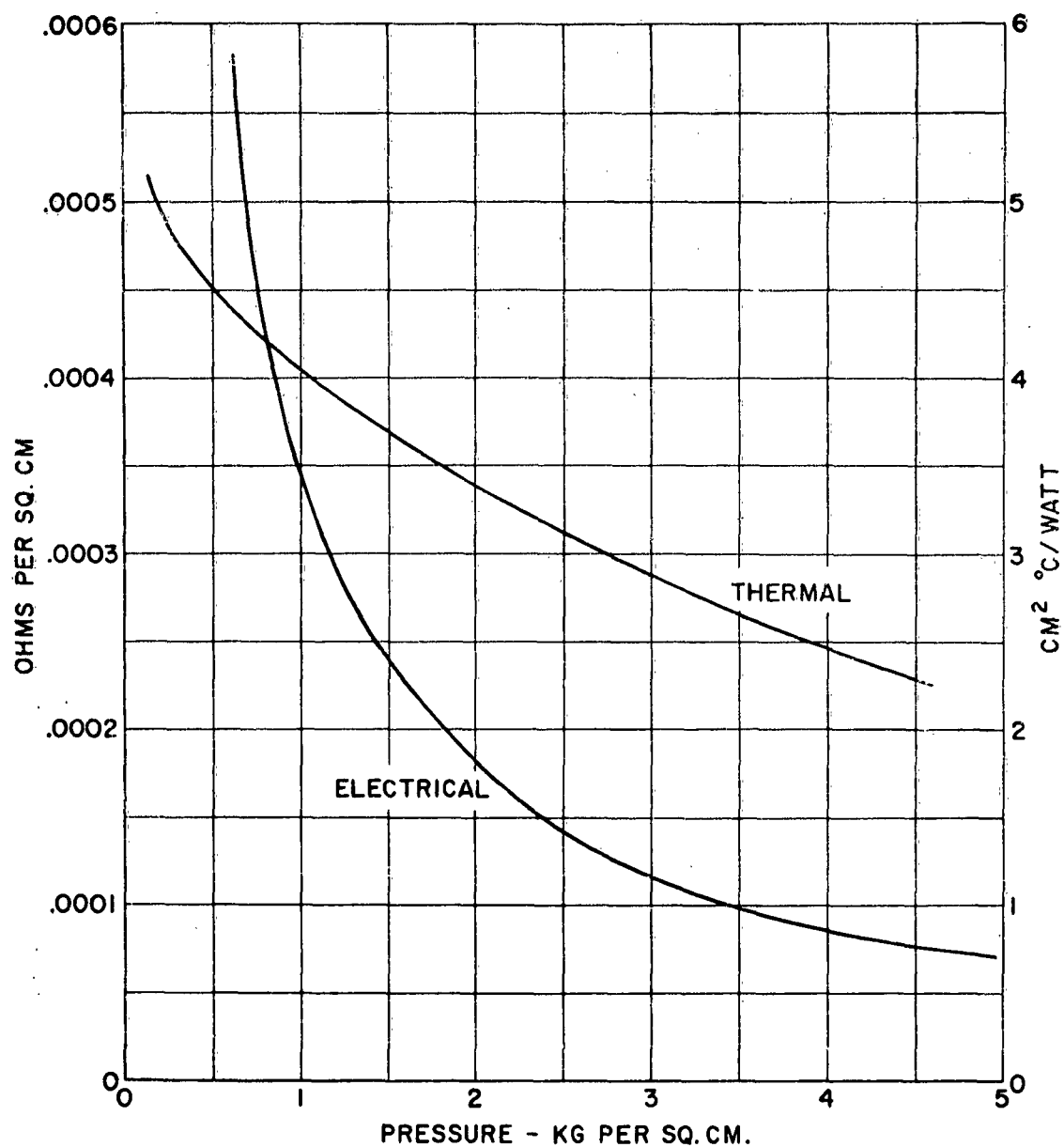


Figure R-9: Contact Resistance vs Pressure.
 Estimated Values from Available
 Data. Plane Surfaces, Ground
 Finish in Vacuum.

$$\tau_c = \frac{.5L^2}{\alpha} = 3 \text{ minutes}$$

where

τ_c = time constant, 63% of final change

L = length of specimen, 1 cm

.5 = Fourier's No. for thin slab for Y = .37

α = Diffusivity, $\frac{\text{thermal conductivity}}{\text{density} \times \text{sp. heat}} = \frac{.005}{.03} = .17$

The above, of course, represents maximum value and normally a faster time response can be expected. The time required to establish equilibrium is from 4 to 5 τ_c thus giving 15 minutes which seems reasonable. The only variable is L and reducing this dimension would improve the time response but for reasons explained below it is not advisable to increase the ratio of $\frac{A}{L}$.

Method of Measurement

For the measurement of thermal conductivity at high temperatures on samples of a size not particularly suited to this type of measurement, it has been found that a comparative type of measurement is most suitable. With this method it is not necessary to determine heat flow by measurement of power input. Instead a standardized reference unit is used.

The thermal conductivity (K) of the sample is then defined by

$$K = \frac{q}{T_1 - T_3} \frac{L}{A}$$

where

q = heat flow, watts

A = area sq. cm of sample

$T_1 - T_3$ = temperature diff. °C across sample

L = length between T_1 and T_3 (CM)

determine q from reference unit by

$$q = k (T_4 - T_1)$$

where

k = constant (watts)

$T_4 - T_1$ = Temperature diff. °C across reference unit

therefore

$$K = k \frac{T_4 - T_1}{T_1 - T_3} \frac{L}{A}$$

when area of sample and reference unit are equal as shown in Figure R-8. k for the reference unit is determined by standardization with materials of known conductivity.

In the comparative method one of the most important factors is that of heat transfer which relates to heat flow thru the sample relative to that thru the reference unit.

The other factor is the thermal resistance between the two contact plates and the surfaces of the sample; this will be referred to as the thermal contact resistance.

Design Factors

Heat Transfer

Inasmuch as the measurements are being made in vacuum the radial heat transfer from an isolated sample, as shown in Figure R-8, is entirely by radiation. Figure R-8 shows the guard ring method which provides a convenient means of keeping these losses to a minimum. An upper and lower heating unit are provided on the guard ring and thermocouples are attached directly opposite those on the contact plates on the sample. By means of individual heat control the thermocouples can be equalized so that

$$T_1 = T_{1g} \quad \text{and} \quad T_3 = T_{3g}$$

The necessity for equalization of these temperatures becomes exceedingly important at the higher temperatures due to the increase in heat transfer by radiation as shown in Table R-1 below.

TABLE R-1
RADIATION HEAT TRANSFER COEFFICIENT (h_r)
 $e = 1$

<u>Temp. °C</u>	<u>W/cm² - °C</u>
500	.011
600	.015
700	.021
800	.029
900	.036
1000	.05

The following are calculations based on a test specimen 1 cm in length, 1.6 cm diameter and a guard ring constructed of a material such as zirconium, having a conductivity $K_g = .008$, emissivity 0.4, I.D. 2 cm, O.D. 6 cm

$$q_a = K \frac{A}{L} (T_1 - T_3)$$

where

q_a = axial heat flow thru specimen, watts

K = thermal conductivity of sample

A = cross sectional area, 2 sq. cm

L = length of test specimen, 1 cm

T_1 and T_3 = degree C

$$q = \frac{T_2 - T_{2w}}{R_1 + R_2 + R_3}$$

where

q_r = radial heat flow from specimen, watts

T_2 = specimen, mean radiation surface temp. °C

T_{2w} = furnace wall, mean temp, °C $\frac{T_{1w} + T_{3w}}{2}$

R_1 = thermal radiation resistance specimen to guard $\frac{1}{h_r A}$ where A = radiating area, 5 sq. cm

R_2 = thermal resistance of guard ring $\frac{1}{K_g \frac{A_g}{L_g}}$ where A_g = mean area to radial heat flow, 12.5 sq. cm and L_g = length to radial heat flow, 2 cm

R_3 = thermal radiation resistance, guard to furnace wall $\frac{1}{19 \times .4 h_r}$ at 1000°C for $T_2 - T_{2w} = 1$

$$q_r = 0.038 \text{ watts}$$

giving

$$T_2 - T_{2g} = .038 R_1 = .15^\circ\text{C}$$

$$T_{2g} - T_{4g} = .038 R_2 = .75^\circ\text{C}$$

$$T_{4g} - T_{2w} = .038 R_3 = .10^\circ\text{C}$$

where

T_{2g} = mean temp. °C. inner surface of guard

T_{4g} = mean temp. °C outer surface of guard

Axial heat flow q_a is a function of $T_1 - T_3$, therefore for reasonable accuracy of measurement a value of at least 5 is desirable and a value of more than 50 would probably be undesirable. The following table gives values of q_r/q_a for a range of values of $T_1 - T_3$ for test specimens of various values of K based on the above radial heat transfer for a 1°C difference between specimen and furnace wall at 1000°C of 0.038 watts.

	K = .005		K = .02		K = .3	
$T_1 - T_3$	q_a	q_r/q_a	q_a	q_r/q_a	q_a	q_r/q_a
5	.05	.76	.20	.19	3.0	.013
10	.10	.38	.40	.09	6.0	.006
20	.20	.19	.80	.05		
25	.25	.15	1.00	.04		
50	.50	.08				

The data above can be used as a guide in determining the most suitable test conditions to obtain the desired accuracy on a particular sample. Heating units are provided on the guard ring and with a suitable control circuit it should be possible to obtain a temperature equalization between specimen and guard so that in most cases only rough control of the furnace heater will be necessary.

Thermal Contact Resistance

As defined under Method of Measurement, the conductivity of the specimen is determined from temperature $T_1 - T_3$. These temperatures are actually the temperature of the contact plates between which the specimen is mounted and therefore these contact resistances are included along with the thermal resistance of the specimen. Ordinarily when measuring insulating materials and high pressures are permissible, the surface contact resistance is so low that it is negligible relative to the high resistance of the specimen. Although a majority of the materials with which we are concerned in this project may fall within this class the desired range of measurement does extend to as high a conductivity as 0.3 watt-cm²/cm-°C.

The k for the reference unit used in this high conductivity range would be obtained from measurements on a standardized specimen under similar conditions and would therefore include these contact resistances. Should the conditions during a measurement be different from those for which the reference unit, k , was obtained, the contact resistance may be different. An estimate of the magnitude of the effect of such variables is therefore desirable.

The factors affecting thermal contact resistance per unit area $1/h_c$, are surface smoothness, hardness of materials, contact pressure and temperature.

The surface of the specimen should be relatively smooth and even so that a uniform contact pressure will be obtained over the whole area. The contact plates can be of platinum, which will withstand the high temperatures and is a relatively soft material which is a desirable property for low contact resistance at low pressures. Pressure should be applied to the reference unit in such a manner that the contact plate can align itself with the face of the specimen.

Contact pressure is probably the most important factor for in the low pressure range, less than 10,000 grams/sq. cm, the contact resistance decreases quite rapidly with increase in pressure. This is shown in Figure R-9 along with the change in electrical contact resistance vs. pressure.

At high temperature in vacuum no deterioration of the surfaces or other effects at low pressures are expected that would affect the contact resistance. Voids resulting from roughness however produce miniature spaces across which, in a vacuum, heat transmission can be by radiation only. At temperatures above 500°C Table R-1 shows that this becomes quite a factor as rather efficient heat transfer takes place although there is no physical contact. Should it be suspected that the surface of a particular sample is questionable, then measurements made at low temperature in air before evacuating could verify this by indicating lower contact resistance due to the conductivity of the air filled voids between the surfaces.

The following is a table calculated from probable contact resistance data at room temperature as taken from Figure R-9. The effect of various pressures on the contact resistance as related to the conductivity of the specimen is shown as

$$\frac{2 \frac{1}{h_c}}{\frac{1}{K}}$$

where

$\frac{1}{h_c}$ = thermal contact resistance, sq. cm°C/watt

$\frac{1}{K}$ = thermal resistivity of specimen, cm² (°C)/watt (cm)

TABLE R-2
EFFECTIVE PRESSURE ON CONTACT RESISTANCE.

	K = .005		K = .02		K = .3
Pressure KG/CM ²	$\frac{1}{h_c}$	$\frac{2}{h_c}/1/K$	$\frac{2}{h_c}/1/K$	$\frac{2}{h_c}/1/K$	$\frac{2}{h_c}/1/K$
.5	4.5	.045	.18		2.7
1.0	4.0	.04	.16		2.4
2.0	3.4	.034	.13		2.0
3.0	2.9	.029	.12		1.8

From the shape of the curves in Figure R-9 and from the above data it is readily seen that a minimum contact pressure of .5 to 1 kg/cm² should be used. At this pressure when measuring specimens with a K as low as .005 the sum of the two contact resistances is only 4% of that of the specimen and a change in pressure of 2 to 1 amounts to only .5% which, in most cases, can be considered negligible.

Up to values of K = .1 a change in contact pressure of 2 to 1 may change the contact resistance by as much as 10% of that of the specimen so that for good accuracy higher pressures are desirable and greater care taken to obtain reproducible results.

For specimens with a $K = .3$ each contact represents a thermal resistance equal to about that of the 1 cm length specimen. Increasing the contact pressure to 10 or 20 kg/cm would give some improvement, but may lead to some mechanical problems. It is to be noted under Heat Transfer that where $K = .3$ the net flow q_a is at a maximum and the radiation losses are at a minimum. For greater accuracy in this range therefore, there are several modifications that could be considered such as

1. Omit the guard ring if necessary and imbed or weld thermocouples directly to the side of the specimen at two definite positions. The distance between them would then be considered as the dimension L .
2. Materials coming within this range would probably be metallic and could be welded, brazed or plated to provide lower contact resistance.
3. Measure the temperature at probes P_1 and P_2 .
4. Greater length could be required for these specimens.

Reference Unit

Standardized reference units will be provided having known values of thermal conductivity. As shown in Figure R-8, there will be a built-in heating unit and two thermocouples, T_1 and T_4 . As mentioned under Thermal Contact Resistance, a platinum contact plate would be desirable. The T_1 thermocouple leads will also provide a means of current connection to the contact plate for the resistance measurement.

In order to adequately cover the wide range of thermal conductivity measurements it is desirable that two or possibly three reference units of various values be used.

Standard samples will be required which will be constructed of materials having known thermal conductivities. For accurate calibrating purposes these should be of the same dimensions as test specimens, thus providing an accurate substitution method. Materials having known thermal properties to within about $\pm 10\%$ are available which are suitable for this purpose.

Seebeck Thermoelectric Effect

Provision is made for setting up a temperature difference across the sample by means of the heating unit built into the reference unit. Platinum potential probes, P_1 and P_2 , connecting the two faces are provided for measuring the thermoelectric voltage. The temperature difference is determined from $T_1 - T_3$.

Heat losses are of no significant importance in the measurement of the Seebeck voltage, therefore the measurement techniques employed at the low temperatures are adequate.

DISCUSSION

An analysis of the various factors pertaining to the measurement of ρ , K and S on test specimens in the temperature range 25 to 1000°C has been presented. Based on the general requirements certain assumptions have been made and in general the only factors considered here are those relating to heat transfer and design requirements

for high temperature operation.

The analysis revealed several features that are desirable for a high temperature facility and Figure R-8 is an outline showing the general arrangement and main features required. At high temperatures adequate shielding against heat losses by radiation is essential and is accomplished by means of the guard ring method as shown. While this method can be applied to test specimens of various sizes, the present discussion has been limited to a test specimen of one specific size and shape not too difficult to obtain. Provision is made so that all measurements can be obtained by means of pressure contacts as mounted in position within a vacuum chamber.

The accuracy of measurement of the electrical resistivity at high temperatures should be of the same order of magnitude as that obtainable at low temperatures on a specimen of comparable size as temperature only and not heat transfer is involved.

Thermal conductivity measurements are dependent upon the measurement of temperature, temperature differentials and associated heat transfer. On the size samples considered, it is shown that temperature equilibrium could probably be obtained within about fifteen minutes after having established a temperature level. Standardized reference units, the constant of which has been predetermined, will be used for the measurement of heat flow thru the test specimen. More than one such reference unit will be required in order to adequately cover the wide range of conductivities. It is expected that the constant for these reference units can be determined to within about $\pm 10\%$ for given conditions.

The radiation heat transfer and thermal contact resistance effects have been considered with respect to their effect on the measurement as they pertain to the maximum and average values of the thermal conductivity range. With adequate control of the guard ring heater it should be possible to attain equilibrium temperatures such that the effect of radiation losses should not amount to more than 2 or 3%.

Thermal contact resistance in the low conductivity range is shown to be a negligible factor. For test specimens of high thermal conductivity falling in the range of .1 to .3 W/cm²/°C/cm the contact resistance under some conditions can approach or exceed that of the test specimen. Extreme care would therefore be essential to attain reasonable accuracy as the test conditions should exactly reproduce those under which the reference unit was standardized. Should it be found that greater accuracy is desired in this range, several modifications have been proposed, one of which would involve a change in the size of the test specimen.

The measurement of the Seebeck thermoelectric effect is made at high temperatures in the same manner as it is obtained at the low temperatures and depends only upon the accuracy of the voltage measurement and the temperature difference across the sample.